

Alma Mater Studiorum – Università di Bologna

DOTTORATO DI RICERCA IN

**Ingegneria Civile, Chimica, Ambientale e dei
Materiali**

Ciclo XXIX°

Settore Concorsuale di afferenza: 08/B3

Settore Scientifico disciplinare: ICAR/09

TITOLO TESI

**Seismic behavior of Cross Laminated Timber (CLT)
structural systems: from traditional steel connections
to low-damage solutions**

Presentata da: Milena Massari

Coordinatore Dottorato

Prof. Luca Vittuari

Relatore

Prof. Marco Savoia

Correlatore

Prof. Andre R. Barbosa

Esame finale anno 2017

Summary

ACKNOWLEDGMENTS	I
ABSTRACT	V
SOMMARIO	VII
CHAPTER 1. INTRODUCTION	1
1.1. OBJECTIVE AND SCOPE.....	6
1.2. CHAPTER OVERVIEW	7
CHAPTER 2. OVERVIEW ON TIMBER CONSTRUCTION TECHNOLOGIES	10
SUMMARY OF CHAPTER 2	12
2.1. HISTORICAL TIMBER STRUCTURES.....	13
2.1.1. <i>Japanese temples</i>	13
2.1.2. <i>Traditional European half-timber frame constructions</i>	15
2.2. MODERN TIMBER STRUCTURES.....	17
2.2.1. <i>Light and Heavy Timber Framing</i>	18
2.2.2. <i>Mass Timber Construction System</i>	22
2.3. SEISMIC BEHAVIOUR OF TIMBER STRUCTURES	30
2.4. COMMENTS	31
PART I: EXPERIMENTAL CAMPAIGN ON CLT TRADITIONAL STEEL CONNECTIONS UNDER COUPLED ACTIONS	33
SUMMARY OF PART I.....	35
CHAPTER 3. INTRODUCTION TO LABORATORY TESTS ON CLT JOINTS	37
3.1. PRESENTATION OF CLT BUILDINGS BEHAVIOUR.....	39
3.2. EXPERIMENTAL TESTS LITERATURE REVIEW ON CLT STRUCTURAL SYSTEM SUBASSEMBLIES	41
CHAPTER 4. MONOTONIC AND CYCLIC TESTS ON HOLD-DOWN CONNECTIONS	46
SUMMARY OF CHAPTER 4	48
4.1. TEST CONFIGURATION AND SETUP.....	49
4.2. SPECIMEN COMPONENTS CHARACTERISTICS	51
4.3. LOADING PROTOCOL	53
4.4. INSTRUMENTATION.....	54
4.5. TEST RESULTS AND DISCUSSION	55
4.5.1. <i>Observed failures</i>	55
4.5.2. <i>Rotation of hold-down steel plate</i>	58
4.5.3. <i>Axial force vs axial displacement curves</i>	60
4.5.4. <i>Shear force vs lateral displacement curves</i>	63

4.6.	ANALYSIS OF THE RESULTS	64
4.6.1.	<i>Procedures for the definition of yielding point</i>	64
4.6.2.	<i>Tri-linearization methods of experimental curves</i>	66
4.6.3.	<i>Comparison with code provisions</i>	72
4.6.4.	<i>Strength degradation</i>	76
4.6.5.	<i>Dissipated energy and viscous damping</i>	77
4.7.	CRITICAL DISCUSSION	78
CHAPTER 5. MONOTONIC AND CYCLIC TESTS ON ANGLE BRACKET CONNECTIONS.....		81
SUMMARY OF CHAPTER 5		83
5.1.	TEST CONFIGURATION AND SETUP	85
5.2.	SPECIMEN COMPONENTS CHARACTERISTICS	86
5.3.	LOADING PROTOCOL	88
5.4.	INSTRUMENTATION.....	90
5.5.	TEST RESULTS AND DISCUSSIONS.....	90
5.5.1.	<i>Observed failures</i>	91
5.5.2.	<i>Deformation of angle-bracket steel plate</i>	94
5.5.3.	<i>Axial force vs axial displacement curves</i>	96
5.5.4.	<i>Shear force vs lateral displacement curves</i>	97
5.6.	ANALYSIS OF THE RESULTS	100
5.6.1.	<i>Procedures for the definition of yielding point</i>	100
5.6.2.	<i>Tri-linearization methods of experimental curves</i>	102
5.6.3.	<i>Comparison with code provisions</i>	107
5.6.4.	<i>Strength degradation</i>	109
5.6.5.	<i>Dissipated energy and viscous damping</i>	110
5.7.	CRITICAL DISCUSSION	112
PART II: LOW DAMAGE SOLUTIONS FOR CLT.....		114
SUMMARY OF PART II.....		116
CHAPTER 6. PRESENTATION OF HYBRID ROCKING SYSTEMS.....		118
6.1.	INTRODUCTION	120
6.2.	ROCKING SYSTEMS.....	121
6.3.	RESEARCH BACKGROUND	125
CHAPTER 7. CLT ROCKING WALL TEST.....		137
SUMMARY OF CHAPTER 7		139
7.1.	DESIGN OF THE WALL EXPERIMENT	141
7.2.	TEST SETUP AND INSTRUMENTATION	150
7.3.	TEST SPECIMEN DETAILING	155

7.3.1.	<i>CLT panel</i>	155
7.3.2.	<i>Post-tensioning solution</i>	157
7.3.1.	<i>Axial energy dissipaters</i>	158
7.3.2.	<i>Wall-dissipater connection</i>	162
7.3.3.	<i>Shear keys and corner skirting</i>	166
7.4.	LOADING PROTOCOL	167
7.5.	EXPERIMENTAL RESULTS	169
7.5.1.	<i>Observed failures and comments</i>	169
7.5.2.	<i>Lateral force vs drift</i>	172
7.5.3.	<i>Overturing moment vs drift</i>	174
7.5.4.	<i>Post-tensioning force</i>	175
7.5.5.	<i>Neutral axis oscillation</i>	178
CHAPTER 8.	NUMERICAL MODEL	184
	SUMMARY OF CHAPTER 8	186
8.1.	NUMERICAL MODELLING - SIMPLIFIED MODEL DESCRIPTION	188
8.1.1.	<i>Model Development – Definition of Elastic Elements</i>	189
8.1.2.	<i>Model Development – Non-linear behaviour of Base Rocking Interaction</i>	191
8.1.3.	<i>Numerical Model Development – Non-linear behaviour of steel dissipaters</i>	193
8.2.	NUMERICAL MODEL VALIDATION	195
8.3.	SIMULATION OF TEST AND CALCULATION OF AREA -BASED EQUIVALENT VISCOUS DAMPING	200
8.4.	NUMERICAL SIMULATION FOR HIGH DRIFT LEVELS	204
CHAPTER 9.	CONCLUSIONS	208
9.1.	EXPERIMENTAL CAMPAIGN ON CLT TRADITIONAL STEEL CONNECTIONS REMARKS	210
9.2.	EXPERIMENTAL TEST CLT HYBRID ROCKING WALL REMARKS	211
9.3.	SUGGESTIONS FOR FUTURE WORK	212
	REFERENCES	217
	FIGURE CAPTIONS	225
	TABLE CAPTIONS	233
	ANNEX A: SETUP DRAWINGS FOR COUPLED ACTIONS TESTS ON CLT TRADITIONAL CONNECTIONS	235
	ANNEX B: SETUP DRAWINGS FOR HYBRID ROCKING CLT WALL TEST	237

Acknowledgments

I would like to take the opportunity to thank those people who have guided and supported me during the past three years of my PhD.

First, I would like to thank my supervisor Prof. Marco Savoia for giving me the opportunity to widen my knowledge and to improve my passion for wooden structures by means of this work. For giving me the chance to travel and learn again, for always having believed in my capabilities.

I would also like to thank Luca Pozza for his valuable scientific input, patience and human support. This work would not be possible without his precious help.

I would like to express my gratitude to Prof. Andre Barbosa for giving me the chance to study at Oregon State University, growing so much as researcher and for reminding me that there are not stupid ideas or questions, but just person that are not able to listen.

My deepest appreciation goes to the following companies and institutions: Baldwin General Contracting Inc., Madden Fabrication, MyTiCon, OSU grants, Soltech and CIRI-Edilizia & Costruzioni laboratories, which all together made this research possible.

In particular, I want to thank my friend Mr. Baldwin, he not only supported economically my research but motivated me as human being.

I would like to acknowledge the whole staff and colleagues that worked with me in Hinsdale Reaserch Waves Laboratory.

A special thanks goes to superSusan, Jimmy & Fifi alias my Oregonian family, I love you so much.

Very special thanks goes to all my friends here and around the world, no matter how close or far we live, they all are the best I can ask for.

I am very grateful to my lovely family for their support in every moment, without which I could not reach this important goal.

Last but not least, my gratitude goes to my boyfriend Lorenzo, his patience and support during the last years have been incredibly important to me. Thank you so much, no words can describe my thoughts.

Abstract

Despite the incredible technological progress on the structural field in terms of construction systems and innovative materials, once again the simplicity on problems resolution and the look directed towards on what nature offers us can be the right response, and this answer today is timber structures.

In fact, timber buildings have always showed great performances, even if past timber structural systems are no longer adequate to fulfil modern building standards. This is why new engineered wood products, such as Cross Laminated Timber (CLT), and renewed structural solutions have been created and employed. The key aspect of CLT buildings, as for timber constructions in general, are the connection systems.

Nowadays, design of CLT wall connections is based on the hypothesis that hold-down connection is subjected only to tension, while angle bracket only to shear. Nevertheless, experimental investigation on CLT walls under seismic action highlighted that the two types of connection may be subjected to significant displacements in both directions, thus to coupled actions.

The first part of this study presents results from an extensive experimental campaign conducted on traditional connections for CLT buildings using a specific setup that allowed to impose prescribed levels of displacements in secondary direction, varying at the same time the main direction displacement in a cyclic and monotonic manner. A total of fifteen specimens, for each connection type, are presented and critically discussed in terms of load-displacement curves, strength, stiffness, energy dissipation, strength degradation and ductility. Moreover, different linear approaches to define the yielding force and comparisons with code provisions are presented.

The second part of the thesis focuses on an experimental and numerical investigation of a two storey 2/3 scaled CLT hybrid rocking wall. The applicability and the response of this relatively new low-damage solution has been studied for the first time applied on a CLT shear wall. The objective of the test has been adapting rocking design principles to

CLT lateral resistant walls. The novel aspects of this technology require original solutions for seismic resilient structures, which need to be tested before accurate design implements can be established. The CLT wall included post-tensioned bars to provide self-centring capabilities and replaceable external steel dissipaters to accommodate energy dissipations. Furthermore, an experimental solution for the dissipater-wood panel link has been implemented. Cyclic lateral load has been applied at two levels, simulating the inertial forces transferred at the floor level. Results are presented in terms of achieved lateral force, overturning moment capacity, variation in the post-tension force, oscillation of the neutral axis depth and energy dissipation. Lastly, a numerical simulation accompanied experimental evidences, to examine the response of the rocking system for higher level of drifts, going beyond test limits.

This study has been conducted with the purpose of contributing to the on-going research on suitable damage prevention connection systems for multi-storey, open plan timber structures under seismic loads. Advantages and disadvantages concerning the response of the test under repetitive cyclic loading are pointed up as well as some specific details and suggestions, that could benefit from further research.

Keywords: *CLT structures, hold-down, angle bracket, coupled action test, CLT connections seismic behaviour, CLT low-damage solutions, CLT rocking wall, energy dissipater devices, post-tensioning, timber hybrid solution, rocking wall numerical modelling*

Sommario

Nonostante gli incredibili progressi tecnologici degli ultimi anni in campo strutturale in termini di sistemi di costruzione e materiali innovativi, ancora una volta la semplicità nella risoluzione dei problemi e lo sguardo rivolto verso ciò che la natura ci offre può essere la risposta giusta, e questa risposta oggi sono le strutture in legno.

Gli edifici in legno hanno infatti sempre mostrato ottime capacità strutturali, anche se le strutture tradizionali in legno, oggigiorno, non sono più adatte a soddisfare i requisiti imposti dai moderni standard per le costruzioni. A tal proposito, innovativi prodotti ingegnerizzati in legno, come l'X-Lam (o CLT), e rinnovati sistemi costruttivi sono stati creati e ampiamente diffusi.

L'aspetto chiave degli edifici in X-Lam, come per tutte le strutture in legno, sono le connessioni. Attualmente, la progettazione delle connessioni nelle pareti X-Lam è basata su ipotesi che considerano gli hold-down soggetti ai soli sforzi di trazione, mentre gli angolari a soli sforzi di taglio. Nonostante ciò, test sperimentali condotti su pareti in X-Lam hanno evidenziato come entrambe le tipologie di connessioni sono soggette in realtà a spostamenti significativi in entrambe le direzioni, e conseguentemente a sforzi combinati.

La prima parte di questo lavoro di tesi presenta i risultati ottenuti da un'estesa campagna sperimentale condotta sulle connessioni tradizionali per gli edifici in X-Lam, per cui è stato messo a punto un particolare setup di prova in grado di imporre spostamenti, ciclici o monotoni, sia in direzione orizzontale che verticale in maniera disaccoppiata. I risultati di quindici test, per ciascun tipo di connessione, sono stati riportati e analizzati mediante la rappresentazione di curve forza-spostamento, valori di resistenza, rigidità, dissipazione d'energia, degrado e duttilità. In aggiunta, diversi metodi di linearizzazione sono stati adottati per il calcolo del punto di snervamento e confronti sono stati fatti con le prescrizioni riportate in normativa.

La seconda parte di questo lavoro è incentrata sullo studio sperimentale e numerico di una parete rocking di due piani in X-Lam in scala 2/3. La fattibilità e la risposta di questa nuova soluzione a basso-danneggiamento è stata per la prima volta studiata applicata su pareti in X-Lam. Lo scopo della ricerca sperimentale è stato quello di cercare di adattare i principi costruttivi delle pareti rocking ibride a pareti resistenti a taglio in X-Lam. Gli aspetti innovativi di questa tecnologia necessitano soluzioni originali per realizzare strutture in legno in grado di sostenere intensi eventi sismici, ma è indispensabile indagare sperimentalmente ogni dettaglio prima di poter riuscire a delineare ben definite linee progettuali. Nel test, alla parete in X-Lam sono state collegate delle barre di post-tensione in grado di fornire capacità ricentanti al sistema e dissipatori esterni capaci di immagazzinare energia. Anche la connessione tra pannello e dissipatore è stata ideata e testata per la prima volta. Il carico ciclico laterale è stato applicato su due livelli, in modo da riprodurre la distribuzione di forze su due piani. I risultati sono presentati in termini di resistenza laterale raggiunta, momento resistente, variazione della profondità dell'asse neutro in funzione del movimento oscillatorio alla base e dissipazione d'energia del sistema. Da ultimo, la schematizzazione numerica del test è stata affiancata e validata dai risultati sperimentali, l'intento è stato quello di indagare il comportamento della parete per livelli superiori di drift, andando oltre i limiti imposti dal test reale.

Lo studio condotto ha come obiettivo quello di poter contribuire alla ricerca in corso per sistemi di connessione a basso danneggiamento applicabili a strutture multipiano in legno soggette a elevati input sismici. Vantaggi e svantaggi riguardanti il comportamento verificatosi nel test sono stati evidenziati. Suggerimenti e accorgimenti adottati nei dettagli sono stati ampiamente descritti, per fare in modo che ogni piccolo contributo possa servire alla ricerca futura.

Parole chiave: *strutture in X-Lam, hold-down, angle bracket, test con sforzi combinati, risposta sismica connessioni X-Lam, sistemi a basso danneggiamento, pareti rocking in X-Lam, dissipatori d'energia, post-tensione, soluzioni ibride, modellazione numerica rocking*

Chapter 1. Introduction

Timber structures are currently experiencing a significant upturn. Reasons for this are their distinct advantages concerning environmental and recycling aspects compared to steel and concrete structures. There are many general advantages in using timber for building purposes, but the key to success of wooden structures is their excellent performance in seismic events.

Timber constructions subjected to earthquake actions provide relevant benefits if compared to traditional materials. Related to its strength, timber has a low mass therefore during earthquakes the mass excited to oscillation (“seismic mass”) is lower than more traditional materials, and therefore resulting forces are smaller.

Despite the great performances of traditional timber buildings, these structural systems are no longer sufficient to meet modern building standards in terms of cost, constructability and structural performances. Consequently, new structural systems have been created using engineered wood products such as Cross-Laminated Timber (CLT or X-Lam), Glue Laminated Timber (GLT) and Laminated Veneer Lumber (LVL).

In particular, the use of CLT panels in buildings has increased over the last few years in Europe, Canada and North America. Cross Laminated Timber (CLT) is a relatively new building system included within a new-defined class of timber products known as massive or “mass” timber. The wood panels consist of several layers of lumber boards stacked crosswise (typically 90°) and glued together. Its particular configuration makes the panel providing relatively high in-plane and out-of-plane strength and stiffness properties, giving it two-way-action capabilities. In addition, the “reinforcement” effect, provided by the cross-lamination, considerably increases the splitting resistance of CLT for certain types of connection solutions.

In timber structures, more than other typologies, is important to pay attention on details to resist lateral loadings, such as wind or earthquakes, and to limit displacements. Lateral loads are transferred to the foundation by structures providing lateral bracing, the best way to guarantee a satisfying behaviour is using shear wall, as CLT panels.

CLT structures are generally platform-type, which means that each floor is constructed and connected on top of each other. Looking at the single storey, the floor diaphragm is supported at the end by shear walls that transfer the load to slab underneath or the foundation level. Therefore, to ensure a properly distributed load path from the top storey directly to the foundation level, the structural parts should be correctly attached to each other. Connections in CLT structures, as in all timber building systems, play an important role in maintaining the integrity of the structure and in providing strength, stiffness, stability and ductility. Consequently, CLT joints require a special attention in designing. However, despite the now widespread use of CLT, due to relatively short time since it has been launched to the market (20 years), the knowledge about cross-lam as a structural material is still limited.

Many studies were carried out recently on this topic in Europe, North America and Japan, in order to define monotonic and cyclic behaviour of mostly used connections, wall assemblies and finally entire prototype buildings. The most comprehensive experimental research on seismic behaviour of CLT systems and connections was carried out by CNR–IVALSA (Italy) under the SOFIE Project (Ceccotti et al. 2013; Sandhaas et al. 2009). Additional studies on the behaviour of special CLT hold-downs and angle brackets connections, characterized by high values of load bearing capacity, were conducted at University of Trento – Italy (Tomasi & Smith 2015). FPInnovations in Canada conducted tests to determine the structural properties and seismic resistance of simple CLT shear walls and 3-D structures (Popovski et al. 2014). Failure mechanisms in large shear-wall systems were studied in several researches conducted in Japan (Yasumura 2012).

In almost all the previous studies conducted in this context, only the overall behaviour of entire CLT wall assemblies or multi-storey buildings was investigated (Pozza et al. 2016). An experimental campaign on single connection elements was conducted by Gavric et al. (Gavric et al. 2014) in order to fully define the behaviour of typical hold-downs and angle brackets under cyclic loadings, but prescribing one individual action only (traction, or alternatively, shear). Nevertheless, during earthquakes, connections are subjected simultaneously to both shear and tension. The interaction between shear and tension forces may affect connector's capacity in terms of strength, stiffness, ductility and dissipation capacity. Moreover, connections subjected to combined tension and shear forces can be subject to brittle failures.

In spite of the simultaneous shear-tension actions on connections in real systems, in the design practice it is actually commonly assumed that angle brackets carry shear forces,

while hold-downs carry tractions, without any rules or guidelines to avoid the tensile – shear coupling. Current design codes as well prescribe this design approach, disregarding the effects of the tension-shear interaction in the connection elements. Experimental tests are fundamental for development of design methods and for verification of design model accuracy. One goal of this research has been investigating the coupled action effect on traditional connection systems, in order to have a better understanding of the actual behaviour of hold-down and angle bracket connections. A research program was defined in order to study the connection response under both shear and tension actions applied simultaneously, evaluating the influence of a secondary direction deformation on the main resisting axis action.

Traditional CLT structural systems surely proved to be a great solution to face seismic events, but another valid perspective as design philosophy is the Performance Based Seismic Design (PBSD). Under the performance based framework it is expected that the structural response to a seismic intensity can be predicted and intelligent, informed decisions can be made for the life cycle consideration of a structure rather than just the initial construction costs (Gupta & Krawinkler 1999).

Among different low-damage technologies, hybrid rocking solutions proved to be a promising and efficient answer, capable of concentrating damages in replaceable sacrificial elements limiting residual displacements. In fact, post-tensioned timber has the potential to address all the above requirements. The concept of post-tensioning solid timber sections for multi-storey buildings (PRESSSTimber) was first developed in 2004 at the University of Canterbury in New Zealand (Palermo et al. 2005). This construction technique was conceived as a direct adaptation of existing precast concrete solutions that were developed by the PRESSS (Precast Seismic Structural Systems) Program at the University of San Diego (Priestley 1991; M J Nigel Priestley et al. 1999), since design concepts at the base of this technology are material independent. Currently, LVL was the only form of structural timber that has been considered for hybrid post-tensioned solution but also CLT is a good alternative to examine more in depth.

The second part of this thesis will present an experimental application of a rocking system concept combining CLT walls with an alternative energy dissipater solution and connection. The rocking system includes post-tensioning which provides post-earthquake re-centering capability to the system, meanwhile additional external elements serves as dissipative fuses.

Until recently, there was no information on the behaviour and design solutions of hybrid post-tensioned CLT timber systems. Some early design recommendations (Palermo et al. 2007; Newcombe et al. 2008a) are based on relatively limited and specific experimental testing and analysis. Therefore, further validation and potentially improvements need to be done in order to be able to take advantage of the rocking system performances applied to CLT structures.

1.1. Objective and scope

The main objectives of this study are to investigate the interaction between shear and tension forces on typical hold-down and angle bracket connections used in CLT structures and to consider an alternative design solution for low-damage system hybrid post-tensioned CLT wall. For the CLT rocking wall, the approach was experimentally and numerically reproduced, adopting rocking system design concepts, which exhibit in other occasions the required prerequisites but have so far not or not sufficiently been studied in the presented context.

The scopes are to provide a more realistic prospective on the actual behaviour of traditional connections in CLT buildings, going beyond accepted codes suggestions and standardized tests, and at the same time improve CLT structural systems giving an opening design idea on how the design for timber structures should project. Going from a traditional, and better know, building solution to an easier (less connection elements) but more effective one.

The work can be subdivided in two main stages:

- **Part I:** Experimental test campaign on hold-down and angle bracket conducted at CIRI Buildings & Construction Laboratory, University of Bologna. Cyclic tests were performed using a specifically developed test setup suitable to apply both tension and shear actions on the connections, simultaneously. The results of these tests, in terms of strength, stiffness, energy dissipation, strength degradation and ductility, are presented and critically discussed. A comparison between the experimental values of load-carrying capacity and stiffness and those obtained with calculations using existing design code provisions are also given.

- **Part II:** Experimental test on a 2/3 scaled CLT hybrid rocking wall conducted at Oregon State University (OSU) laboratory. A new seismic connection system has been tested under pseudo-static cyclic lateral loading. The connection system consists of a structural fuse connected to the CLT panel, which can be replaced after an earthquake. In addition, the wall was post-tensioned to provide self-centring capabilities to the structural system. Testing results are presented to provide much needed data on performance of rocking CLT wall systems to the engineering design community for possible future projects. Finally, a numerical model, using SAP2000, has been developed to reproduce and overcome the limit of the test specimen. Comparison between the numerical simulation and the experimental evidences are reported.

1.2. Chapter overview

The present thesis is divided in two main parts, as previously described, with a total amount of nine chapters.

Chapter 2 gives a preliminary overview on the evolution of timber products and construction technologies. Focusing on the various types of connections traditionally used for different timber solution systems. Going through the passage, more and more visible, from timber joints to steel connectors. Presenting also a seismic characterization for the introduced timber building systems.

Chapter 3 provides the research background for the first part. Studies that were carried out on traditional CLT assemblies in Europe, North America and Japan, to define monotonic and cyclic behaviour of mostly used connections, wall assemblies and finally entire prototype buildings are here summarised.

Chapter 4 described the experimental testing of the hold-down connection. Details of the test apparatus and loading protocols are given. Test results are presented, and conclusions are drawn by examining the experimental data, also comparing what obtained with codes design provisions.

Chapter 5, similarly to Chapter 4, described the parallel experimental campaign conducted on angular bracket connections. Also here, details of the test apparatus,

specimen and loading protocols are given within the presentation of final results and observations.

Chapter 6 provides the research background for the second part. This chapter revisits existing hybrid connection practice as proposed by the PRESSS program and its developments applied to different construction materials. Subsequently, the evolution of post-tensioned timber is described from its conception to current state-of-the-art research. A summary of existing post-tensioned design solutions are provided.

Chapter 7 the design of the 2/3 scale hybrid post-tensioned CLT wall is described. The building geometry, connection details and material specifications are provided. Details of the test apparatus and loading protocols are given. The test results are presented, and conclusions are drawn by examining the experimental data.

Chapter 8 a simplified numerical models, using SAP2000, is developed to model the lateral force-displacement response of the CLT rocking wall. The numerical model is compared and validate with experimental results. Comparisons in term of lateral force, overturning moment, dissipated energy and re-centring capability are presented.

Chapter 9 present the overall conclusions and possible future work.

Fig. 1.1 shows the flow-chart of the thesis organization.

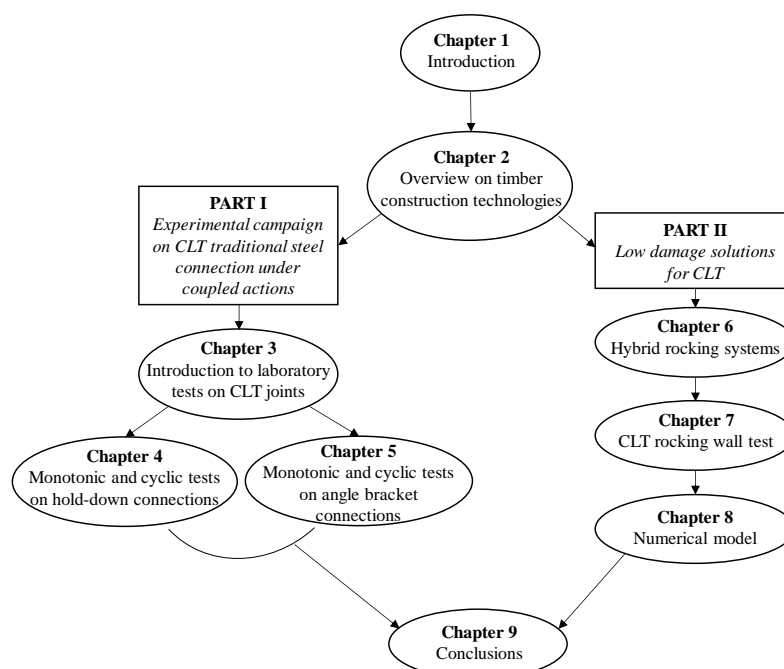


Fig. 1.1 Flow-chart of thesis organization

Chapter 2. Overview on timber construction technologies

Summary of Chapter 2

This Chapter presents a synthetic look through centuries on wood construction technologies focusing on the type of connections, from the old Japanese pagoda to the modern Cross Laminated Timber (CLT) building system. There are many general advantages in using timber for building purposes. It is an environmentally friendly, renewable, easily recyclable material and the energy consumption during production is very low compared to other building materials. However, key to the success of the wooden structures is nowadays their excellent performance in earthquake. Wood has been a most useful construction material for thousands of years and the development of engineered wood-based elements, mostly within the 20th century, has had a significant effect on wood use and opened new opportunities for creative and versatile products from a changing wood prospective in constructions.

2.1. Historical timber structures

Japanese temples

Wood is the primary material of Japanese architecture, the product of the rich forest environment of this country. Japanese wooden buildings range from the smallest architectural spaces to one of the largest wooden existing buildings in the world (the ^{2.1.1.} Todaj-ji Daibutsu-den), a great Buddhist temple 57 meters in width and 47 meters in height, with a floor area of 2880 square meters.

Among Japanese wooden architectural monuments, the oldest existing example is the western temple precinct of Horyu-ji, built at the end of the 7th century. The buildings in this precinct are also the oldest remaining wooden buildings in the world (Fig. 2.1).



Fig. 2.1 (a) *Todaj-ji Daibutsu-den* Buddhist temple (b) *Horyu-ji* temple and its structure

The fundamental characteristic of Japanese architecture is the wooden post-and-beam structure. This type of structure uses a system of joinery in which the structural members meet at right angles and are joined by means of mortise-and-tenon connections using wooden wedges and pegs to secure the joints. Where long members are required, spliced connections with wedges and pegs are used to join shorter lengths of wood together. Metal fasteners such as nails and cramps are sometimes used, but only for relatively small members which have no primary structural role. The basic system of the frame structure composed of posts and beams is known as a “*rigid-frame structure*”, constructed to resist the bending moment at each joint, but in effect the overall system acts as a flexible structure which allows a certain degree of flexure and sway in response to lateral external forces. This is a very practical type of system in an earthquake-prone country such as Japan.

Connections have to be strong enough to transfer forces such as bending, torsion, and shear, also appearance is an important factor. Japanese typical joints include various shapes that connect into each other with ease. Tendon and mortise splice (Fig. 2.2) are effective against torsion but cannot resist any tensile forces, therefore they are often combined with splicing plates bolted throughout.

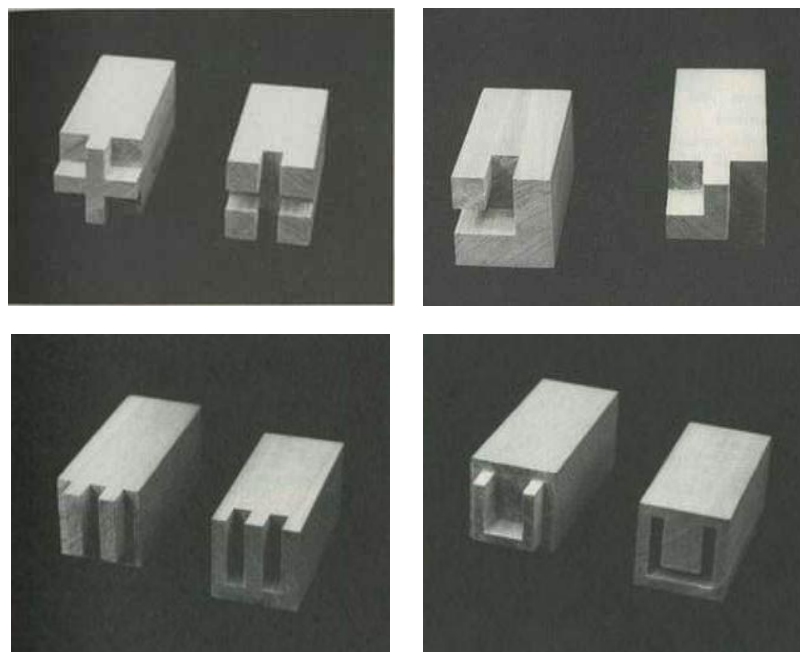


Fig. 2.2 Japanese tenon and mortise splices joints (*mechiire*)

Traditional European half-timber frame constructions

The origin of timber frame structures probably goes back to the Roman Empire, but timber was used in masonry walls even in previous cultures. In historical periods, half-timbered constructions spread not only throughout Europe, such as Portugal (edifícios pombalinos), Italy (casa baraccata), Germany (fachwerk), Greece, France (colombage or pan de bois), Scandinavia, United Kingdom, Spain (entramados) etc., but also in India (dhajji-dewari) and Turkey (himis) (Fig. 2.3) (Langenbach 2010; Tampone 1996).



Fig. 2.3 Traditional half-timber frame constructions in (a) Portugal: *gaiola* walls, (b) France: *colombage*, (c) Turkey: *himis*, (d) India: *dhajji-dewari*, (e) Italia: *casa baraccata*, (f) Germany: *fachwerk*

In each country, different typologies were used, but the common idea is that the timber frame can resist to tension, contrary to masonry, which resists to compression, thus providing a better resistance to horizontal loads.

Timber elements act as a sort of confinement to the masonry structure, improving the mechanical properties to shear loads. In various country this system was adopted specifically as a seismic-resistant construction, sometimes with specific regulations or codes (i.e. Portugal, Italy and Greece Lefkas Island).

Timber frame constructions have also widely been used in South America. In Perù, for example, the *quincha* (Fig. 2.4) presents a one story timber frame made of round and square wood (bamboo is often used) and filled with cones covered with earth and gypsum (Gülkan & Langenbach 2004).

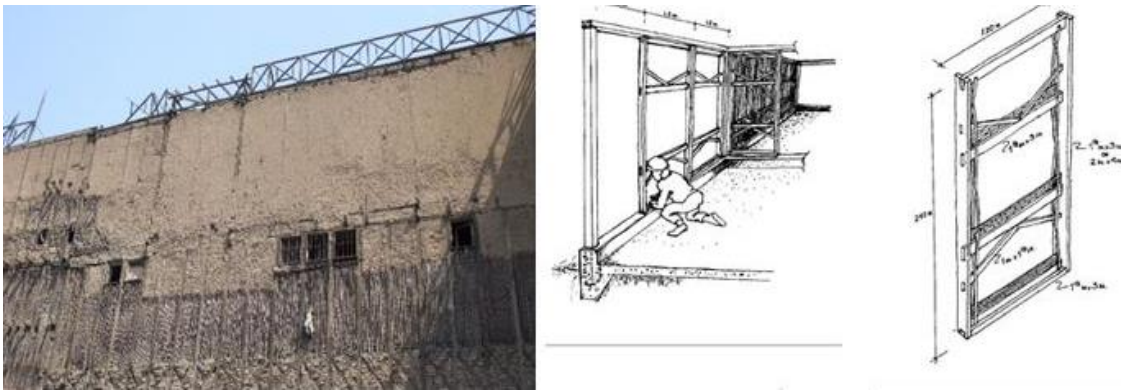


Fig. 2.4 Example and schematic representation of *quincha* (Perù) construction system

Though the general arrangement and geometry of timber frame walls is similar in most countries, variability exists in terms of timber species, cross-section of the timber elements, type of connections, type of infill, spacing between posts and presence of bracing elements. Usually, mechanical connections such as half-lap joints or mortise and tenon were adopted, while the diagonals were connected with simple noched connections or simply nailed.

Timber frame construction can be seen in urban and vernacular buildings in several countries around the world, either motivated by the availability of materials and construction tradition or by the need of reducing the seismic vulnerability of existing buildings, namely in Italy, Portugal and Greece.

2.2. Modern timber structures

Modern wood buildings combine structural types used in the past with wood products of the “future”.

Currently new engineered wood materials, mainly glue laminated elements (Glue Laminated Timber - GLT) and innovative timber panels, allow wood to be employed for long-span structures and multi-storey buildings. The possibility to overstep dimensional limitations and natural defects, in addition to realize different shapes has led to a rebirth of wood as a valid alternative in construction materials.

In fact, a decline in the building market was observed over the second half of the 20th century due to the technological advantages of materials such as steel and concrete, and the desire of both architects and engineers to grow in height.

A century later, technical advances in fabrication techniques and connection engineering, coupled with a renewed interest in timber as an environmentally friendly building material, have driven renewed interest in the building material. Wood products are being re-examined for new opportunities, in a wider range of building types and reaching greater heights than ever before. Modern timber structures compound the beauty of architectural design with smart engineered system solutions, some examples are shown in the pictures below (Fig. 2.5).

Another important aspect that differentiates modern structures from the historical ones is the use of steel connections more than carpentry, this because are relatively easy to realize and it is possible in part to take advantage of steel ductility capacity, really important in seismic condition.

Hereinafter a brief description of the principal structural systems that can be divided in two major categories as follows:

- Light and Heavy Timber Framing
- Mass Timber Construction System

The main characteristics and connection solutions of each sub-included constructive typology are presented and discussed.

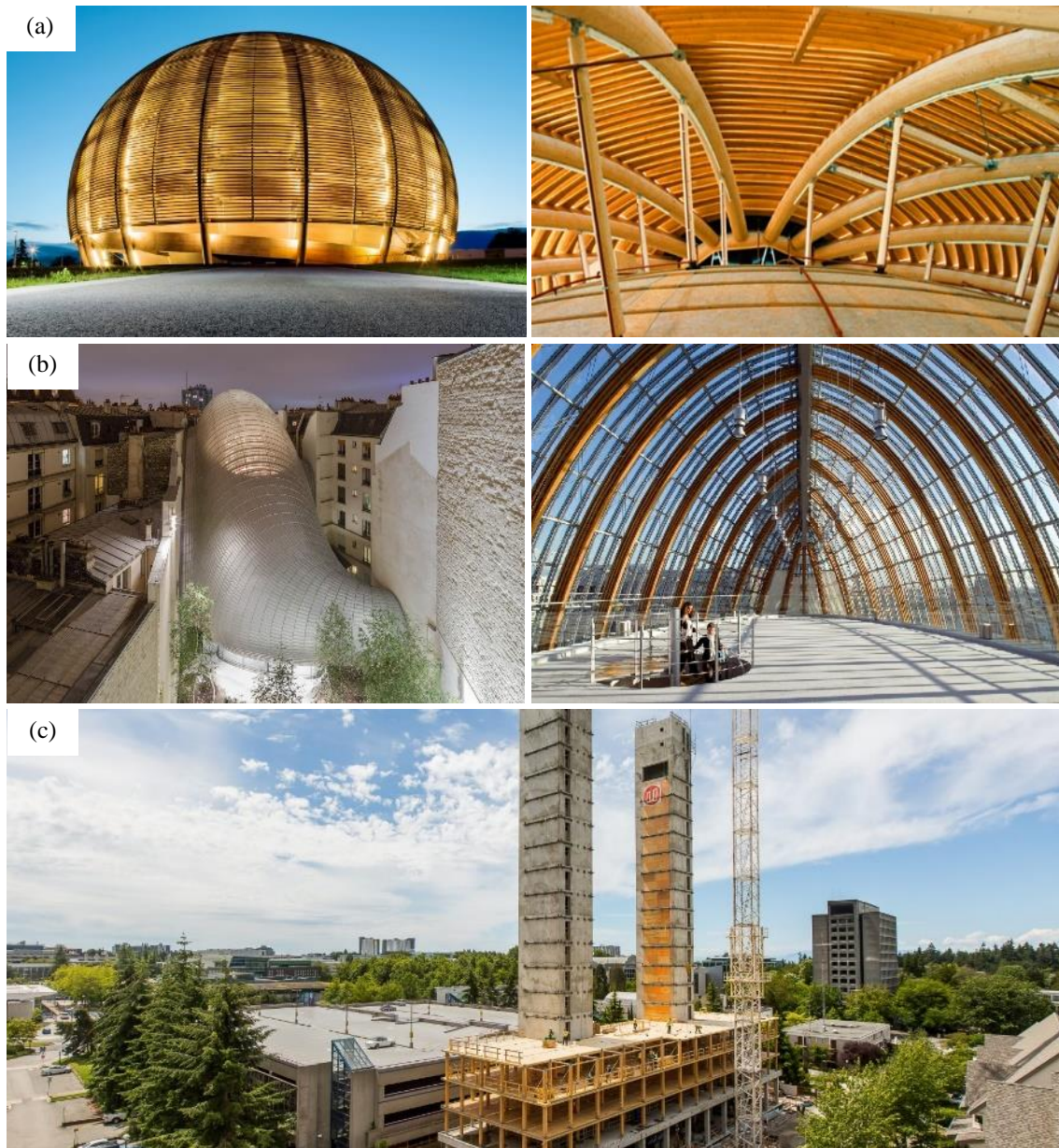


Fig. 2.5 Modern timber structures : (a) *The Globe of Science and Innovation*, CERN Museum, (b) *Fondation Jérôme Seydoux-Phaté* by Renzo Piano, (c) *Brock Commons*, the tallest mass timber building under construction in Canada.

2.2.1.

Light and Heavy Timber Framing

Light wood framed construction is one of the most popular types of building method, mostly used in residential houses, both in the United States and part of Europe.

This type of construction is light, and allows quick construction with no heavy tools or equipment. Every component can be easily carried by hands and the house basically becomes a large carpentry job.

Around the 1930s, a construction method called *Platform Framing* was invented and still use today. This new system enabled to cut labor and material costs respect to the previous *Baloon Frame* system (Fig. 2.6).

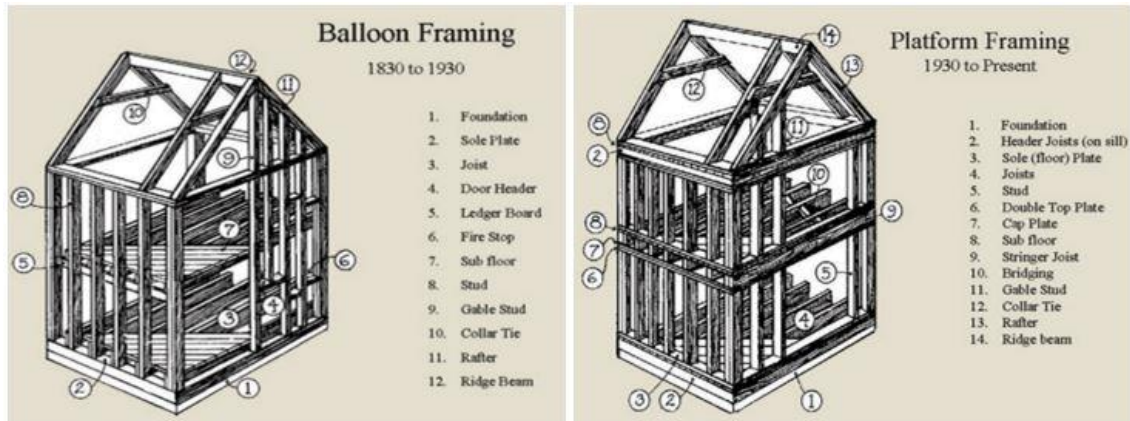


Fig. 2.6 Balloon Frame vs. Platform Frame system

Balloon framing was one of the earlier wood construction methods, in which light frames of wood are constructed around studs which run continuously from top to bottom of a building. The roof is a truss structure that consists of horizontal ceiling joists and sloping rafters. Platform framing comes after the previous described system, it is a more modern approach in construction. It utilizes plates to enable the upward extension of a building. Floor joists for each story are supported by the top plate of the floor underneath. The main difference between the two types occurs at the floor lines.

As a result of industrialization and economical efficiency today's light wood framed structures are assembled into panels in manufacturing facilities either manually or in an automatic system and, then, transported over long distances to the site where are assembled in a short period of time.

Another building system in use is the so-called *Heavy Timber Framing* (or post-and-beam construction), originally designed and used primarily for industrial and storage purposes, today has been expanded to include many other occupancies (i.e. schools, churches, auditoriums ecc.). Many of the modern heavy timber buildings are large in area and one story in height. This type differs from light-wood framing (Fig. 2.7) because of the bigger dimensions of the timber elements, and therefore for its better fire resistance.



Fig. 2.7 Examples of *Platform Frame* structural system (left) and *Heavy Timber* construction (right)

Timber framing's advantages include durability, sustainability, strength and aesthetic appeal. Material choices vary, from glulam, Parallel Strand Lumber (PSLs), Laminated Veneer Lumber (LVLs), and other engineered wood products to traditional sawn lumber of available wood species.

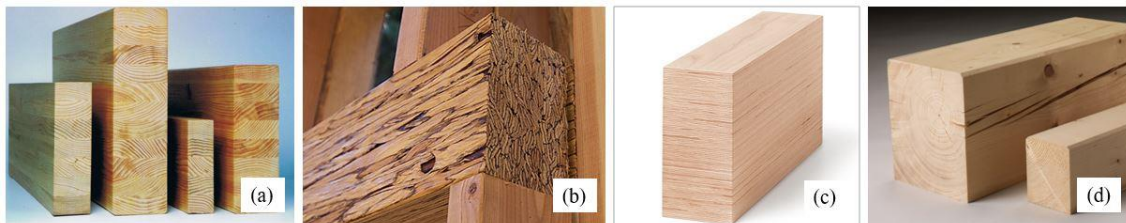


Fig. 2.8 (a) Glue Laminated Timber, (b) PSL, (c) LVL and (d) sawn lumber wood element

In most wood structures, connections are one of the most important, but least understood components. The performance and efficiency of any structure, including timber structures, depend on the connections that join their components. Connections provide continuity to the members and strength and stability to the system. Joint solutions may consist entirely of wood members (Fig. 2.9) but frequently involve the connection of wood to steel (Fig. 2.10). Traditional joinery techniques (usually carpentry joints) have mostly been superseded by heavy metal connectors, split rings, timber rivets, knife plates, and concealed connection kits.

Mechanical connections are usually constructed using two general fastener types: dowel and bearing-fasteners. Dowel types, such as nails, screws and bolts, transmit either lateral or withdrawal loads. Lateral loads are transmitted by bearing stresses developed between the fastener and the members of the connection. Withdrawal loads are axial loads parallel to the fastener axis transmitted through friction or bearing to the connected materials. Metal connector plates are a special case of dowel-type fasteners; they combine the lateral load actions of dowels and the strength properties of the metal plates. Bearing-type

connections, such as shear plates and split ring connectors, transmit only lateral loads through bearing on the connected materials.

The selection of a fastener for a specific design application depends of the type of connections and the required strength capacity. Each connection must be designed to transmit forces adequately and provide satisfactory performance for the life of the structure without causing splitting, cracking or excessive deformation of the wood members. The strength of wood connections is often limited by the resistance of the wood in bearing or withdrawal rather than the capacity of the fastener. As a result, connection design is affected by many of the same factors that influence the strength properties of wood. In addition to the type, number, and size of fasteners, connections strength also depends on factors as the wood species, direction and duration of load, and condition of use.

Seismic design leads to an improvement in ductility and redundancy, as well as ensuring the interconnection of the structure. Therefore, in the particular case of timber structures, seismic design requires a much closer attention to detailing of connections, since they play a major role in ductile capacity of the whole structure.

Timber framed constructions, utilizing standardized elements, have become the dominant building technique in the United States of America, Canada and Australia, due to economical factors. Furthermore, for the same factors, in addition to the ecological concerns and the excellent performance under earthquakes, this method is gaining ground in Europe and certain Asian countries.



Fig. 2.9 Examples of wood joints in timber frame constructions



Fig. 2.10 Various solutions of wood-steel connections

2.2.2.

Mass Timber Construction System

Mass timber is a category of framing styles typically characterized by the use of large solid wood panels or logs for wall, floor or roof construction (Fig. 2.11). Mass wood weighs less than other materials and has a consequent number of potential benefits, including smaller foundation requirements and lower forces for seismic resistance.

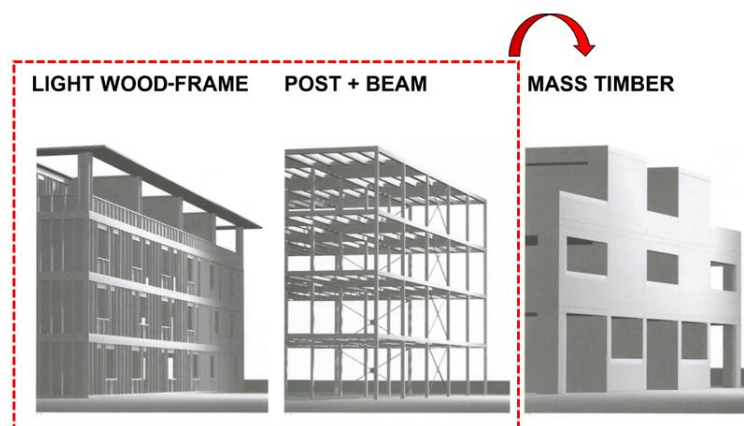


Fig. 2.11 Mass timber constructions are a complement to light wood and post-and-beam systems

Products in the mass timber family include:

- Handcrafted or milled logs;
- Glue-Laminated Timber (glulam);
- Structural Composite Lumber (SCL);
- Cross-Laminated Timber (CLT);
- Nail-Laminated Timber (NLT);
- Dowel-Laminated Timber (DLT)
- Wood-Concrete composites;

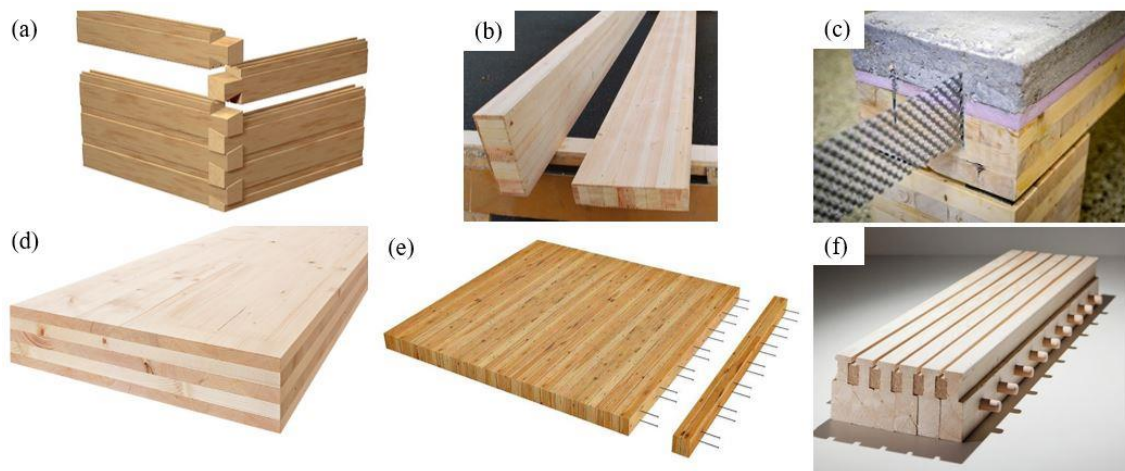


Fig. 2.12 (a) Milled logs (*log house*), (b) plank orientation glulam (*floor or roof*), (c) wood-concrete element (*floor*), (d) CLT panel, (e) NLT panel, (f) DLT panel

The different wood elements are used for various purposes. Blockhouse system use logs, as described more in detail after. Glulam is typically adopted for beams and columns but can also be used in the plank orientation for floor or roof decking. The remaining wood engineered products are particular structural panel solutions that can be employed either for wall (membrane behaviour) and floor (plate behaviour). At a product level, most of the panels described can be made into a wood-concrete composite by applying a concrete topping in such a way that the two materials act as one. An example is CLT-concrete slab hybrid section that provide extreme stiffness and minimal deflection which, along with an insulation layer between the materials, provided good acoustic separation between floors. Other than composite materials, wood-concrete solutions can be defined as a constructive system where timber can be coupled with other construction material such as steel or concrete in a building. Generally reinforced concrete shear walls and cores are used to resist the lateral loads and act as seismic force resisting systems while wooden structure bear the gravity loads.

In particular, this work will focus on Cross Laminated Timber panel construction system, with a specific interest on the behaviour of traditional connections under seismic loading and other innovative system solutions.

Hereinafter a brief introduction on the main structural concepts for the constructive solutions with logs and panels (referring to CLT) will be given.

2.2.2.1. *Blockhouse*

Blockhouse type is a very old method of log building. The construction system used for Blockhouse, or Log House, wooden homes or buildings is typical of Central-Northern Europe and the Alps. This is a massive type construction system comprising overlaying trunks or, in more modern systems, squared-off rounded horizontal elements and with beams that may also be duo beams, generally connected to each other using screws, and thereby forming the support walls (Fig. 2.13). The corner joint between the walls is generally obtained by means of a visible male-female carpentry knot or dovetail joint and potentially reinforced with metal bars or screws.



Fig. 2.13 Houses built with *log house* system

The connection between wooden walls and the reinforced concrete foundations is obtained using resin-coated metal bars. Blockhouse mainly entrusts resistance to static action (vertical loads and wind) and seismic action almost exclusively to the wood (resistance to horizontal action is guaranteed by the tapping of the crossover and friction between overlaying beams or trunks) and the mechanical connection elements are used to a very limited degree. Therefore, in this system steel connections do not play an essential role. This type of construction solution is not suitable for zones with high seismic risk since it has a low dissipative capacity. Its use in some seismic areas is specifically prohibited.

2.2.2.2. *CLT structural system*

Cross-Laminated Timber (CLT) building system is a new potentially cost-competitive and wood-based solution that is a suitable candidate for applications that currently use concrete, masonry and steel. CLT is an innovative wood product that was first developed in Austria and Germany and ever since has been gaining popularity in residential and non-residential applications in Europe, Canada and USA.

Experience shows that CLT construction can be competitive, particularly in mid-rise and high-rise buildings. Easy handling during construction and high level of prefabrication facilitate rapid project completion. Good thermal insulation and good performance under fire are added benefits that come as a result of a massive wood structure.

CLT panel consist of several layers of boards stacked crosswise (typically at 90 degrees) and glued together on their wide faces (Fig. 2.14) and, sometimes, on the narrow faces as well. A cross-section of a CLT element has at least three glued layers of boards placed in orthogonally alternating orientation to the neighbouring layers. In special configurations, consecutive layers may be placed in the same direction, giving a double layer (e.g. double longitudinal layers at the outer faces and additional double layers at the core of the panel) to obtain specific structural capacities. Thickness of individual boards may vary from 10 mm to 50 mm and the width may vary from about 60 mm to 240 mm. Boards are fingerjoined using structural adhesive and are previously visually or machine stress-rated and are kiln dried to a moisture content of $12\% \pm 3\%$.

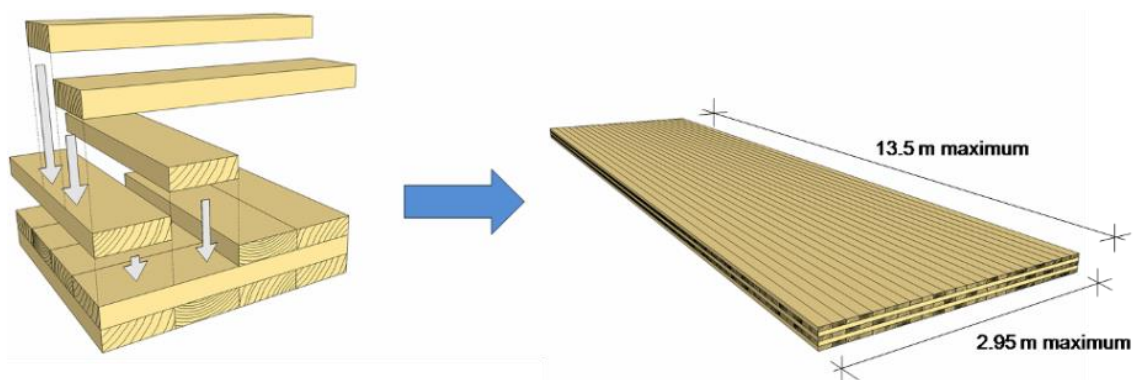


Fig. 2.14 Cross-Laminated Timber (CLT) panel

CLT is made of layers of smaller beams, thus it can reduce waste by using odd-shaped, knotty timber that lumber mills would otherwise reject.

Cross-Laminating provides relatively high in-plane (main axis) and out-of-plane strength and stiffness properties in both directions, giving these panels a two-way action capability similar to a reinforced concrete slab.

CLT buildings are a platform type of structural system and tend to be less susceptible to develop soft story mechanisms than many other structural systems of the same type. Since the nonlinear behaviour (and the potential damage) is localized in the hold-down and bracket connection areas only, the panels, that are also the vertical load carrying elements, are virtually left intact in place, even after failure of the connections.

In addition to the steel connections applied at the base of the panels, the use of half-lapped joints in longer walls can be an effective solution to reduce the wall stiffness and thus the seismic input load, and also to improve ductility. Moreover, it is important to take into account that CLT walls contribute to the lateral resistance, thus providing an added degree of redundancy and a system sharing effect.

In general, connections in timber construction including those built with CLT, play an important role in maintaining the integrity of the timber structure and in providing strength, stiffness, stability and ductility. Consequently, steel connections require a particular attention. Common types of connections in CLT assemblies include: panel-to-panel (in floors, walls and roofs), wall-to-foundation, wall-to-wall intersections and wall-to-floor/roof, some examples are shown in Fig. 2.15.

Literature review on research work conducted around the world, results from a series of quasi-static tests on CLT wall panels conducted at FPInnovations and more in-plane cyclic tests on CLT wall panels with different layouts of connections and opening (Ceccotti et al. 2006), demonstrate that CLT wall panels can be used as an effective lateral load resisting system.

Shear-wall tests to date have also shown that the CLT wall panels demonstrated adequate seismic performance when nails or slender screws are used with steel brackets to connect the walls to the floors, ensuring a ductile failure. Results from small and full scale shake table tests on two CLT buildings in Japan by the Trees and Timber Institute of Italy (CNR-IVALSA) under the SOFIE project in 2009 (Ceccotti 2007) proved that CLT structures perform very well when subjected to seismic forces (Fig. 2.16).

CLT construction system has already been used to build hundreds of structures across Europe, Canada and, more recently, in North America. In many cases, CLT has also been used in combination with other wood based products such as glulam or with other construction materials such as concrete or steel to form hybrid building systems. Despite

the extensive use of wood based products some incongruities and lacks are present in seismic codes in the timber section mainly because of the relatively recent development of new building systems, this is particularly true for CLT technology.

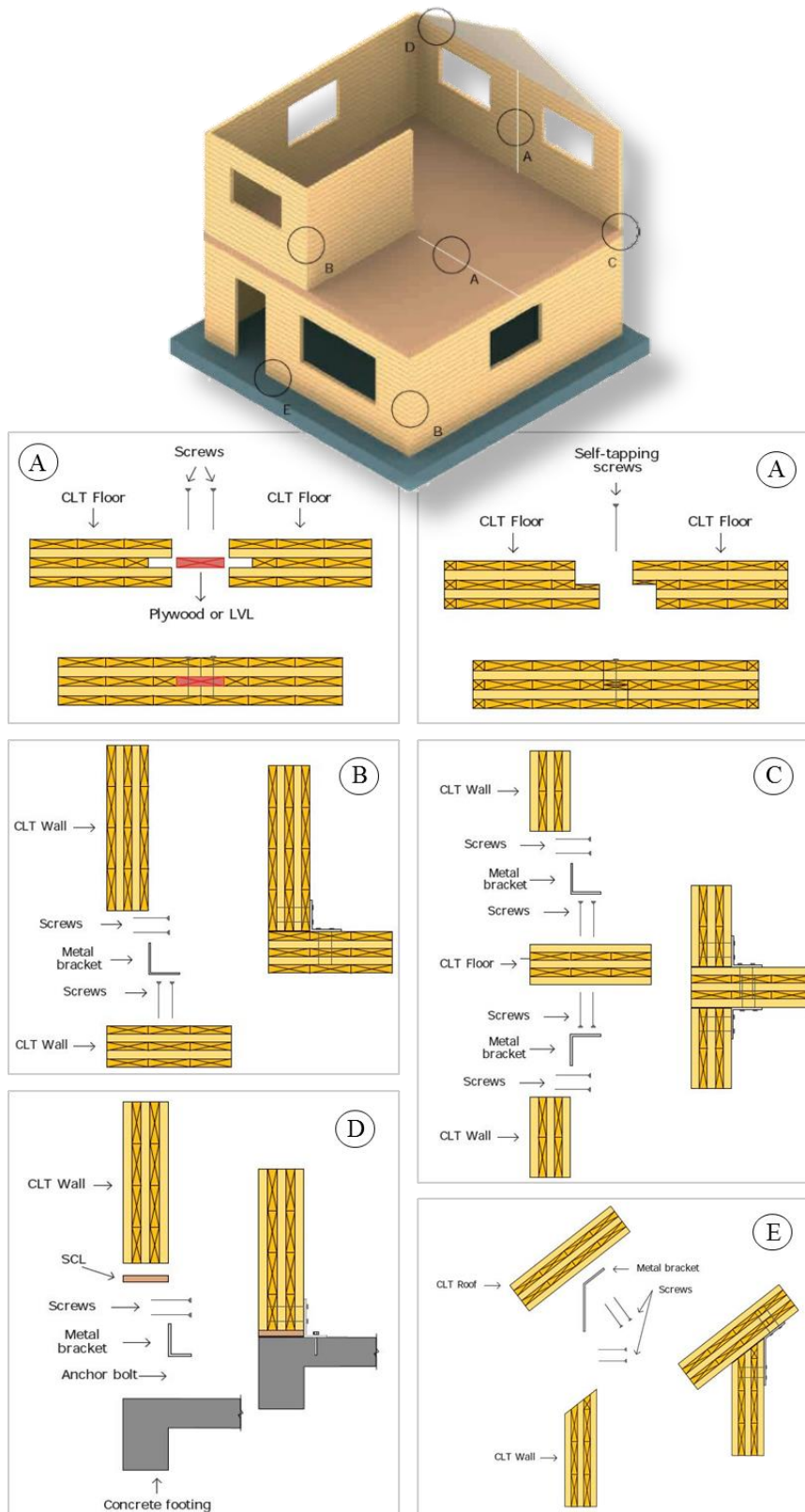


Fig. 2.15 Examples of types of connections typically used to establish panel-to-panel and wall-to-floor connections in CLT construction



Fig. 2.16 In-plane CLT wall tests and CLT building shaking table tests conducted by CNR-IVALSA under SOFIE project.

Fig. 2.17 presents some interesting examples of building built around the world using CLT elements, going from a simple single-family house to the tallest hybrid multi-storey building in Canada.

An unknown variable about CLT could be the safety and longevity of the glues holding CLT panels together. For this reason other panel products, such as NLT and DLT, can be adopted as a valid alternative for future applications.

Nail-Laminated Timber (NLT) was originally invented in 1970s and it is simply made by individual lumber members fastened together, but the presence of metallic fasteners is a problem when cuts in the panel are needed. “Dowelled wood” has been introduced after, and refers to the inclusion of wood dowels which replace the nails and glues of earlier systems. DLT involve inserting hardwood dowels into pre-drilled holes perpendicular to the posts. The two elements are combined and the different moisture content makes the dowels expanding to achieve moisture equilibrium locking this way the posts together.

CLT, NLT and DLT are different wood massive panel solutions that can be either implemented in the structural system described above, but with a main difference that is the beauty of CLT in its orthotropic quality.



Fig. 2.17 Examples of CLT building: (a) Family house (Austria); (b) Kindergarten in Poggio Picenze (Aquila); (c) Hotel Nautilus, 7-storey (Pesaro); (d) Social housing-Via Cenni, 9-storey (Milano); (e) Student Residence Brock Commons, 18-storey (Vancouver)

2.3. Seismic behaviour of timber structures

Timber constructions subjected to earthquake actions provide relevant advantages if compared to traditional materials, especially because of its lighter weight and a favorable strength/density ratio. In seismic design a careful balance of stiffness, strength and ductility is required in order to ensure a good structural performance in terms of serviceability and safety.

In timber structures the energy is dissipated during cyclic loading in the connections via mechanical fasteners. On this basis, structural systems ductility levels are mainly due to the expected capability of joints within them to do plastic work if loaded over the yielding limit (Piazza et al. 2011a). On the other side, wood elements have a limited capacity to deform inelastically (Smith et al. 2007) providing an ineffective plastic contribute.

A simple approach to design structures under seismic loading is the method suggested in seismic codes as EC8 (EN-1998-1), where a simple global linear elastic analysis is required for timber structures. Earthquake analysis by response spectra is based on the assumption that the system behaves linearly but following, Ultimate Limit State criteria, damages are expected and so yielding, therefore it will lead to inelastic response of the structure. For this reason a so-called behaviour factor q is introduced to reduce the forces obtained from a linear-elastic analysis, in order to account for the non-linear resources of a structure.

Despite the q -factor is associated with multiple variable levels of the structure design in fact is just a modification factor and it must be such that the design procedure are satisfied. This definition explains why we refer to a code-dependent q -factor, thus the importance of establishing a proper behaviour factor for different timber structural systems (Ceccotti & Sandhaas 2010). Blockhouse type is classified being low dissipative system and must be design elastically ($q=1.5$). The q -factor associated to light frame systems correspond to a value up to 5. The heavy-frame system is less dissipative compared to the light-frame, and the design of this system can be performed adopting a q -factor equal to 4. Regarding CLT solutions, a q -factor value of 2 results proper for walls with un-jointed panels, while a q -factor of 3 for jointed CLT wall panels (Ceccotti 2008a; Pozza & Scotta 2015), it follows that the number of connections used to assemble CLT structures is substantial. In between of rigid panel (i.e. CLT) and light frame systems, there are wall systems with deformable panels characterised by a q -factor of 4. Last but not least, hybrid wood-concrete systems present a high ductility and dissipative capacity. The wood-concrete

system is comparable to the light-frame, therefore a q-factor of 5 is applicable (Pozza et al. 2016; Pozza et al. 2015).

2.4. Comments

In most wood structures, connections are one of the most important, but least understood, components. Connections provide continuity to the members and strength and stability to the system. Moreover, in timber structures the connections are the only structural parts where energy dissipation will occur as the timber itself behaves elastic, but they also are the weakest link in the structure. Joints may consist entirely of wood members, but nowadays they usually involve connection of wood-to-steel or other members. Each connection must be designed to transmit forces adequately and provide satisfactory performance for the life of the structure without causing splitting, cracking, or excessive deformation of the wood members. In timber structures the failure of wood members in tension or bending is not favourable because of its brittle characteristics, and all failures should occur in the connections. Therefore, it is very important to understand and characterize joint components to ensure an adequate seismic response in timber buildings. Seismic design of CLT structures follows, as the other construction types, the capacity design principles that are of major importance in seismic design in general. By considering certain modes of deformation, we can ensure that the brittle elements have the capacity to remain intact, while inelastic deformations occur in selected ductile elements. Consequently, it is suggested that all non-linear deformations and energy dissipation in the case of CLT structures should occur in the connections (i.e. angle brackets, hold-downs) that connect the wall to the floor panels and in the vertical step joints in the walls. All other connections shall be designed to remain linear elastic, with a strength that is slightly higher than the force induced on each of them. Another important consideration is that all connections used for energy dissipation in CLT structures should be designed to fail in fastener yielding mode, avoiding brittle failures. Since the nonlinear behaviour (and the potential damage) is localized to the hold-down and bracket connection areas only, the panels that are also the vertical load carrying elements are virtually left intact in place, and well connected to the floor panels, even after a major seismic event. In addition, all walls in one storey of a CLT construction contribute to the lateral and gravity resistance, thus providing a degree of redundancy and a system effect.

Part I: Experimental campaign on CLT traditional steel connections under coupled actions

Summary of Part I

Connections in heavy timber construction, including those built with CLT, play an essential role in providing strength, stiffness, stability and ductility to the structure; consequently, they require careful attention by designers. Nowadays, design of CLT wall connections is based on the hypothesis that hold-down connections are subjected only to tension and angle-brackets only to shear. Nevertheless, experimental investigations on CLT walls under seismic action highlighted that hold-downs may be subjected also to significant lateral displacement, and consequently to a coupled action. Similarly, angle brackets are subjected simultaneously to shear and axial stresses. Aim of this work is to experimentally investigate the axial-shear interaction in typical CLT steel connections. To this purpose, an extensive experimental campaign has been conducted with a specific setup allowing to impose prescribed levels of displacement in the secondary axis and varying along the main direction the displacement in monotonic or cyclic way. Test results, for the different configurations taken into consideration, are presented and critically discussed in terms of load-displacement curves, strength, stiffness, energy dissipation, strength degradation and ductility. In addition, different approaches for the definition of the connection's yielding limit are used, according to a multi-linear approximation of the experimental load-displacement curve. Forces and stiffness provided by these methods are compared with those predicted by code provisions.

Chapter 3. Introduction to laboratory tests on CLT joints

3.1. Presentation of CLT buildings behaviour

The use of CLT panels in buildings has increased over the last few years in Europe, Canada, USA, Australia and New Zealand. Numerous impressive buildings and other types of structures built around the world using CLT have become a good testimony of the many advantages that this product can offer to the construction sector. The easy handling in construction and the high level of prefabrication involved that facilitate a quick erection time are just some of the key advantages. Nonetheless, no specific addressed design codes for CLT constructions have been published yet, therefore extensive researches on the field have been performed by research groups in Europe and overseas. Experimental test results are fundamental to develop design methods and for verification of design model accuracy.

Seismic design of CLT structures follows the capacity design principles that are of major importance in seismic design in general. This design approach is based on the simple understanding of the way a structure sustains large deformations under severe earthquakes. By choosing certain modes of deformation, we can ensure that the brittle elements have the capacity to remain intact, while inelastic deformations occur in selected ductile elements. These “dissipative zones” act as dampers to control the force level in the structure. In timber structures, however, the failure of wood members in tension or bending is not favourable because of wood material brittle characteristics, and all failures should occur in the connections.

CLT constructions are usually a platform type structural system, where structural continuity among vertical elements must be realised by means of connectors able to transmit vertical and horizontal forces (Fig. 3.1).

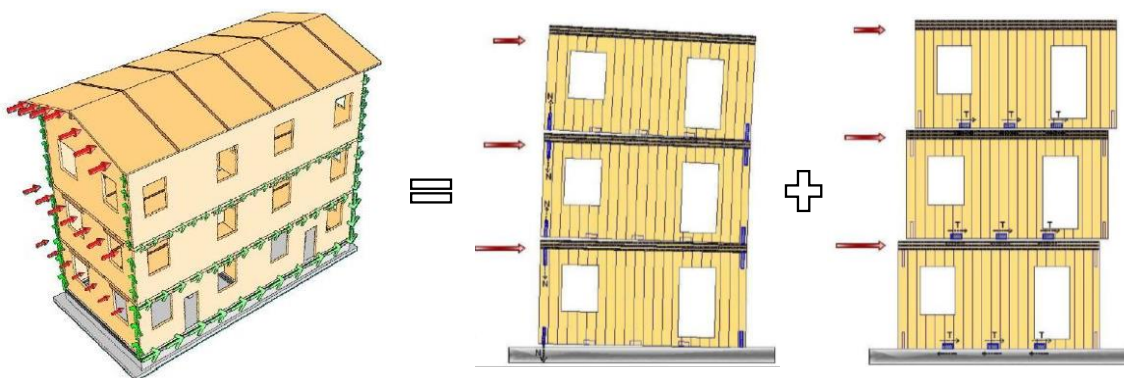


Fig. 3.1 Lateral load path in a platform system and detail of CLT wall consequent deformation

The most basic approach to calculate the force distribution in the connections of a CLT wall is to assume that the panel remains rigid and all deformations come from rotation and translation of the panel. The vertical forces due to rocking of the panel are generally assumed to be resisted only by the hold-downs, which are normally placed at the corners. The base shear forces due to horizontal slip of the panel are usually expected to be taken by the angle brackets, and the vertical shear forces between adjacent wall panels are taken by the in-plane screwed joints. In this basic design approach, the axial stiffness and strength of angle brackets are neglected, as well as the shear stiffness and strength of hold-downs.

Hold-down elements prevent the uplift and rotation of the wall. They are designed with a particular geometry usually L-shape metal plates endowed with ribs in order to transfer the vertical force (aligned with the vertical flange symmetry axis) to the anchor bolt placed centrally to the base flange. Angular brackets are regular steel bracket, of various sizes, that have different holes to attach them through ringed nails to wood and anchored to foundation with bolts. Fig. 3.2 shows the traditional connectors at the base of a CLT wall.

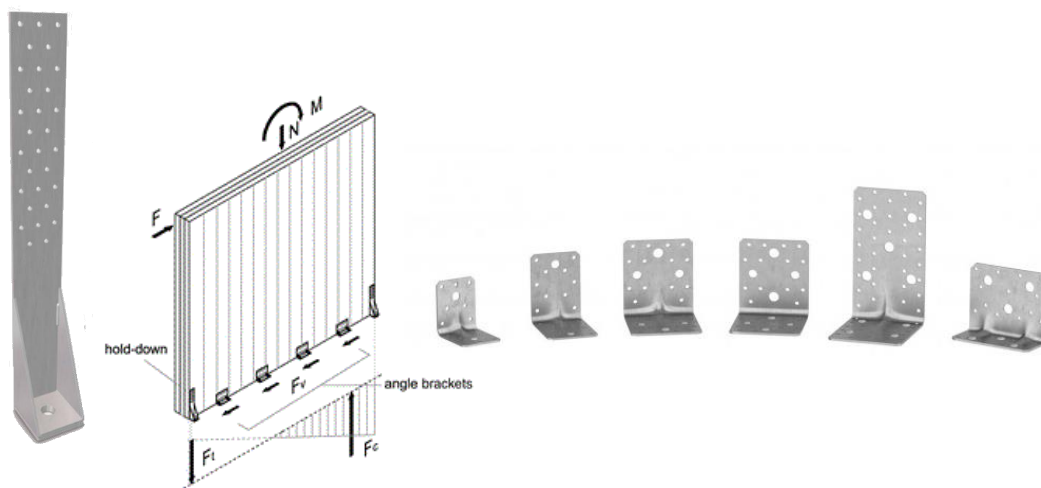


Fig. 3.2 Schematic representation of a CLT wall and typical joints (i.e. hold-down and angle bracket)

Although the simplified design assumptions currently in use, during earthquakes, connections are subjected simultaneously to both shear and tension. The interaction between shear and tension forces may affect connector's capacity in terms of strength, stiffness, ductility and dissipation capacity. Therefore, according to the capacity design rules for a safe sizing of the connection system, the hold-down and angle bracket load-carrying capacity must be defined also under bi-directional actions.

In addition, for a more reliable definition of the building response, a full characterization of the connection mechanical behaviour is necessary, especially in seismic conditions.

In the present chapter, results of an experimental campaign conducted at CIRI Edilizia & Costruzioni laboratories of the University of Bologna on steel traditional connectors for CLT are presented. Connections response under shear and tension actions applied simultaneously was studied, also the variation of principal direction axis strength, while deformed in the other one was investigated. Moreover, from test results all the significant mechanical properties of the connection (e.g. stiffness, yielding and failure condition, ductility etc.) subjected to combined axial-shear actions were defined adopting different methods. Results show that the engineering design practice is not coherent with the experimental evidences and may represent an unsafe calculation procedure when connectors are subjected to coupled tension-shear actions. Current design codes as well disregard the possible tension-shear interaction in the sizing of the connection elements.

3.2. Experimental tests literature review on CLT structural system subassemblies

Background literature on buildings constructed with CLT shear walls reveals crucial structural design issues to be those pertinent to reliable definition of the strength and stiffness of shear wall-to-foundation connections and inter-story connections.

Studies were carried out recently in Europe, North America and Japan, in order to define the behaviour of mostly used connections, wall assemblies and entire prototype buildings under monotonic or cyclic actions.

Within the SOFIE project, a research program conducted by the CNR-Ivalsa, an extensive experimental campaign on CLT buildings was carried in collaboration with various Japanese Institutes. Experimental tests on full scale buildings (one, three and seven story CLT building) provided very positive outcomes, as the structures were able to survive strong recorded earthquake (i.e. Kobe earthquake) almost undamaged, while showing a significant energy dissipation (Ceccotti 2008b). In 2005, as a first step of SOFIE project (Ceccotti 2007), experimental tests to quantify seismic behavior of CLT wall panels were performed.

The test program included different connections layouts of single wall panels, including wall with openings, subjected to different levels of vertical loads. Wall-to-foundation and

wall- to-floor connections were tested with different metal connectors used in SOFIE full-scale prototype structures.

In parallel, another campaign on CLT shear wall was conducted at the University of Ljubljana by Dujic (Dujic 2004). Here, wall panels were subjected to different levels of vertical load and monotonic or cyclic horizontal load applied. Boundary conditions were also another parameter for the tests to develop deformation in the wall, either behaving as a cantilever or in pure shear.

In 2010, similar tests on CLT wall assembly were conducted at FPInnovations research institute, Canada (Popovski et al. 2010), one of the typical CLT wall configuration is reported in Fig. 3.3.

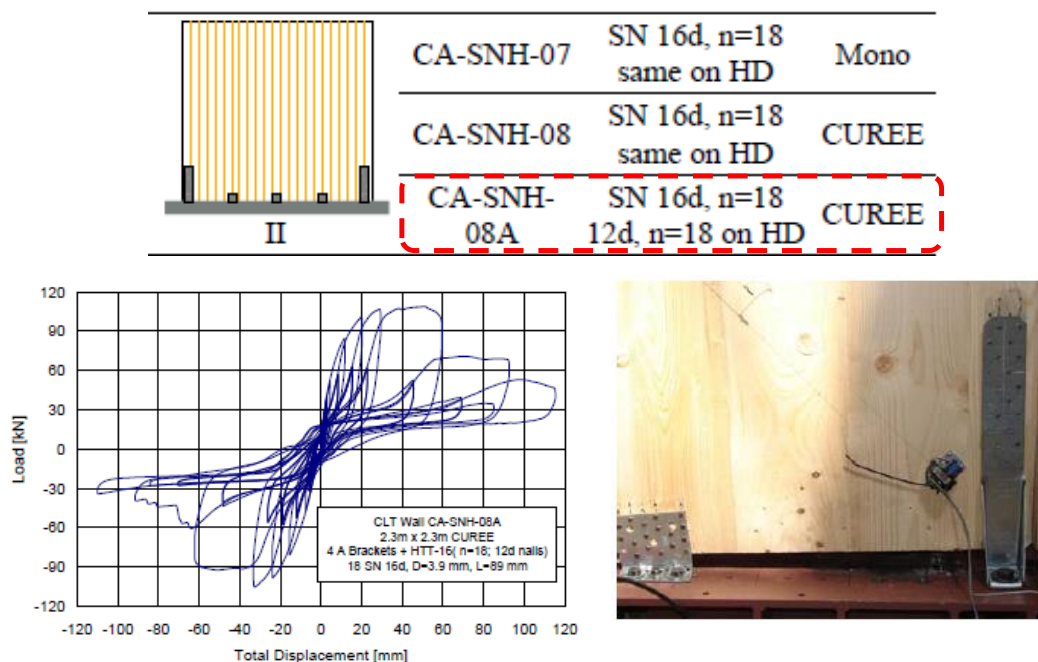


Fig. 3.3 Case of CLT wall test with hold-downs and angle brackets, hysteresis loop response and uplift corner detail (Popovski et al. 2010)

Different configurations, types of connectors and fastener were used, as well as different aspect ratio.

Additionally, wall tests on a single story CLT wall (Fig. 3.4) were conducted between 2010 and 2011 at CNR-Ivalsa by Gavric et al. (Gavric et al. 2012). In conjunction with CLT shear wall tests, Gavric et al. also investigate the cyclic behaviour of the metal connections individually. Shear and pull-out monotonic and cyclic tests were carried out on twenty different configurations of CLT connections used in the SOFIE buildings (Gavric et al. 2012; Gavric et al. 2014).



Fig. 3.4 Experimental setup on full scale CLT walls: single wall and coupled wall (Gavric et al. 2012)

As reference point for the experimental programme on typical CLT connections was the three-storey SOFIE building, which was tested on shaking table in Tsukuba, Japan.

Two different types of hold-down and angle bracket connections were tested under monotonic and cyclic loading: CLT panel-steel base foundation and panel– panel connections, representative of wall panels to foundations and wall-to-floor panels connections, respectively. Both hold-down and angle bracket tests were performed in two directions: shear and tension, separately (Fig. 3.5). The hold-down was a relatively new type that matched well the geometry and thickness of the older type HTT22 of hold-down, originally used at the ground storey of the building, while the angle bracket was exactly the same type.

Cyclic tests of hold-downs in axial (tension) direction revealed mainly deformation of nails due to vertical displacement, while the steel part of hold-down was virtually undamaged. In the shear direction, mainly deformation of the steel parts of hold-down was observed, leading to failure of the steel due to local buckling or to a combination of bending of steel and withdrawal of nails. Therefore, as the tests highlighted, having a shear component (lateral deformation) applied on the hold-down may significantly affect the resulting capacity of the connection.

Regarding angle brackets even if the principal load-carrying direction is shear, tests showed also a relatively good behaviour in tension. This is due to the geometry of the angle bracket, in fact this type of steel bracket was thought to be used in both direction (i.e. traditional CLT Canadian building system), hence it is more stable and compact with a proper distribution of fasteners.

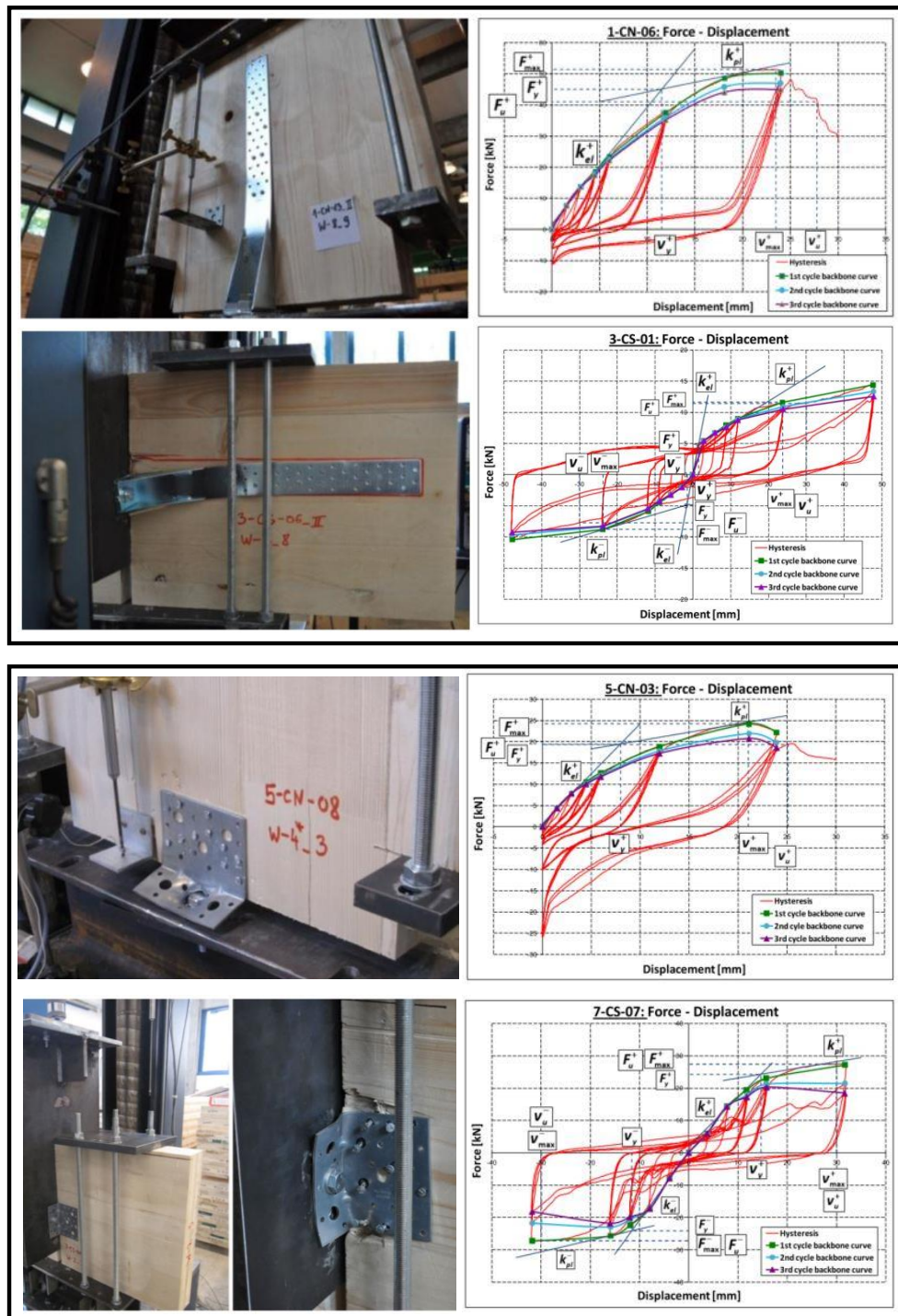


Fig. 3.5 Unidirectional cyclic tests on typical CLT connections conducted by Gavric et al. (Gavric et al. 2014)

In terms of strength and stiffness, the behaviour of the angle brackets is fairly similar in tension and shear, despite the failure mechanisms being rather different. This fact leads to the conclusion that angle brackets contribute quite significantly to the overall wall resistance not just with their shear resistance but also with their tension resistance.

Chapter 4. Monotonic and cyclic tests on hold-down connections

Summary of Chapter 4

The present Chapter is aimed at investigating the interaction between shear and tension forces on typical hold-down connections used in CLT structures. Test setup, specimen geometry, mechanical properties and loading protocol procedures will be illustrated. The outcomes of the experimental campaign conducted on hold-down connections at CIRI-Edilizia & Costruzioni laboratories of the University of Bologna will be hereafter presented. The campaign includes both monotonic and cyclic loading tests on the hold-down connection. The response of the joint system, subjected to shear and tension actions simultaneously applied, has been studied. Moreover, the principal mechanical properties of the connection (e.g. stiffness, yielding and failure condition, ductility etc.) have been defined adopting different linearization methods.

Results show how the common design practise is based upon simplifying hypothesis that may not always represent the real connection response under certain conditions. These assumptions can conduct to an unsafe estimation of the connections capacity, and therefore of the all system.

4.1. Test configuration and setup

Experimental tests on both type of connections were performed using a specifically designed test setup suitable to prescribe both lateral and axial deformation to the assembly of a CLT panel specimen with the joint. The experimental setup is depicted in Fig. 4.1.

The test specimen, rotated of 90° with respect to the configuration in an actual in-situ application, is fixed to the steel profiles of the supporting rigid steel frame in the principal direction of the load application considered for the specific case, thus transferring the displacement directly to the joint. Moreover, being the CLT panel virtually non-deformable the deformation of the specimen is due to the connection only.

In order to avoid rotations of the specimen and reducing friction between moving parts during the test, rolling bearing devices are used in both directions.

In this test setup, the two degrees of freedom (axial and lateral displacement) for the connection are uncoupled and measured with respect to the fixed supports by means of electronic transducers. The instrumentation will be described more in detail for the two specific configuration in the next paragraphs.

Finally, two actuators are used to impose the load protocols in the lateral and axial direction respect to the connector position. Due to the need of reproduce withstand axial forces due to overturning moments on the CLT wall panel for the hold-down connections, usually with higher values than the other reactions, different actuator capacity are used. A horizontal actuator, with the loading capacity of 500 kN, is used to prescribe axial displacement (named axial-actuator), whereas a vertical 50 kN actuator is used to prescribe lateral displacement (named lateral-actuator), see Fig. 4.2.

The CLT panel is fenced in the steel “cage” that is connected to the contrast steel frame trough a system with rolling bearing devices. Also, to prevent out of plane movements, the CLT panel is blocked both sides in the four corners.

The connectors (i.e. angle bracket or hold-down) has been connected to the panel by the use of nails, while on the right view slide (representing the foundation) trough one or more bolts.



Fig. 4.1 Pictures of the test setup without the CLT specimen

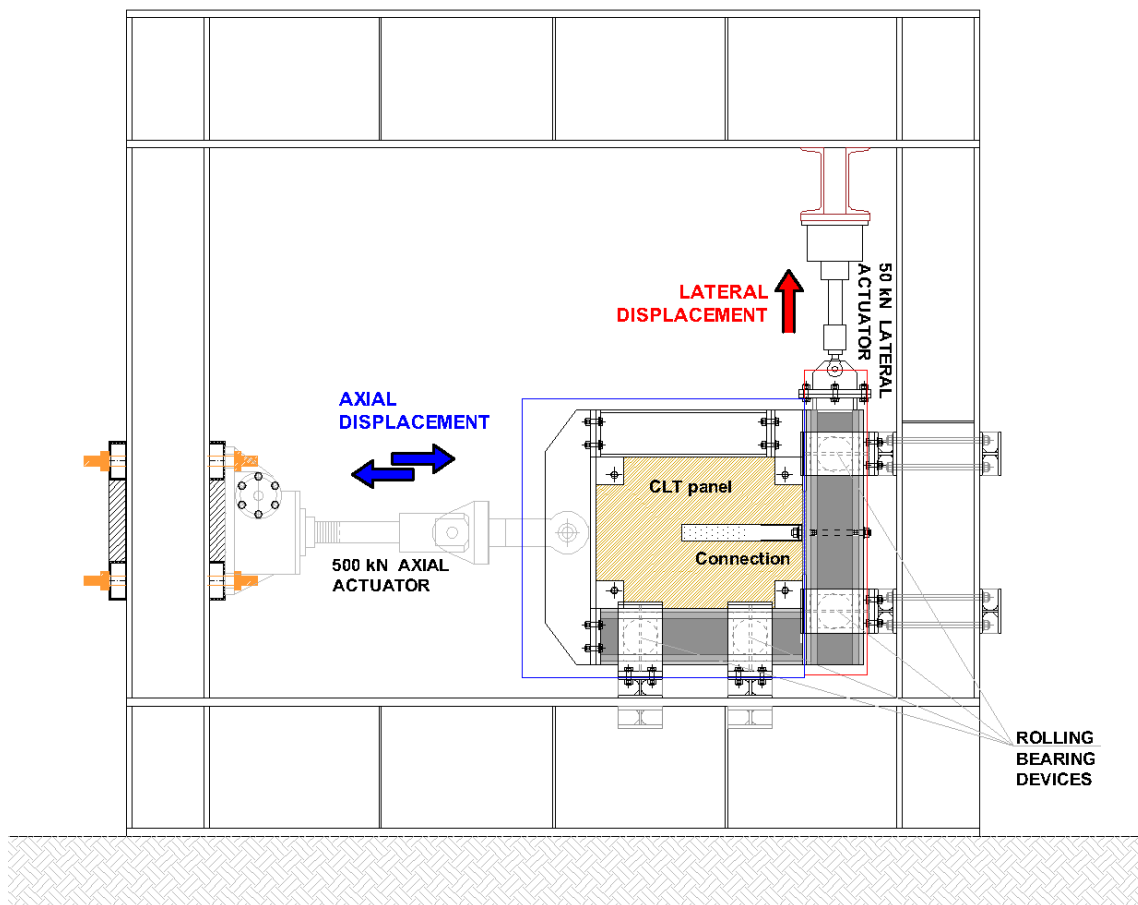


Fig. 4.2 Test setup representation with the specimen and description of load directions

4.2. Specimen components characteristics

Specimens consist of two parts: CLT panel and the hold-down connector plus the fasteners.

CLT panels (C24 grade) made with five crosswise laminated board layers and a total thickness of 140 mm (40-20-20-20-40 mm) were used in the tests (Fig. 4.3). The panel is certified according to European Technical Approval (ETA-14/0349) prescriptions. Specimen dimensions are 750 mm × 550 mm. As prescribed by EN 1380 (EN-1380) the panels were conditioned at (20±2)°C temperature and (65±5)% relative humidity for 15 days before performing the tests.

The hold-downs used in the tests are WHT540 type, with 12 annular ringed nails (4 x 60 mm) (ETA-04/0013), and were anchored to the base support with 16 mm diameter bolts (8.8 grade). The type of hold-down and the number of fasteners are the same used in the previous unidirectional tests conducted by Gavric, in order to have a possible comparison between the two experimental campaign results.

The standard dimensions for WHT540 hold-downs follow the European Technical Approval (ETA-11/0086). Two lateral stiffening plates are present at the two sides of the plate anchored to the CLT panel (ribbed portion), as shown in Fig. 4.4.

Additional details of the specimen assembly are reported in Fig. 4.5.

C panels		The grain direction of the cover layers is always parallel to the production widths.		Panel design [mm]					
Thickness [mm]	Panel type [-]	Layers [-]	Panel design [mm]						
			C***	L	C***	L	C***	L	
60	C3s	3	20	20	20				
80	C3s	3	20	40	20				
90	C3s	3	30	30	30				
100	C3s	3	30	40	30				
120	C3s	3	40	40	40				
100	C5s	5	20	20	20	20			
120	C5s	5	30	20	20	20	30		
140	C5s	5	40	20	20	20	40		
160	C5s	5	40	20	40	20	40		


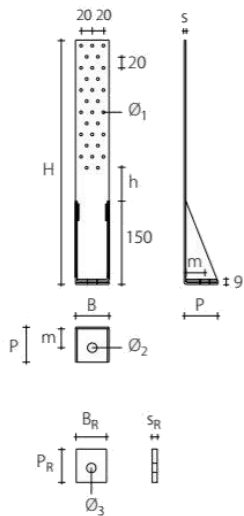


Fig. 4.3 Distribution and detail of the CLT panel layer thickness

GEOMETRY



WHT ANGLE BRACKET		WHT340	WHT440	WHT540	WHT620
Height	H [mm]	340	440	540	620
Width	B [mm]	60	60	60	80
Depth	P [mm]	63	63	63	83
Thickness	s [mm]	3	3	3	3
Hole position in timber	h [mm]	40	60	40	40
Hole position in concrete	m [mm]	35	35	35	38
Flange holes	Ø1 [mm]	5,0	5,0	5,0	5,0
Base hole	Ø2 [mm]	17,0	17,0	22,0	26,0
WHT washer	type	-	WHTBS50	WHTBS50L WHTBS50	WHTBS70L WHTBS70

WHTBS WASHER		WHTBS50	WHTBS50L	WHTBS70	WHTBS70L
WHT Angle bracket	type	WHT440 / WHT540	WHT540	WHT620	WHT620
Width	BR [mm]	50	50	70	70
Depth	PR [mm]	56	56	77	77
Thickness	SR [mm]	10	10	20	20
Washer hole	Ø3 [mm]	18,0	22,0	22,0	26,0

Fig. 4.4 Hold-down WHT540 dimensions (Rothoblass catalogue)

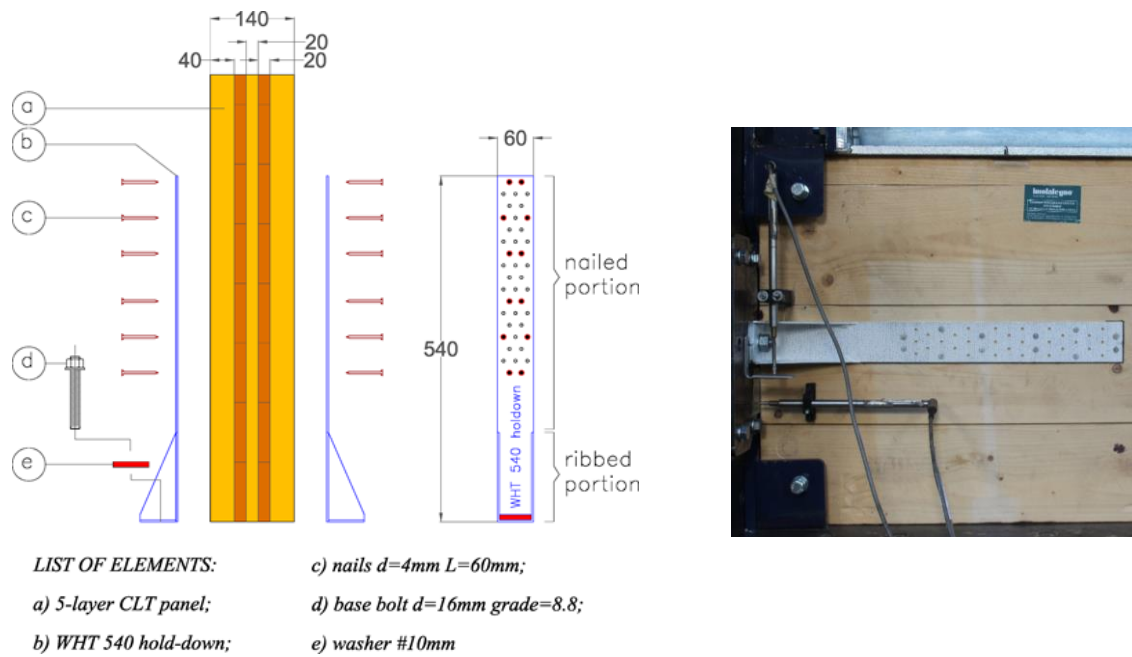


Fig. 4.5 Specimen details and assembly

4.3. Loading protocol

In order to evaluate the effect of a lateral deformation on the axial behavior of the hold-down connections, five different test series have been performed. For each of them, three specimens were tested varying the protocol adopted for the axial loading phase: one specimen was tested following the monotonic procedure prescribed by EN 26891 (EN-26891), while the protocol prescribed by EN 12512 (EN-12512) for cyclic tests was adopted for two specimens. The five different test series refer to different values of the prescribed lateral displacement.

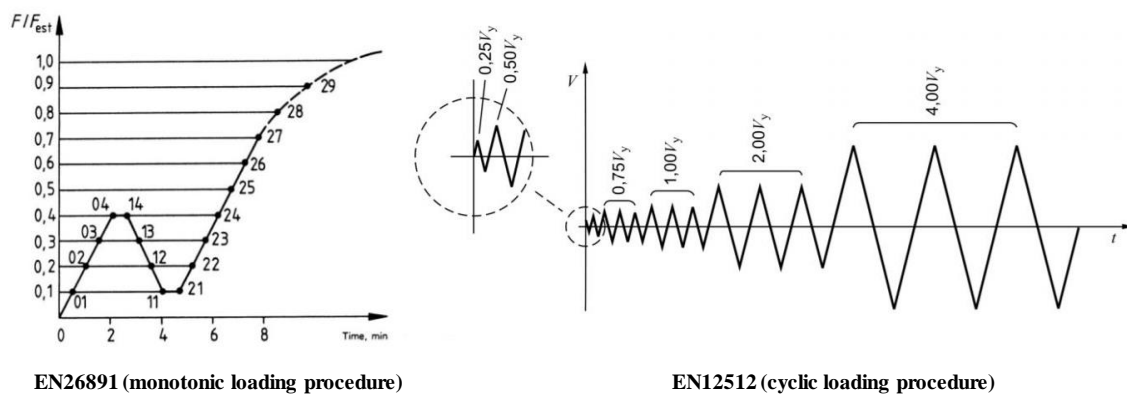


Fig. 4.6 Standard monotonic and cyclic loading procedure for timber structures

The tests labeled as follows: LD–XY are performed with lateral displacement maintained equal to “XY” mm during the total axial monotonic or cyclic phase.

For all tests, the adopted procedure followed these steps: (1) a monotonic lateral displacement was prescribed to the connection up to the target value and kept constant during the test (called “lateral displacement phase” or “lateral phase”);

(2) the axial displacement was then prescribed (called “axial displacement phase” or “axial phase”), following the protocol for monotonic test or the protocol for cyclic test, maintaining constant the lateral displacement up to the end of the test.

The different level of lateral displacement are: $XY = 0, 7.5, 15, 30, 45$ mm, for the five test series. Figures below show the displacement protocols adopted for both lateral and axial displacement phases for the monotonic (Fig. 4.7) and for the cyclic (Fig. 4.8) tests, respectively.

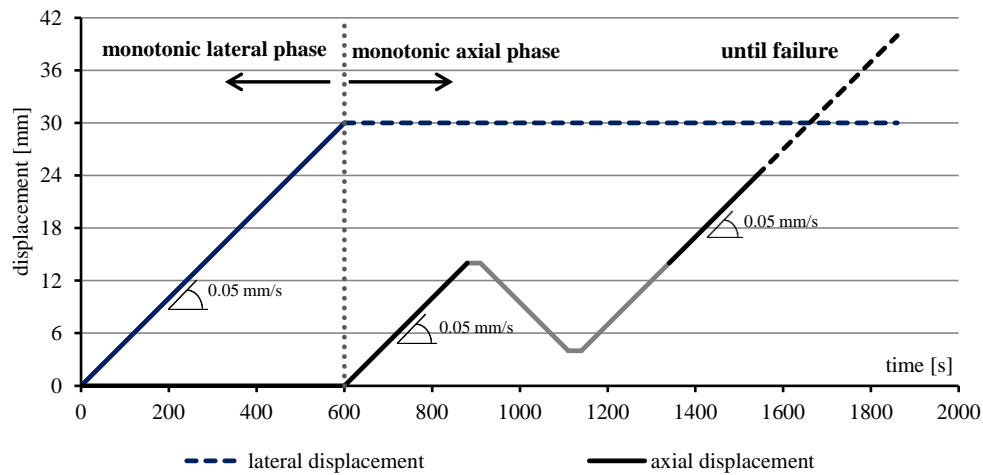


Fig. 4.7 Protocol followed for monotonic tests (LD-30 as example)

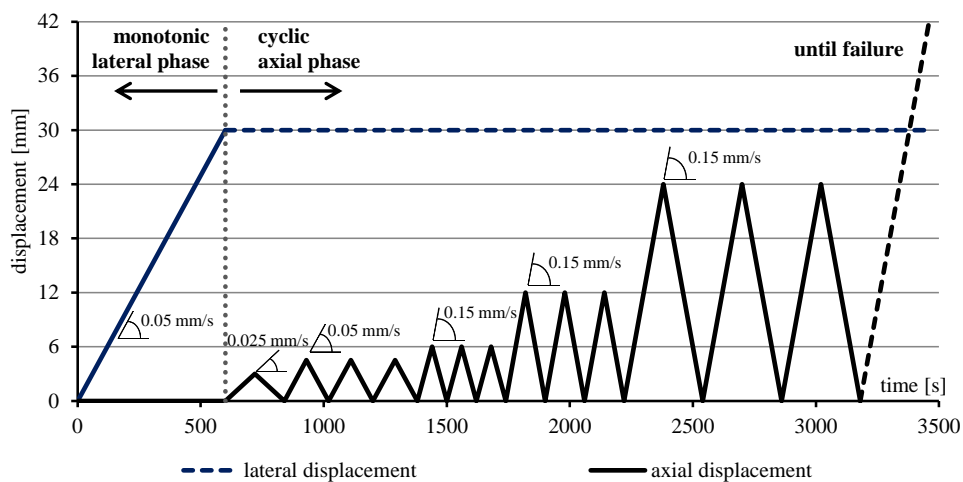


Fig. 4.8 Protocol followed for cyclic tests (LD-30 as example)

The rate has been increased during the cyclic loading phase, after the beginning cycles, following the European Standard prescriptions.

4.4. Instrumentation

In this test setup, the two degrees of freedom (axial and lateral displacement) for the connection are uncoupled and measured with respect to the fixed supports by means of two electronic transducers (LVDTs) per side (i.e. CH.2 (side A) – CH.3 (side B), and CH.4 (side A) – CH.5 (side B)), see Fig. 4.9. On one side (side A), three additional vertical LVDTs (CH 6, 7, 8) and one potentiometer (CH 9) are installed along the hold-down length to measure the lateral rotation and axial deformation of the connection.

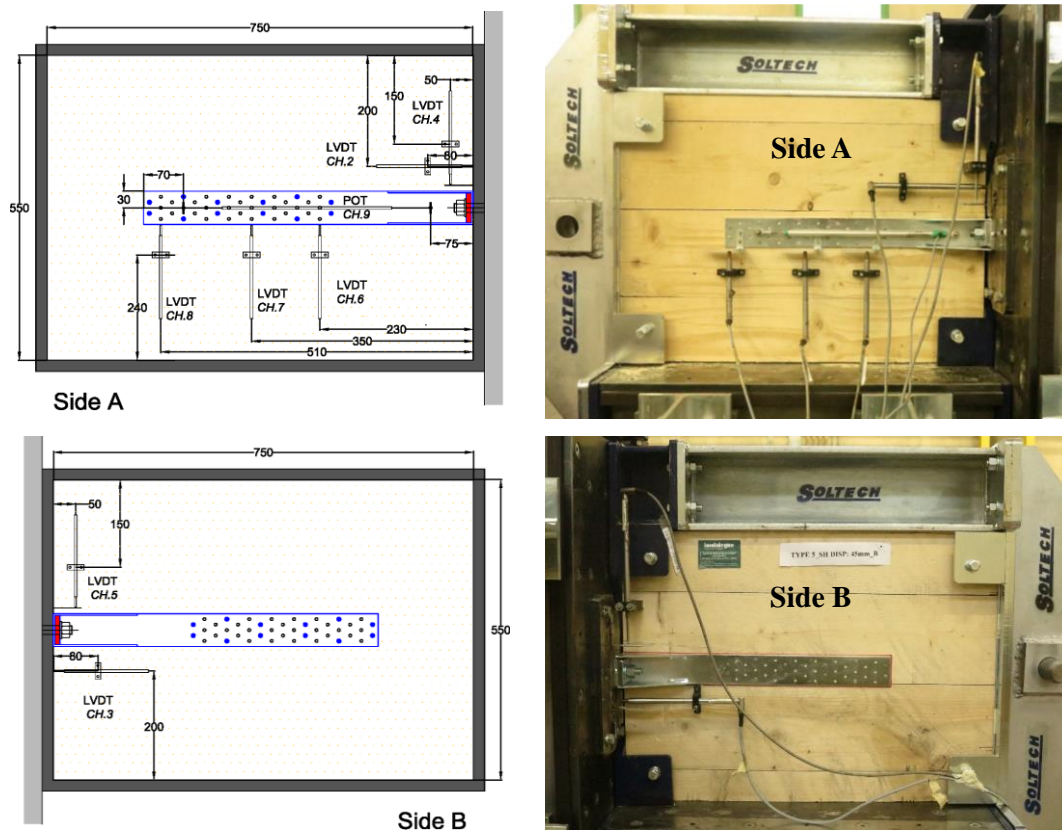


Fig. 4.9 Side views of the test setup and position of measurement instruments

4.5. Test results and discussion

In this section, the results of monotonic tests (5 specimens) and cyclic tests (10 specimens) are shown. Failure modes are investigated and the most significant load - displacement curves are reported.

4.5.1. Observed failures

Due to the specific test procedure, it is interesting to verify the connection deformation. In particular at the end of the first test phase, when the lateral displacement is monotonically incremented up to the target level, and at the end of the second phase when the axial displacement is prescribed.

Fig. 4.10 shows, for the examined series LD-0, -7.5, -15, -30 and -45, the hold-down deformed shape at the end of the shear displacement phase and at the end of the 1st cycle with a prescribed 24 mm axial displacement. A solid black line on the panels indicates the original position of the hold-down at time 0s. The failure mode observed at the end of

all experimental tests principally involved the nails used to connect the steel plate of the hold-down to the CLT panel.

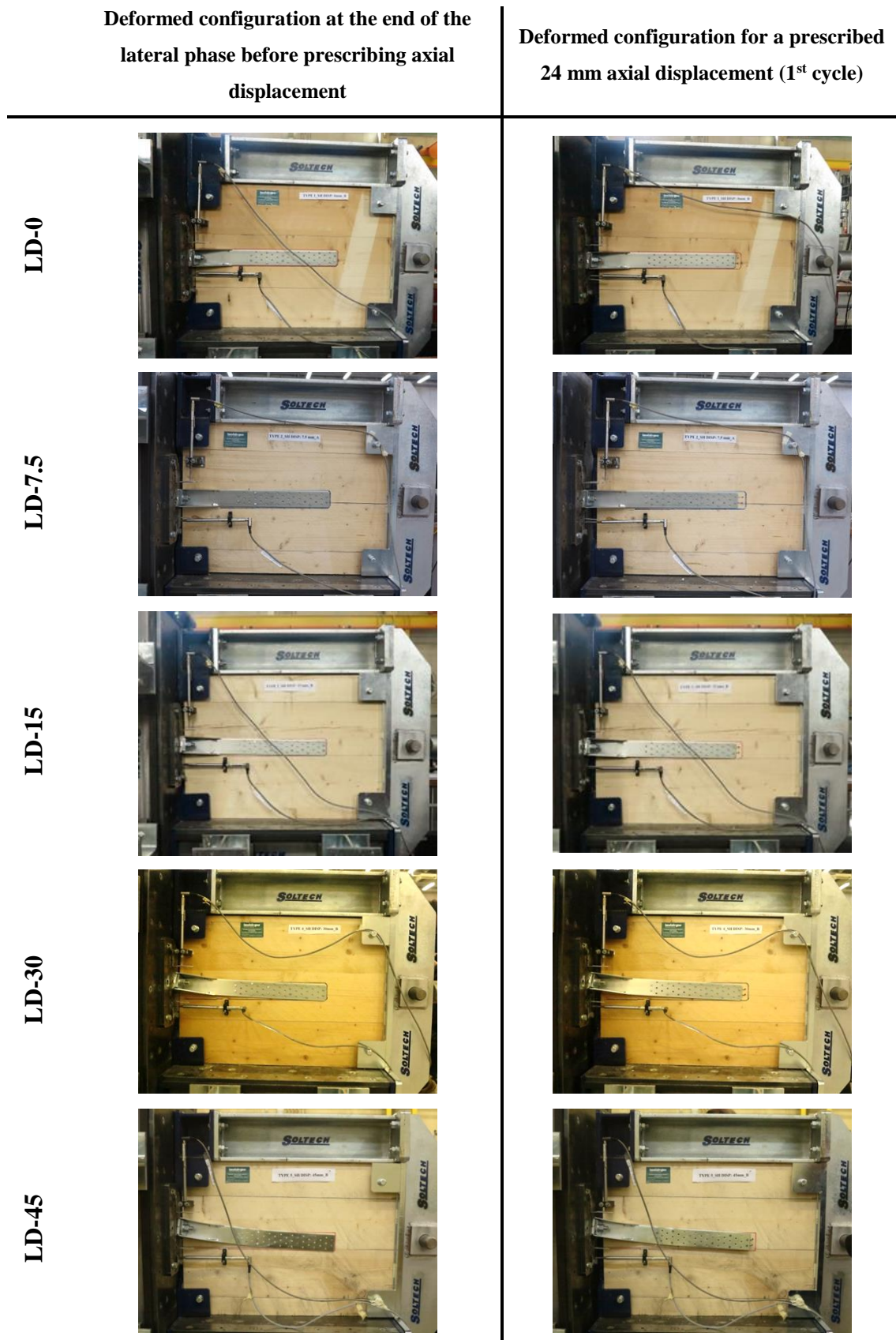


Fig. 4.10 Deformed shapes of specimens for different values of lateral and axial displacements

Two plastic hinges can be recognized in the nails, one under the cap and another one in the shank (about 20 – 25 mm below), see Fig. 4.11

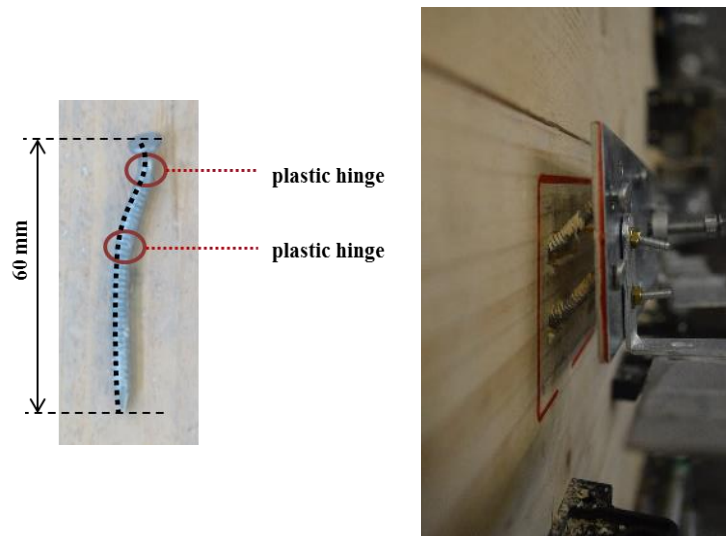


Fig. 4.11 Deformed nails with double plastic hinge formations

In addition, localized embedment of wood around the nail shank, oriented in the load direction, can be observed (Fig. 4.12). In fact, embedment failure together with the formation of plastic hinges in the fastener are the mechanisms considered by Johansen's theory to calculate the capacity of the single connector, by ensuring a ductile behavior. Brittle failure involving the fracture of the steel plate never occurred during tests, thanks to the correct design of the number of nails adopted for the connections (Jorissen & Fragiaco 2011).



Fig. 4.12 Localized embedment of wood caused by loaded fasteners

For specimens subjected to a large value of imposed lateral displacement (i.e., LD-45), the hold-downs deformation at the end of the lateral phase exhibited a rigid rotation of the base ribbed portion of the steel connection, see Fig. 4.13. The rigid rotation is caused by the eccentricity between the bolts axis and the steel plate of the hold-down, inducing an out-of-plane deformation of the latter, with consequent extraction of the nails and localized crushing of the wood in the contact area between the panel and the ribbed plate.

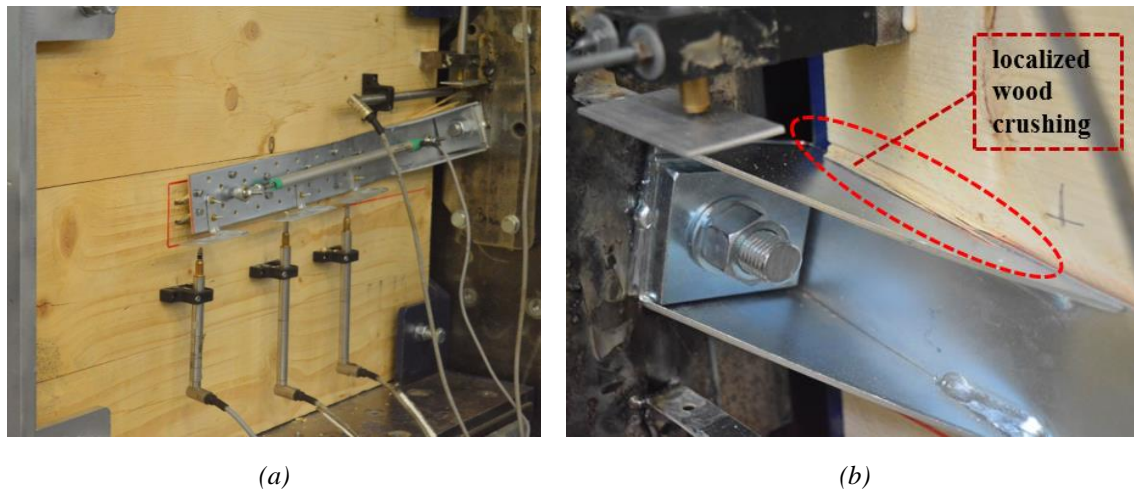


Fig. 4.13 Detail of rigid rotation of the ribbed based portion of hold-down for large value of lateral displacement imposed (i.e., LD-45): (a) out-of-plane deformation of the steel plate with accompanied extraction of nails, (b) localized crushing of wood panel below the ribbed portion of connection

4.5.2. Rotation of hold-down steel plate

Adopted measurement setup allowed to detect the transverse and longitudinal deformation of the hold-down steel plate, during both the lateral and axial loading phases. Relative lateral displacements between steel plate of the hold-down and CLT panel were measured in three different points along the nailed portion of the connection (instruments are indicated with CH 6,7,8 in Fig. 4.9). In addition, the relative displacement between connection and external support was also recorded during the tests (see CH.4).

Fig. 4.14 shows the measured displacements for the five different test configurations with different values of prescribed lateral displacement ($0 \div 45$ mm). Curves in Fig. 4.14 show the steel plate deformation at the achievement of the prescribed lateral displacement (XY).

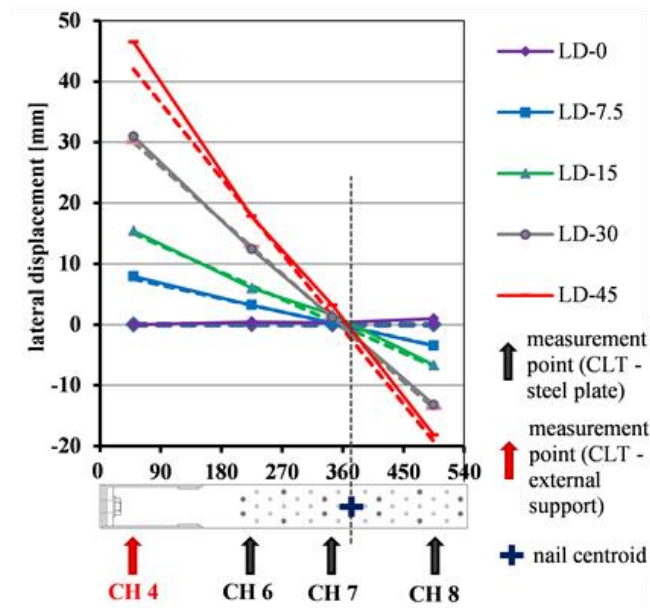


Fig. 4.14 Lateral displacement along the hold-down plate at the end of lateral displacement phases

For series LD-0, -7.5, -15 and -30, the lateral deformation of the hold-down is a rigid rotation of the steel plate without significant distortion, as confirmed by the good fit between the points representing the measured lateral displacements and the ideal line corresponding to a rigid rotation of the hold-down around the nails centroid (short dashed line), see Fig. 4.14. For configuration LD-45, in addition to the rigid rotation of the plate around the nail centroid, a local distortion of the based ribbed portion of the steel connection is also registered, as confirmed by Fig. 4.13 and the failure mode illustrated in Fig. 4.14.

The elongation of the hold-down was measured by means of the potentiometer (the instrument indicated with CH 9) installed along the steel plate. Table 1 reports, for the specimens tested following the cyclic protocol, the mean values of the steel plate elongation reached at the end of the 1st cycle with amplitude equal to 6 mm, 12 mm and 24 mm, together with the values registered at the achievement of the peak axial force (denoted as “P”).

Table 1 Mean values of hold-down axial elongation at different levels of the axial cyclic displacement.

Axial displacement	LD-0	LD-7.5	LD-15	LD-30	LD-45
6.00 mm	0.80 mm	0.53 mm	0.49 mm	0.45 mm	0.26 mm
12.00 mm	1.06 mm	0.72 mm	0.73 mm	0.67 mm	0.39 mm
<i>P</i>	1.21 mm	1.05 mm	0.85 mm	0.83 mm	0.45 mm
24.00 mm	1.12 mm	1.02 mm	0.75 mm	0.75 mm	0.33 mm

From Table 1, it is possible to observe that:

- (i) increasing the axial cycle amplitude, the axial elongation of the hold-down steel plate increase until the achievement of the peak axial force and then decreases;
- (ii) increasing the imposed lateral displacement, the axial elongation of the hold-down steel plate decreases due to the reduction of the axial forces acting on the connection. In any case, the steel plate always remained in the linear range so that any residual plastic deformation at the end of the tests.

4.5.3. Axial force vs axial displacement curves

The axial displacement and the corresponding axial force will be reported for all the test series, both monotonic and cyclic.

In Fig. 4.15, results from the monotonic and the two cyclic axial tests (named “cyclic 1” and “cyclic 2”), starting from different levels of prescribed lateral displacement (LD-XY), are compared.

As first, monotonic and cyclic tests exhibit a very good agreement, both in the ascending and softening branches. This result leads to the conclusion that the connection capacity, in terms of strength and ductility, is not significantly affected by the cyclic loading.

The same curves are superposed and plotted in Fig. 4.16(a) collecting results from monotonic tests, and in Fig. 4.16(b) for one of the two series subjected to the cyclic load protocol.

Experimental results show that the effects of the initially prescribed lateral deformation on the axial response of the specimens can be relevant in terms of reduction of the maximum force achieved during the test (up to 25% from LD-0 to LD-45). Moreover, an increment of the initial stiffness can be observed, especially for large values of the lateral displacement. This is due probably because of its initial lateral deformation, while axial phase is starting the connectors is not aligned with the load direction thus resulting a stiffer connector configuration. Analogously, an increasing of reloading stiffness after unloading (at 15 kN, for all specimens) with the imposed lateral displacement (Fig. 4.16(a)) can be observed.

On the contrary, no significant correlation was found between the imposed lateral displacement LD-XY and the conventional ultimate displacement (corresponding to a 20% load reduction) in traction.

Finally, it is interesting to examine the variation of both shear and axial force during the axial cyclic tests. The mean shear and axial force values, obtained from the two specimens investigated using the cyclic protocol, are reported in Fig. 4.16 and Fig. 4.17 respectively.

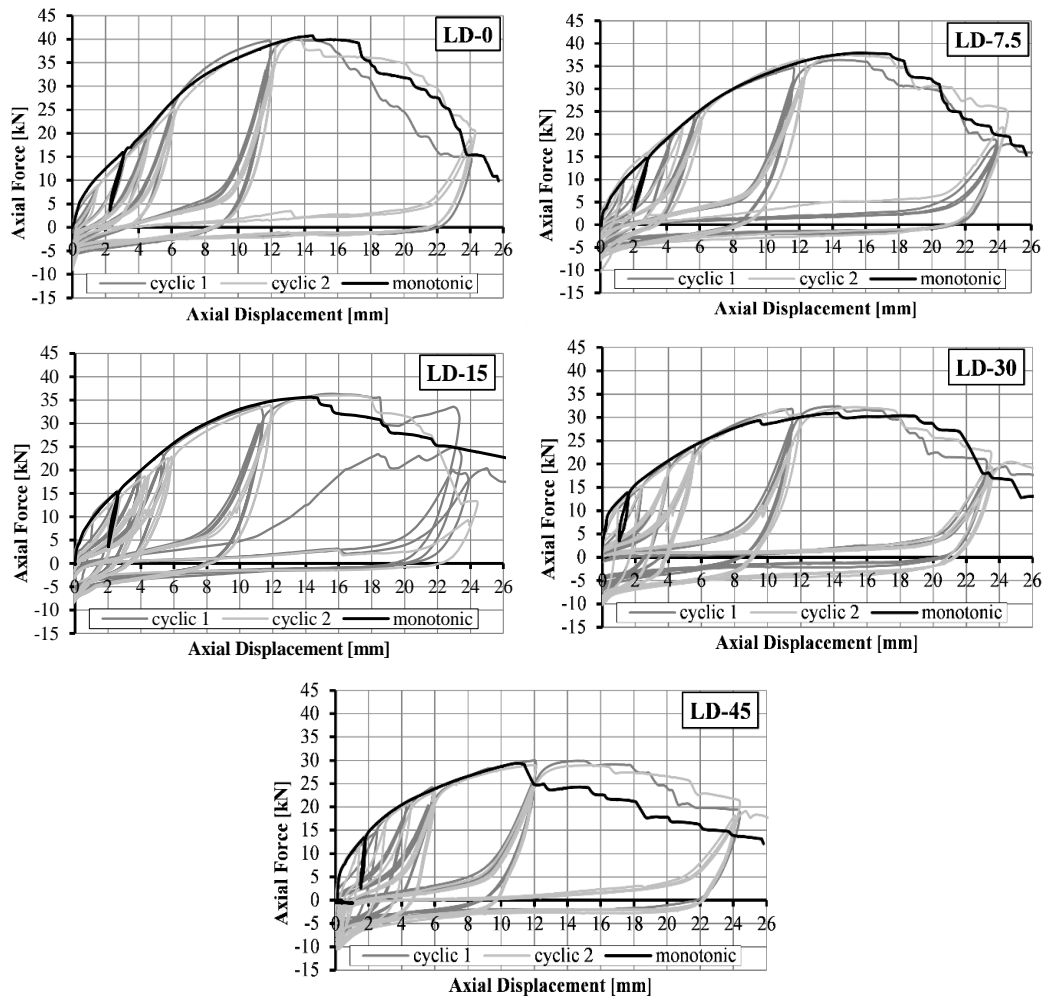


Fig. 4.15 Axial force vs. axial displacement curves for the 5 test series with different prescribed lateral displacement values (LD-0, 7.5, 15, 30, 45 mm): comparison of results from monotonic and cyclic tests

The axial displacement for each cycle is indicated while, in the last cycle, “*P*” denotes the attainment of the maximum (i.e., peak) traction force in the hold-down.

Fig. 4.16 shows the axial force for the cycles before the peak value (*P*) and then in the softening branches.

Fig. 4.17 shows a significant reduction of the shear force during the test for all the tested configurations (LD-7.5, -15, -30, -45). However, the evolution of the shear forces is oscillatory increasing the cycle axial displacement. In detail, the variation of the shear force is small up to the 6 mm axial cycle, after it becomes relevant due to the combined effect of shear-tension into the fastening system of hold-down connection.

This oscillatory behavior is quite significant for series LD-30 and LD-45, denoting the relevance of the axial force - shear interaction.

Comparing the axial force values achieved at each cycle amplitude, it is evident that:

- (i) for small amplitude cycle displacement (up to 6 mm), specimens with higher values of imposed lateral displacement are characterized by higher values of axial forces;
- (ii) for high amplitude cycles (from 6 mm to peak – P), specimens with higher values of imposed lateral displacement reach lower values of axial force;
- (iii) for all values of imposed lateral displacement, results show an axial strength degradation for repeated cycles at the same displacement amplitude.

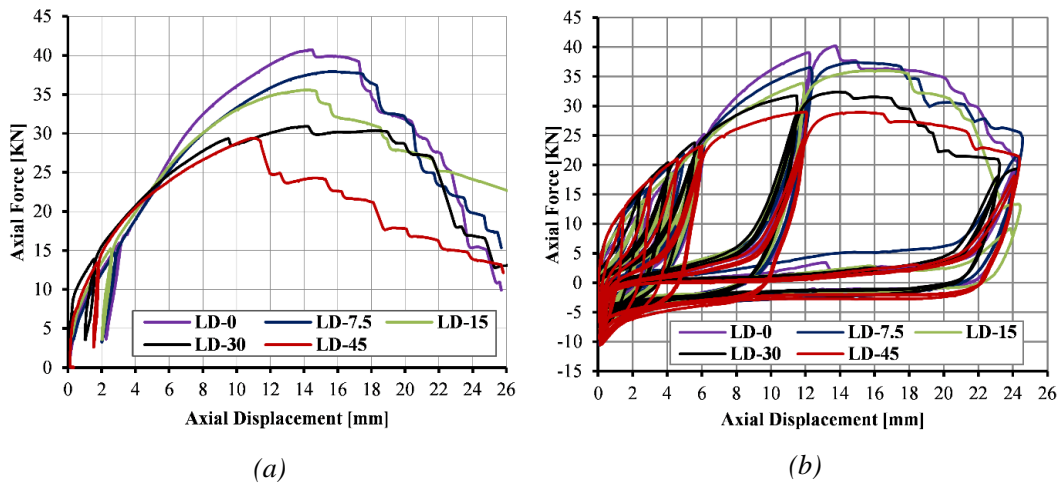


Fig. 4.16 Axial force vs. axial displacement: (a) monotonic and (b) cyclic curves for the 5 test series with different prescribed lateral displacement values (0, 7.5, 15, 30, 45 mm)

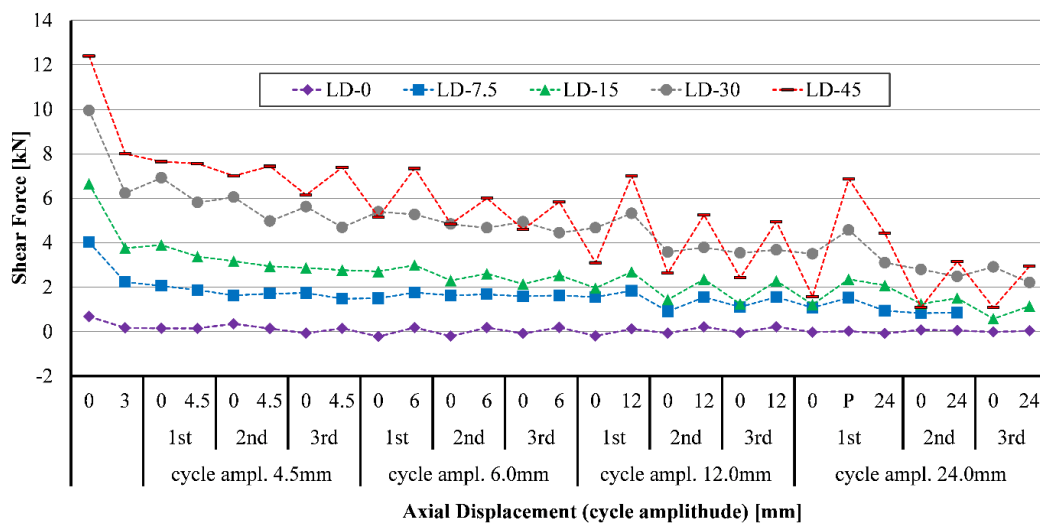


Fig. 4.17 Force evolution during the cyclic axial phase - Mean values of shear force

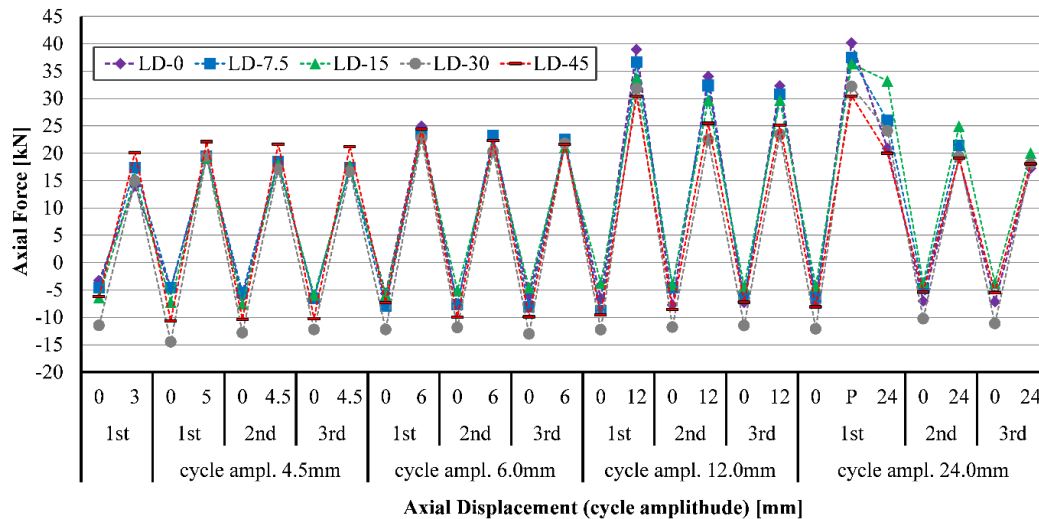


Fig. 4.18 Force evolution during the cyclic axial phase - Mean values of axial force

4.5.4. Shear force vs lateral displacement curves

For all the five test series the lateral displacement was preliminary imposed and then kept constant to the prescribed value.

Shear force vs. lateral displacement curves are plotted in Fig. 4.19, for the monotonic and the cyclic tests. In addition, Fig. 4.19 reports, with different symbols, the points corresponding to the mean force-displacement values at:

- (i) the end of the lateral displacement phase (i.e., achievement of the maximum imposed lateral displacement equal to 0, 7.5, 15, 30 and 45 mm);
- (ii) the achievement of the maximum axial force;
- (iii) the achievement of an axial displacement equal to 24 mm during the 3rd cycle.

Curves in Fig. 4.19 show the same trend up to the different step of prescribed lateral displacement values. The chart reports the superposition of monotonic and cyclic progressions, overlapping with each other, with the exception of LD-45 series where a small difference between the curves is displayed.

After reaching the fixed lateral displacement, the deformed configuration is maintained (almost) constant during the axial displacement phase of the test, and a gradual loss of shear force is registered for all the five series. When the peak axial force is reached, the shear force in the connection is reduced of about 50% with respect to the maximum value for all investigated configurations LD-XY. At the end of the tests, the shear force reduced even more. See for instance the residual shear forces corresponding to the achievement of a 24 mm axial displacement during the 3rd cycle.

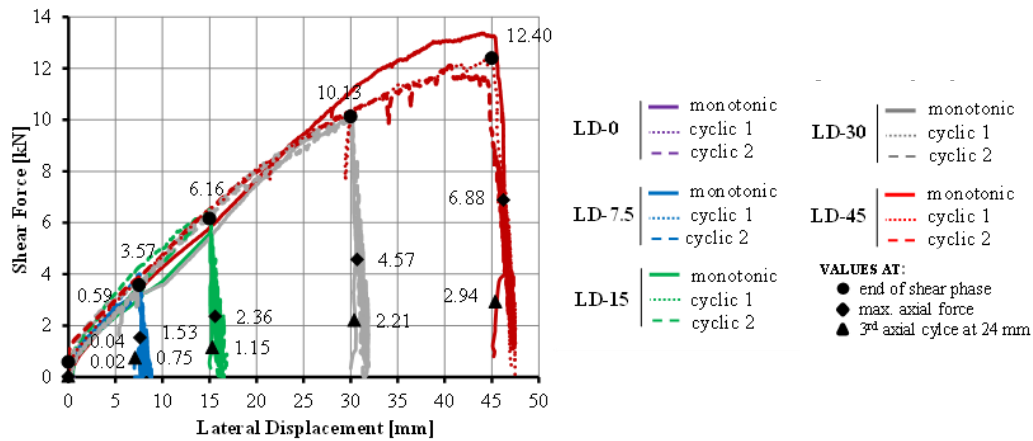


Fig. 4.19 Shear force vs. lateral displacement curves for the tests with different values of prescribed lateral displacement (0, 7.5, 15, 30, 45 mm)

As shown in Fig. 4.19, the imposition of the lateral displacement does not lead to the failure of the connections even for the largest applied lateral displacement. The peak shear force values increase with the imposed lateral displacements LD-XY, as expected. The force decrease is due to the subsequently imposed axial deformation, damaging the connection at the nail-wood level, with a significant reduction in the shear stiffness. Moreover, both shear forces, measured at the attainment of the maximum axial force and after a 24 mm axial displacement during the 3rd cycle, increase with the imposed lateral displacement for all the specimens tested.

4.6. Analysis of the results

In this section, results of the axial displacement phase of the tests are analysed according to the procedure prescribed by EN 12512 (EN-12512) and EN 26891 (EN-26891) for cyclic and monotonic tests, respectively. The mean values of force and stiffness for each specimen are defined, together with strength degradation and equivalent viscous damping registered at every cycle.

4.6.1. Procedures for the definition of yielding point

The experimental capacity curve of steel-to-timber connection generally does not show a well-defined yielding limit.

Two different criteria can be adopted for the definition of the yielding condition starting from experimental results (Piazza et al. 2011a): the first one is based on EN 12512 (EN-

12512) provisions, while the second one is based on an energetic approach (the so called Equivalent Energy methods (Jorissen & Fragiaco 2011)). For traditional steel-to-timber connections, the first criterion is usually adopted.

EN 12512 (EN-12512) provisions propose a bi-linearization of the experimental curves using the following two different criteria: method “a” which is adequate for a load-slip curve with two well-defined linear branches; method “b” for other cases (Fig. 4.20).

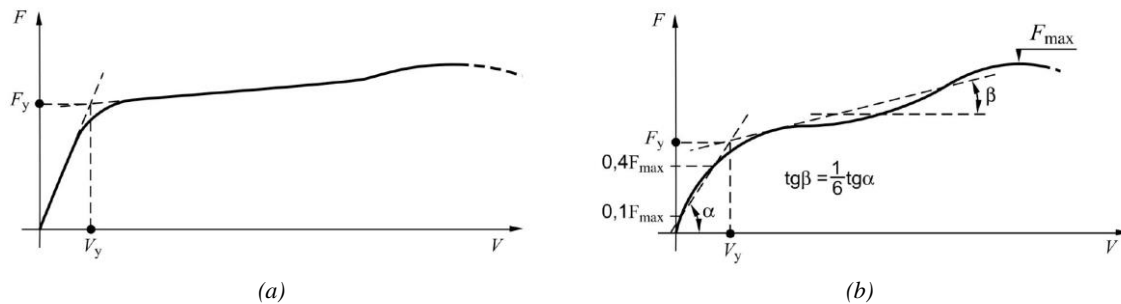


Fig. 4.20 EN-12512 definition of yield values for a load-slip curve with (a) with two well defined linear parts, (b) without two well-defined linear parts

The experimental load-displacement curves presented in this study (see Fig. 4.16) are not characterized by a marked variation of the gradient at the level of yielding condition, therefore the method “b” of EN 12512 was adopted. This method defines the yielding point ($d_y; F_y$) as the intersection between the branch with slope α , defined as the line through the point intersecting the experimental first loading curve at $0.1 F_{max}$ and $0.4 F_{max}$, and the branch tangent to the loading curve with a slope equal to $\beta = \alpha / 6$ (see Fig. 4.20). According to this approach, the slope of the second branch is imposed a priori, disregarding the actual shape of the experimental curve or other mechanical aspects such as the gradient of the post elastic branch. Consequently, the yielding point definition is affected by this assumption.

In order to seize the features of the experimental curves, an alternative approach for the definition of the yielding point is considered. The substitute approximation refers to the Equivalent Energy method (Piazza et al. 2011b; Munoz et al. 2008; Pozza & Scotta 2015). Here the slope of the second branch (β^*) is defined by forcing the passage through the peak force point ($d_{F_{max}}; F_{max}$) and the equivalence of strain energy (in the range $0 - d_{F_{max}}$) between the experimental envelope curve and the piecewise linear approximation.

Method “b” of EN 12512 (EN-12512 2011) is labeled as ENb, whereas the Equivalent Energy methods is labeled as EEH, see Fig. 4.21.

Finally, independently of the method used to define the yielding limit, the failure condition ($d_{Fu}; F_u$) is conventionally assumed as the point corresponding to the achievement of a force equal to $0.8 F_{max}$ in the softening branch of the experimental load displacement curve (EN-12512).

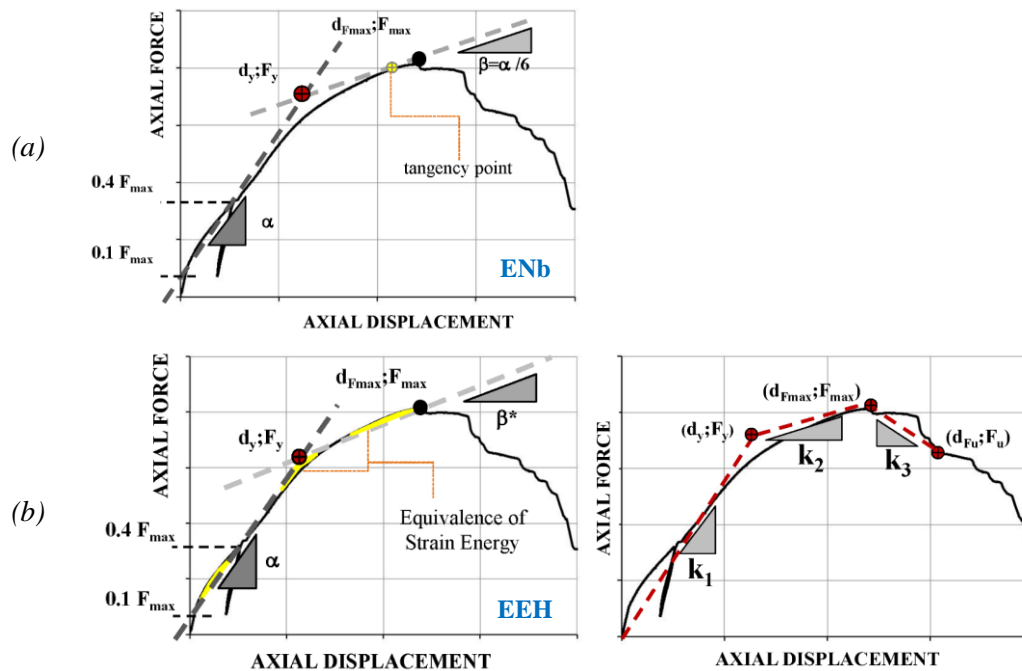


Fig. 4.21 Schematic representation of (a) ENb and (b) EEH methods for the definition of yielding point and corresponding tri-linear approximation

4.6.2. Tri-linearization methods of experimental curves

Once defined the yielding limit, the tri-linear approximation of the experimental load-displacement curve can be delineated.

As depicted in Fig. 4.21(b), the tri-linear approximation is obtained joining the following points: the origin of the axis (0; 0), the yielding point ($d_y; F_y$), the peak point ($d_{Fmax}; F_{max}$) and the point corresponding to the failure condition ($d_{Fu}; F_u$). The so obtained three branches are characterized by the stiffness: k_1 (elastic stiffness), k_2 (post-elastic stiffness) and k_3 (softening stiffness). Clearly, two different tri-linear approximations are obtained varying the method used to define the yielding limit.

From the experimental curves, the tri-linear approximation has been drawn referring to the mean values of the yielding, peak and failure points obtained from the cyclic and monotonic tests. Fig. 4.22 (a-e) show the mean tri-linear curves for all the tested specimens LD-0, -7.5, -15, -30, -45, where the points are obtained according to ENb and EEH methods. In Fig. 4.22 (a-e), the tri-linear approximations are overlapped to the

experimental monotonic curves for an immediate comparison. This way, it is possible to observe that for all the examined configurations the approximation provided by the EEH approach is closer to the experimental curve with respect to that provided by ENb method.

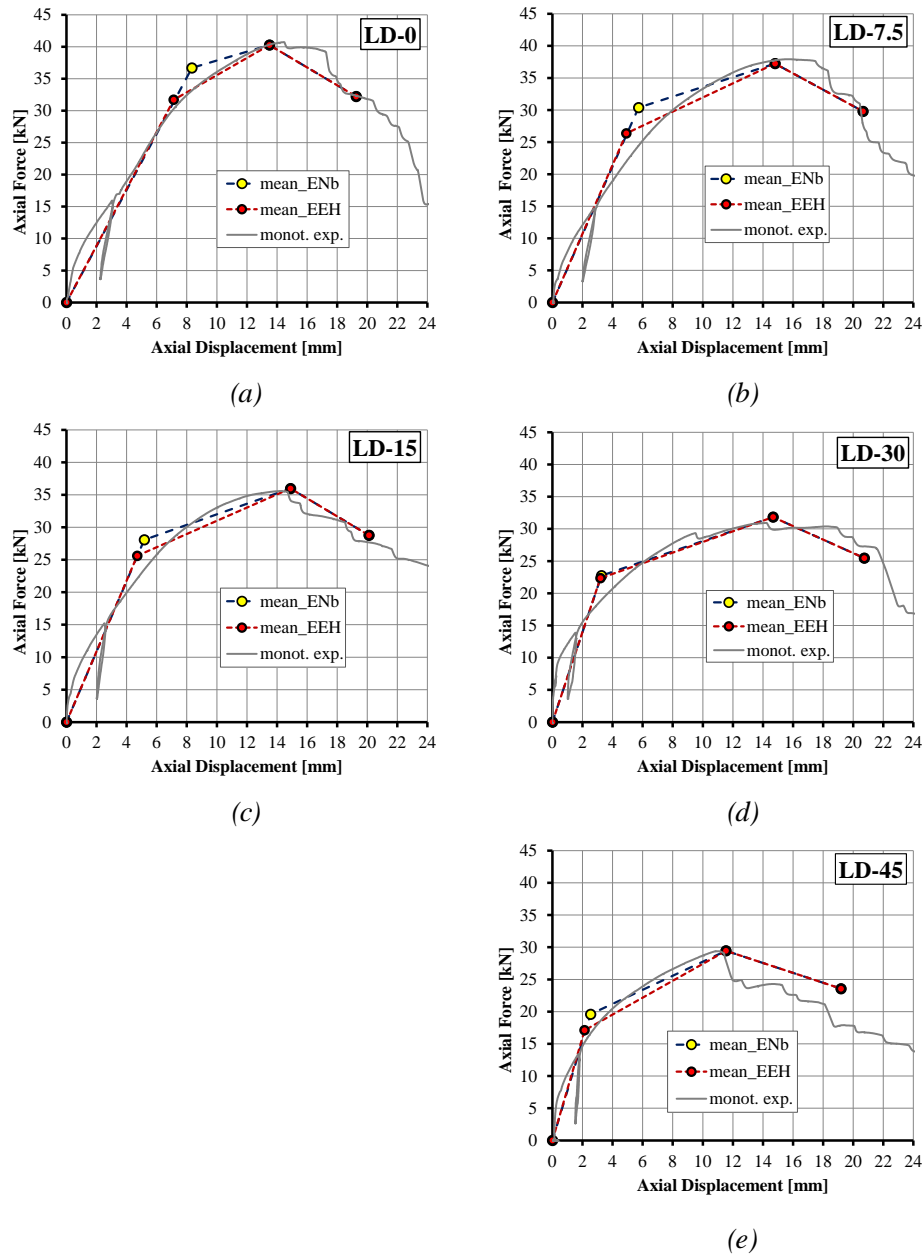


Fig. 4.22 Tri-linear approximations superimposed to the monotonic experimental curves for the specimen subjected to different prescribed lateral displacement (0, 7.5, 15, 30, 45 mm)

Table 2 reports the values of the significant parameters (force-displacement values and stiffness of three branches) characterizing the tri-linear curves obtained for the specimens with different prescribed lateral displacement values (0, 7.5, 15, 30, 45 mm) and adopting

both methods, ENb and EEH. Values obtained for each monotonic or cyclic test as well as the mean values are reported in Table 2, and in the below charts.

Table 2 Resulting values from the different tri-linearization methods

	LD	dy ENb	dy EEH	dFmax	dFu	Fy ENb	Fy EEH	Fmax	Fu	k1 ENb	k21EEH	k2 ENb	k2 EEH	k3	krel
MONOTONIC	0	7.45	6.06	14.19	19.00	35.48	29.36	40.74	32.59	4.76	4.84	0.78	1.40	1.69	12.80
	7.5	5.87	4.92	15.61	20.50	30.84	26.16	37.92	30.33	5.25	5.31	0.73	1.10	1.55	15.10
	15	4.33	3.82	14.19	19.50	28.30	25.22	35.59	28.47	6.53	6.61	0.74	1.00	1.34	19.65
	30	3.06	2.92	14.22	22.02	22.22	21.32	30.92	24.74	7.25	7.30	0.78	0.85	0.79	26.30
	45	2.11	1.89	10.90	15.38	18.50	16.77	29.39	23.51	8.79	8.88	1.24	1.40	1.31	34.33
CYCLIC	0	8.79	7.66	13.15	19.40	37.32	32.89	40.04	32.03	4.26	4.29	0.62	1.30	1.34	
	7.5	5.66	4.91	14.40	20.73	30.14	26.47	36.91	29.53	5.33	5.39	0.77	1.13	1.17	
	15	5.59	5.15	15.25	20.43	27.96	25.81	36.16	28.93	5.06	5.07	0.85	1.03	1.41	
	30	3.35	3.33	14.90	20.10	23.00	22.86	32.28	25.83	6.86	6.87	0.80	0.82	1.24	
	45	2.61	2.63	11.87	21.15	20.29	20.43	29.48	24.55	7.68	8.00	0.98	0.97	0.96	
MEAN VALUE	LD	dy ENb	dy EEH	dFmax	dFu	Fy ENb	Fy EEH	Fmax	Fu	k1 ENb	k21EEH	k2 ENb	k2 EEH	k3	
	0	8.12	6.86	13.67	19.20	36.40	31.13	40.39	32.31	4.51	4.57	0.70	1.35	1.52	
	7.5	5.76	4.92	15.01	20.61	30.49	26.32	37.41	29.93	5.29	5.35	0.75	1.11	1.36	
	15	4.96	4.48	14.72	19.96	28.13	25.51	35.88	28.70	5.79	5.84	0.79	1.01	1.37	
	30	3.21	3.12	14.56	21.06	22.61	22.09	31.60	25.28	7.06	7.08	0.79	0.83	1.02	
45	2.36	2.26	11.38	18.26	19.40	18.60	29.43	24.03	8.23	8.44	1.11	1.18	1.14		

Fig. 4.23 shows the displacements corresponding to the yielding point (d_y), the achievement of the peak force (d_{Fmax}) and of the ultimate force (d_{Fu}) for the five levels of lateral displacement (0, 7.5, 15, 30, 45 mm).

It is possible to observe that:

- (i) the yielding displacement (d_y) decreases increasing the imposed lateral displacement LD, independently from the method used for the definition of the post elastic stiffness (i.e., ENb or EEH method);
- (ii) the displacements at the peak force (d_{Fmax}) and at failure (d_{Fu}) remain almost constant varying the imposed LD;
- (iii) the yielding displacements (d_y) obtained from the monotonic tests are smaller with respect to the mean values obtained from cyclic ones for both methods ENb and EEH;
- (iv) EEH method provides lower estimation of the yielding displacement with respect to the ENb method, even if the differences decrease for higher lateral displacement (LD=30 mm and 45 mm).

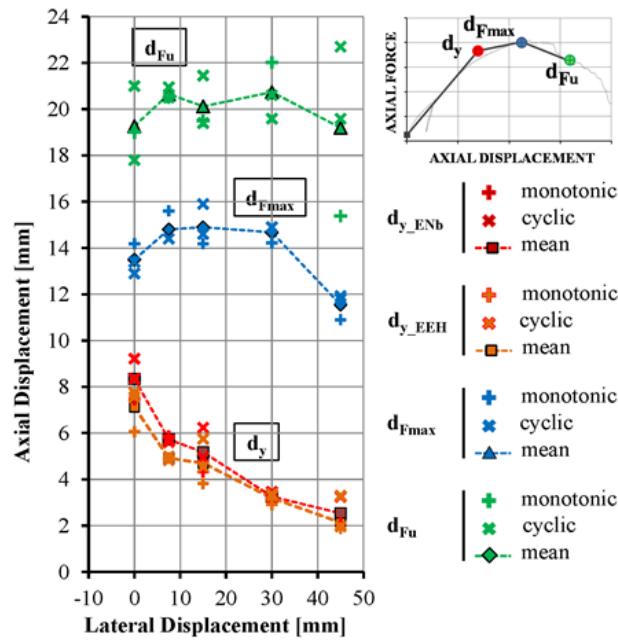


Fig. 4.23 Displacement values of the tri-linear curves for the specimens with different prescribed lateral displacement (LD=0, 7.5, 15, 30, 45 mm).

Fig. 4.24 reports the forces corresponding to the yielding (F_y) obtained with both ENb and EEH methods and the force at the achievement of the peak force (F_{max}) for the five levels of lateral displacement.

It is possible to observe that:

- (i) all the force values (F_y ; F_{max}) decrease increasing the lateral displacement LD-XY;
- (ii) the mean yielding force for LD-45 specimens is about 50% with respect to the LD-0 specimens for both ENb and EEH methods;
- (iii) the peak force for LD-45 specimens is reduced of about 25% with respect to LD-0 specimens (i.e., less than the yielding force reduction); the ultimate force is subjected to the same reduction because is conventionally defined as 0.8 F_{max} ;
- (iv) the yielding force values obtained with EEH method are always smaller than those obtained with ENb method.

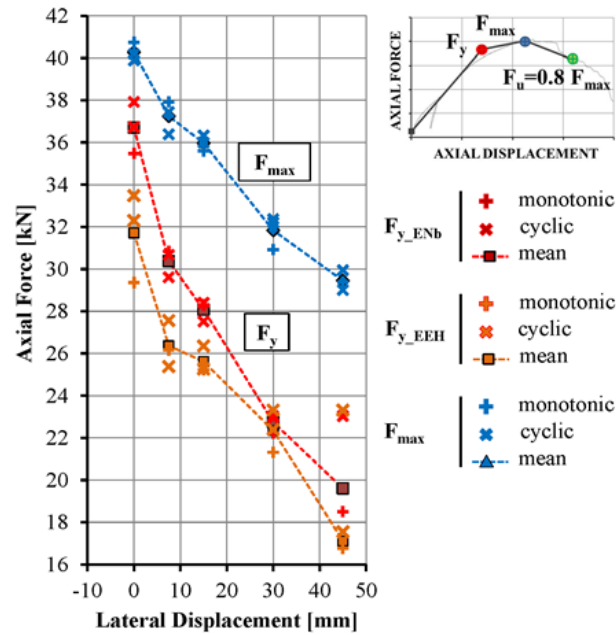


Fig. 4.24 Force values of the tri-linear curves for the specimens with different prescribed lateral displacement (LD=0, 7.5, 15, 30, 45 mm)

As last, Fig. 4.25 shows the stiffness values of the first elastic branch (k_1), the second post-elastic branch (k_2) and the softening branch (k_3) of the tri-linear curves obtained for the five levels of lateral displacement LD-XY.

It is possible to observe that:

- (i) elastic stiffness (k_1) increases for increasing LD,
- (ii) ENb and EEH methods give analogous estimation of the elastic stiffness (k_1),
- (iii) the post-elastic (k_2) stiffness is not significantly influenced by the imposed LD;
- (iv) post-elastic stiffness (k_2) obtained following the ENb method is smaller than that obtained with the EEH method except for specimen LD-45;
- (v) stiffness of the post-peak branch (k_3) slightly decreases for increased LD.

When the hold-down connection is subjected to small lateral displacement (i.e. the entire CLT wall assembly behaves elastically), the effect of the elastic stiffness variation is negligible. As far as the first comment is concerned, the initial stiffness k_1 increases with the imposed LD because the initial configuration changes making the connection stiffer with respect to the non-deformed configuration. In fact, a higher value of axial force is necessary to obtain the same axial deformation (see Fig. 4.18).

However, even if the imposed LD causes an increase of the initial stiffness, the presence of a lateral displacement reduces the registered maximum force, thus the connection strength.

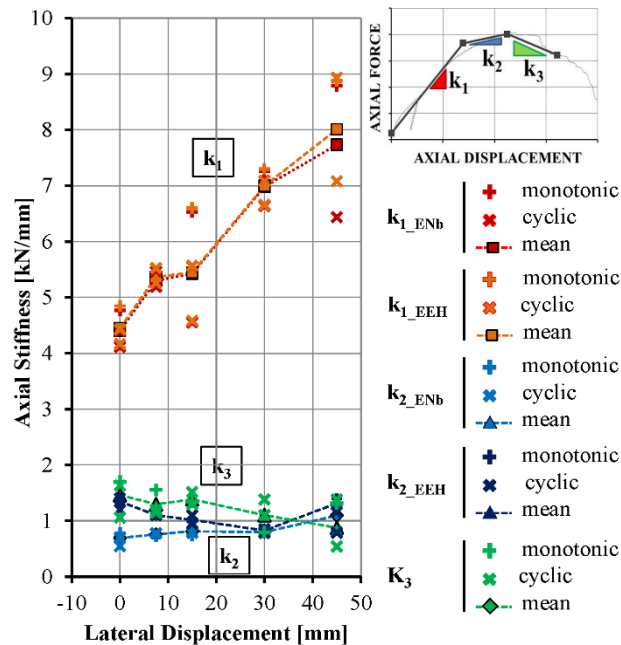


Fig. 4.25 Stiffness values of the backbone curves for specimens with different prescribed lateral displacement (LD=0, 7.5, 15, 30, 45 mm)

Starting from the values of yielding and ultimate displacements, the ductility in traction (μ) of the hold-down connection can be estimated. Table 3 reports the ductility value as $\mu = d_{Fu} / d_y$, i.e., ratio between the mean value of the displacement at the ultimate force (d_{Fu}) and at the yielding force (d_y) for the series LD-0, 7.5, 15, 30 and 45. Ductility values have been computed referring to the yielding estimation provided with both ENb and EEH methods, for comparison.

Table 3 Mean values of ductility in traction (μ) for different levels of lateral displacement (LD=0, 7.5, 15, 30, 45 mm)

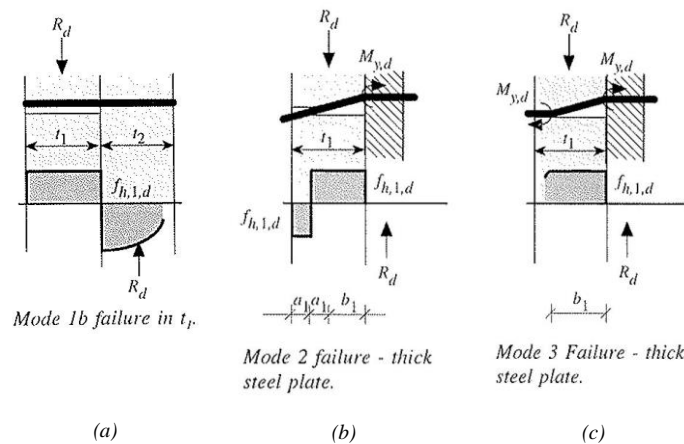
μ	LD-0	LD-7.5	LD-15	LD-30	LD-45
ENb	2.31	3.60	3.89	6.37	7.57
EEH	2.70	4.20	4.28	6.49	8.98

The results show the increasing of the ductility values with the imposed lateral displacement. This trend is mainly due to the reduction of the yielding displacement when

the imposed lateral displacement is increased, while the ultimate displacement (i.e., the effective displacement capacity of the connection) remains substantially constant.

4.6.3. Comparison with code provisions

Current standards provide design criteria to calculate the strength capacity of a nailed connection according to Johansen's theory (Johansen 1949) for glue laminated timber and other engineered wood elements. However, CLT panels and corresponding connections (e.g. hold-downs) are still not included in standards, requiring the use of harmonized technical specifications, such as European Technical Assessments (ETAs). The European Yield Model (EYM) (Johansen 1949) is typically adopted for computing the load-carrying capacity of nailed connections. This model is based on an ideal perfectly rigid-plastic behavior for both the fastener's moment capacity and the embedment strength of nails in timber. Accordingly, the load-carrying capacity of a single fastener joint loaded in shear for steel-to-timber joints with thick steel plates is (see Hilson (Hilson 1995)):



$$R_v = \min \begin{cases} f_h t_1 d & (a) \\ f_h d t_1 \left[\sqrt{2 + \frac{4M_y}{f_h d t_1^2}} - 1 \right] & (b) \\ 1.4 \sqrt{2M_y f_h d} & (c) \end{cases} \quad (1)$$

where f_h = value of embedment strength, t_1 ; d = fastener penetration depth and diameter, M_y = fastener yielding moment.

Eqn 1(a) represents the force corresponding to a rigid failure mechanism involving the only embedding of the timber, while Eqn 1(b) and Eqn 1(c) give the single fastener

capacity in the case of formation of, respectively, one and two plastic hinges in the metal connector, plus the embedding of the timber around the fastener.

Equation (1) does not take into account, for the two ductile failure mechanisms (b) and (c), the strength increase due to the so called “rope effect” that involves the withdrawal capacity of the nails (EN-1995-1-1 2009).

According to Eqn (1), the lowest value obtained identifies the failure mechanism of the single fastener joint.

In order to compare the experimental results with the analytical value of load-carrying capacity provided by EYM model (Johansen 1949), two different criteria can be used. The first criteria follows Eurocode 5 (EN-1995-1-1 2009) provisions and defines the 5-percentile characteristic load-carrying capacity of the connection adopting the 5-percentile characteristic values for all the parameters in Eqn (1). Computed characteristic load-carrying capacity can be then compared with the 5-percentile characteristic value of the maximum force (F_{max}), obtained from tests according to statistical method suggested by EN 14358 (EN-14358 2006). Since the set of experimental data available is lower than the minimum required by EN 14358 (EN-14358), this approach is not applicable in the present case.

The second approach aimed at comparing the mean values of the connection load-carrying capacity, obtained experimentally and analytically adopting in Eqn (1) in the latter, the mean values of the mechanical parameters. Mean values of yielding moment (M_{y_m}) and embedding strength (f_{h_m}) for an individual nail are defined according to Sandhaas et al. (Sandhaas, Carmen; Mergny) and Blass & Uibel (Blaß, H. J. ; Uibel 2006).

$$M_{y_m} = 0.18 f_{tu_m} d^{2.99} \quad (2)$$

$$f_{h_m} = 0.13 d^{-0.53} \rho_m^{1.05} \quad (3)$$

where f_{tu_m} = mean ultimate tensile strength of the steel nails (obtained from experimental tests, e.g. Izzi et al. (Izzi et al. 2016)) and ρ_m = mean density values of wood (obtained from experimental tests or defined according to EN 338:2004 (EN-338)).

The actual strength of a single nail is finally obtained by adding to the load-carrying capacity (R_v) the so called “rope effect” contribution (R_{ax}) (EN-1995-1-1 2009). According to ETA-04/0013 (ETA-04/0013), this additional strength contribution is defined as a quote of the withdrawal capacity of the nail (F_{ax}) but must be limited to the 50% of the load-carrying capacity (R_v) as prescribed by Eurocode 5 (EN-1995-1-1 2009):

$$R_{ax} = \min(0.5F_{ax}; 0.5R_y) \quad (4)$$

The formula derived from Blass & Uibel (Blaß, H. J.; Uibel 2007) was adopted to compute the mean values of the withdrawal strength value (F_{ax}):

$$F_{ax} = 0.16d^{0.6}l_{eff}\rho_m^{0.8} \quad (5)$$

Where l_{eff} is the profiled length of the nail shank .

The structure of the Eqns (2-5) is the same of those provided in Eurocode 5 (EN-1995-1-1 2009) for calculation of the characteristic values of yielding moment, embedment strength and withdrawal capacity, with some modification in the coefficients that are specifically calibrated, being the equations adopted here defined with reference to the mean values of the input parameters $f_{tu,m}$, ρ_m .

The above-listed capacity parameters and corresponding input values for Eqns (2-5) are reported in Table 4

Table 4 Adopted parameters for computing connection's load-carrying capacity

PARAMETER	VALUE
d	4.00 mm
t_1	57.00 mm
$f_{tu,m}^*$	722.70 N/mm ²
$M_{y,m}$	8.21 Nm
ρ_m^{**}	420.00 kg/m ³
$f_{h,m}$	35.42 N/mm ²
l_{eff}	45.00 mm
F_{ax}	2.07 kN
R_v	2.15 kN
R_{ax}	1.05 kN
$R_v + R_{ax}$	3.20 kN
n	12.00
F_v	38.44 kN
F_{max}	40.27 kN
* from Izzi et al. (Izzi et al. 2016)	
** C24 according to EN 338:2004 [36]	

Due to the large spacing between nails, no reduction effects are considered to compute the overall lateral capacity (F_v) of the hold-down connection, which is then obtained multiplying the resistance of single nail ($R_v + F_{ax}$) by the number of nails (n).

It is worth noting that the evaluated load-carrying capacity is representative of the ideal condition of pure traction in the hold-down, without any lateral action (i.e. LD-0 test

conditions). The experimental mean value of the peak forces for the configuration LD-0 (F_{max}) is compared in Table 4 with the analytical mean value (F_v).

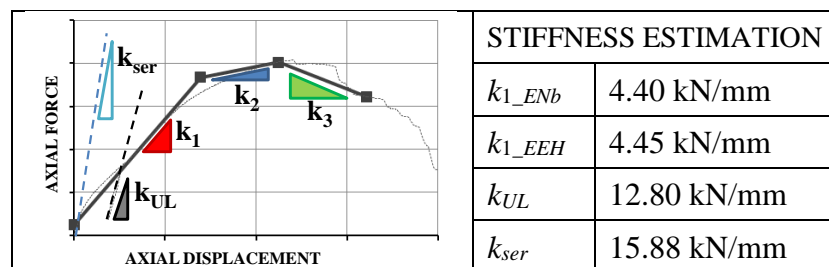
Table 4 shows that the analytical predicted mean values of the connection load-carrying capacity (F_v) agree very well with the experimental mean values of the peak forces for the configuration LD-0 (F_{max}), with a difference less than 5%. The adopted approaches then is quite appropriate for the estimation of the load-carrying capacity of nailed hold-down connection subjected to traction.

Regarding to the stiffness of the connection, Eurocode 5 (EN-1995-1-1 2009) provides a reliable model to predict the mean values of the instantaneous slip modulus (k_{ser_nail}) of a nailed timber-to-timber joint, suggesting to doubled it up for the timber-to-steel case:

$$k_{ser_nail} = 2\rho_m^{1.05} d^{0.8} / 30 \quad (6)$$

Similarly to the strength, the hold-down stiffness (k_{ser}) is obtained multiplying the nail slip modulus by the number of fasteners (see Table 5).

Table 5 Comparison between the estimation of elastic stiffness of hold-down connection for the configuration LD-0



The experimental elastic connection's stiffness is generally defined as the slope of the first branch of the tri-linear approximation of the experimental load-displacement curve. Many studies available in literature (Pozza et al. 2015; Piazza et al. 2011a) demonstrate that such definition of the connection stiffness is strongly affected by the method adopted for the linearization of the experimental curve and is, in general, not coherent with the k_{ser} value obtained following the code provisions. On the contrary, the definition of the actual elastic stiffness of the connection provided by the EN 26891 (EN-26891) is typically more accurate and representative of the elastic behavior of the connection without any approximation due to the adopted linearization method of experimental curve. According to the EN 26891 (EN-26891) provision, the unloading stiffness (k_{UL}) obtained from the monotonic tests can be assumed representative of the elastic behavior of the connections.

Table 5 lists, for the series LD-0, the mean stiffness values obtained with the previously described linearization method ENb and EEH (k_{1_ENb} and k_{1_EEH}), the unloading stiffness (k_{UL}) from the monotonic tests according to the EN 26891 (EN-26891 1991) and the estimation provided by codes (k_{ser}).

Comparing the values reported in Table 5, it is possible to observe that:

- (i) the analytical elastic stiffness (k_{ser}) is much greater than the estimations of the elastic stiffness obtained following the ENb and EEH approaches;
- (ii) the analytical elastic stiffness (k_{ser}) is a good estimation of the unloading stiffness obtained from monotonic tests (i.e. k_{UL}).

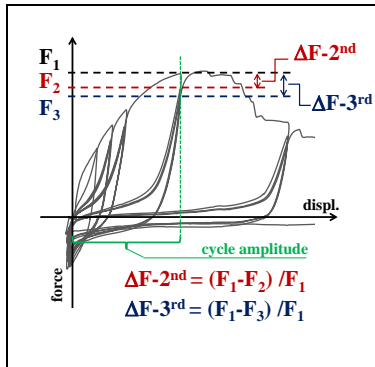
4.6.4. Strength degradation

In order to verify the capability of the connection to withstand cyclic loads, the force degradation registered at the end of 2nd and 3rd cycles (of prescribed axial displacement level) has been examined. According to EN 12512 (EN-12512), force degradation ΔF is defined as the percentage difference between the force registered at the second (or third) cycle ($F_{2(or\ 3)}$) and that reached at the first cycle (F_1) (i.e., $(F_1 - F_{2(or\ 3)}) / F_1 \cdot \%$).

Table 6 reports the mean values of ΔF registered at the 2nd and at the 3rd cycles for the specimens subject to different levels of lateral displacement (LD-0, -7.5, -15, -30 and -45). The results show that the reduction in the cycle peak forces increases with the initially lateral deformation (from 0 mm to 45 mm), except for LD-45 specimens.

Table 6 Mean values of strength degradation (ΔF) registered during the cyclic tests at different levels of the axial displacement (4,5 - 24 mm)

Cycle Amplitude	STRENGTH DEGRADATION – EN 12512					
	ΔF	LD-0	LD-7.5	LD-15	LD-30	LD-45
4.5 mm	2 nd	8.3%	5.0%	5.9%	16.4%	2.0%
	3 rd	6.2%	11.1%	7.7%	17.3%	3.9%
6.0 mm	2 nd	5.1%	1.2%	11.0%	15.8%	8.6%
	3 rd	9.9%	4.1%	10.2%	16.6%	11.6%
12.0 mm	2 nd	11.9%	11.5%	12.0%	10.0%	16.4%
	3 rd	14.0%	16.0%	11.9%	14.2%	17.6%
24.0 mm	2 nd	8.2%	5.6%	25.4%	15.1%	16.0%
	3 rd	17.1%	12.5%	39.9%	21.6%	15.6%



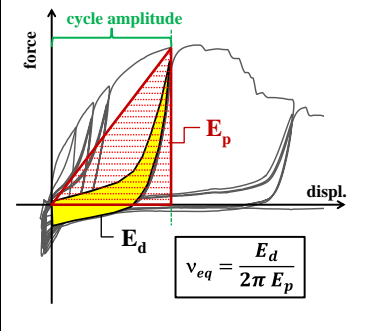
However, strength degradation is limited to the range 10%-15% for the axial displacement up to 12 mm, confirming that this phenomenon is not detrimental of the load-carrying capacity in the typical working displacement range of hold-down connections.

4.6.5. Dissipated energy and viscous damping

According to EN 12512 (EN-12512), the capability of the connection to dissipate energy in case of cyclic loading can be estimated through the equivalent viscous damping (v_{eq}). Table 7 reports the average values of the viscous damping for series LD-0, -7.5, -15, -30 and -45 when subject to different amplitudes of axial displacement cycles.

Results reported in Table 7 show an increasing trend of the equivalent viscous damping with the level of the lateral displacement, with some exceptions in the case of LD-45. Moreover, comparing the values of viscous damping for the 2nd cycle and the 3rd cycle, a very small reduction for all the examined cycle amplitudes and lateral displacement levels can be observed, confirming that strength degradation phenomenon is not relevant and does not affect the dissipative capacity of hold-down connections subject to tests.

Table 7 Mean values of equivalent viscous damping (v_{eq}) from cyclic tests conducted at different levels of axial displacements



Cycle Amplitude	EQUIVALENT VISCOUS DAMPING v_{eq} – EN 12512					
	v_{eq}	LD-0	LD-7.5	LD-15	LD-30	LD-45
4.5 mm	2 nd	3.79%	5.76%	10.46%	17.44%	19.18%
	3 rd	3.49%	5.16%	10.67%	17.34%	19.16%
6.0 mm	2 nd	3.98%	6.43%	9.53%	14.34%	10.26%
	3 rd	3.60%	6.35%	9.60%	13.57%	10.63%
12.0 mm	2 nd	4.40%	6.20%	6.81%	10.93%	7.74%
	3 rd	4.11%	5.57%	6.30%	10.19%	7.13%
24.0 mm	2 nd	6.38%	7.16%	14.50%	6.31%	8.74%
	3 rd	5.81%	6.31%	6.80%	5.70%	8.28%

In order to better understand the actual dissipative capacity of the hold-down connection at different levels of prescribed lateral displacement, the mean values of the dissipated energy for each cycle displacement amplitude are plotted in Fig. 4.26.

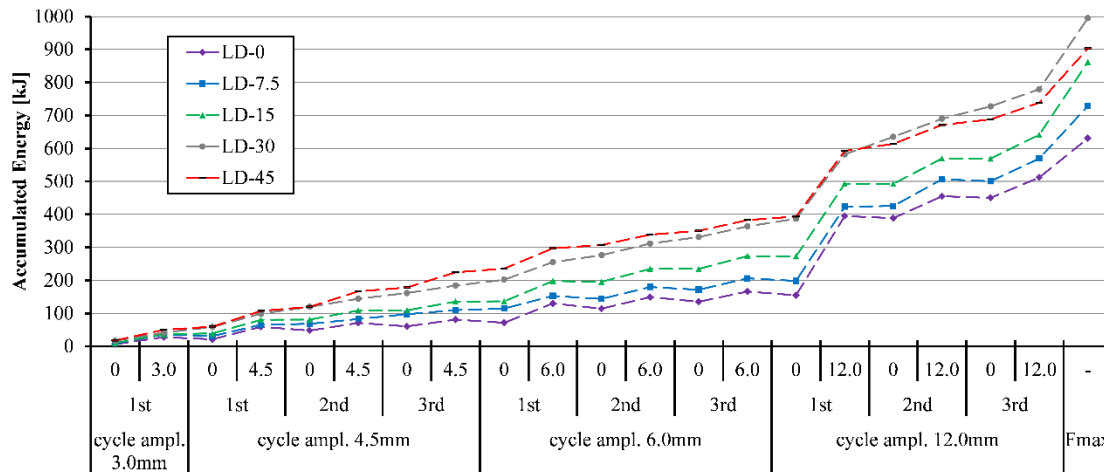


Fig. 4.26 Mean values of the dissipated energy for each axial cycle at prescribed values of lateral displacement (0, 7.5, 15, 30, 45 mm)

Comparing the total amount of dissipated energy, an increasing trend with the level of prescribed lateral deformation can be observed, with some exceptions for LD-45. This result is coherent with the trend of the equivalent viscous damping values registered for the different configuration up to the peak force value reported in Table 7.

4.7. Critical discussion

The results of tests performed on 15 specimens subjected to different levels of imposed lateral deformation confirm that stiffness, yielding displacement, and load-carrying capacity are affected by the coupling shear-tension action on hold-downs. The obtained results show good repeatability, confirming the quality and adequacy of the designed test setup.

Data processing has been done using two methods, the one suggested by EN 12512 (EN-12512 2011) which defines the linearization points of the experimental curve depending on the F_{max} achieved, and the Equivalent Energy method (Munoz et al. 2008) based on energy equivalence considerations. In both cases, a significant dependence of axial behaviour of the hold-down on the imposed lateral deformation is highlighted, especially in terms of: maximum strength, yielding point, elastic stiffness, ductility and equivalent viscous damping. Consequently, design practice should be updated, taking the interaction between axial and lateral behaviour of hold-down connections into account.

Experimental results compared to analytical estimation of the load-carrying capacity demonstrate that the adoption of the mean values of the mechanical parameters (i.e. wood

density, fastener yielding moment etc.) in the general model suggested by Johansen (Johansen 1949) provides reliable estimation of the load-carrying capacity of nailed hold-down connection subjected to traction (without imposed lateral displacement). On the other hand, the load-carrying capacity of the configuration with imposed lateral displacement cannot be predicted with the standard approach and then specifically developed models are necessary.

Finally, results from monotonic and cyclic tests on hold-down connections can be used to define guidelines and models for a safety design of metal connectors in CLT structures. Last but not least, they provide a basic information for advanced and reliable investigation on CLT structures, by means of specifically calibrated analytical models suitable to define the actual hold-down axial resistance at different level of lateral displacement.

Chapter 5. Monotonic and cyclic tests on angle bracket connections

Summary of Chapter 5

The purpose of Chapter 5 is evaluating the interaction between shear and tension forces on typical angle bracket connections used in CLT structures, as it has been done for hold-down connectors in the previous chapter. The same test setup has been exploited for both campaigns on CLT traditional joints. Specimen geometry, mechanical properties and loading protocol procedures will be illustrated. The angle brackets experimental campaign is the continuing of the work conducted on hold-down connections at CIRI-Edilizia & Costruzioni laboratories of the University of Bologna. Results from monotonic and cyclic tests will be reported and critically discussed. In particular, the connection response has been studied under lateral and axial loads simultaneously applied. From test results, all the significant mechanical properties of the connection (e.g. stiffness, yielding and failure condition, ductility etc.) will be defined adopting different methods. Furthermore, also the variation of angle bracket's shear strength while deformed axially will be delineated. As conclusion, test outcomes highlighted that the engineering design practice is not sufficiently coherent with the showed experimental response, and may represent an unsafe calculation procedure when angle brackets are subjected to bidirectional solicitations.

5.1. Test configuration and setup

The test setup used for the experimental campaign on angle bracket connection is the same employed for the hold-down tests, and previously described more in detail. The particular disposition of the actuators, with respect to the connection rotated at 90°, is aimed at imposing simultaneously axial and lateral deformations. Fig. 5.1 shows the test setup configuration for the angle bracket connection experimental campaign.

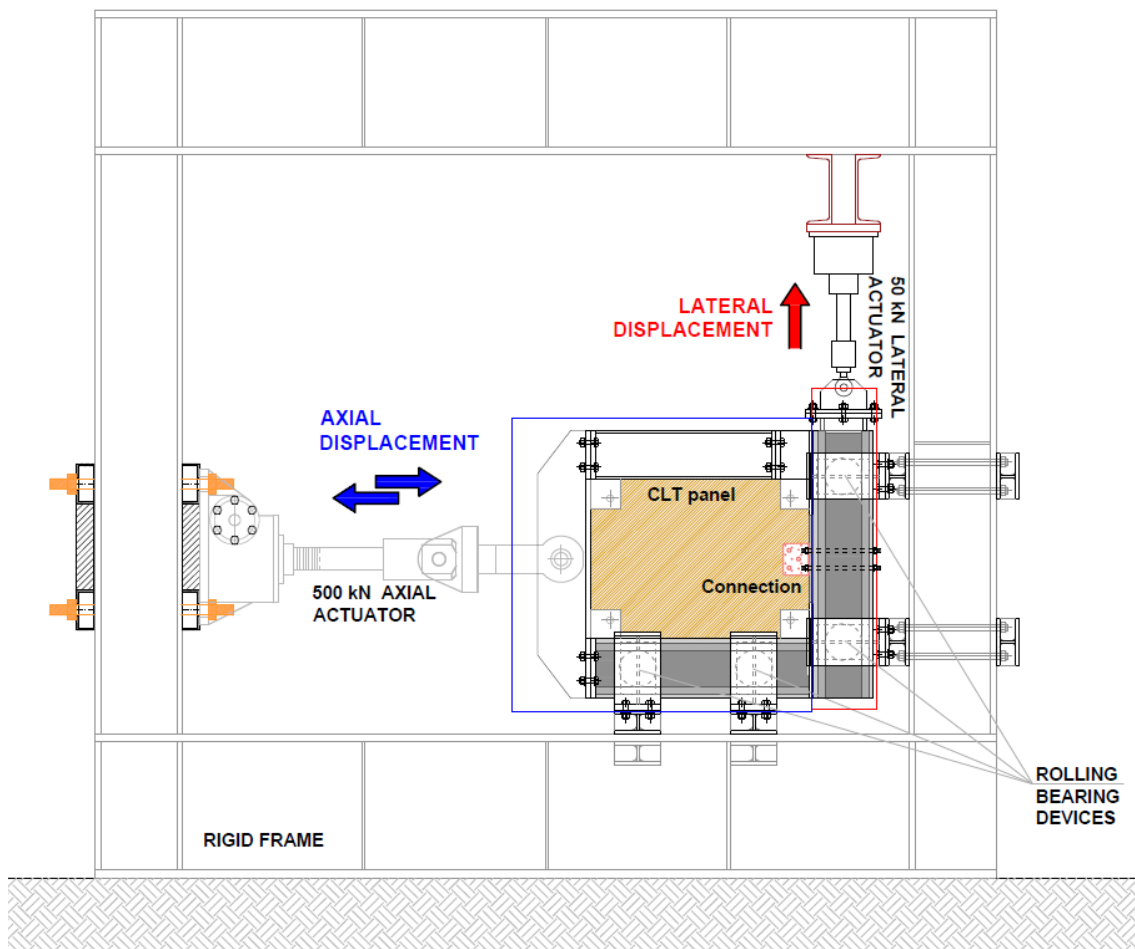


Fig. 5.1 Drawing of the test setup for angle bracket connection

First set of experimental tests on hold-down validate the proper functioning of the setup excluding eccentricity in the system. Therefore, for this second part of the campaign only one side of the CLT panel was connected to the angle bracket.

As Fig. 5.2 displays, the CLT panel has been inserted in a steel cage that was connected to the external rigid frame through rolling bearing devices.

To prevent out-of-plane displacement the panel has been blocked by four corner bolts. The angle bracket has been fixed to the CLT panel by the use of eight nails, while to the steel base side with two bolts.



Fig. 5.2 Angle bracket connection setup

In hold-down connections the principal direction was the axial one, since they are used mainly to resist traction, and so they were investigated with an imposed lateral displacement. For angle brackets that principally operate to resist shear force the main direction is the lateral one, therefore the imposed displacement in in this case was axial.

5.2. Specimen components characteristics

Each specimen is composed by two main parts: 5-ply CLT panel and angle bracket plus nails. The CLT panel (C24 grade) was made of spruce and has 5 layers configuration for a total thickness of 140 mm, refer to Fig. 5.3. CLT panels are certified according to European Technical Approval (ETA-14/0349) prescriptions. Specimen dimensions are 750 mm × 550 mm. As prescribed by EN 1380 (EN-1380) the panels were conditioned at $(20 \pm 2)^\circ\text{C}$ temperature and $(65 \pm 5)\%$ relative humidity for 15 days before performing the tests.

C panels			Panel design [mm]						
The grain direction of the cover layers is always parallel to the production widths.			storänsso						
Thickness [mm]	Panel type [-]	Layers [-]	C***		L		C***		C***
			C***	L	C***	L	C***	L	
60	C3s	3	20	20	20				
80	C3s	3	20	40	20				
90	C3s	3	30	30	30				
100	C3s	3	30	40	30				
120	C3s	3	40	40	40				
100	C5s	5	20	20	20	20	20		
120	C5s	5	30	20	20	20	30		
140	C5s	5	40	20	20	20	40		
160	C5s	5	40	20	40	20	40		


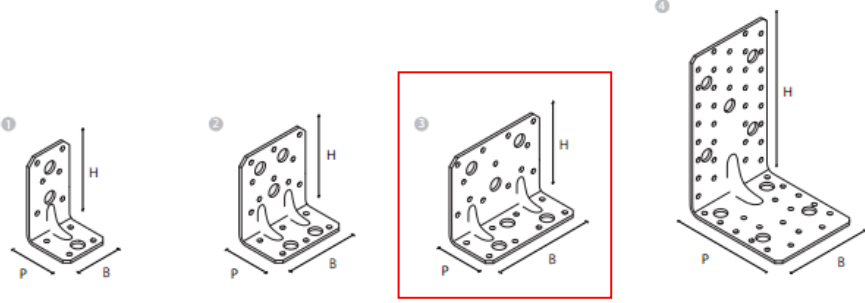


Fig. 5.3 CLT panel layer configuration

The angle brackets used in the test are WVS90110 type (same used in SOFIE project and by Gavric (Gavric et al. 2014)) with eight annular ringed nails 40x60 mm (ETA-04/0013), and were anchored to the base support with 12 mm diameter bolts (8.8 grade). Standard dimensions for WVS90110 angle bracket follow the European Technical Approval (ETA-09/0323), as Fig. 5.4 reports.

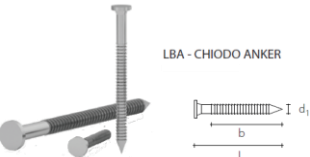
WVS 9050 + WBR 170
With reinforcement

CE 5328 GALV



code	type	B [mm]	P [mm]	H [mm]	s [mm]	n Ø5 [pcs]	n Ø11 [pcs]	n Ø13 [pcs]	pcs/box
1	PF101050 WVS90050	50	50	90	3,0	10	-	3	100
2	PF101055 WVS90080	80	50	90	3,0	16	-	5	100
3	PF101060 WVS90110	110	50	90	3,0	21	-	6	50
4	PF100125 WBR170	95	110	170	3,0	53	-	9	25

LBA - CHIODO ANKER



codice	tipo	d ₁ [mm]	L [mm]	b [mm]	pz/conf
PF601440	LBA440		40	30	250
PF601450	LBA450		50	40	250
PF601460	LBA460	4	60	50	250
PF601475	LBA475		75	60	250
PF601410	LBA4100		100	80	250

Fig. 5.4 Angle bracket and nail geometry (Rothblaas catalogue)

Fig. 5.5 illustrates the exploded view drawing of the specimen components, only one side of the panel was connected to an angle bracket.

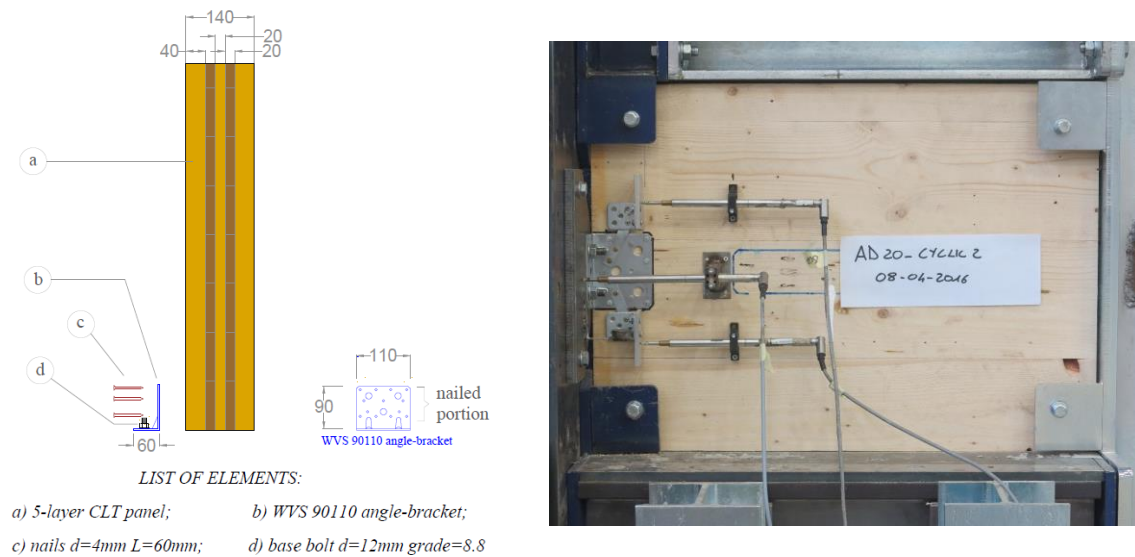


Fig. 5.5 Explode view and assembly of the test specimen

5.3. Loading protocol

The objective of the tests is evaluating the influence of the axial deformation on the lateral capacity and stiffness of the angle bracket connection. To define and better understand the behavior of the joint, cyclic and monotonic tests have been conducted using five different levels of imposed axial displacement. In particular, two cyclic and one monotonic tests were planned for each level of displacement, for a total of fifteen specimens.

Using a horizontal actuator the axial displacement (and a corresponding axial force) was applied and kept constant, in Table 8 five desired displacement levels are listed.

Table 8 Different levels of imposed axial displacement

AXIAL DISPLACEMENT (AD-XY) mm					
Imposed XY axial displacement values	0	5	10	15	20

After reaching the predefined axial displacement, through a second vertical actuator, the lateral displacement has been applied, either with cyclic and monotonic load paths. Thanks to the load cells positioned in the actuators also the variation of forces, for both

directions, were recorded. The monotonic procedure is prescribed by EN 26891 (EN-26891), while the cyclic protocol is prescribed by EN 12512 (EN-12512), both were showed in Fig. 4.6.

The tests labeled as follows: AD–XY are performed with lateral displacement maintained equal to “XY” mm during the total axial monotonic or cyclic phase.

For all tests, the adopted procedure followed these steps: (1) a monotonic axial displacement was prescribed to the connection up to the target value and kept constant during the test (called “axial displacement phase” or “axial phase”); (2) the lateral displacement was then prescribed (called “lateral displacement phase” or “lateral phase”), following the protocol for monotonic test or the protocol for cyclic test, maintaining constant the axial displacement up to the end of the test. Figures below show the displacement protocols adopted for both axial and lateral displacement phases for the monotonic (Fig. 5.6) and for the cyclic (Fig. 5.7) tests, respectively.

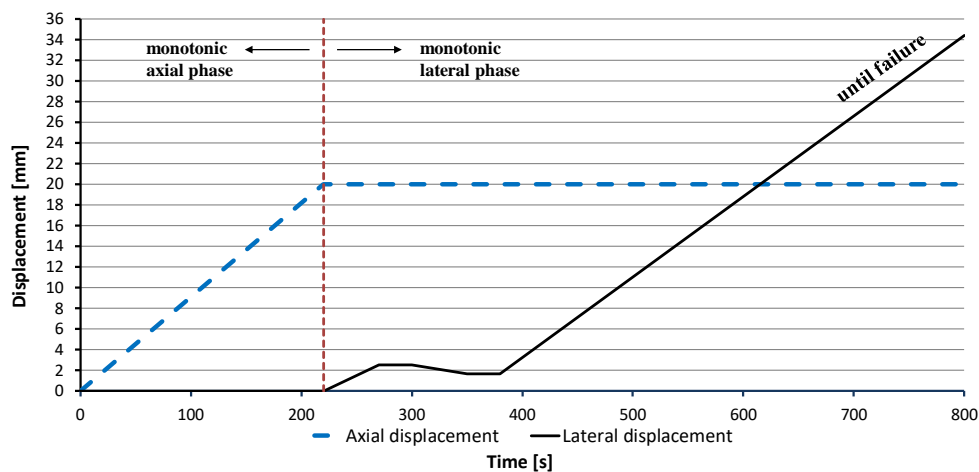


Fig. 5.6 Protocol followed for monotonic tests (AD-20 as example)

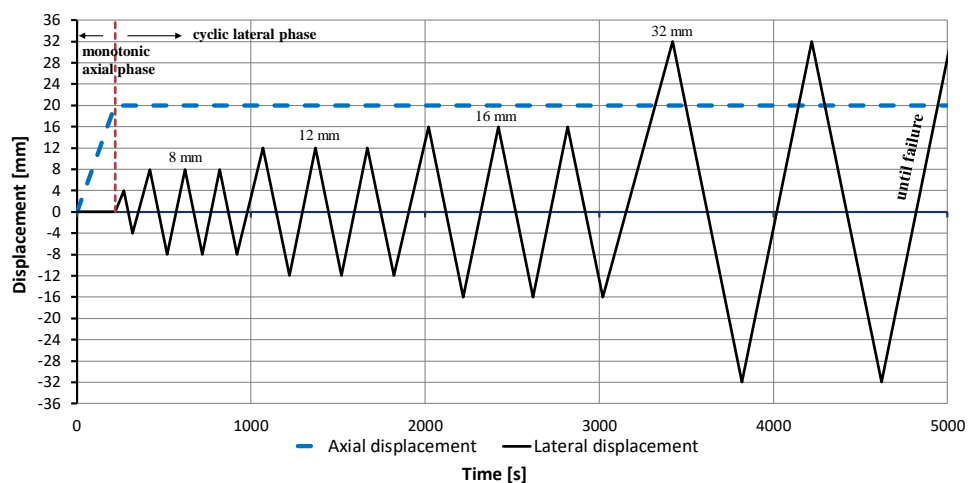


Fig. 5.7 Protocol followed for cyclic tests (AD-20 as example)

The rate has been maintained constant during cycles (0.2 mm/sec).

5.4. Instrumentation

As for the hold-down configuration, the two uncoupled degrees of freedom (axial and lateral displacements) were measured respect to the fix support using two electronic transducers (LVDTs). The LVDT named CH.2 reads the axial displacement, while CH.4 evaluates the lateral displacement, see Fig. 5.8.

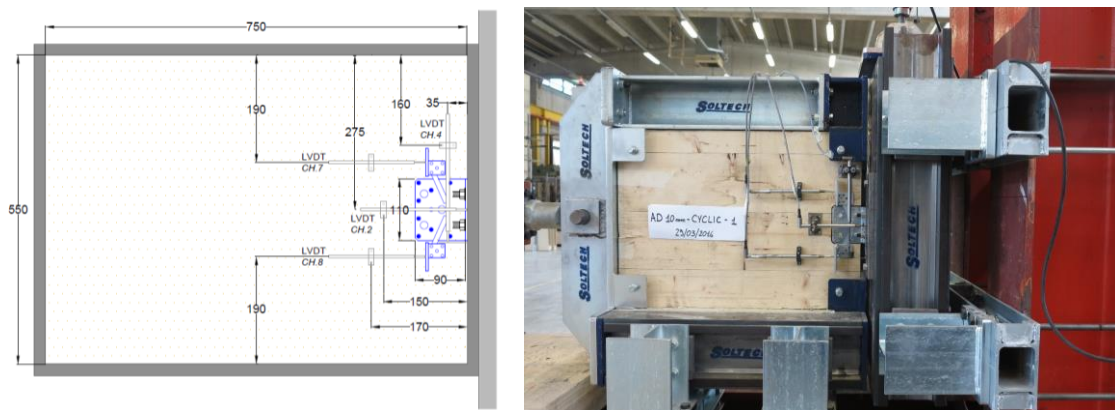


Fig. 5.8 Side view of the specimen and position of the measurement instruments

Two additional LVDTs were placed (CH.7 and CH.8) in the axial direction to quantify the relative displacement between the CLT panel and the angle-bracket connector, in order to evaluate the nails deformation and the rotation of the bracket.

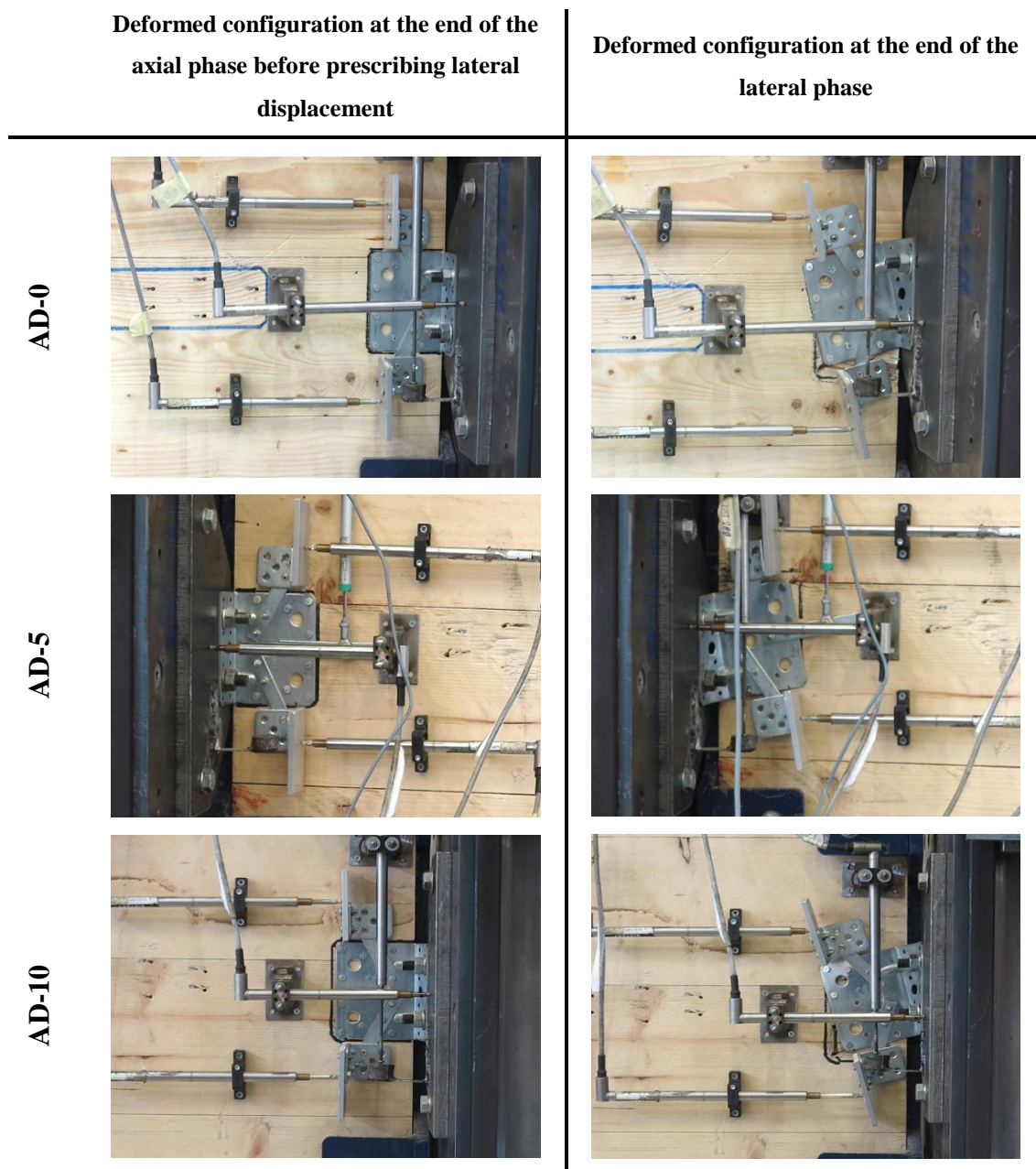
5.5. Test results and discussions

In this section, the results of monotonic tests (5 specimens) and cyclic tests (10 specimens) are shown. Failure modes are investigated and the most significant load - displacement curves are hereinafter reported.

5.5.1. Observed failures

The application of the load in two directions makes interesting focusing on the progression of the deformation phases in the angle brackets.

Fig. 5.9 illustrates, for all the imposed axial displacement sets, the deformed configuration of the bracket at the end of the axial phase and after the second lateral phase. A black line marked the non-deformed position of the angle bracket.



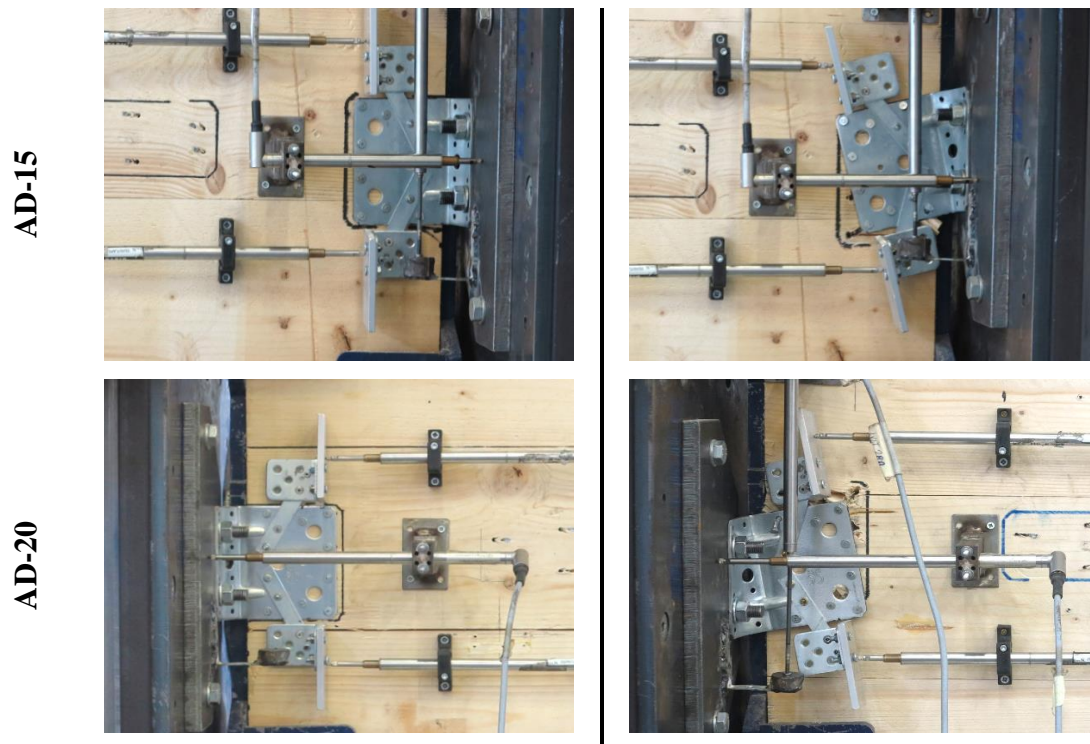


Fig. 5.9 Deformed shapes of test specimens for different values of axial displacement

The failure at the end of the connection tests was concentrated in the fasteners (Fig. 5.10) used to attach the angle bracket to the CLT panel. The ultimate response on the angle bracket follows what expected from Johansen's theory (Johansen 1949), that is the formation of two plastic hinges in the nails plus the embedment of the wood in the hole contour.

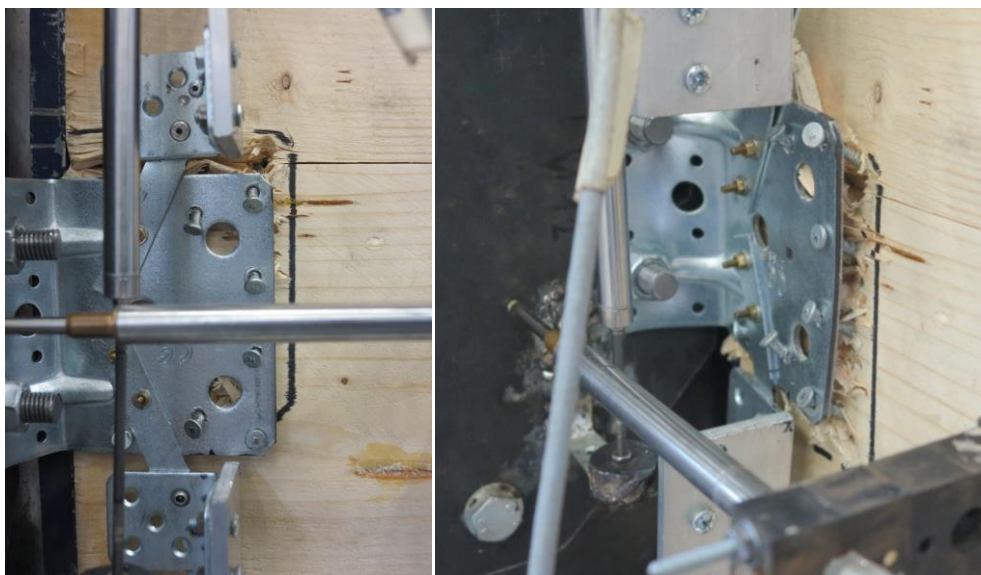


Fig. 5.10 Failure of the connection with plasticization in the nails

Fig. 5.11 shows the final damages in the wood and in the angle bracket. In fact, part of the axial force was taken by the steel bracket, in particular the steel plate deformed in correspondence of the fold where there were not nearby connectors.

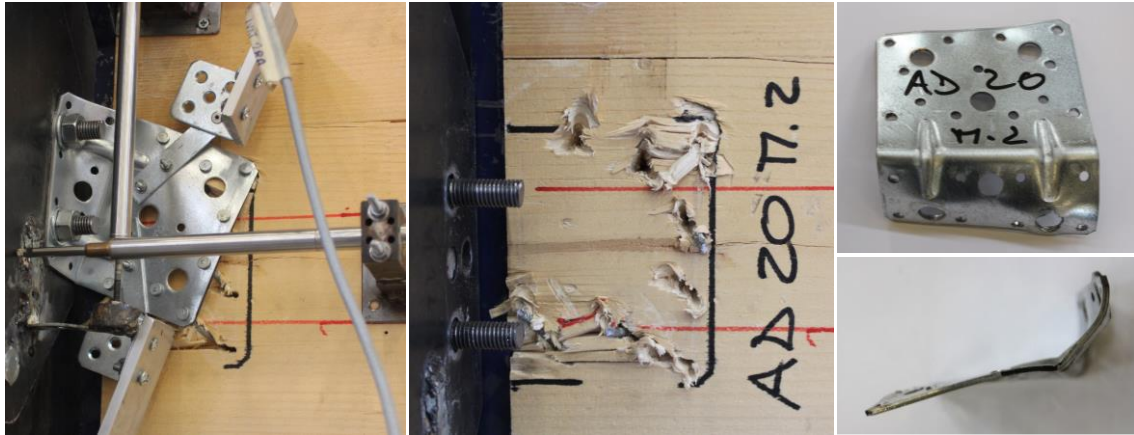


Fig. 5.11 Failure of the connection with consequent embedment in the panel and deformed steel bracket

The passage of the shear force, from the base bolts to the nails centroid in the wood, implies the formation of twisting moments in two directions, one in plane due to the vertical eccentricity and another out-of-plane due to the horizontal eccentricity (Fig. 5.12).

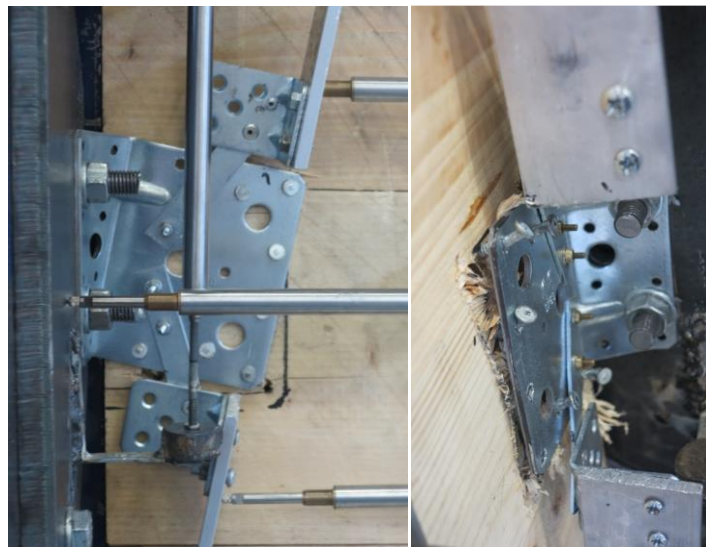


Fig. 5.12 In-plane and out-of-plane rotation of the angle-bracket

For higher levels of imposed axial displacement, such as AD-15 and AD-20, this rotation was amplified, causing a local crushing in the wood and almost the complete extraction of the fasteners (Fig. 5.13).

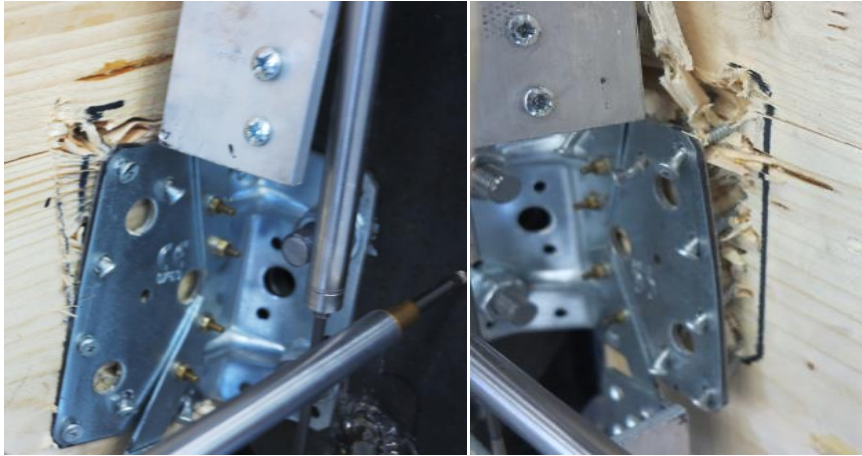
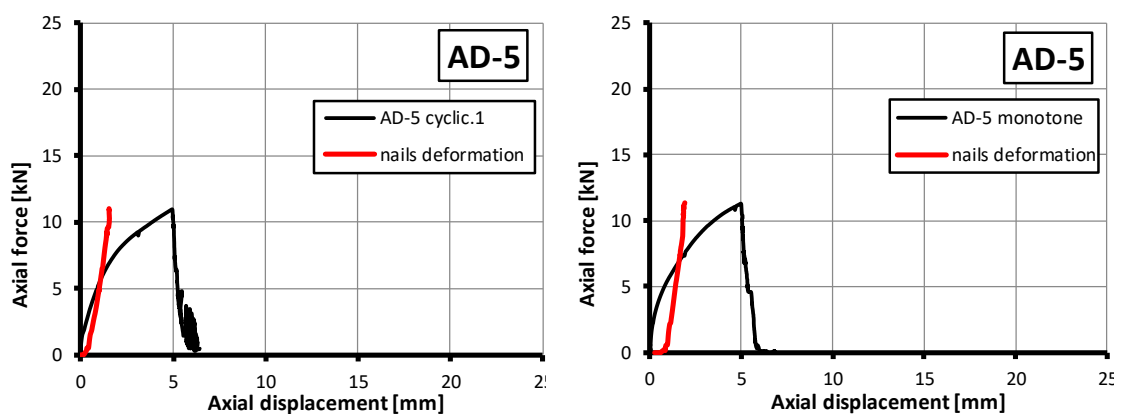


Fig. 5.13 Corner wood crushing and nails pull out

However no brittle failures were observed thanks to the correct design of the number of nails adopted for the connections (Jorissen & Fragiaco 2011).

5.5.2. Deformation of angle-bracket steel plate

The angle bracket steel plate showed a relevant plastic deformation, as previously highlighted, and therefore it is interesting to better look how the read in axial deformation was split between the deformation in the fasteners and the steel plate itself. In order to do so, measurements from the two additional vertical transducers (CH.7-8) were taken as the relative axial displacement of the nails. Fig. 5.14 shows the plots of the axial force versus the axial displacement for the five different imposed axial target levels, both for cyclic and monotonic load tests. The graphs compare the reading values from the actuator to the ones derived from the LVDTs, giving a direct estimation of the relative vertical movement in the connection.



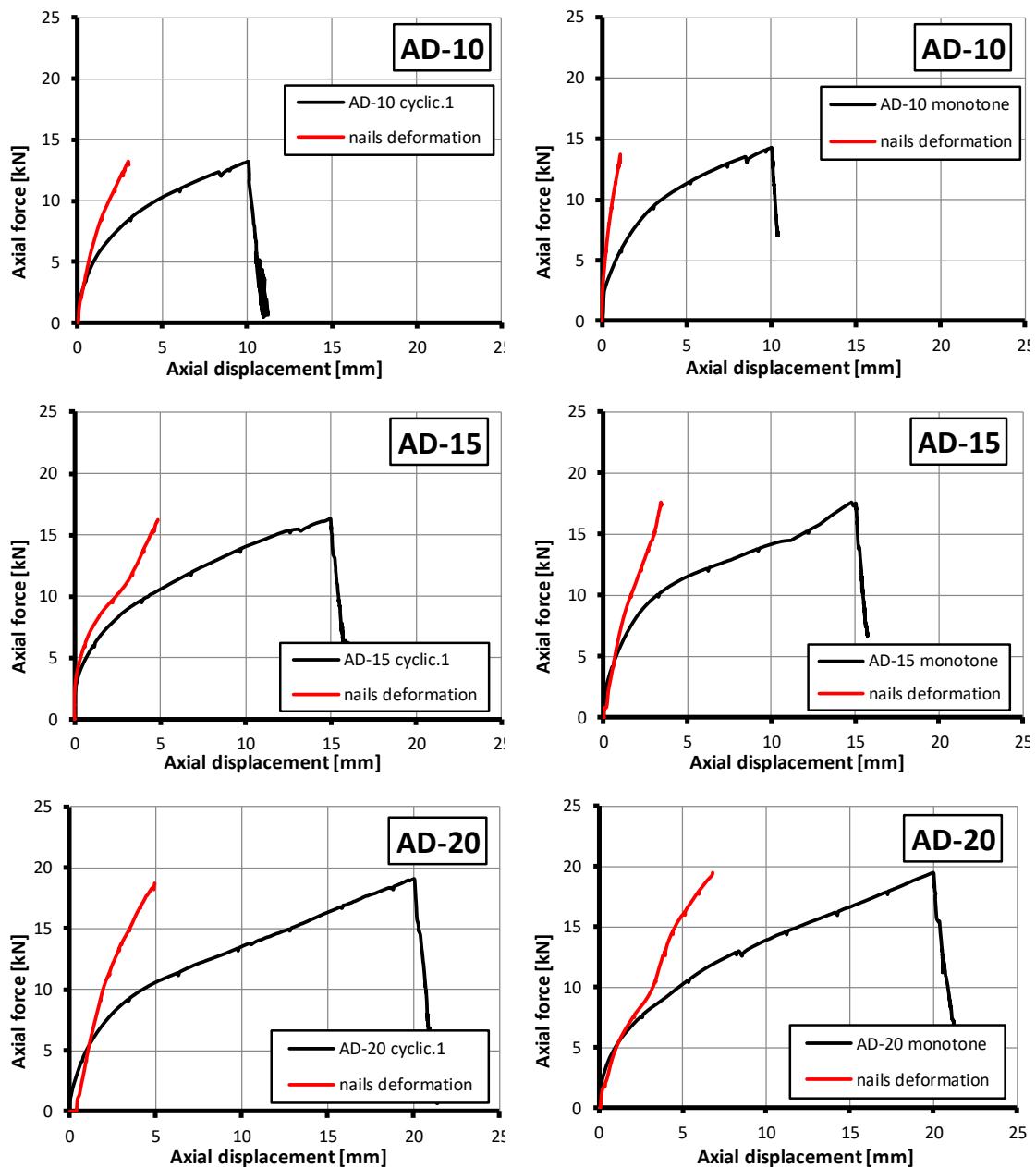


Fig. 5.14 Imposed axial displacement on the connection and nails deformations for cyclic (left) and monotonic (right) tests

The axial deformation is mainly concentrated in the steel plate, the nails contribution is relatively small. For higher imposed displacement levels, the percentage of fasteners deformation slightly increase, as reported in Table 9 and Table 10.

This is probably due to a slackening in the portion fixed to the CLT panel, since an increase in the axial force correspond to a growth of a secondary out-of-plane moment. This way the fasteners release in part the steel bracket but are still under traction.

Table 9 Comparison between the imposed axial displacement and nails deformation for lateral cyclic loading

Cyclic (mean value 1&2)	Angle bracket connection axial deformation			
	Nails displacement (mm)	Def. %	Angle bracket displacement (mm)	Def.%
AD-0	–	–	–	–
AD-5	1.5	30%	3.5	70%
AD-10	3	30%	7	70%
AD-15	5	33.3%	10	66.7%
AD-20	5	25%	15	75%

Table 10 Comparison between the imposed axial displacement and nails deformation for lateral monotonic loading

Monotonic	Angle bracket connection axial deformation			
	Nails displacement (mm)	Def. %	Angle bracket displacement (mm)	Def.%
AD-0	–	–	–	–
AD-5	1.5	30%	3.5	70%
AD-10	2	20%	8	80%
AD-15	3.5	23.3%	11.5	76.7%
AD-20	7	35%	13	65%

5.5.3. Axial force vs axial displacement curves

For the complete five test series the axial displacement was initially imposed and kept constant to the prescribed value during the lateral phase.

Axial force vs. axial displacement curves are illustrated in Fig. 5.15 for the monotonic trial, and Fig. 5.16 for the cyclic tests. Figures below reports, with different symbols, the points corresponding to the mean force-displacement values at:

- (i) the end of the axial displacement phase (i.e., achievement of the maximum imposed lateral displacement equal to 0, 5, 10, 15 and 20 mm);
- (ii) the achievement of the maximum lateral force;
- (iii) the achievement of a lateral displacement equal to 32 mm during the 1st cycle.

The graph of monotonic tests (Fig. 5.15) calls the attention to the drop of the axial force from the end of the axial phase to the achievement of the maximum lateral force in the

connector. The reduction of the axial force value decrease slightly with the increase of the imposed level.

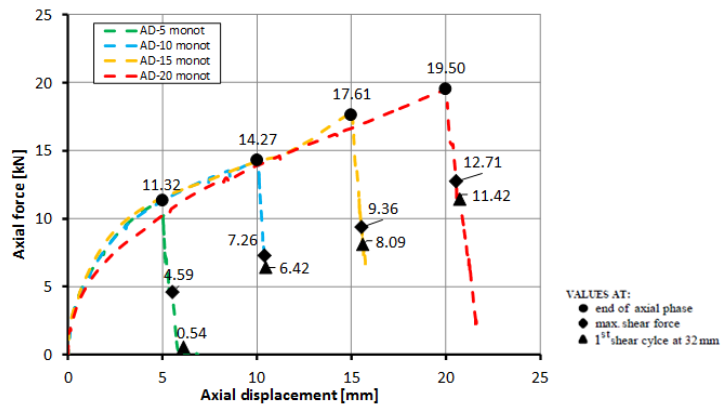


Fig. 5.15 Axial force vs. axial displacement for monotonic tests (AD 0-5-10-15-20)

For lateral cyclic tests the reduction of the axial force is almost total, this leads to the fact that within cycles the axial force fades little by little.

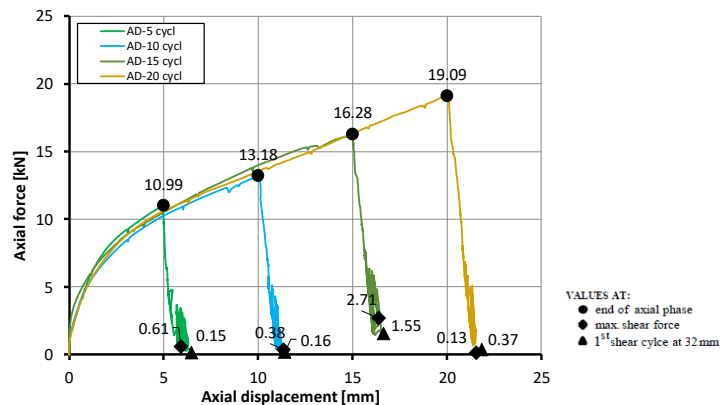


Fig. 5.16 Axial force (mean value) vs. axial displacement for cyclic tests (AD 0-5-10-15-20)

5.5.4. Shear force vs lateral displacement curves

Lateral displacements and the associated shear forces will be reported for all the test series, both monotonic and cyclic. In Fig. 5.17 results from monotonic and the two cyclic lateral tests (named “cyclic 1” and “cyclic 2”), for the different level of imposed axial displacement (AD-XY), are compared.

The superposition of the cyclic and monotonic curves shows not evident differences in terms of strength and ductility, this presupposes that the overall behavior of the connection is not strongly influenced by the cyclic load.

Similar observations to those done for the hold-down connections can be made for the angle brackets. In fact, looking at experimental results it can be noted that for increasing values of imposed axial displacement, a consequent reduction of the maximum force achieved during the tests is observed (about 23% from AD-0 to AD-20). Moreover, an increase of initial stiffness can be noticed for upper values of axial displacements.

The reason would probably be that when the steel bracket deforms axially, at first, the shear stiffness relies on the steel plate, and then is related to the fasteners.

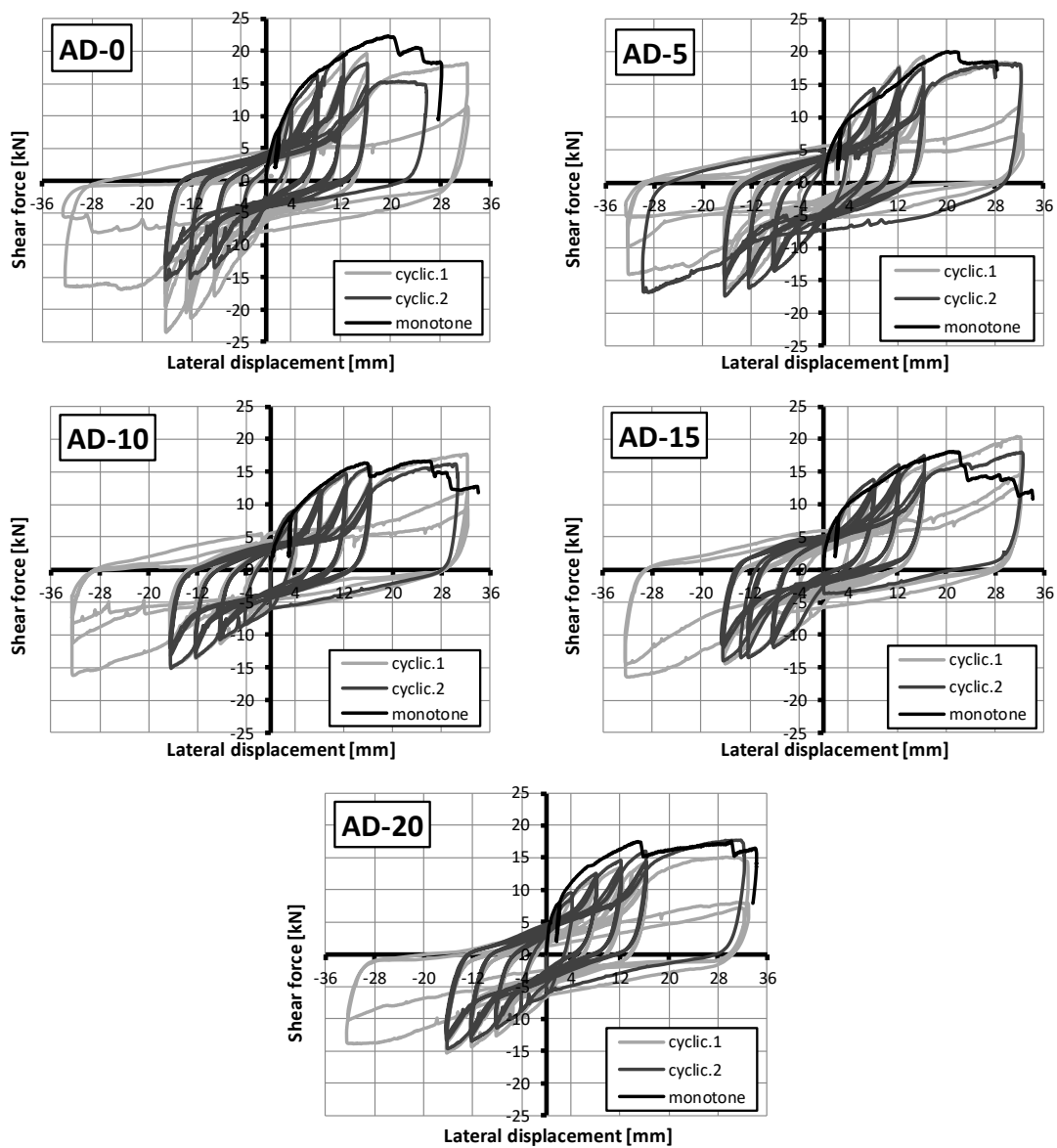


Fig. 5.17 Shear force vs. lateral displacement curves for the five test series (AD 0-5-10-15-20): comparison of monotonic and cyclic results

Fig. 5.18 summarizes and presents monotonic and cyclic curves, comparing the response for the different displacement target levels (AD_{XY}). No significant correlations was

found between the ultimate lateral displacement (defined correspondent at 20% load reduction) and the imposed axial displacement.

In particular, from the monotonic curves summary, it is possible to observe (better from the monotonic curves) a rise in the ascending branches possibly caused by the deformations and rotations in the steel bracket, that was becoming more and more a resistant part of the connection.

The force jumps, visible in the monotonic plots, are due to the progressive loss of nails and the consequent redistribution of the force in the remaining fasteners.

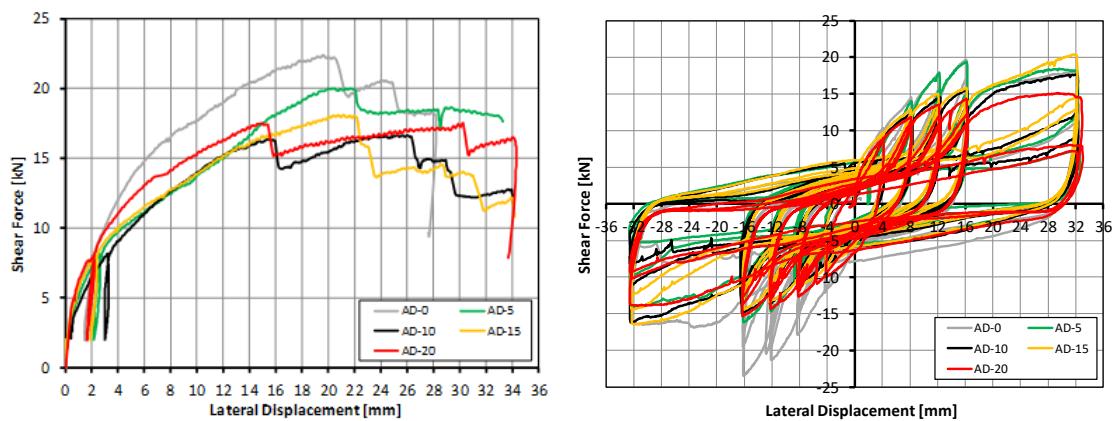


Fig. 5.18 Shear force vs. lateral displacement for monotonic (right) and cyclic (left) tests

Fig. 5.19 displays the significant reduction of the axial force over the cyclic lateral load protocol, for all the examined configurations (AD 0-5-10-15-20).

In particular, AD-15 and AD-20 targets show an oscillatory trend started close by where the lateral yielding displacement was expected, as a demonstration of the interaction between the two loading directions.

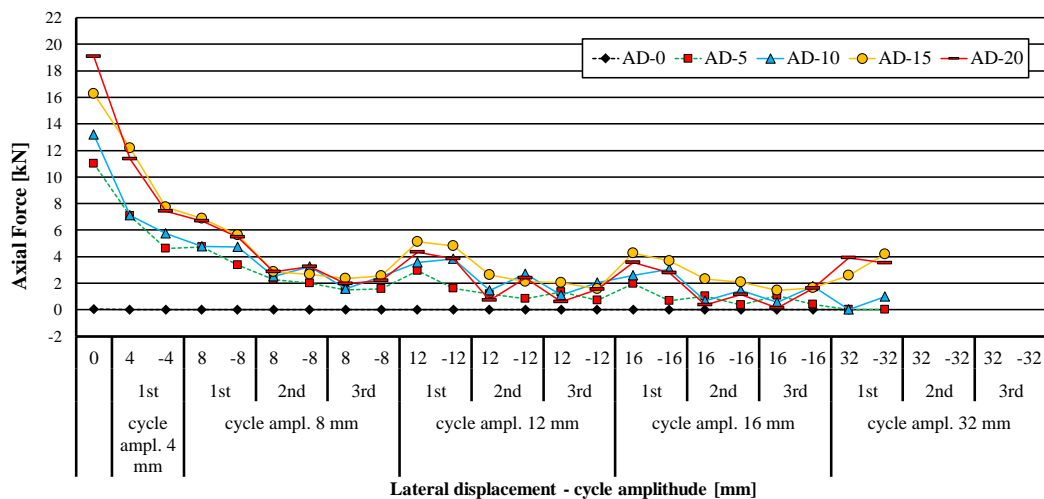


Fig. 5.19 Axial force (mean value) evolution during the cyclic loading

The trend of the shear force during repeated cycles have a down gradient, as Fig. 5.20 reports. The difference of peak forces between repeated cycles for the same lateral displacement is more evident for low values of the imposed axial displacement, while the degradation decrease for higher levels of axial deformation. This is the result of having, for bigger level of axial displacement, a connection that have been already despoiled of part of its initial stiffness, consequently to the vertical deformation.

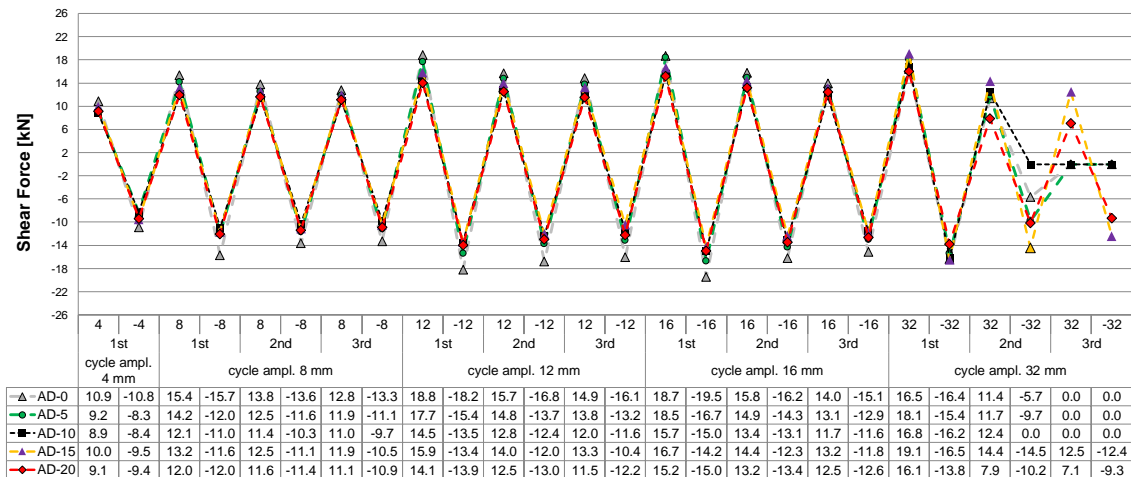


Fig. 5.20 Shear force (mean value) evolution for repeated lateral displacement cycles

5.6. Analysis of the results

In this section, results of the lateral displacement phase of the tests are analysed according to the procedure prescribed by EN 12512 (EN-12512) and EN 26891 (EN-26891) for cyclic and monotonic tests, respectively. The mean values of force and stiffness for each specimen are defined, together with strength degradation and equivalent viscous damping registered at every cycle.

5.6.1. Procedures for the definition of yielding point

The experimental capacity curve of steel-to-timber connection generally does not show a well-defined yielding limit, therefore simplified procedures are defined to delineate the points of interest to describe the connection behaviour.

Different criteria can be adopted for the definition of the yielding condition starting from experimental results. To elaborate angle bracket results, four different linearization

methods have been used and compared. The first one is based on EN 12512 (EN-12512) provisions and the second one is based on an energetic approach (the so called Equivalent Energy methods (Jorissen & Fragiaco 2011)). The first two listed criteria were previously described, and adopted to characterize the hold-down connection as well.

Additionally, other two methods have been introduced in this part: the Equivalent Energy Plastic Curve (EEEP) and the Yamasura & Kawai criteria (Y&K) (Munoz et al. 2008).

The EEEP linearization approach is based on energy equivalence principles and has been mainly applied for steel and concrete systems. The yielding force (P_y) is defined by the following formula:

$$P_y = \left(\Delta_{failure} - \sqrt{\Delta_{failure}^2 - \frac{2 \cdot w_{failure}}{K}} \right) \cdot K \quad (1)$$

Where $\Delta_{failure}$ is the ultimate displacement correspondent to the 80% of the maximum force, $w_{failure}$ is the experimental accumulated energy and K is the initial stiffness defined as illustrate in Fig. 5.21.

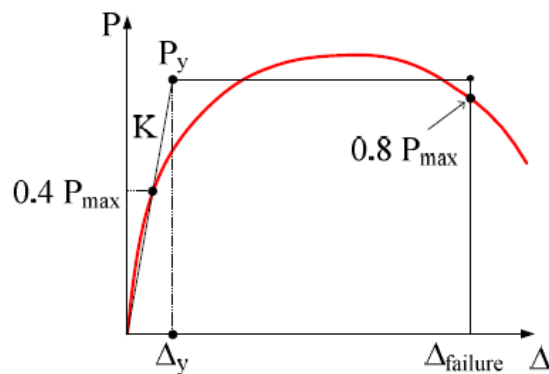


Fig. 5.21 Equivalent Energy Plastic Curve (EEEP) method

In Yamasura and Kawai (Y&K) criteria the initial stiffness is calculated between 10% and 40% of the peak load. After that, a straight line between 40% and 90% of the peak load and a straight line tangent to the load–displacement curve and parallel to the 40% and 90% secant line are determined. This last line represents the immediate post-elastic zone before reaching the peak load. Finally, the point of intersection between the initial stiffness with this new tangent is projected horizontally towards the load–displacement curve to obtain the respective yield point displacement (Fig. 5.22).

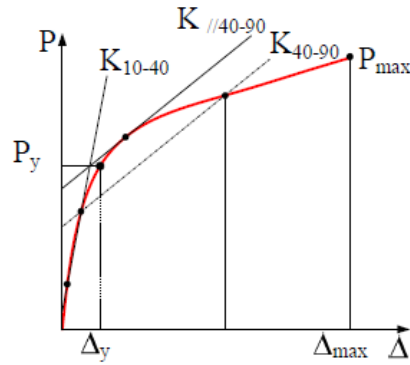


Fig. 5.22 Yasumura and Kawai analysis method for the determination of the yield point

5.6.2. Tri-linearization methods of experimental curves

Once defined the yielding limit, the tri-linear approximation of the experimental load-displacement curve can be defined.

As represented in Fig. 5.23, the tri-linear approximation is obtained joining the following points: the origin of the axis (0; 0), the yielding point ($d_y; F_y$), the peak point ($d_{F_{max}}; F_{max}$) and the point corresponding to the failure condition ($d_{F_u}; F_u$). The so obtained three branches are characterized by the stiffness: k_1 (elastic stiffness), k_2 (post-elastic stiffness) and k_3 (softening stiffness).

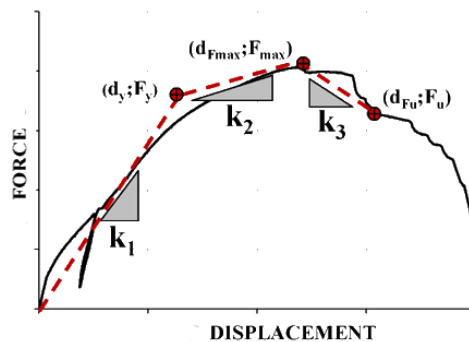


Fig. 5.23 Tri-linearization of experimental curve

Evidently, from the above listed different methods, four tri-linearization curves have been defined based on the criteria used to define the yielding limit.

Fig. 5.24 shows the tri-linear approximation for cyclic (mean values from the two) and monotonic tests for all the axial displacement configurations (AD 0-5-10-15-20).

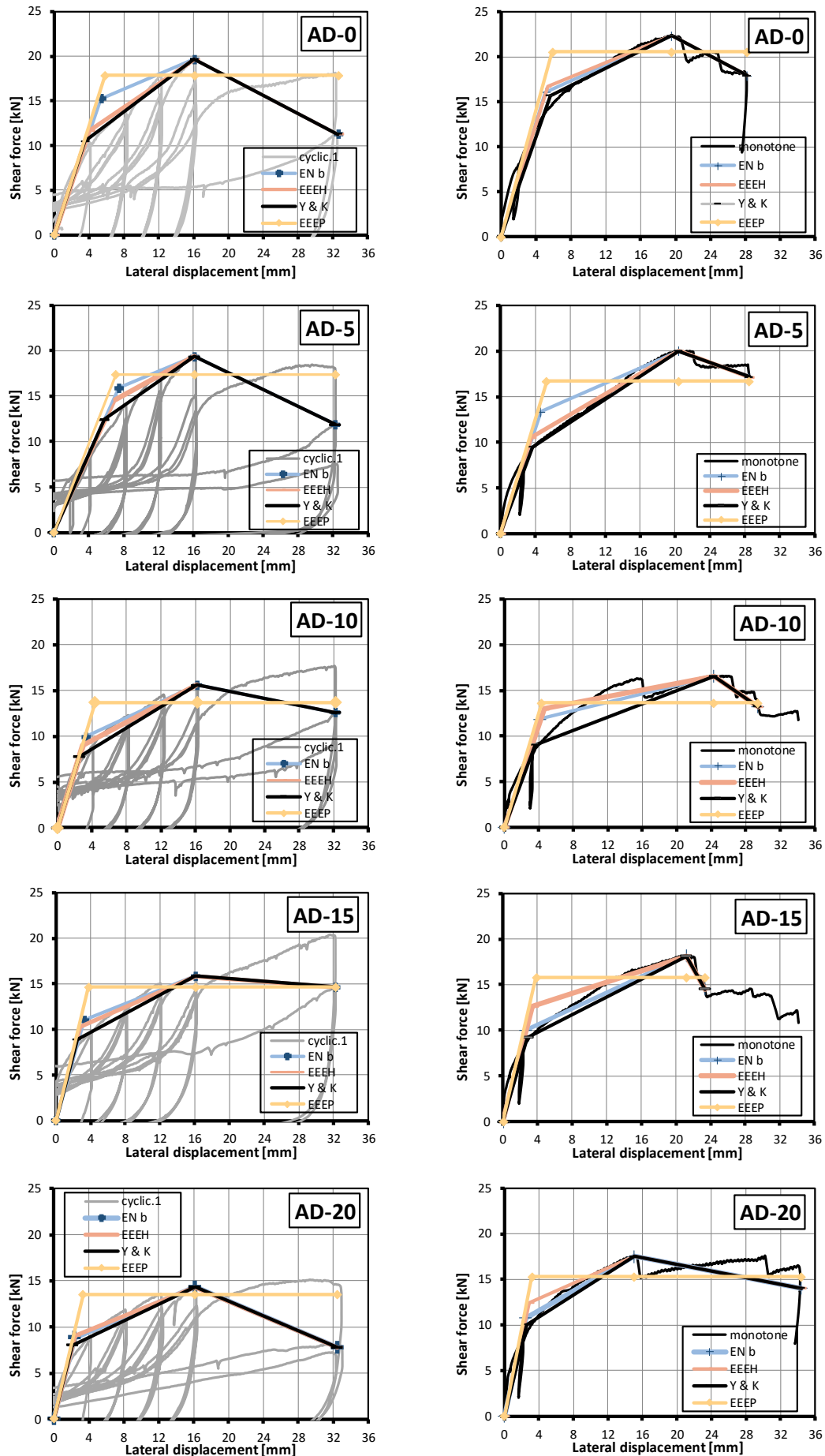


Fig. 5.24 Tri-linear approximation curves for cyclic and monotonic results for imposed AD-XY levels

From the overlapped tri-linearization curves for each test specimen, it is possible to observe how ENb, EEH, Y&K criteria gives closer values (especially for the cyclic tests), whereas EEEP method that is intended to simplify the experimental curve through an elastic-perfectly plastic behaviour amplifies the resultant yielding force.

In this case, while for the monotonic curves the ultimate point has been considered $0.8F_{max}$, for cyclic curves the ultimate point has been chosen as the force at the second cycle of the maximum imposed lateral displacement (32 mm).

Fig. 5.25 reports the displacements corresponding to the yielding point (d_y), the achievement of the peak force (d_{Fmax}) and of the ultimate force (d_{Fu}) for the five levels of axial displacement (0, 5, 10, 15, 20 mm).

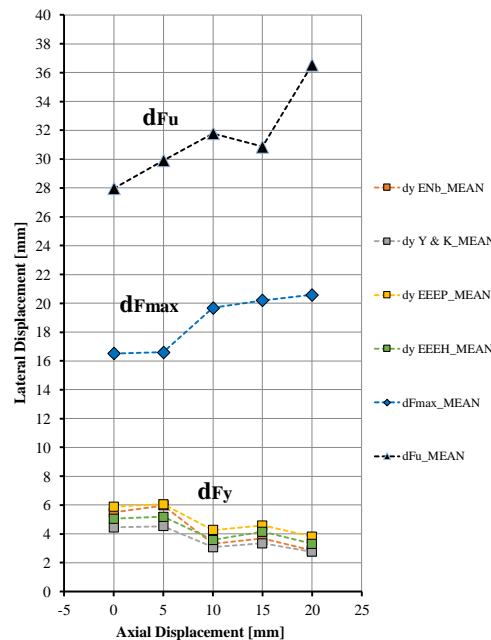


Fig. 5.25 Displacement point values of the tri-linearization curves (mean value) for different prescribed axial displacement (AD 0-5-10-15-20)

It is possible to observe that:

- (i) the yielding displacement (d_y) decreases for higher imposed axial displacement target, independently from the method used to define the post-elastic stiffness;
- (ii) the trends of yielding displacement following the increase of axial displacement are the same for the four methods, only shifted in values;
- (iii) maximum and ultimate displacements raise when the imposed axial displacement far up;
- (iv) for higher axial displacements the ductility of the connection increases;

Fig. 5.26 shows the forces corresponding to the yielding (F_y) value obtained from the different methods, the peak (F_{max}) and the ultimate values (F_u).

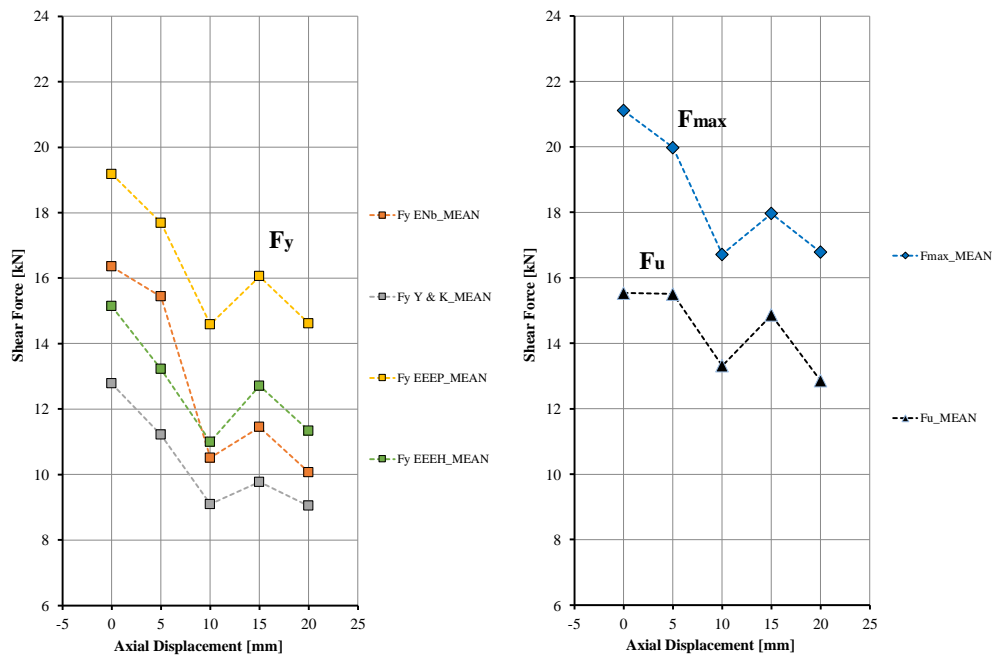


Fig. 5.26 Force point values of the tri-linearization curves (mean value) for different prescribes axial displacement (AD 0-5-10-15-20)

From the graphs is possible to notice that:

- (i) the force values decrease increasing the axial displacement up to AD-10, for higher target of axial displacements the lateral force indicate a correlation with the secondary direction movement;
- (ii) the reduction in terms of achieved force varying the axial displacement is evident in all the four methods (about 30% between AD-0 and AD-20);
- (iii) the yielding force value is strongly affected by the adopted method of linearization (as expected), Y&K and EEEH standards are the closest to the experimental behaviour;
- (iv) The peak force, as the ultimate, decrease increasing the axial displacement (about 20% from AD-0 to AD-20).

As last, Fig. 5.27 shows the stiffness values of the first elastic branch (k_1), the second post-elastic branch (k_2) and the softening branch (k_3) of the tri-linear curves obtained for the five levels of axial displacement AD-XY.

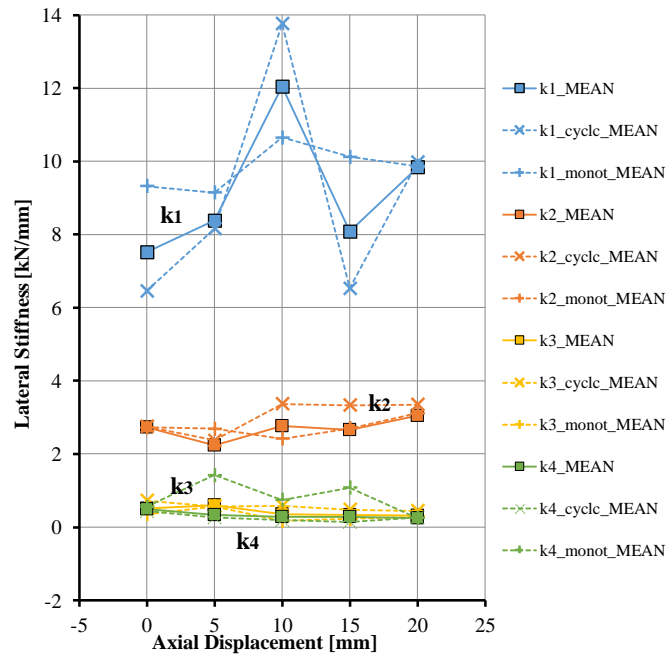


Fig. 5.27 Stiffness values of the backbone curves for different prescribed axial displacement (AD 0-5-10-15-20)

It is possible to observe that:

- (i) elastic stiffness (k_1) oscillates for increasing AD,
- (ii) the post-elastic (k_2) stiffness is not significantly influenced by the imposed AD;
- (iii) stiffness of the post-peak branch (k_3) slightly decreases for increased LD.

When the angle bracket connection is subjected to small axial displacement (i.e. the entire CLT wall assembly behaves elastically), the effect of the elastic stiffness variation is relevant (up to AD-10). As far as the first comment is concerned, the initial stiffness k_1 increases with the imposed AD because the initial configuration changes making the connection stiffer with respect to the non-deformed configuration. In fact, a higher value of shear force is necessary to obtain the same axial deformation (see Fig. 5.24).

However, even if the imposed AD causes an increase of the initial stiffness, the presence of an axial displacement reduces the registered maximum force, thus the connection strength.

In fact, what really change in the response of the connection growing in imposed axial displacements are the maximum force value reached and the yielding limit condition.

Finally, starting from the values of yielding and ultimate displacements, the ductility in shear (μ) of the angle bracket connection can be estimated.

Table 11 reports the ductility value as $\mu = d_{Fu} / d_y$, i.e., ratio between the mean value of the displacement at the ultimate force (d_{Fu}) and at the yielding force (d_y) for the series AD-0, 5, 10, 15 and 20.

Ductility values have been computed referring to the yielding estimation provided with all methods, for comparison.

Table 11 Mean values of ductility (μ) for different levels of axial displacements (AD 0-5-10-15-20)

μ	AD-0	AD-5	AD-10	AD-15	AD-20
EN(b)	5.14	5.59	10.37	10.21	13.20
Y & K	6.59	6.70	10.84	11.13	13.81
EEEP	4.79	4.96	7.38	7.66	9.72
EEEH	5.84	6.33	9.22	9.23	11.87

The results show a raise of the ductility values with the imposed axial displacement. This is due mainly for two reasons: the yielding displacement decreases for growing AD and part of the ductility is attributed to the steel bracket that keeps deforming.

5.6.3. Comparison with code provisions

To compare the experimental results with analytical formulations same theory, parameters and formulas described in Chapter 4 have been applied.

Angle bracket connections react mainly to shear load, therefore the principal direction of action is exactly 90° rotated respect to the hold-down connector.

The lateral load (as the real case) was applied at the base bolts through the movement of the vertical slide, the resulting shear force needs to be transferred to the nails centre and doing so, because of the double eccentricity, generates secondary moments in the bracket. The first is an out-of-plane moment that pull out the nails in one side and compress the other half, while the second cause an in-plane rotation (Fig. 5.28). This force equilibrium refers to a normal condition, which means not considering additional axial force.

Since the nails are pulled out, the contribution of the rope effect has been neglected in the fastener capacity.

It has been assumed that the connection behaves rigidly (all nails are contributing) until reaching the maximum force, rotating around its fastener centroid (Fig. 5.9).

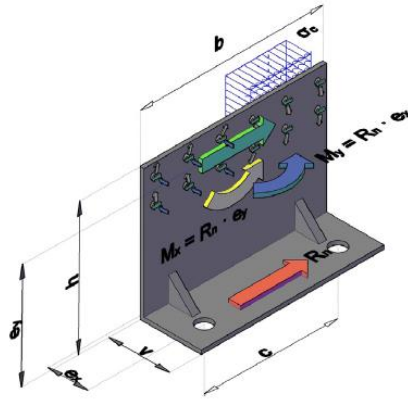


Fig. 5.28 Influence of the angle bracket geometry on force patterns on the nails fastener group (Tomasi & Sartori 2013)

To calculate the lateral capacity of every single fastener, the only parameter that has been changed is the embedding strength, considering its variation with the angle of action of the resulting force from the vectors sum.

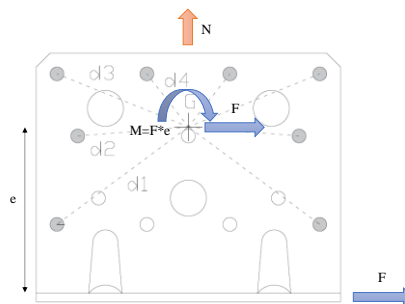


Fig. 5.29 Resulting forces in the angle bracket connector

A detailed calculation showed, in accordance with on what suggested in EC5 (EN-1995), that for small diameters fasteners (such as nails) the resulting embedment strength, and consequently the resulting capacity, is not strongly affected by the action angle respect to the wood fibres orientation.

Finally, following simplified procedures and equations the resulting capacity for the angle bracket does not change considerably with an increase in the axial load, departing from experimental values with the grow of the imposed axial displacement, as Fig. 5.30 and Table 12 report.

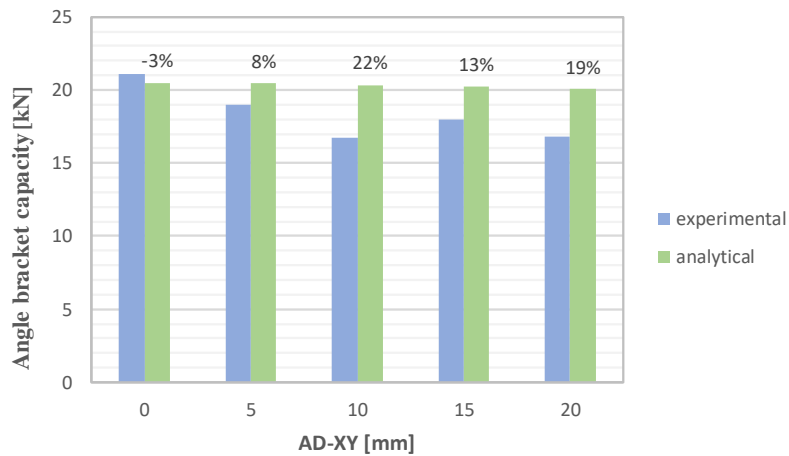


Fig. 5.30 Comparison between experimental and analytical angle-bracket connection capacity

Table 12 Analytical and experimental angle bracket connection capacity results

	$F_{max,mean}$ [kN]	$F_{analytical}$ [kN]	Δ
AD-0	21.11	20.50	-3%
AD-5	19	20.45	8%
AD-10	16.7	20.35	22%
AD-15	17.96	20.25	13%
AD-20	16.8	20.05	19%

5.6.4. Strength degradation

In order to verify the capability of the connection to withstand cyclic loads, the force degradation registered at the end of 2nd and 3rd cycles (of prescribed axial displacement level) is reported.

According to EN 12512 (EN-12512), force degradation ΔF is defined as the percentage difference between the force registered at the second (or third) cycle ($F_{2(or\ 3)}$) and that reached at the first cycle (F_1) (i.e., $(F_1 - F_{2(or\ 3)}) / F_1 \cdot \%$).

Table 13 reports the mean values of ΔF registered at the 2nd and at the 3rd cycles for the specimens subject to different levels of axial displacement (AD-0, 5, 10, 15 and 20). The results show that the reduction in the cycle peak forces decreases with the increase of the initial axial deformation (from 0 mm to 20 mm).

As mentioned above, a non-negligible strength degradation regards the more rigid configurations for shear in the connection (lower AD), while the phenomena is reduced for the latest AD since the connection has already been deformed.

Table 13 Mean values of strength degradation (ΔF) registered during the cyclic tests at different levels of the axial displacement (4,5 - 24 mm)

Cycle Amplitude	STRENGTH DEGRADATION - EN12512					
	ΔF	AD-0	AD-5	AD-10	AD-15	AD-20
8 mm	2 nd	10.02%	11.50%	5.61%	4.70%	3.39%
	3 rd	16.56%	16.29%	9.41%	9.58%	7.35%
12 mm	2 nd	16.31%	16.51%	11.92%	11.40%	10.96%
	3 rd	20.66%	22.23%	17.22%	16.20%	18.18%
16 mm	2 nd	15.94%	18.94%	14.96%	13.53%	13.18%
	3 rd	25.45%	29.09%	25.36%	20.89%	18.10%
32 mm	2 nd	37.27%	35.45%	29.09%	29.21%	45.05%
	3 rd	-	-	-	38.47%	50.49%

However, strength degradation is limited to the range 10%-17% for the lateral displacement up to 12 mm, confirming that this phenomenon is not detrimental of the load-carrying capacity in the typical working displacement range of angle bracket connections.

5.6.5. Dissipated energy and viscous damping

According to EN 12512 (EN-12512), the capability of the connection to dissipate energy in case of cyclic loading can be estimated through the equivalent viscous damping (v_{eq}). Table 14 reports the average values of the viscous damping for series AD-0, 5, 10, 15 and 20 when subject to different amplitudes of lateral displacement cycles.

Results reported in Table 7 show an increasing trend of the equivalent viscous damping with the level of the axial displacement, with some exceptions in the case of AD-15.

Moreover, comparing the values of viscous damping for the 2nd cycle and the 3rd cycle, a very small reduction for all the examined cycle amplitudes and lateral displacement levels can be observed, confirming that strength degradation is not relevant and does not affect the dissipative capacity of angle bracket connections subject to tests.

Table 14 Mean values of equivalent viscous damping (ν_{eq}) from cyclic tests conducted at different levels of axial displacements

		EQUIVALENT VISCOUS DAMPING % - EN12512														
		cycle ampl. 4 mm			cycle ampl. 8 mm			cycle ampl. 12 mm			cycle ampl. 16 mm			cycle ampl. 32 mm		
		1st	2nd	3rd	1st	2nd	3rd	1st	2nd	3rd	1st	2nd	3rd	1st	2nd	3rd
AD-0		20.8	22.3	19.3	19.5	19.9	18.1	17.8	18.9	18.0	18.0	23.5	13.0	-		
AD-5		10.8	23.0	17.4	17.0	18.6	17.1	17.1	18.2	17.4	18.2	23.3	11.6	-		
AD-10		13.4	24.9	18.4	18.2	20.8	17.7	17.3	18.4	18.4	18.7	24.0	12.2	-		
AD-15		13.0	22.6	16.4	15.2	18.2	18.1	14.9	17.4	16.3	16.8	19.9	11.3	-		
AD-20		13.1	24.4	18.2	17.2	20.2	18.1	18.1	18.6	18.8	18.1	26.4	15.0	-		

In order to understand better the actual dissipative capacity of the angle bracket connection at different levels of prescribed axial displacement, mean values for the dissipated energy at each cycle displacement amplitude are plotted in Fig. 5.31.

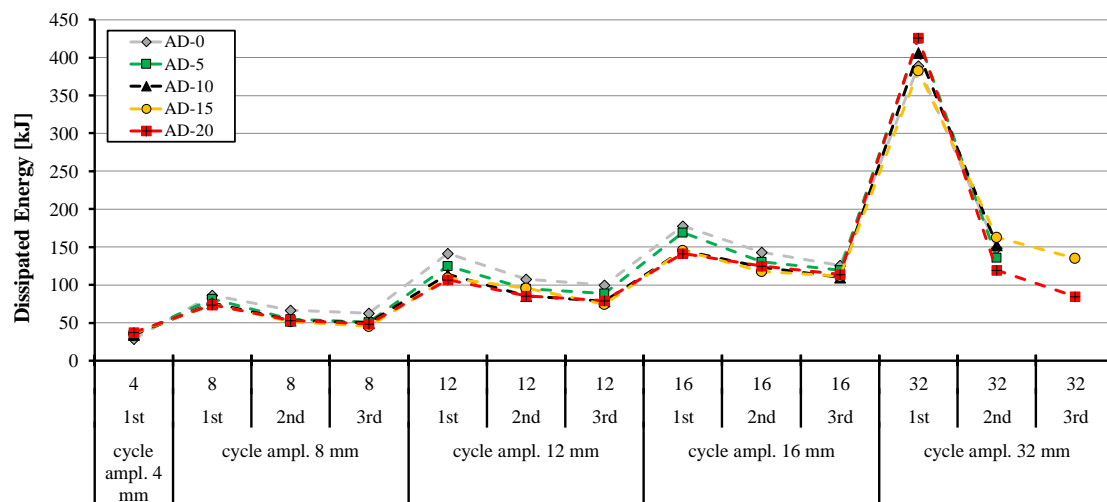


Fig. 5.31 Mean values of the dissipated energy for each axial cycle at prescribed values of axial displacement (0, 5, 10, 15, 20 mm)

Comparing the total amount of dissipated energy, an increasing trend can be observed when the lateral cycle displacement increase, as expected, while decrease after the first cycle repetition. This result is coherent with the trend of the equivalent viscous damping values registered for the different configuration up to the peak force value reported in Table 14.

5.7. Critical discussion

The results of tests performed on 15 specimens subjected to different levels of imposed axial deformation confirm that stiffness, yielding displacement, and load-carrying capacity are affected by the coupling shear-tension action on angle brackets.

Data processing has been done using four methods, in all cases, a significant dependence of shear behaviour of the angle bracket on the imposed axial deformation is highlighted, especially in terms of: maximum strength, yielding point, elastic stiffness. Consequently, design practice should be updated, taking the interaction between axial and lateral behaviour of angle bracket connections into account.

Experimental results compared to analytical estimation of the load-carrying capacity demonstrate that the adoption of the mean values of the mechanical parameters (i.e. wood density, fastener yielding moment etc.) in the general model suggested by Johansen (Johansen 1949) provides reliable estimation of the load-carrying capacity of nailed angle bracket connection subjected to shear (without or for small imposed axial displacement). On the other hand, the load-carrying capacity of the configuration with imposed axial displacement cannot be predicted with the standard approach, therefore further studies and specifically developed models are necessary.

Finally, results from monotonic and cyclic tests on angle bracket connections can be used to define guidelines and models for a safety design of metal connectors in CLT structures. In addition, they provide a basic information for advanced and reliable investigation on CLT structures, by means of specifically calibrated analytical models suitable to define the actual angle bracket lateral resistance at different level of axial displacement.

Part II: Low damage solutions for CLT

Summary of Part II

An alternative construction technology for multi-story timber buildings is solid timber building system. In particular, Cross-Laminated Timber panels, thanks to the cross-banded lay-up elements can carry loads in both directions either horizontally or vertically as free-standing components. Quasi-static and dynamic test results highlighted that the layout and design of the joints strongly influence the overall behavior of the structural system.

It is confirmed that all the dissipated energy is resulting from the connections and the ductility capacity of the system is limited or controlled by the detailing of the connections region.

One of the most desirable connection systems that resulted from precast concrete research (M. J. N. Priestley et al. 1999) is termed *hybrid connection*. The hybrid system includes post-tensioning which provides post-earthquake re-centering capability to the system, meanwhile additional external or internal steel elements serves as dissipative fuses.

This chapter presents an innovative hybrid system solution for lateral resistant CLT walls. In this section the design procedure, construction detailing, experimental results and a comparison with a simple numerical model of a 2-story 2/3 scale hybrid rocking CLT wall assembly will be presented. The behaviour of the hybrid system was investigated under quasi-static reversed cyclic loading protocol.

Experimental results showed a satisfying response, negligible damage in the CLT wall and a limited residual displacement. In addition, the rocking oscillation of the CLT panel will be illustrated in terms of variation of the neutral axis depth.

Results obtained from this test should be a start to improve and better understand the application of hybrid rocking design concepts to CLT wall panel, to reduce the number of traditional connections and at the same time incrementing shear wall response capacity.

Chapter 6. Presentation of hybrid rocking systems

6.1. Introduction

Nowadays, as in the past, all around the world we are facing as engineers the power of seismic events with better and better structural innovative building solutions. Nevertheless, the design goal considering major events has always been the “life safety” at the expense of the structural integrity. This means that structures designed in accordance with modern buildings codes are expected to sustain damage during a severe earthquake; however; these structures are expected to protect the lives of the occupants. On the other side, it is also important to consider that damages to the structures can require expensive repairs; significant business downtime; and in some cases the building reconstruction. Damages in constructions may include yielding, buckling or fracture of structural elements and permanent horizontal displacements after the earthquake, referred to as residual drift.

In this new context, the conventional prescriptive serviceability/life-safety design methodology of earthquake-engineered-buildings is no longer enough. Control of damage, definition of operational levels and other performance parameters are expected to be incorporate in seismic codes to define the required seismic performances. To address these shortcomings with current seismic lateral force resisting systems and to work towards more resilient; sustainable cities; a new class of seismic lateral force resisting systems that sustains little or no damage under severe earthquakes has been developed in the past. These new seismic lateral force resisting systems reduce or prevent structural damage to non-replaceable structural elements by softening the structural response elastically through gap opening mechanisms.

Rocking systems, with the help of unbonded pre-tensioning elements, tend to return to their original non-deformed position at every cycle and therefore display a self-centering response. A supplemental key feature to rocking system has been the addition of internal or external energy-dissipating devices that act as structural fuses by producing high initial system stiffness and then yielding to dissipate energy from the input loading and protect the remaining portions of the structure from damage.

6.2. Rocking systems

The so called rocking, or self-centering, systems are supplemental damping solutions that incorporate self-centering properties, allowing the structural system to return to, or near to, its original position after an earthquake. More in detail, rocking systems can be subdivided in two categories: *joined* (only post-tensioning) and *hybrid* (post-tensioning and energy dissipation devices) (Fig. 6.1).

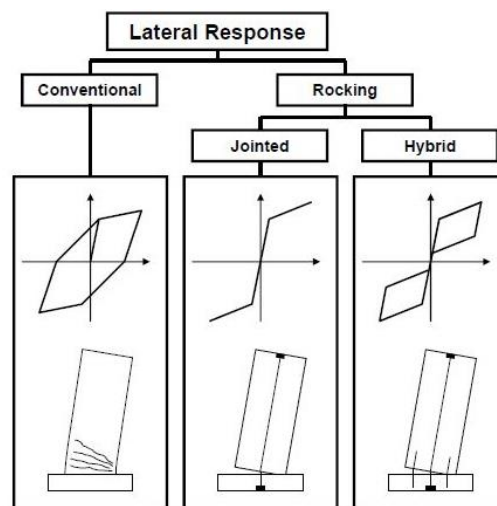


Fig. 6.1 Hysteretic response of various structural systems

Conventional seismic lateral force resisting systems are designed to dissipate energy through inelastic behaviour (i.e. permanent damage) of structural elements.

The joined design philosophy is the prevention of damage in the structural elements designed as the lateral load resisting system in a building. This is achieved by the preclusion of plastic hinges development. The system performance may be described as non-linearly elastic with formation of a gap at the base level (Fig. 6.2).

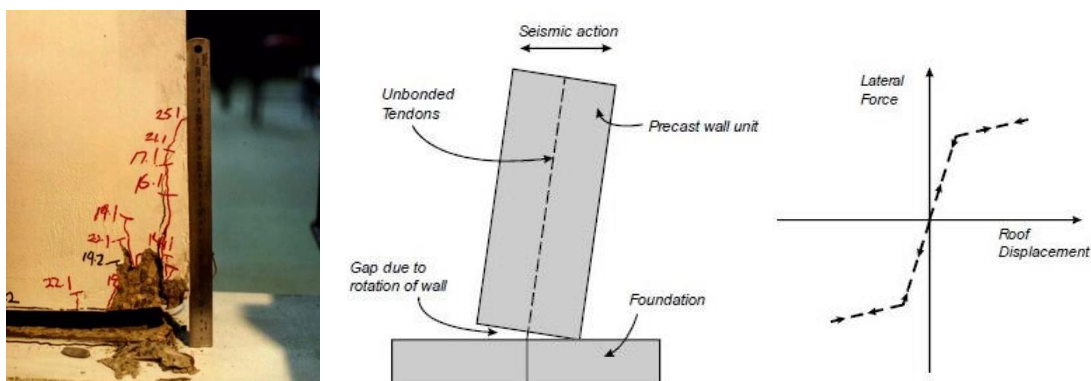


Fig. 6.2 Gap opening and schematic representation of a self-centering wall (Rahman & Restrepo 2000)

This gap results in a reduction in stiffness which is recovered as the elastic pre-stressing tendons or bars (act as a spring) restore the elements to their original position.

The prevention of inelastic deformations in the pre-stressed bars is a primary objective, as this will preclude post-earthquake residual drifts and affects the overall system response.

The rocking concept was combined with added energy dissipation devices in the design of the “stepping” railway bridge over the south Rangitikei River in New Zealand as the early application of self-centering system. Nevertheless, the first modern self-centering systems for concrete frames and walls were developed under the decade-long PRESS (PREcast Seismic Structural Systems) program in the United States in the 1990s, coordinated at the University of California, San Diego (Priestley 1991; M. J. N. Priestley et al. 1999; Nakaki et al. 1999).

The so-called “hybrid” rocking system was at a later time proposed, here self-centering and energy-dissipating properties were combined through the use of unbonded post-tensioning tendons or bars and longitudinal mild steel (or other dissipative devices) designed to yield and provide supplemental damping to the rocking system.

In particular, a fundamental aspect in this type of structural system is the energy dissipation that provides a channeling of seismic energy in a previous- defined “sacrificial” element. The concept of hybrid system is material independent and it has subsequently been extended from concrete to steel structures (Christopoulos et al. 2002) and to engineered wood structural systems (A. Palermo et al. 2006; Smith et al. 2007; Sarti et al. 2012).

The hybrid connection has the properties of both self centering and energy dissipation, by combining the moment contribution from energy dissipators and the post-tensioning. This particular dissipative and re-centering mechanism is described by “flag-shape” hysteresis behavior (force-displacement or moment-rotation cyclic behavior) (Fig. 6.3).

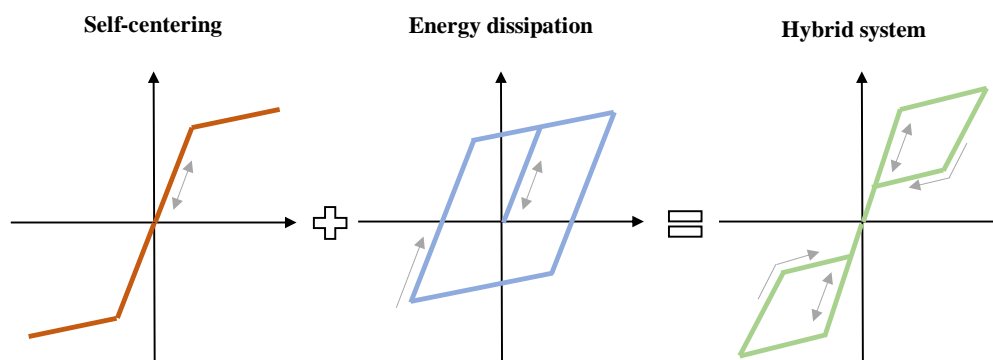


Fig. 6.3 Idealized hysteresis loops

When pure post-tensioned rocking section are used, typically multi-linear elastic hysteresis behaviour is observed and no hysteretic damping is provided. On the other side, when a dissipative post-tensioned rocking system is wanted, the integration of damping devices connected to the structural element is needed. The hybrid system's mechanics is summarised in Fig. 6.4.

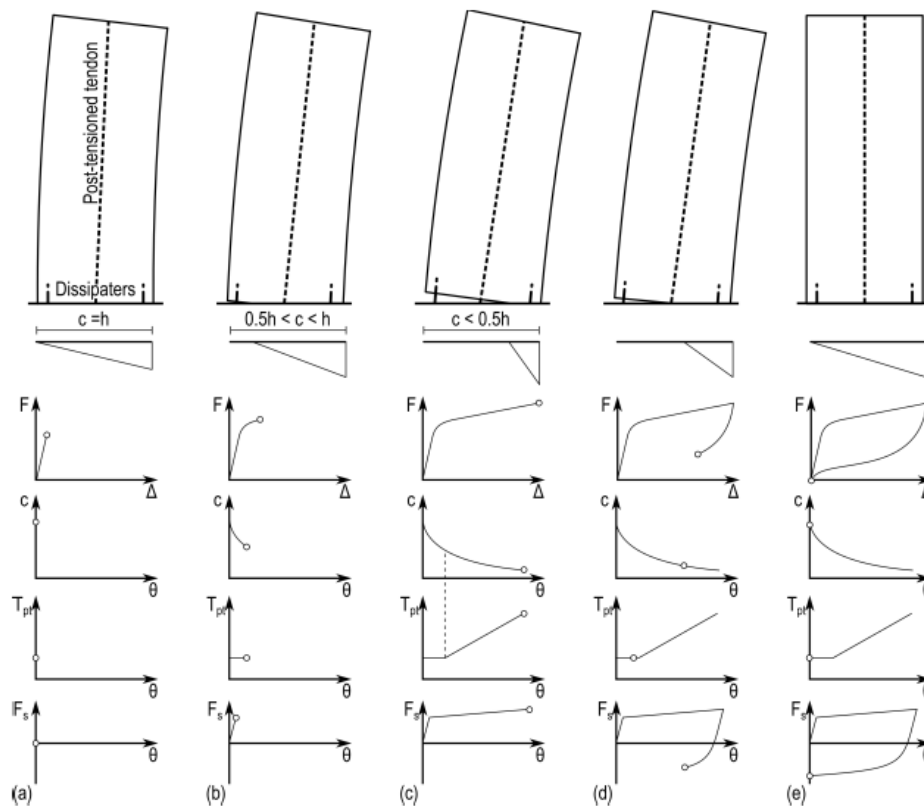


Fig. 6.4 Hybrid rocking system mechanisms: (a) decompression, (b) tensile yielding of the steel dissipater, (c) PT elements elongation, (d) compressive yielding in the steel dissipater and (e) re-centring (Sarti 2015)

Depending on the moment contribution ratio between self-centring and energy dissipaters a wide range of hybrid system flag shaped responses can be obtained. The design parameter λ represents the ratio between the moment contribution provided by the dissipative devices (M_s) and the total moment contribution (M_t). It follows that a relevant aspect of these systems is that they can be tailored to provide a specific amount of energy dissipation. The flag-shaped hysteretic response can be achieved using specialized energy dissipation devices (Passive Energy Dissipation, PED) or through innovative structural systems using traditional materials.

There are different energy dissipater types used to mitigate seismic effect as: hysteretic dampers (yielding of metals), friction dampers (frictional sliding) or viscoelastic or viscous-fluid dampers (deformation of viscoelastic solids or fluid), as shown in Fig. 6.5.


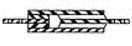
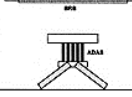
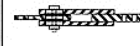
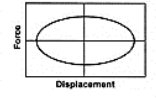
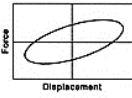
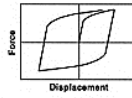
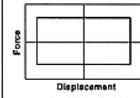
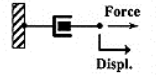
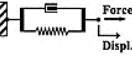
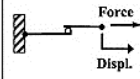
	Viscous Fluid Damper	Viscoelastic Solid Damper	Metallic Damper	Friction Damper
Basic Construction				
Idealized Hysteretic Behavior				
Idealized Physical Model			Idealized Model Not Available	
Advantages	<ul style="list-style-type: none"> - Activated at low displacements - Minimal restoring force - For linear damper, modeling of damper is simplified. - Properties largely frequency and temperature-independent - Proven record of performance in military applications 	<ul style="list-style-type: none"> - Activated at low displacements - Provides restoring force - Linear behavior, therefore simplified modeling of damper 	<ul style="list-style-type: none"> - Stable hysteretic behavior - Long-term reliability - Insensitivity to ambient temperature - Materials and behavior familiar to practicing engineers 	<ul style="list-style-type: none"> - Large energy dissipation per cycle - Insensitivity to ambient temperature
Disadvantages	<ul style="list-style-type: none"> - Possible fluid seal leakage (reliability concern) 	<ul style="list-style-type: none"> - Limited deformation capacity - Properties are frequency and temperature-dependent - Possible debonding and tearing of VE material (reliability concern) 	<ul style="list-style-type: none"> - Device damaged after earthquake; may require replacement - Nonlinear behavior; may require nonlinear analysis 	<ul style="list-style-type: none"> - Sliding interface conditions may change with time (reliability concern) - Strongly nonlinear behavior; may excite higher modes and require nonlinear analysis - Permanent displacements if no restoring force mechanism provided

Fig. 6.5 Passive energy dissipation devices in earthquake resistant buildings

Metallic yield dampers dissipate earthquake energy input through inelastic deformation of metals. Some particularly desirable features of these devices are their stable hysteretic behaviour, low-cycle fatigue property, long term reliability, and relative insensitivity to environmental temperature. A typical example can be X-shaped plate damper or ADAS (added damping and stiffness). Another example is the tension/compression yielding brace, also called the unbonded brace (or buckling restrained brace, BRB), which consists of a core steel profile encased in a concrete-filled (or epoxy-filled) steel tube. A special coating is provided between the core part and the filling in order to reduce friction. The internal mild steel profile provides stable energy dissipation by yielding under reversed axial loading, while the surrounding concrete-filled steel tube prevents compression buckling (Fig. 6.6):

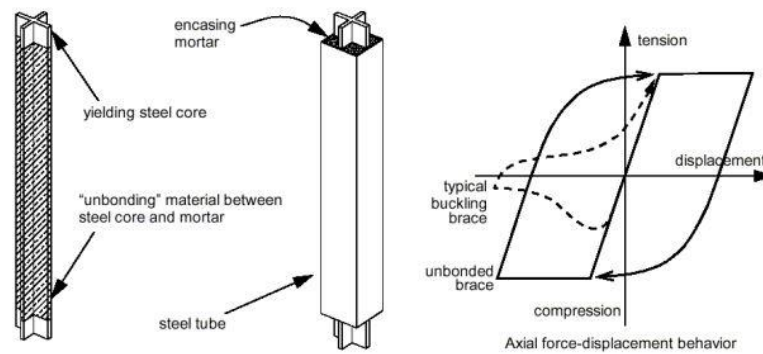


Fig. 6.6 Buckling-resistant unbonded brace (BRB)

Metallic energy dissipative devices are designed to yield during a large earthquake event but must be replaced afterwards; this leads to potentially expensive maintenance costs for system with internal dissipaters (mild steel bars) or with fixed connections (e.g. welded), which led to the development of externally mounted dissipaters.

6.3. Research background

The conceptual innovation of 'capacity design' introduced by professors Park and Paulay in the 1960s and 1970s is universally recognised as a major milestone in the development of earthquake engineering, and of seismic design philosophies in particular. Similarly, the concept of ductile connections able to accommodate high inelastic demand without suffering extensive material damage, developed in the 1990s, is the next development in high performance damage-resistant structural systems.

- Application in precast concrete structures

As previously outlined, one of the first applications of the above described concepts is the Rangitikei Railway Bridge in New Zealand that has been in operation since 1981, where rocking is combined with a hysteretic energy dissipation device.

After that, hybrid technological solution and the associated conceptual design were developed in the 1990s as an outcome of the collaboration U.S.-Japan research program under the title of the PREcast-Seismic-Structural-Systems (PRESSS), that has been a major force in the development of jointed ductile precast connections (Priestley 1991).

The intent of this research program was to improve the inelastic response, analytical modelling, design recommendations, and to improve the understanding of “ductile” precast buildings.

Hybrid systems have firstly been developed on concrete precast beam column subassembly where mild steel dissipaters were coupled to post tensioned cables (Stanton et al. 1997), as shown in Fig. 6.7. The similar self-centring concept was used by Stanton and Nakaki (Stanton & Nakaki 2002) in the development of the post-tensioned split rocking wall system.

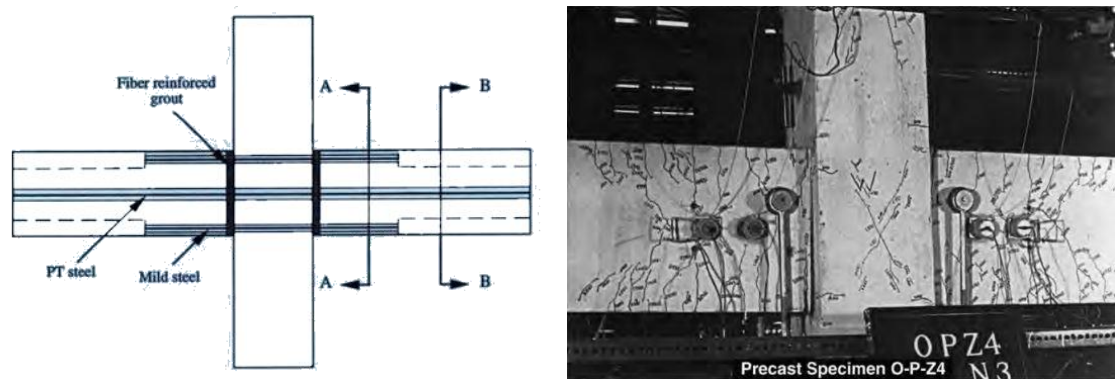


Fig. 6.7 Jointed precast hybrid frame (Nakaki et al. 1999)

Several self-centering systems have been studied as part of the co-coordinated four-phase PRESSS research program on precast concrete systems in the United States. This program culminated with the testing of a 60% scale five-story building (Nakaki et al. 1999; M J Nigel Priestley et al. 1999). U-shaped rolling stainless steel plates, as shown in Fig. 6.8, were designed for energy dissipation and used to couple the walls.

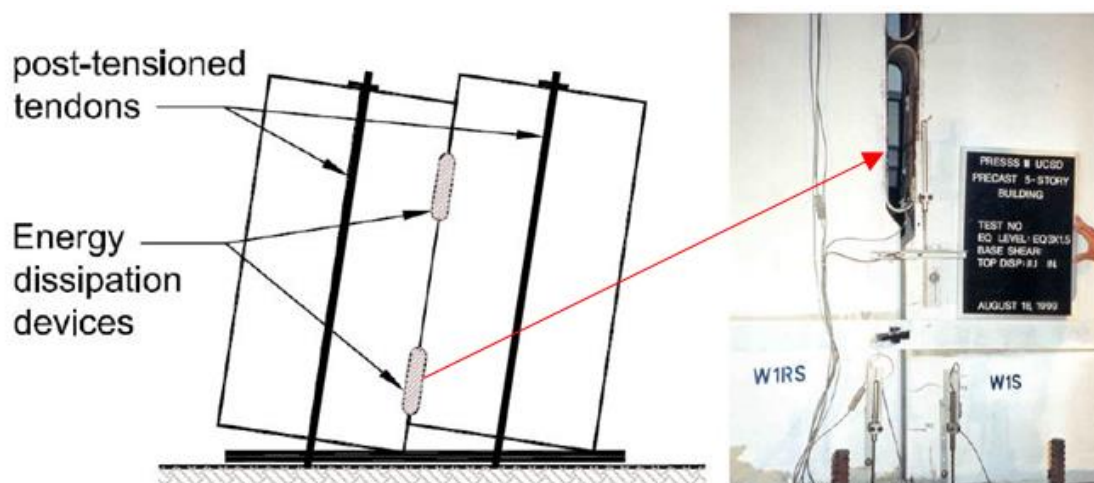


Fig. 6.8 Precast concrete post-tensioned rocking wall with u-shaped lateral dissipator (Stanton 2003)

The use of rocking systems has increased also in bridge structures in the last fifteen years. One of the last experimental work has been conducted by Guerrini et al. 2015, and consists on posttensioned self-centering precast concrete dual-shell steel columns with external or internal energy dissipators (Fig. 6.9). This work has been an enhancement to the research completed by Restrepo et al. 2011.



Fig. 6.9 Hybrid precast concrete dual-shell steel columns (Guerrini et al. 2015)

- Application in steel structures

The PRESS systems developed for concrete frames have also been extended to steel frame structures (Ricles et al. 2001; Christopoulos et al. 2002). Fig. 6.10 illustrates the hybrid post-tensioned connection developed for steel moment-resisting frames (MRF). Different kinds of dissipaters have been used as steel angles, high strength bars and friction devices.

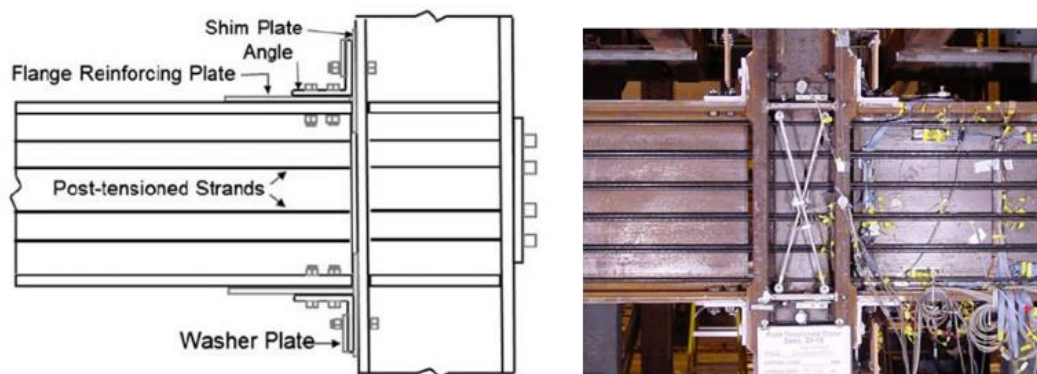


Fig. 6.10 Steel Moment Resisting Frame joint (Ricles et al. 2001)

As for precast concrete the rocking concept has been widening to the entire steel frame system, as schematized in Fig. 6.11.

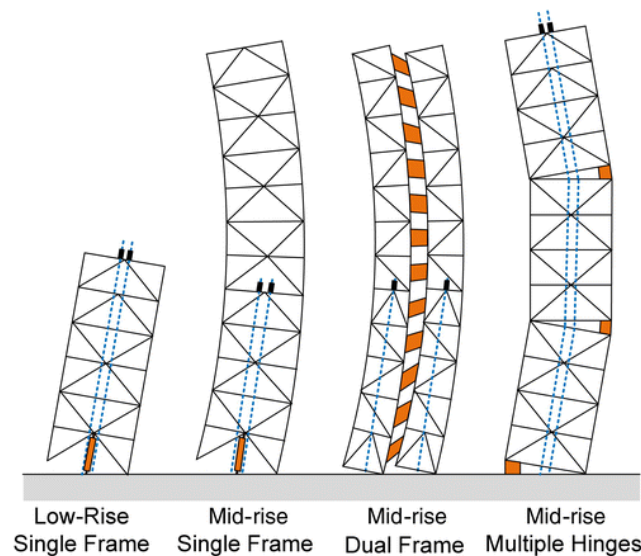


Fig. 6.11 Controlled rocking self-centring steel-braced frames (Eatherton et al. 2014)

- Application in masonry structures

As an add-on to the previous described different material hybrid system solutions, the same concept has been applied for masonry walls. Toranzo (Toranzo 2002; Toranzo et al. 2004; Toranzo et al. 2009) proposed the use of rocking confined masonry systems incorporating low-cost external hysteretic energy dissipation devices. The wall unit in the test was built with brick masonry infill, and included the slabs, as shown in Fig. 6.12. The columns were designed for strain control to ensure small shear distortions would occur in the wall panel, while the wall rocked at the foundation. Energy dissipation devices, in the way of tapered levers designed to yield in bending with constant curvature, were installed at the wall toes, as shown in Fig. 6.13.

Although the hysteretic loops of the flexural dissipaters are smaller than the ones obtained with a dissipater yielding axially, dissipaters designed in this way proved to be more reliable and stable.

The developments in damage-resistant design of rocking post-tensioned multi-storey buildings have been additionally implemented and transferred to timber structures since 2004 (Palermo et al. 2005; A. Palermo et al. 2006; Smith et al. 2007; Sarti et al. 2012).

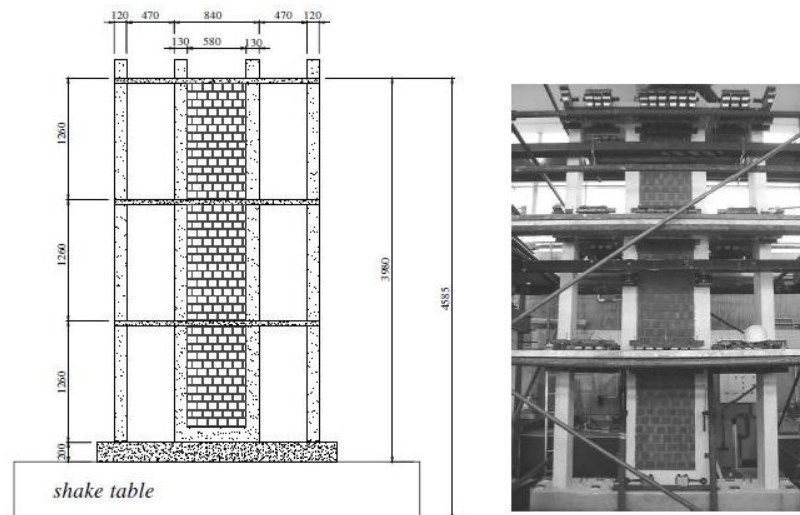


Fig. 6.12 Rocking confined masonry system (Toranzo et al. 2009)

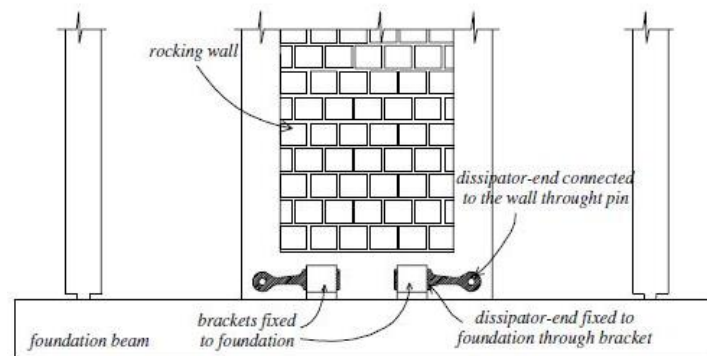


Fig. 6.13 Flexural energy dissipation devices (Toranzo et al. 2004)

- Application in timber structures

Related to timber structures, special attention has been given to the hybrid connections, which combine post-tensioning bars with internal or external steel dissipaters.

The post-tensioned timber concept effectively combines lessons learnt from the PRESSS program and research on glulam elements by Buchanan & Fairweather 1993, here beams and columns constructed from Glue-Laminated (GL) timber were connected by epoxied steel rods or gusset connections, as illustrated in Fig. 6.14.

One of the most extended and known research campaign on rocking timber system named Pres-Lam was conducted by researchers of the University of Canterbury. The Pres-Lam timber system covers both seismic resistant timber frames and walls, with particular emphasis on Laminated Veneer Lumber (LVL) components.

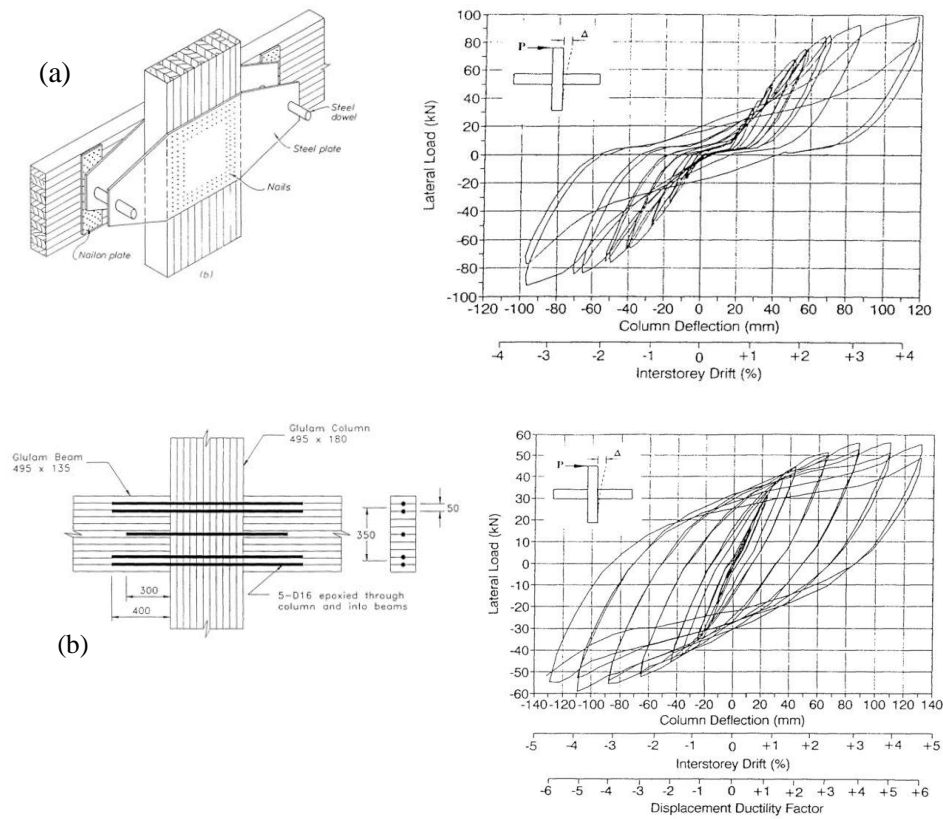


Fig. 6.14 (a) Nailed and (b) epoxied steel rods connection for glulam beam-column joint

The interest in using engineered wood products, as LVL, is because that the final timber product results devoid of defects, such as knots, contrary to sawn timber and therefore with higher properties even if they are coming from the same wood species. Timber strength characteristics do not strongly affect the effectiveness of the hybrid system mechanism but it is important to be careful on providing proper confinement on the compression areas to avoid crushing.

Pres-Lam program laboratory tests on structure sub-assemblies have shown good results, with small residual damage in the supporting elements (M. J. N. Priestley et al. 1999; a. Palermo et al. 2006; Newcombe 2007; Sarti et al. 2014). The extensive experimental campaign can be separated in three parts: the first includes beam-column subassemblies, column-to-foundation connections and shear wall specimens; the second focuses on the global seismic performance of rocking LVL systems with hybrid solutions while the third phase investigates the displacement incompatibility between lateral-load resisting structural systems and the floor diaphragms.

The first test on a PT timber system was performed on a reduced scale external beam-column subassembly (Palermo & Pampanin 2006) considering both only post-tensioning and hybrid solutions with internal or external energy dissipation, as shown in Fig. 6.15.

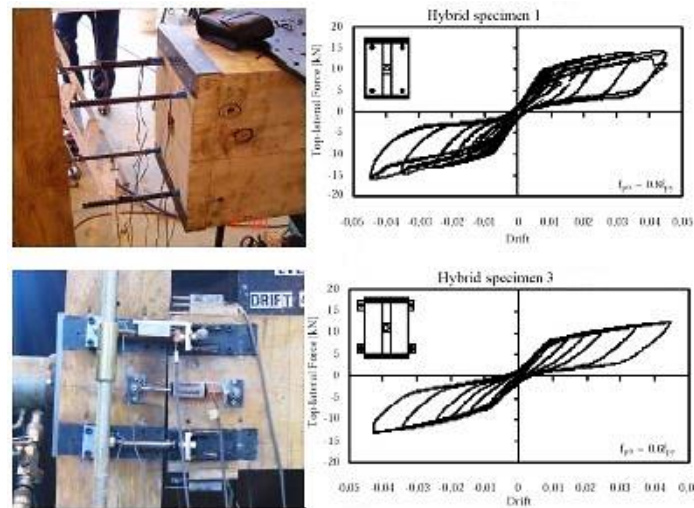


Fig. 6.15 LVL beam-column hybrid solutions under Pres-Lam program

As a part of the investigation of the frame components also cantilever columns and lateral-resistant walls were tested under quasi-static and dynamic loading using similar solution to those adopted for beam-column joints. Similar seismic performance can be obtained from columns and walls. Fig. 6.16 shows the experimental tests conducted on wall-to-foundation subassemblies with the so-called *plug and play* external dissipator devices.



Fig. 6.16 Post-tensioned LVL rocking wall system with externally mounted plug-and-play dissipaters

For the wall different arrangements of dissipater types were considered: internal fuses mild steel bars, external timber-steel epoxied dissipaters and external buckling restrained brace devices (*plug and play*), details are showed in Fig. 6.17. The principal difference between choosing internal vs external dissipation device solutions, other than more stable hysteretic response cycles, is that the last one can be easily replaced, with a beneficial time-consuming repair.

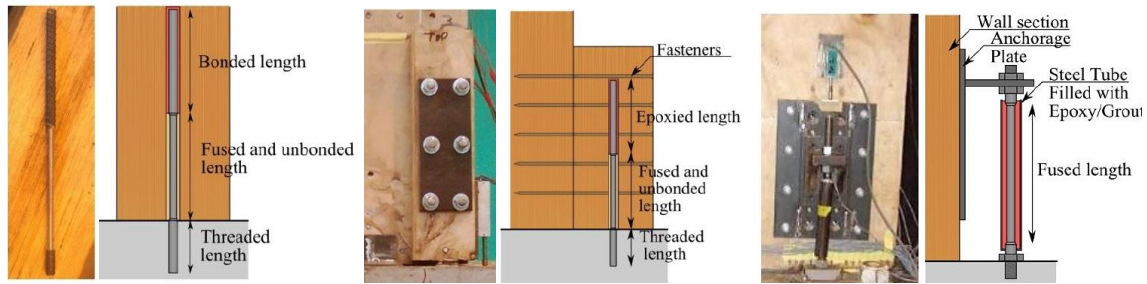


Fig. 6.17 Internal mild steel bars on the left, LVL-epoxyied steel dissipaters on the centre and *plug-and-play* solution on the right (Sarti et al. 2012)

Marriott (Marriott et al. 2008) performed dynamic testing on the same hybrid wall foundation joint detail, adding to the hysteretic axial dissipater also viscous damping devices.

Next step on the research has been double-wall-subassemblies (Smith et al. 2007; Iqbal et al. 2012), where the energy dissipation was ascribed to the U-shaped plates that were coupling aside the post-tensioned walls or wall-to-column (Sarti et al. 2014), as depicted in Fig. 6.18.



Fig. 6.18 Scheme of Coupled Wall System with UFP devices (left), Test set up of Coupled Wall System (centre), Particular of UFP devices (right) (Iqbal et al. 2007)

After investigating 3-D LVL hybrid frame and rocking walls behaviour, looking to the overall interaction between structural components potential solutions regarding the displacement incompatibilities of diaphragms in hybrid timber structures have been investigated by Moroder et al. (Moroder et al. 2014). The floor diaphragms are subjected to out-of-plane bending when the wall starts rocking, because the wall is rotating and uplifting from the foundation. As the gap opening at the base is a peculiarity of the rocking

system and is used to activate the dissipaters; it is important to pay attention on the vertical displacement incompatibilities as the floor diaphragm tends to remain straight.

Following the research program described on post-tensioned LVL timber buildings at the University of Canterbury, real applications of the Pres-Lam technology can be seen in several post-tensioned timber buildings in New Zealand, as the commercial building NMIT in Nelson and the Carterton Events Centre, located north of Wellington (Fig. 6.19).



Fig. 6.19 NMIT building with steel UFP devices (*top*) and Carterton Events Centre with internal dissipater bars (*bottom*), New Zealand

Based on the experimental research on LVL timber systems conducted by the University of Canterbury, other found inspiration to modify and adapt similar concepts to CLT structural elements. This kind of structural system along with timber buildings has been of great interest on the US west coast to implement tall wood buildings in high seismicity regions. Existing CLT structures do not use such systems, relying on conventional hold-downs and connectors (e.g., screws and angle brackets), as described in the previous chapters, that have limited deformation capacity and result damaged after a strong earthquake. Experimental tests were conducted by the University of Washington to investigate CLT lateral force resisting wall solutions that combine post-tensioning to U-

shaped flexural plate devices (UFPs). Double-walls test specimens response is reported in Fig. 6.20, either full scale single story walls or 0.4 scale multi-storey walls were tested.

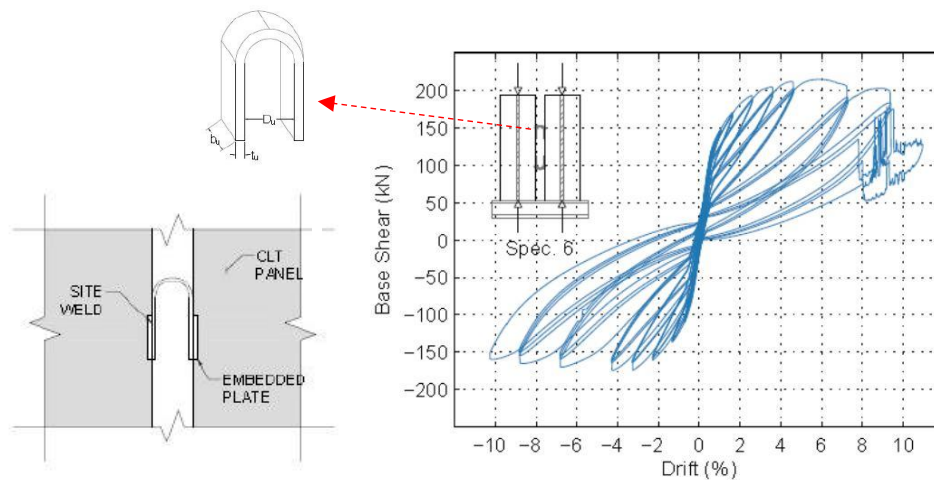


Fig. 6.20 CLT self-centering timber wall with supplemental UFPs dissipating devices (Ganey et al. 2016)

Proceeding with hybrid system component tests for CLT structures, part of the present research conducted at Oregon State University (OSU), has been the follow-up of a previous experimental work conducted by Kramer et al. (Kramer et al. 2013) on the performance of an axial steel energy dissipater to be used with CLT rocking lateral resisting wall (Fig. 6.21). Although the solutions for various types of energy dissipaters are available in the literature, these were not tested with CLT.

The proposed energy dissipaters were fabricated following concepts used in developing steel buckling restrained steel braces (BRB), having a milled portion, which is designed to yield and is enclosed within a grouted steel pipe.

In general, BRBs must be designed and detailed to accommodate inelastic deformations without permitting undesirable modes of behaviour, such as overall instability of the brace or bearing of the non-yielding zones of the core on the sleeve. Buckling-restrained brace have full, balanced hysteretic behaviour, with compression yielding similar to tension-yielding performance. They achieve this through the decoupling of stress-resisting and flexural-buckling resisting aspects of compression strength. To postpone unasked failure modes in compression, as it is possible to catch in Fig. 6.21 between case (a) and case (b), the restrained length play an essential role with an increase in the dissipater's capacity.

In order to accommodate axial yielding of the sleeve core, and to prevent instability of the sleeve, the detailing of BRB end connections must be able to transmit forces to the core without permitting significant stress to develop in the sleeve.

Local buckling may be initiated by typical rigid connections that are prescribed between the device and the main structural component, which may induce undesired bending moments at the connection ends (Guerrini et al. 2015). This is an undesired mode of failure because it reduces the efficiency of the design. Given this possible unwanted behaviour, the new ends restrain solution for the axial dissipater has been connecting it to the CLT panel trough pinned joints, with the intent to allow rotation of the dissipating device to reduce internal moments.

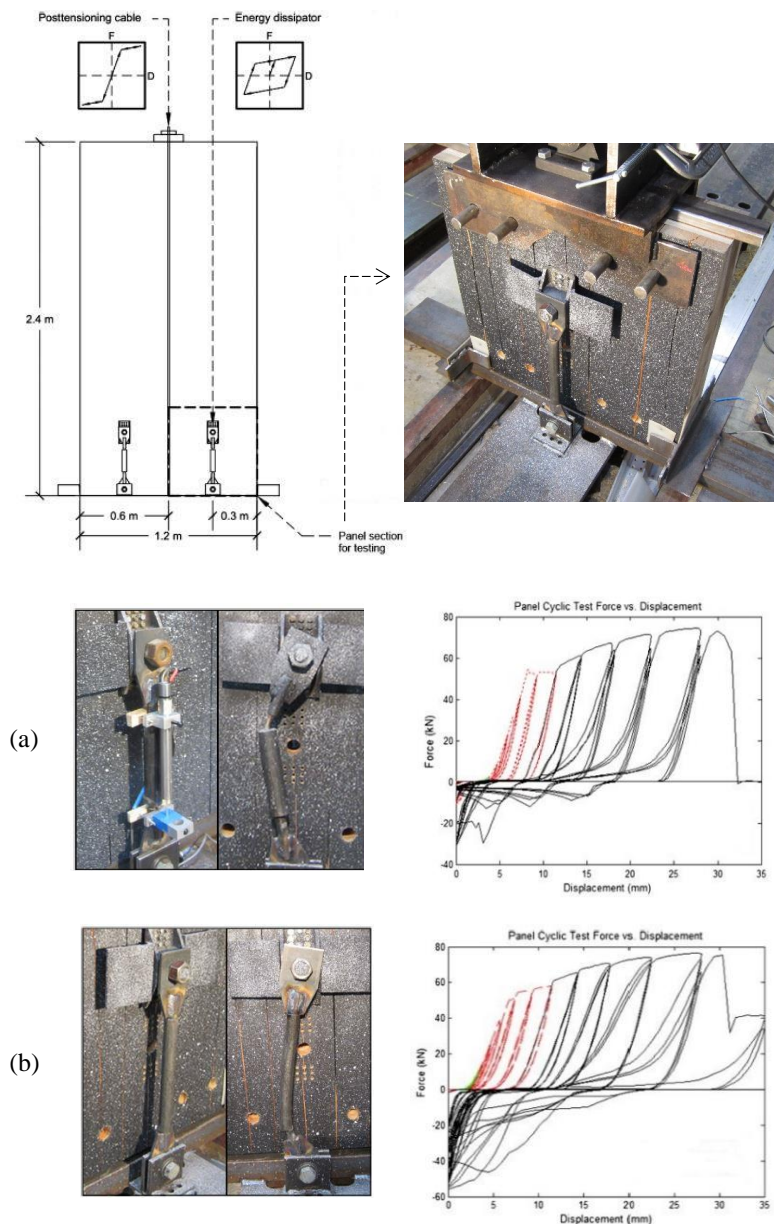


Fig. 6.21 Tests on pinned axial energy dissipaters for CLT rocking wall: (a) with reduced restrained buckling length, (b) increase in restrained length for the dissipater (Kramer et al. 2013)

Chapter 7. CLT rocking wall test

Summary of Chapter 7

In this Chapter, a simplified design procedure for a Cross Laminated Timber (CLT) hybrid rocking wall will be described, together with details of the components, results and limits of the test.

As previously reported, rocking system concepts and solutions have been mostly applied to LVL wood elements thanks to the research conducted under PRES-LAM program (University of Canterbury, New Zealand).

A valid and interesting alternative to LVL is CLT, this type of wood engineered products are gaining more and more popularity all over.

The objective of the experimental study was adapting hybrid rocking system principles to CLT lateral resistant walls. The novel aspects of this technology require innovative solutions for seismic resilient structures, which need be tested before proper design tools can be developed.

In particular, a new seismic connection system has been developed, which was tested under pseudo-static cyclic lateral loading. The connection system consists of a structural external fuses joined with a particular connection solution to the CLT wall, which can be replaced after a seismic event.

The shear wall system included post-tensioned bars to provide self-centering capabilities to the structural system. The wall specimen (Douglas-Fir CLT wall panel) was 2.44 m wide and 4.88 m tall. The cyclic lateral load was applied at two levels, simulating the inertial forces transferred at the floor levels. Differential deformations due to flexure, shear, and/or rocking of the wall are assessed.

Test results can be used to provide more information on CLT rocking wall systems performances to the scientific and engineering design community, possibly to be used in the near future for further researches and several CLT projects.

7.1. Design of the wall experiment

The followed simplified design approach can be broken down in few main steps:

- 1) As first step is necessary to evaluate the seismic design actions in terms of moment, shear and axial forces from seismic (ELF method) and gravity loads respectively;
- 2) Define a re-centering ratio (λ) value and evaluate moment contributions;
- 3) Through an iterative process considering rigid rotation equilibrium, starting from a guess value of the neutral axis depth, it is possible to evaluate the required post-tensioning and the additional mild steel contribution (axial dissipater) for a given edge distance;

A case study building has been identified to do the preliminary design for the CLT rocking wall test. This prototype follows a previous building case considered by Sarti et al (Sarti et al. 2012), some preliminary information were assumed from there.

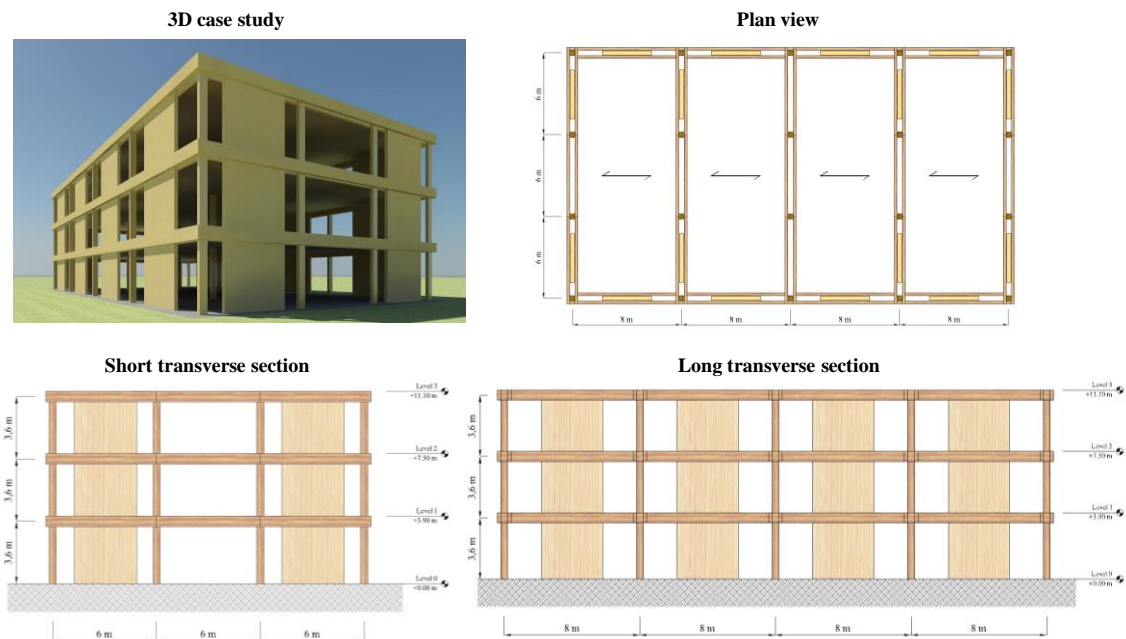


Fig. 7.1 3D model and different views of the adopted case study

It is assumed that shear post-tensioned rocking (single) walls are used for the seismic resistance in both directions. CLT walls are 3.6 m wide and 0.178 m thick (5 layers). The structure is a 3-storey building, the lateral resistant walls have been thought as post-tensioned till the 2nd level and classically connected to the floor in the upper storeys.

Internal frames are designed to support gravity loads, and as an additional lateral strengthening to ensure also a box-like behaviour to the structure. Floors would be timber-concrete composites and oriented in the shorter dimension.

The vertical uplift generated by the gap opening at the base of the wall element can cause displacement incompatibility issues when interacting with the diaphragm system. That vertical displacement can bring to damage in the diaphragm when the connection is not properly conceived, thus influencing its capacity (Moroder et al. 2014). Moreover, the interaction of the two systems can increase the vertical load on the wall. The increased axial force amplifies the capacity of the wall system but reduces the energy dissipated of the system since the dissipaters might not be activated. Considering also these problems in the real system, the slab has been considered connected to the frames by sort of shear plates or rollers that allow vertical uplift and no transmission of vertical loads (Fig. 7.2).

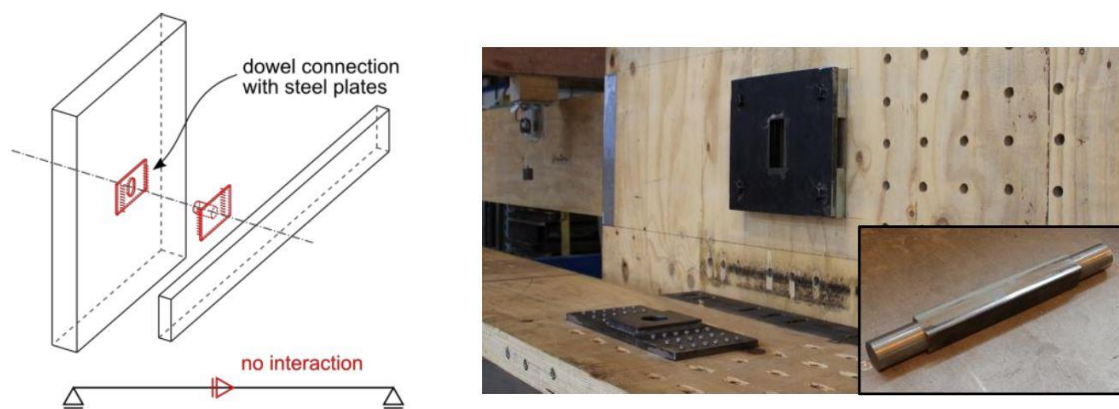


Fig. 7.2 Hypothesize wall-to-beam pinned connection (Moroder et al. 2014)

The equivalent static lateral force method (ELF) has been adopted to estimate the forces resulting from a seismic action on the structure, and consequently on the CLT wall. The equivalent static lateral force method is a simplified technique to substitute the effect of dynamic loading of an expected earthquake by a static force distributed laterally on a structure for design purposes. It assumes that the building responds in its fundamental lateral mode. For this to be true, the building must be low rise and must be fairly symmetric to avoid torsional movement under ground motions.

The building has three levels with regular and symmetric plan, the seismic weight for each floor have been decided following the New Zealand case study building (244 ton each floor and 192 ton for the roof).

The building has been considered situated in Seattle (WA), referring to the correspondent elastic response spectra. It is important to underline that the representation of seismic demand in ASCE/SEI 7-10 is based on Risk Targeted Maximum Credible Earthquake maps (MCE_R), which is defined as an earthquake with 2% probability of exceedance in 50 years (2475 years return period), while the Design Base Earthquake (DBE) level represents a 475 years return period event. Therefore, as suggested (Yenidogan & Erdik 2016), the DBE event is assumed to be 2/3 of the MCE_R event.

To obtain the design spectrum from the elastic one for the ELF analysis is necessary to introduce the behaviour factor q , as know this parameter is used to take into account the capacity of the structural system to resist seismic actions in the non-linear range thus designing for reduced seismic forces. In particular for CLT structures, apart from recent studies (Ceccotti & Sandhaas 2010; Pozza et al. 2015; Pozza et al. 2016), there are no specific provisions on the behaviour factor value.

The reference seismic code in the European area is Eurocode 8 (EN-1998-1) which gives the guide lines for all the other national standards, according to what reported in ductility classes and behaviour factors for timber structures paragraph, a q value of 2 has been adopted.

Following the equivalent static lateral force method steps and calculating the fundamental period T with the simplified formula:

$$T = C \cdot H^{3/4} \quad (1)$$

Where C is a constant equal to 0.05 and H is the total height of the building, it is possible to obtain the lateral forces resulting at each level of the structure.

Fig. 7.3 shows the design spectrum and the corresponding value for the study case building.

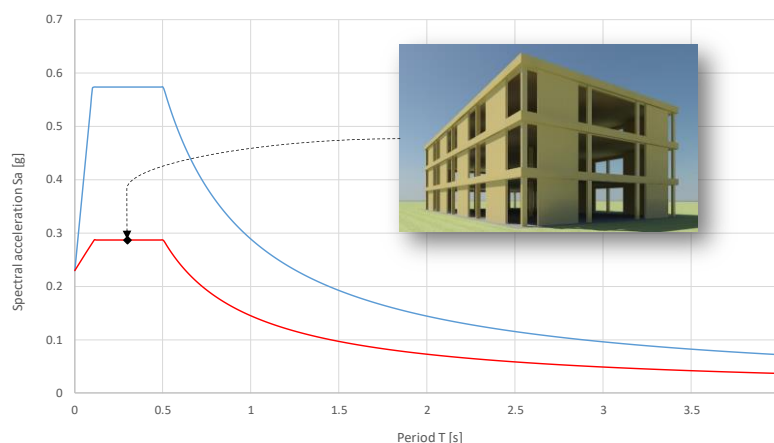


Fig. 7.3 Seattle (WA) elastic response spectra and design spectra with a q -factor of 2

All these assumptions were taken in a safety prospective, since the rocking system solution will not behave as rigidly as a regular structure solution. Therefore, a detailed model would be necessary to define a more accurately fundamental period and viscous damping associated. Lateral forces have been determined ignoring the presence of energy dissipation (or hysteretic damping). Hence, the elastic design has been performed with an assumed elastic damping equal to 5% of critical damping.

A total number of eight post-tensioned walls are assumed in each direction (Fig. 7.1) so the base shear and overturning moment for each wall are 310 kN and 2517 kNm, respectively. A design drift level of 1% was considered.

Lateral displacements and drift ratio limits have immediate effects on the structure response, such as consequent damages on structural and non-structural elements, plus displacements can affect adjacent structure. However the recommended drift limit values are vary widely in worldwide codes (i.e. Europe 1%, USA 2%, New Zealand 2.5%).

In particular, designing rocking timber system, due to the peculiar material properties (i.e. flexibility, reduced seismic mass), it is important to contain the deformations, as well as ensuring lateral strength.

The scaling factor for the CLT rocking wall is two-thirds ($\gamma=2/3$), it follows that all phenomena involved in the test are scaled according to a similitude law. Cauchy similitude law was chosen in the present case, which implies the relations for the different parameters in terms of the geometrical scale factor presented in Table 15.

Table 15 Scale factors according to Cauchy similitude

Parameter	Symbol	Scale factor
Length	L	γ
Modulus of elasticity	E	1
Specific mass	ρ	1
Area	A	γ^2
Displacement	Δ	γ
Rotation	θ	1
Force	F	γ^2
Moment	M	γ^3

Therefore, the specimen design shear and moment demand are:

$$N_{2/3} = \gamma^2 \cdot N_b = \left(\frac{2}{3}\right)^2 \cdot 41 = 18 \text{ kN} \quad (2)$$

$$V_{2/3} = \gamma^2 \cdot V_b = \left(\frac{2}{3}\right)^2 \cdot 310 = 138 \text{ kN} \quad (3)$$

$$M_{2/3} = \gamma^3 \cdot M_b = \left(\frac{2}{3}\right)^3 \cdot 2517 = 745 \text{ kNm} \quad (4)$$

The concept of post-tensioned timber walls was initially proposed by Palermo et al. (Palermo et al. 2005). The followed procedure is the approach recommended to determine the moment-rotation response of post-tensioned precast concrete connections (Pampanin et al. 2006). The presence of unbonded tendons violates the strain compatibility in the section, therefore a compatibility condition is needed to solve the problem. The member compatibility considered rely on the Monolithic Beam Analogy (MBA), introduced by New Zealand researchers (Pampanin et al. 2001; Palermo et al. 2004) for precast concrete structures. Using the MBA analogy corresponds to define the strain as a function of the imposed rotation at the base connection. After fixing an impose rotation (or drift level) and guessing an initial neutral axis position, through an iterative section equilibrium is possible to evaluate both resulting post-tension bars and energy dissipater forces. The iteration process is summarized below (Fig. 7.4):

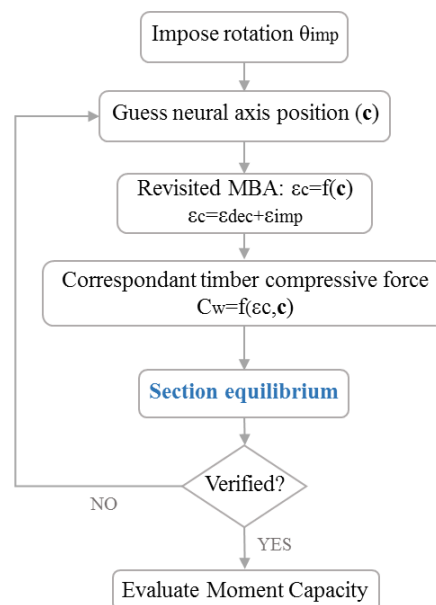


Fig. 7.4 Summary flow-chart of the section equilibrium procedure

In order to obtain the required steel area of the axial dissipater and the number of post-tension bars, it has been assumed a dimensionless neutral axis depth of $\gamma = c/b_w = 0.30$ to estimate an internal lever arm.

In addition, a ratio between the moment contribution provided by the axial dissipater and the moment contribution provided by the post-tensioned bars is normally adopted in order

to guarantee a controlled rocking mechanism. In order to overcome the force required to return the energy dissipater to its original position, after plastic deformation, a re-centring factor (λ) of approximately 1.15 was used (Palermo et al. 2007).

The equations for λ , β , α are the following:

$$\lambda = \frac{M_{pt} + M_N}{M_s} \geq \alpha \quad (5)$$

$$\beta = \frac{M_s}{M_{tot}} = \frac{1}{1 + \lambda} \quad (6)$$

$$\alpha = 1 - \beta \quad (7)$$

Where M_s is moment contribution from the energy-dissipating bar; M_{pt} is the moment provided by the unbonded post-tensioning; and M_N is the moment provided by axial load, which includes only the self-weight of the wall since a slotted pin connection has been supposed between the CLT wall and the resisting gravity frame.

The material properties of the dissipater steel (S275 or A36) and the post-tension bars (Dywing) are listed in Table 16 and Table 10.

Table 16 Post-tension bars steel properties

PT bars	
E	200000 [MPa]
f_{ypt}	825 [MPa]
f_{upt}	1030 [MPa]

Table 17 Axial dissipater steel (S275)

S275 steel dissipater	
E	200000 [MPa]
f_y	275 [MPa]
f_u	440 [MPa]

Accordingly, this would lead to choose a 26 mm (1inch) diameter milled section for the energy dissipater and two Dywidag bars of 35mm (1-3/8 inch). The number and geometrical dimensions of the post-tensioning bars derived also from practical needs to realize the laboratory test.

After having established the steel components areas (A_{diss}), it is possible to repeat the iterative sequences described below. Fig. 7.5 schematizes the CLT rocking wall balance.

a) *Determination of dissipater mild section and number of PT bars*

$$M_s \geq \beta \cdot M_{tot} \quad (8)$$

$$A_{diss} = \frac{M_s}{d_s \cdot f_y} \quad (9)$$

Where A_{diss} is area of the milled section for the external dissipater, consequently the diameter can be derived from there.

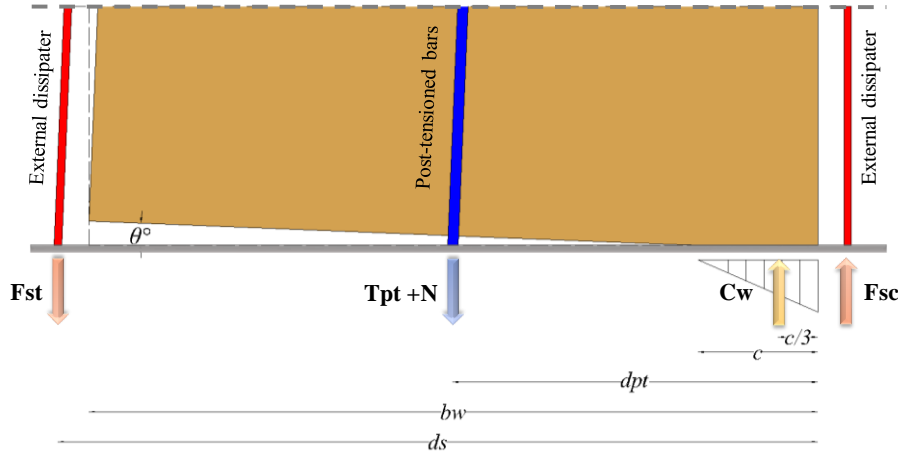


Fig. 7.5 Rocking wall section balance

Regarding the minimum number of post-tension bars:

$$M_{pt} + M_N = (T_{pt} + N) \cdot d_{pt} \geq \alpha \cdot M_{tot} \quad (10)$$

Where T_{pt} is the total force within the post-tensioned tendons at the design drift, while N is the scaled axial load

$$T_{pt} \geq \frac{M_{tot} \cdot \alpha}{d_{pt}} - N \quad (11)$$

$$n_{min} \geq \frac{T_{pt}}{80\% \cdot A_{pt} \cdot f_{ypt}} \quad (12)$$

It is crucial for the post-tensioning bars to remain elastic until the maximum expected drift rotation, since they act in the system as re-centring springs. In order to guarantee an elastic behaviour of the PT bars the tensile capacity is reduced by the 80%, as recommended in the information provided by the manufacturer.

b) Iterative section equilibrium steps

The following steps need to be repeated until the section equilibrium (Eqn. 13-14) will be satisfied

$$T_{pt} + N + F_s - C_w - F_{sc} = 0 \quad (13)$$

Where T_{pt} is the total force within the post-tensioned tendons at the design drift, N is the scaled axial load, F_s is the tensile force acting on the dissipater in the uplifting corner, F_{sc} is the compression force on the other side dissipater and C_w the wood compression force on the base contact portion.

Since the connection between the panel attach and the head of the dissipater has been thought through a hinged constrain within a slotted hole, to delay the occurrence of buckling phenomena, F_{sc} has not been taken into account in the equilibrium. Even if, the presence of small tolerances in the slotted hole will generate friction reaction, those are not considered in this phase. Therefore, Eqn 13 became:

$$T_{pt} + N + F_s - C_w = 0 \quad (14)$$

This way the dissipated energy results reduced, but it would be possible to exploit more the plastic resources in traction of the axial dissipater.

To define the force components it is necessary to derive the strain on each element correspondent to the imposed rotation level.

The passages are described more in detail below:

- *PT reaction*

$$\varepsilon_{pt}(\theta_{imp}) = \frac{\Delta_{pt}}{l_{pt}} = \frac{\theta \cdot b_w \cdot (0.5 - \gamma)}{l_{pt}} \quad (15)$$

$$\Delta T_{pt} = E_{pt} \cdot \varepsilon_{pt}(\theta_{imp}) \cdot n_{pt} \cdot A_{pt} \quad (16)$$

$$T_{pt,initial_req} = T_{pt} - \Delta T_{pt} \quad (17)$$

$$T_{pt,initial_real} = \% f_{ypt} \cdot n_{pt} \cdot A_{pt} \cong T_{pt,initial_req} \quad (18)$$

$$\frac{f_{pt}}{f_{ypt}} < 80\% \quad (19)$$

The post-tension force should guarantee the re-centring of the system and the closure of the base gap after the yielding in the dissipater. That is why the initial post-tension contribution should be such as to ensure the desired mechanism but also not so elevate.

In fact, considering that over a certain limit the dissipater elements have served their purpose, the post-tensioning solution itself nonetheless provides a good seismic response of the building system, as long as it remain in the prescribed elastic range.

- *Tensile force in the external dissipater*

$$\varepsilon_s = \frac{\Delta_s}{l_{fuse}} = \frac{\theta \cdot (d_s - \gamma \cdot b_w)}{l_{fuse}} \quad (20)$$

The stress is determined from a bilinear stress-strain relationship with a hardening branch slope ratio of $r = 1\%$

$$f_s = f_y \cdot \left[1 + r \cdot \left(\frac{\varepsilon_s}{\varepsilon_y} - 1 \right) \right] \quad (21)$$

$$F_s = A_{diss} \cdot f_s \quad (22)$$

- *Compression force in the panel*

Table 18 summarises the wood physical and mechanical properties of the CLT panel

Table 18 Douglas fir (Oregon pine) physical and mechanical characteristics

Wood characteristics	
ρ_m (12% MC)	600 [kg/m ³]
E_{0°	12000 [MPa]
E_{90°	$E_{0^\circ}/30$
f_{c0°	50 [MPa]
f_{i0°	100 [MPa]

Since CLT is made out of crosswise layers (Fig. 7.6 5 layers panel) an equivalent elastic modulus (Eq.23) is considered for the compression force calculation

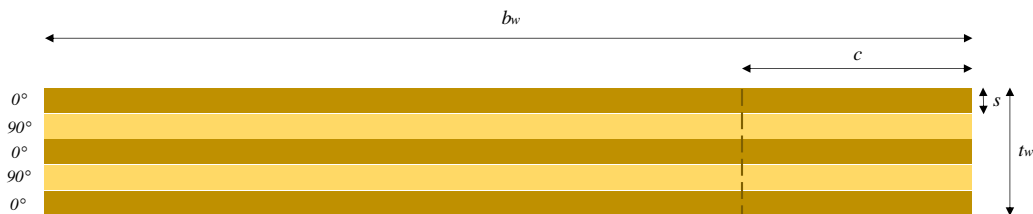


Fig. 7.6 Base layers subdivision of the CLT panel

$$E_{eq} = (E_{0^\circ} \cdot 3s + E_{90^\circ} \cdot 2s) / t_w \quad (23)$$

$$\varepsilon_c = \varepsilon_{dec} + \varepsilon_{imp} \quad (24)$$

$$\varepsilon_{dec} = \frac{\left(\frac{(T_{pt,initial} + N) \cdot 0.5b_w}{t_w \cdot b_w^2} \right)}{E_{eq}} \quad (25)$$

$$\varepsilon_{imp} = \left(\frac{\theta_{imp}}{h_w} \right) \cdot c \quad (26)$$

Where h_w is the height of the rocking panel, considering a rigid rotation of the panel. Therefore, having the hypothetical strain in the compression area and taking into consideration a triangular distribution of the stresses, the compressive force is calculated as follows:

$$C_w = \frac{\varepsilon_c \cdot E_{eq} \cdot c \cdot t_w}{2} \quad (27)$$

- *Resulting neutral axis and moment capacity*

The dimensionless resulting value for the neutral axis depth is approximately

$$\gamma = \frac{c}{b_w} = 0.25 \quad (28)$$

Having been provided all the variables, it is possible to verify the moment capacity

$$M_c = (T_{pt} + N) \cdot \left(\frac{b_w}{2} - \frac{c}{3} \right) + F_s \cdot \left(d_s - \frac{c}{3} \right) \cong 800 \text{ kNm} \geq M_{2/3} \quad (29)$$

The system capacity fulfil the demand in terms or resisting moment. For a more rigorous calculation a safety coefficient can be applied to the different resistant contributes.

7.2. Test setup and instrumentation

The objective of the test is the determination of the lateral load response of a single two-storey post-tensioned two-third scale rocking CLT wall with external dissipaters reinforcement. The CLT hybrid rocking panel has been subjected to a quasi-static cyclic testing regime with an imposed triangular distribution of lateral forces to simulate the seismic load response of the shear wall. Lateral and side views are showed respectively in Fig. 7.7 and Fig. 7.8.

The applied point loads were achieved using a 2.74 m (108 inch) long distribution steel beam (W8x40 american steel section) which was attached to the actuator trough bolts, while to the CLT side wall with steel hinges. The centre-to-centre distance between the top and the bottom pin hinges was 2.22 m (87.5 inch) and the hydraulic actuator (max force 1450 kN and 1.2 m stroke) was positioned at 0.76 m from the top hinge. The hydraulic actuator fixed end was bolted to the reinforced concrete reaction wall.

Applying horizontal loading consisted of pushing and pulling the CLT wall (in the north-south direction) to predetermined drift ratio levels. In order to do so, an “embraced” system with bolted and tied bars side-to-side at lateral force application level was adopted.

The footing of the rocking wall was composed of two combined steel beams (W14x145 American steel section) 2.85 m long (112 inch) fixed to the strong floor.

Post-tensioning bars and the base attach for the external lateral dissipater were connected to the base steel support. CLT walls in real application can be supported either by raised concrete footing, more resistant timber elements and particular steel or aluminium profile to facilitate the levelling of the siting and protecting the wood from humidity. For this reason, and time-consuming cost, the last option has been adopted.

PT bars were placed externally only because of technically feasible reasons for the test, in a real application they can be inserted in drawn up cavity in the thickness of the CLT panel made simply eliminating wood boards from the layers. This way would be also possible to protect the PT bars from corrosion.

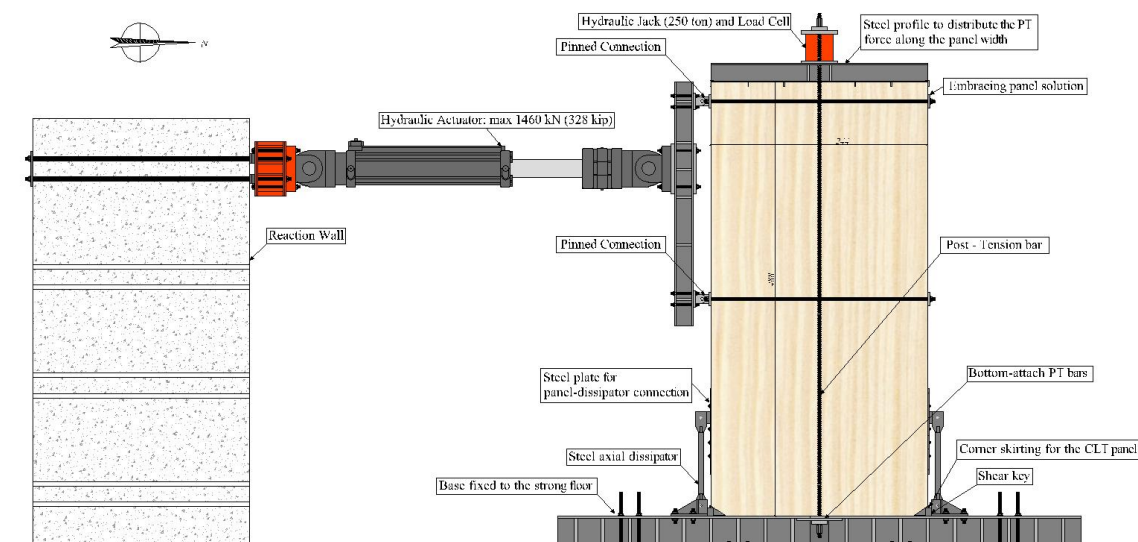


Fig. 7.7 Setup description

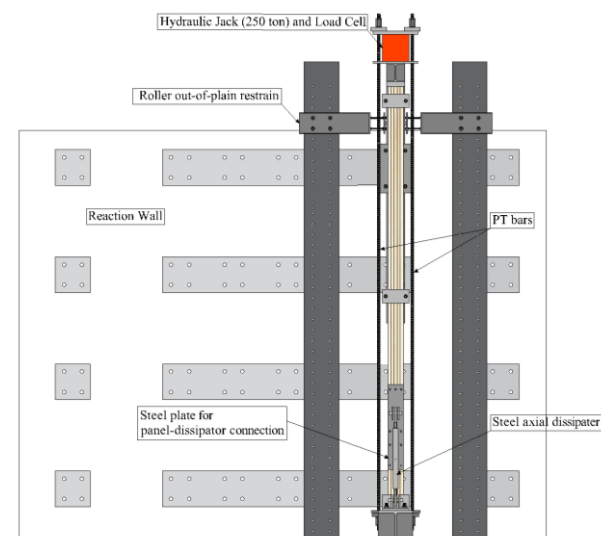


Fig. 7.8 Side view of the setup

The setup initiated with applying an axial centred post-tensioning force to the CLT wall. To distribute along the total width the vertical compression resulting from the post-tensioning a steel profile (W8x40 American steel profile) was placed on top of the CLT wall and prevented from sliding.

Axial load was applied with a hydraulic jack located between the top steel beam and a thick steel plate where the PT bars were hooked. The initial post-tensioning force applied was about 12% of the f_{ypt} .

Regarding the post-tensioning, especially for timber structures, it is crucial to exploit as much distribution area as possible. The reason is to reduce the short-term post-tension losses caused by the local deformation in the wood element.

Lastly, to prevent out-of-plane displacement the wall was restrained in two points per lateral side with rollers bolted to steel profiles connected to steel lateral column (Fig. 7.9).



Fig. 7.9 Out-of-plane retains detail (left), global view of CLT wall in position (right)

Once all the components were set on position, the external dissipaters were pinned to the wall connection system and to the base restraint that was acting also as shear key.

Details will be described more thoroughly in the following paragraph.

The completed test setup is shown in Fig. 7.10.



Fig. 7.10 Multiple full views of the test specimen

Lateral forces and post-tensioning load were measured by load cells, respectively positioned in the head of the hydraulic actuator and below the hydraulic jack. Load cells are transducers that convert force into a measurable electrical output.

The displacement measurements of the top and bottom CLT wall rocking movement, and the relative displacements to monitor the wood panel deformations were taken placing several string potentiometers (SP). String potentiometer (also known as “yo-yo-sensor”) are transducers used to detect and measure, through a potentiometer or a rotary encoder, the linear position by using a flexible cable and spring-loaded spool.

Two strain potentiometers were positioned respectively to measure the actuator openness (SP0) and the top displacement (SP1) of the panel to derive the correspondent drift level. A total of eight string potentiometers (SP13-14-15-16-17-18-19-20) were placed at the base of the CLT panel in the NE side to monitor the variation of the neutral axis depth, while other two were positioned in the other side (SP21-24).

To check the CLT panel deformation vertically, horizontally and diagonally for each floor a total of eleven string potentiometers were positioned (SP2-3-4-5-6 and SP7-8-9-10-11-12).

Two string potentiometer were placed to check also the out-of-plane displacement in each side (SP22-23) and another one (SP25) for the base panel lateral displacement.

Multiple LVDT were used to monitor the relative displacements between the steel connection and the panel (LVDT10-11), the panel shear restrain and the steel profile footing (LVDT4-5) and the lateral and uplift displacement of the footing within respect to the strong floor (LVDT6-7-8-9-12). Linear Variable Differential Transformers (LVDT) are types of electrical transformers used for measuring linear displacement.

The instrumentation is shown in Fig. 7.11 and Fig. 7.12.

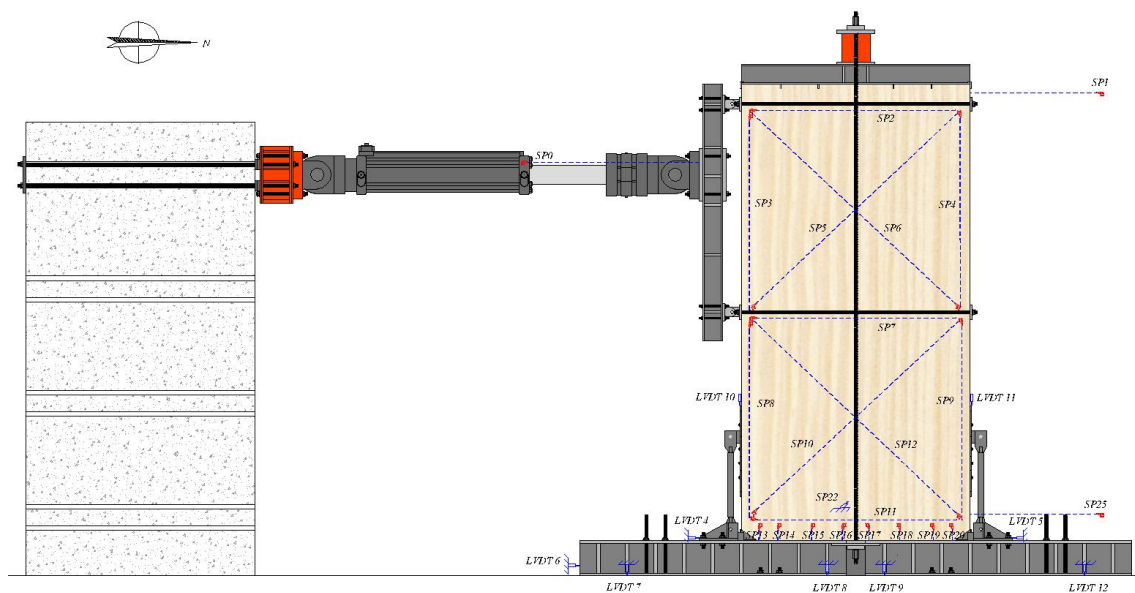


Fig. 7.11 North-East side view instrumentation

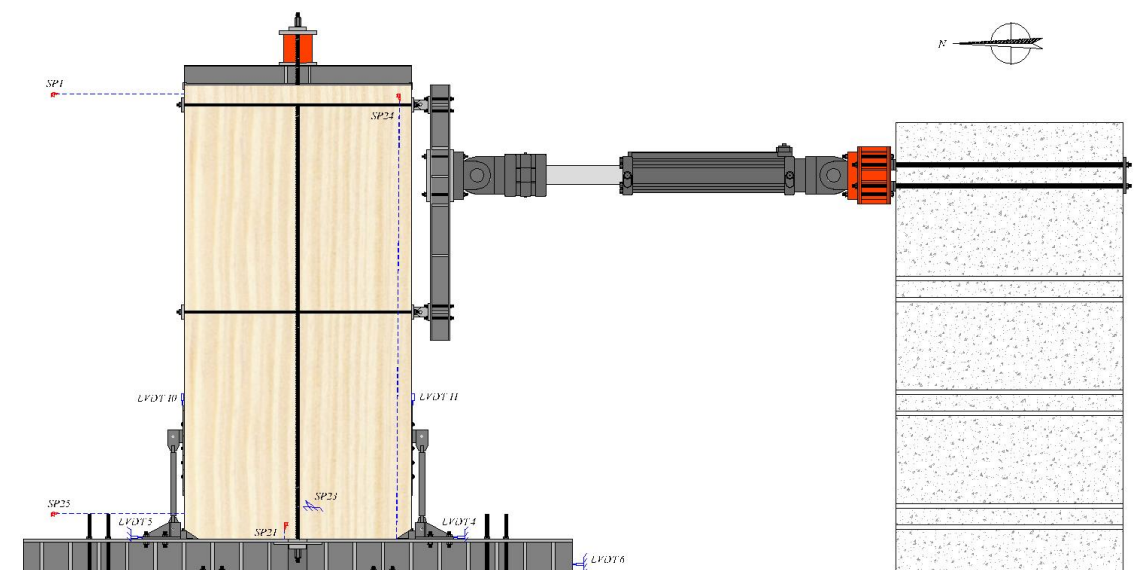


Fig. 7.12 North-West side view instrumentation

7.3. Test specimen detailing

The different components of the rocking wall test specimen such as CLT panel, PT system, external axial dissipaters, panel-to-dissipater trial connection, shear key solutions and corner skirting protection are hereinafter described in greater detail.

7.3.1. CLT panel

The Cross Laminated Timber (CLT) wall consisted of a 5-layers wood panel of Douglas Fir (Oregon pine) with dimensions of 4.88 m in height, 2.44 m in width and 0.18 m thick (Fig. 7.13). The panel was provided by D.R. Johnson Co., which is the first company in the U.S. in possession of a certification (American National Standard-ANSI/APA PRG 320 2012) to manufacture CLT panels.



Fig. 7.13 CLT wall panel dimensions and thickness layers detail

The panel dimensions were scaled from the case study building, and the total height represents the two first floors for the study case building.

The thickness of the wall (number of layers) was established considering the possible compression problems at the base of the wood panel, since while the neutral axis depth reduces the compressed area decreases as well. Also taking into account the entity of the axial load for higher level of drift, caused by the increment of post-tensioning force, and for the out-of-plane stability of the panel.

A pin-type moisture meter was used to measure the moisture content (MC%) of the panel (Fig. 7.14), the measurements confirmed with good approximation the 12% standard moisture content as shown in Table 19. Pin-type moisture meter function by measuring the electrical resistance between two electrodes (inserted in the wood element), when moisture is present within the wood, electricity flows more “easily”.



Fig. 7.14 Moisture content measure instrument

Table 19 Moisture content records

Moisture Content	
Date	Value [%]
15/01/2016	12.4%
09/02/2016	11.8%
07/03/2016	12.6%
21/03/2016	13%
05/04/2016	13.2%

The content of water inside the wood cells is important for several factors, starting from gluing efficacy to structural performances and biological attacks.

7.3.2. Post-tensioning solution

The post-tension was applied thanks two (one for each side) external Dywidag threaded bars of 36 mm diameter (1-3/8 inch). The total tensioned length of each side bar was about 5.5 m (18 feet), to achieve the needed length two bars were joined with a coupler. The nuts and the corresponding anchor support simulated a pin restraint, therefore the bar was free to rotate at the ends.

Fig. 7.15 shows different views of the post-tensioning solution for the CLT rocking wall test.

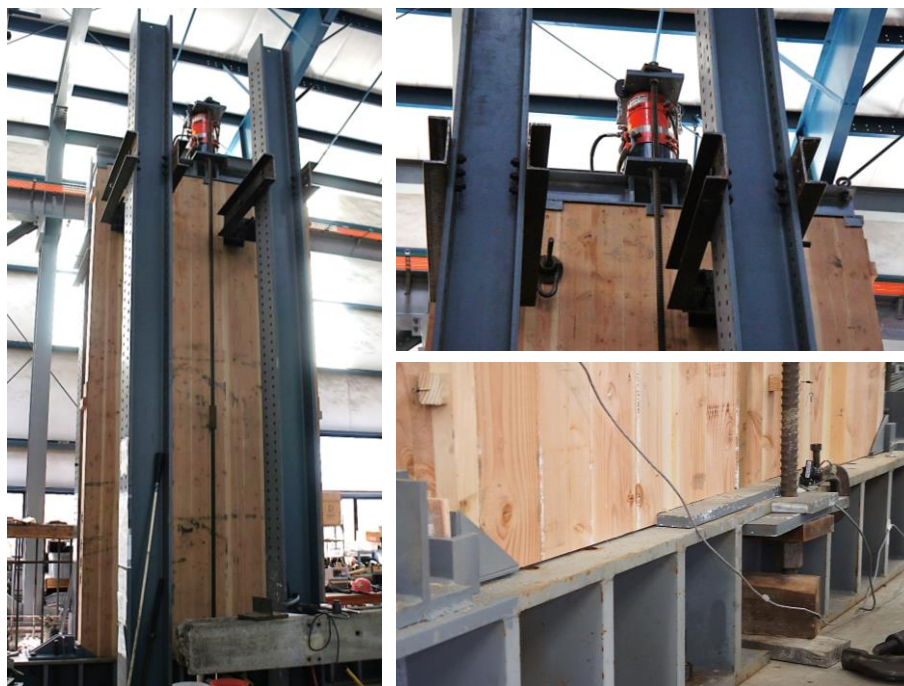


Fig. 7.15 Post-tensioning solution for the test

PT bars are positioned further than the panel surface to avoid friction while the spring try to elongate during the uplifting, and enough to leave space for the passing of the “embracing” horizontal system.

The drift level of the test was limited by the base anchorage of the PT bars since it was done relying on the footing steel beam stiffness (reinforced), given the impossibility to use the strong floor as anchorage point and the amount of time available. In a real building, the post-tensioning bars can be anchored down to the concrete foundation, leaving the steel profile only as support for the timber wall.

7.3.1. Axial energy dissipaters

Previously an overview of different kind of dissipater devices has been done and the typical behaviour of each have been briefly described. The external dissipaters used for the CLT rocking wall test refer in particular to the buckling resistant unbonded brace type (BRB).

Similar dissipaters have been already used associated to other materials, and just recently modified and adapted for wood engineered elements (Palermo et al. 2005).

The dissipaters adopted are similar to the solution with smaller dimensions tested at Oregon State University by Kramer (Kramer et al. 2013).

First, the characteristics of being external and pinned at both ends confer to the dissipater the possibility to be replaced after a seismic event, if needed. Since energy dissipaters are designed to act as sacrificial fuses, the possibility for them to be damaged is very elevate and so being replaceable is an important quality.

The energy dissipation devices where realized with a mild steel bar surrounded by a confining material and encased in a steel tube, the hook ends were made out of shaped steel plates welded to the “body” bar (Fig. 7.16).

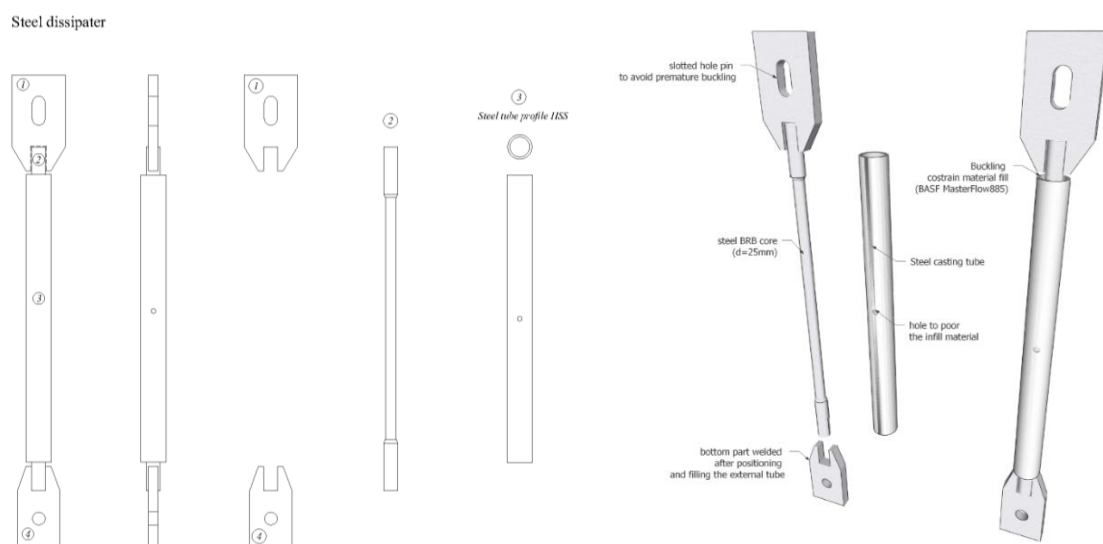


Fig. 7.16 Axial energy dissipater with non-assembled parts

The infill material was a cement-based metallic aggregate grout (BASF MasterFlow 885). The grout compound is the equivalent of the previous formula BASF Embeco 885, which has been shown to perform well for the same purposes under cyclic loading (Guerrini et al. 2012).

The central “body” of the axial dissipater was made from hot rolled S275 (A36) 33 mm (1-5/16 inch) steel bar. Two bars of the same length and diameter were machined along the axial direction with a reduced diameter ($d = 26$ mm or 1 inch) over a specific length. The central part with a small diameter is the fuse length where the steel yield. The fuse length was defined so that the maximum expected uplift of the wall does not exceed a fraction of the deformation at the ultimate strain of the steel. The percentage considered was about 20% of the ultimate strain ($\varepsilon_{su} = 20\%$). In Toranzo (Toranzo 2002) is suggested to use a 25% for a “Rare” seismic event (475 years return period).

The maximum displacement expected in the energy dissipater position derives from the imposed rotation consequent to the rocking movement and the wall geometry, together with relatively rigidity of the CLT panel.

The passages are described below by equations:

$$\varepsilon_{diss} = 20\% \varepsilon_{su} = 0.04 \quad (30)$$

$$\Delta_{diss_max} = \theta_{imp} \cdot (d_s - c) \quad (31)$$

$$l_{fuse} = \frac{\Delta_{diss_max}}{\varepsilon_{diss}} \quad (32)$$

Where ε_{diss} is the design strain for the dissipater length, Δ_{diss_max} the requested displacement by the rocking in the dissipater and l_{fuse} the active length of the axial dissipater.

The steel tube has to be designed to resist to the lateral pressure due to the buckling of the bar that pushes on the confining material. Therefore, the thickness of the tube was chosen considering the worst case scenario which corresponds to the bar that, buckling, produces in the external tube a concentrated force at the mid length (Fig. 7.17).

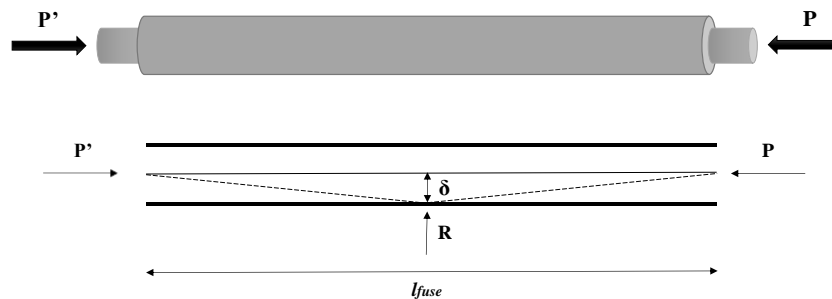


Fig. 7.17 Simplified scheme of buckling

The preliminary design was done not taking into account the effects of the infill material on reducing the allowed displacement of the buckled bar inside.

The required thickness is so determined:

$$R = \frac{4 \cdot P \cdot \delta}{l_{fuse}} \quad (33)$$

$$F_{tube} = \frac{A_v \cdot f_{yk_tube}}{\sqrt{3} \cdot \gamma} = \frac{(d_{fuse} \cdot t) \cdot f_{yk_tube}}{\sqrt{3} \cdot \gamma} \quad (34)$$

$$t_{min} = \frac{R \cdot (\sqrt{3} \cdot \gamma)}{d_{fuse} \cdot f_{yk_tube}} \quad (35)$$

Where P is the compressive force acting on the dissipater, δ the allowed displacement, R the reaction in the external tube profile and F_{tube} the shear resistance of the infinitesimal portion of the steel tube to derive the required minimum thickness.

For the applied load P , the maximum value was considered 1.5 times the yielding force of the middle section bar. A value of about 5 mm thickness of the tube can guarantee a value of stress within the elastic range, the flexural yield in the middle of the external tube was so avoided. Once the minimum thickness was derived the tube size was chosen according to U.S. standard size (HSS 2.375x0.218). The steel tube was located around the steel bar all along the available free length. In this regard, it has been demonstrated that, enlarging the restrained buckling portion in the dissipater, a significant increase in the compression response is obtained (Kramer et al. 2013).

The connection extremities have been oversized to secure that the fuse was the active part. Both were cut from a steel plate of 22 mm (7/8 inch) thick. The top connector had a slotted hole with 35 mm gap, while the bottom one a regular hole to insert a 32 diameter (1-1/4") pin.

The two dissipaters were assembled in the laboratory following few steps (Fig. 7.18), as instructed below:

➤ **STEP I**

The steel "body", with one extremity welded, was horizontally positioned on brackets and covered with grease over its entire length. The bigger diameter portion rolled up with rubber tape. This was done to avoid friction between the steel part and the grout-infill. In order to ensure a proper functioning of the BRB device it is necessary that the steel bar slides freely in traction.

➤ **STEP II**

As second phase, the external tube was positioned thanks to different level brackets to make concentric the two elements. As shown in Fig. 7.18 one end was free without the

connector plate, this to permit the assemble passages. Once the parts were in position the extremity holes were sealed.

➤ **STEP III**

Only the required amount of grout to fill a single dissipater was mixed at time. The used cement based grout is a fast-setting type and it is more fluid compared to regular cement pastes.

➤ **STEP IV**

The grout was poured through holes made along the tube length by the use of a funnel. Once filled, they had been left in place for about a week. Finally, also the other connection end was welded.

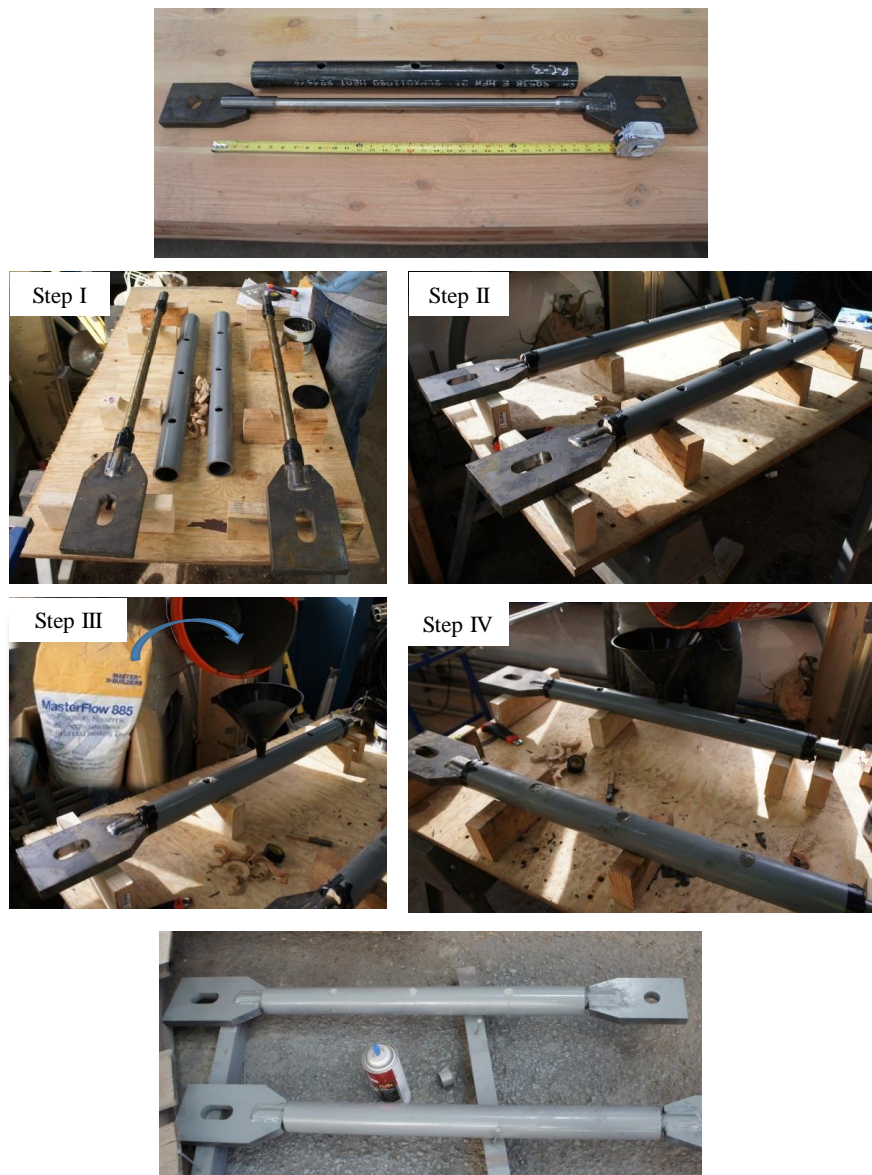


Fig. 7.18 Execution phases for the external axial dissipater

7.3.2. *Wall-dissipater connection*

An experimental type of connection has been adopted for the CLT rocking wall link between the external dissipater and the wood panel.

The necessity of studying a new connection solution different from the ones previously used, it has due to the distinctive position of the energy dissipation device.

Usually, for hybrid rocking timber wall systems, the dissipative devices have been fixed in the timber panel face. Using this arrangement, the advantage is the possibility to reduce the required elongation consequent to the rocking in the axial dissipater plus having a bigger wood area to distribute the connection.

On the other side, positioning aside the dissipating steel device increases the imposed uplift but at the same time the correspondent lever arm.

Furthermore, being in line within the thickness may help avoiding out-of-plane forces after the dissipater's yield. In the other case, it would be sufficient a non-symmetric behaviour to cause a pull-out-plane force.

Unfortunately, the new position for the dissipater cause difficulty on designing a wood connection able to transmit high shear force and moment (due to the distanced dissipater). In wider terms, the field of timber engineering is strongly affected by efficient, reliable jointing techniques so that the individual structural members can fulfil their function in resisting heavy loads. An adding limit for wood connection that should remain rigid, regardless the type of fasteners used, is also the resulting embedment in the wood after repeated cycles.

For the 2/3 scaled CLT rocking wall test an experimental solution to link the panel-to-dissipater was chosen. Through the use an innovative (non-commercial) type of connector called "ZD-plate" (MyTiCon) with the addition of screws, see Fig. 7.19. mediante l'utilizzo

This ZD-plate (Fig. 7.20) is made from two 86 mm x 55 mm steel parts with yield strength $\geq 550 \text{ N/mm}^2$. One part ("base") is pre- installed to the vertical member using four 10 mm by 280 mm ASSY VG plus full thread screws (MyTiCon) arranged at an angle of $\pm 30^\circ$ to the shear plane. Two screws are intended to transfer stresses in tension and two are intended to transfer stresses in compression. Therefore, forces acting parallel to the screw axis can be determined using truss principles. Because of the design of the ZD-plate a gap of approximately one to two millimetres between the lid surface and the head of the

screws exists. Due to this gap the compression screws do not contribute to the connection capacity before a certain deformation occurs.

The second part (“lid”) is pre-installed using two 4 mm x 10 mm pins that are driven into holes that penetrate the lid and partially penetrate into the base. These pins temporarily fix the lid to the base, until a permanent connection between the external steel plate (15 mm thick) and the ZD-plates will be established using a M16 - 10.9 metric bolt on site.

The manufacturing standards for MyTiCon structural wood screws require the steel wire material to be of high grade and strength. ASSY screws are typically manufactured using a steel wire material with 330 N/mm^2 yield strength and must provide an ultimate tensile strength of 410 N/mm^2 . ASSY screws with a diameter of 10 mm yield a characteristic tensile strength of 24 kN with 45 Nm characteristic torsional strength and a characteristic yield moment ($M_{y,k}$) of 35.8 Nm.

To fit the required steel bracket and ZD-plates appropriately onto a specimen, quite extensive milling work had to be done in the vertical wood panel (Fig. 7.19).



Fig. 7.19 Alternative connection solution for the panel-to-dissipater link

The ZD-plate solution was chosen, instead of a sort of a more common “big lateral hold-down” with an inclined arrangement of the screws between 90° and 30° to the wood grain, because previous tests on typical shear connection with inclined screws (Closen 2012) shown less rigidity and not exactly symmetric response for reverse loading directions.

$$R_{ZD,tot} = R_{ax,c} \cdot 3 \cdot n_{ZD} \geq F_{st} \quad (37)$$

Where $R_{ax,c}$ is the minimum value between the withdrawal resistance of the full thread wood screw or the tensile capacity of the screw steel, n_{ZD} is the number of the ZD-plates counting for shear in the connection.

The moment demand was considered as:

$$M = F_{st} \cdot (e_{diss} - e) \quad (38)$$

Where e_{diss} is the distance between the dissipater and the connection plate, e is the distance between the plate and the contact point of the ZD-plate (Fig. 7.21).

Finally, the resisting moment was considered:

$$M_R = R_{ax,c} \cdot n_{screw} \cdot d_{screw} + (R_{ax,c} \cdot 4 \cdot \sin 30^\circ) \cdot d_{ZD1} \geq M \quad (39)$$

Where n_{screw} and d_{screw} are respectively the number of screw working in traction and the distance from the line(s) of screw to the rotational point, while d_{ZD1} is the lever arm of the ZD-plate from the rotation point (assuming a rigid rotation).

Fig. 7.22 shows a schematic representation of the connection and the final assembly.

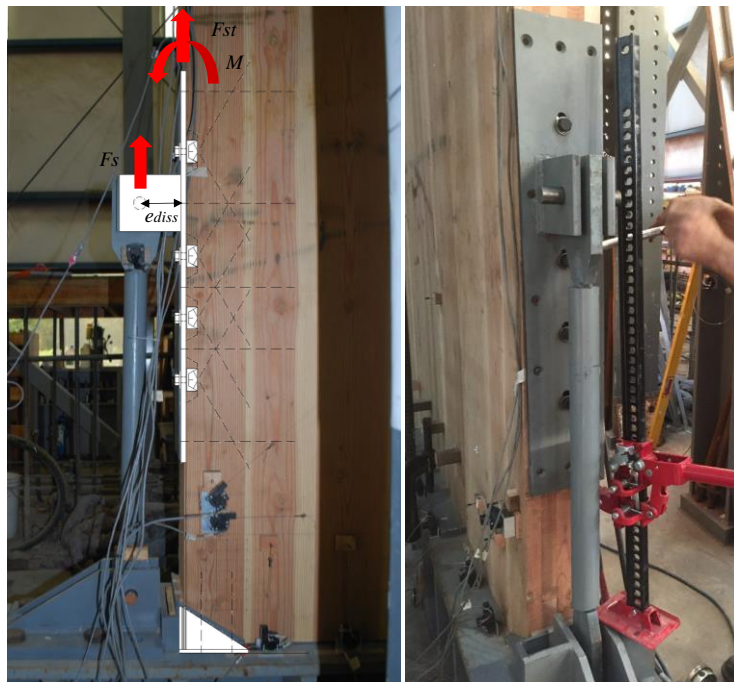


Fig. 7.22 Panel-to-axial dissipater connection assembly

7.3.3. Shear keys and corner skirting

The base attachment system for the external dissipater had a dual functionality. In fact, besides providing the hook for the bottom pin of the dissipater also functioned as lateral restraint for the CLT wall (Fig. 7.23).

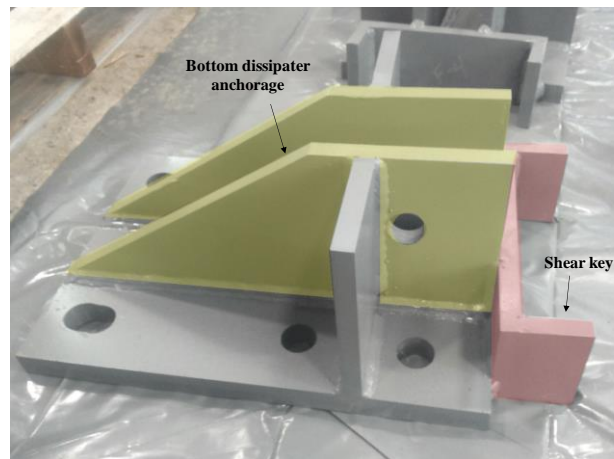


Fig. 7.23 Double function of the shear key solution

The CLT wall, without shear keys resisting lateral loading and blocking the panel from sliding, would not be able to rock. Despite the friction (wood-to-steel friction coefficient about 0.15) expected at the base of the wall due to the high compressive force, it was not enough to resist shear.

The dissipater attachment solution has been designed ad hoc for the test. It included vertical welded stiffened steel plates to accommodate the bottom pin and a steel C shaped “hand” to embrace the panel in its thickness.

To allow for construction tolerance, slotted holes were drilled for connecting the shear key to the foundation with four bolts. The detail of the shear key is shown in Fig. 7.24.

Another issue was highlighted in previous experimental tests on rocking timber system solution, it regards the crushing at the wall’s toe (Dunbar et al. 2014). A possible solution to avoid this problem was found in protecting the base wall corner with a particular steel skirting, see Fig. 7.25.

The steel protection was connected to the panel with four screws that act also as a reinforcement for the compressed wood area.

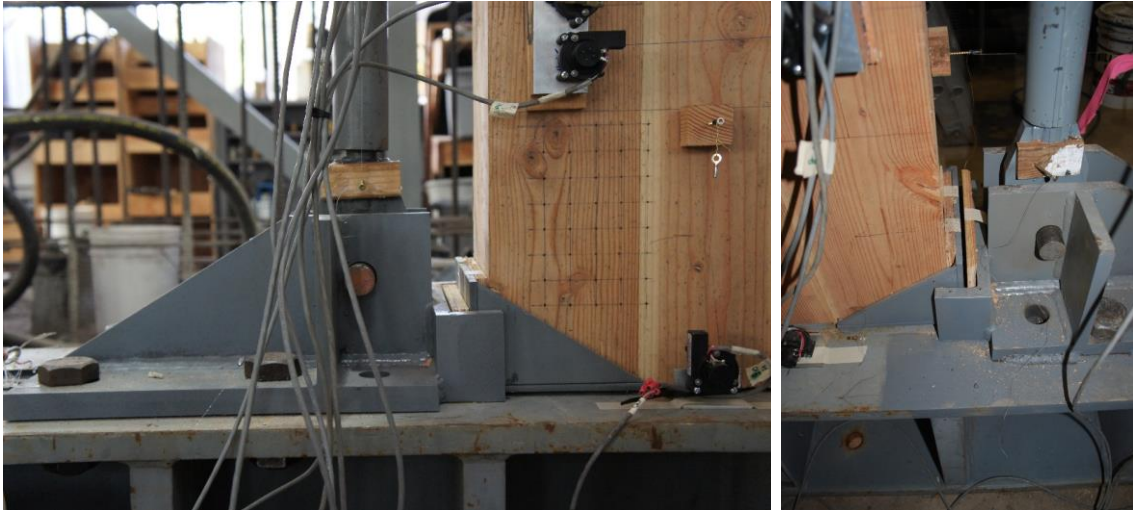


Fig. 7.24 Base corner solution shear key, working also as bottom attachment of the axial dissipater

This element prevented the direct contact between the wood and the steel of the shear key while the rocking motion was ongoing. An adding detail that was adopted, it is the sacrificial interchangeable plywood piece between the shear key and the skirting to leave space for the rotation movement and to absorb energy from the contact. The plywood resulted damaged, as expected, after major cycles as it would be after a seismic event, but also easy to replace.

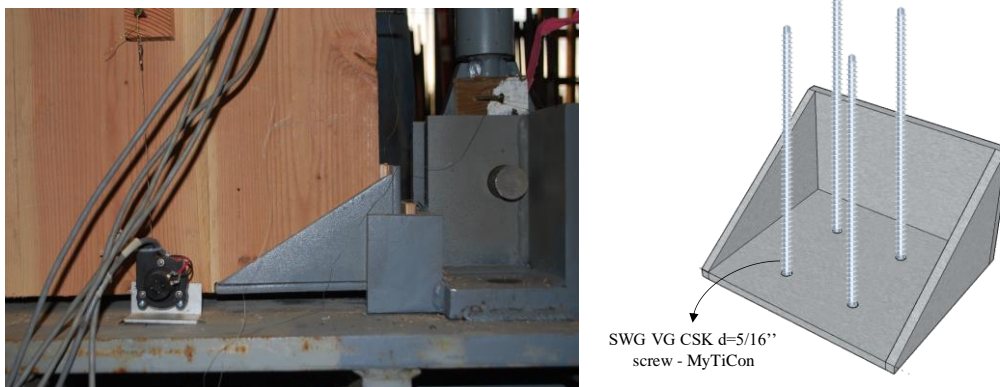


Fig. 7.25 Steel skirting protection for the CLT wall toe

7.4. Loading protocol

The CLT rocking wall test initiated with pre-stressing the wall, an initial post-tension force of about 175 kN (40 kip) was applied.

Table 20 lists the testing protocol and Fig. 7.26 shows the profile in terms of drift ratio versus number of cycles. Applying lateral loading consisted of pushing and pulling the wall (north-south direction) to predetermined drift ratio levels.

Table 20 Loading profile of CLT rocking wall test

Loading protocol		
drift ratio cycle [%]	n° cycles	rate [mm/sec]
0.5	1	0.5
0.5	2	1
0.75	3	2
1	3	4
1.25	3	4
2	3	4
2.5	2	4

Each drift ratio level consisted of three cycles (six peaks) and two cycles for the 2.5% drift ratio level: the cycle started at zero displacement, was then displaced in the positive direction towards the positive peak (north), was then displaced in the negative direction towards the negative peak (south), and then returned back to zero displacement.

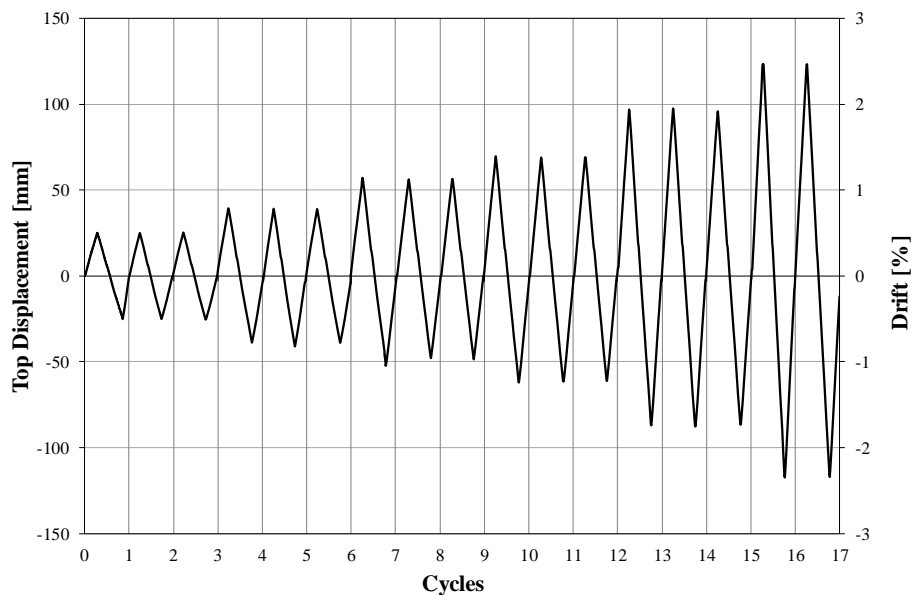


Fig. 7.26 Lateral loading protocol (displacement control)

7.5. Experimental results

In this paragraph a summary of the seismic response for the described hybrid CLT rocking wall test is given.

Results are presented in terms of achieved lateral force, overturning moment, variation of post-tensioning force and neutral axis oscillation versus drift levels.

Further considerations on the dissipated energy of the system will be presented in the next chapter, as a comparison with the numerical model.

7.5.1. Observed failures and comments

A summary of the damages that occurred in the CLT rocking wall test during quasi-static reverse loading testing is provided to better understand the results presented after.

An undesired failure started around 1% drift level displacement in the connection between the CLT panel and the external dissipater, the ZD-plate in tension begun pulling-out converging to create a plastic deformation in the steel plate. This kind of failure mechanism is similar to the other test was done using ZD-plates for a moment resisting base connection (Closen 2012). Figures below show both deformed type of connections, the top represent the one used for the rocking wall (Fig. 7.27) while the bottom the moment resisting connection with a big steel bracket (Fig. 7.28).



Fig. 7.27 Failure started at 1% drift in the connection



Fig. 7.28 Previous test on a moment connection using ZD-plates (Closen 2012)

Once the failure started the deformation in the connection has progressed until the complete breakdown in the upper tensioned part of the connection, see Fig. 7.29.

Therefore, the response of the system is well captured up to about 1% drift, while the cycles after take into account the degradation of the link between the dissipater and the panel (jumps in the force and reduced stiffness). The numerical model have the intent to overcome this problem and show an ideal hysteretic response of the system.



Fig. 7.29 Breaking in the panel-to-dissipater connection

Influent in the cyclic response of the panel it is also the bottom corners solution, previously described, in terms of shifted hook of rocking movement. This is due to some initial lateral tolerance of the panel-shear keys positioning plus the deformation caused

by the compression in the interposed plywood (Fig. 7.30), no significant sliding displacements were registered in the lateral restrains.



Fig. 7.30 Uplift in the base corner and subsequent repositioning contact for the reverse cycle

A first sliding motion slightly delay the beginning stiffness of the rocking hysteretic response but also prevents damages in the resisting elements. This way the wall is allowed to have small lateral displacements, but always in a controlled manner.

Lastly, in this particular test setup, the PT bars anchor is not a perfectly rigid restrain (as could be anchoring to the concrete foundation) but have a certain elastic stiffness (Fig. 7.31) that represented the limit to the achieved drift level for the test.



Fig. 7.31 PT bars bottom anchoring

7.5.2. Lateral force vs drift

Results are here presented in terms of lateral force (base shear force) versus drift levels (or top displacement). The drift ratio has been derived from measurements of the global top string potentiometer (SP1), connected externally to a fin point, by the height of the string potentiometer position.

Since the wall rotates at its base during the test, the actuator load and global string-pot readings were recorded at an angle. Nevertheless, in both cases it has been found that the correct horizontal value is very close to the uncorrected inclined value.

Fig. 7.32 shows the hysteretic response of the test for all imposed drift levels, while in Fig. 7.33 and Fig. 7.34 the results are separated respectively before and after the design drift ratio level (1%).

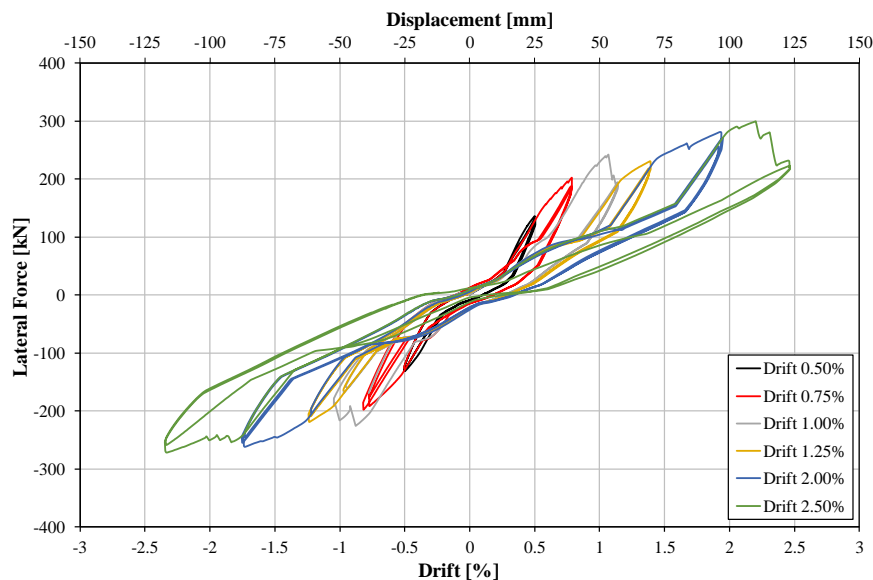


Fig. 7.32 Lateral force vs drift

As previously mentioned, the response starts with a low angle slope representing the slide at the base of the CLT wall, until it gets in contact with the shear key and starts the rocking movement (change in the cycle stiffness).

After reaching 1% drift level, the lateral loading started decreasing with a different tangent, accompanied by a sudden variation in peak force, due to the begin of the failure mechanism in the wall- axial dissipater connection. This caused a consequent reduction in the stiffness of the system, since the progressive detachment of the steel plate from the panel was acting as a rotational spring reducing the contribute efficiency of the external

axial dissipater in traction. Although the connection, after an initial decline, started redistributing the reaction force in the remaining active connectors.

In Fig. 7.33 it is possible to better appreciate that at 1% drift the request in term of shear demand has been exceeded.

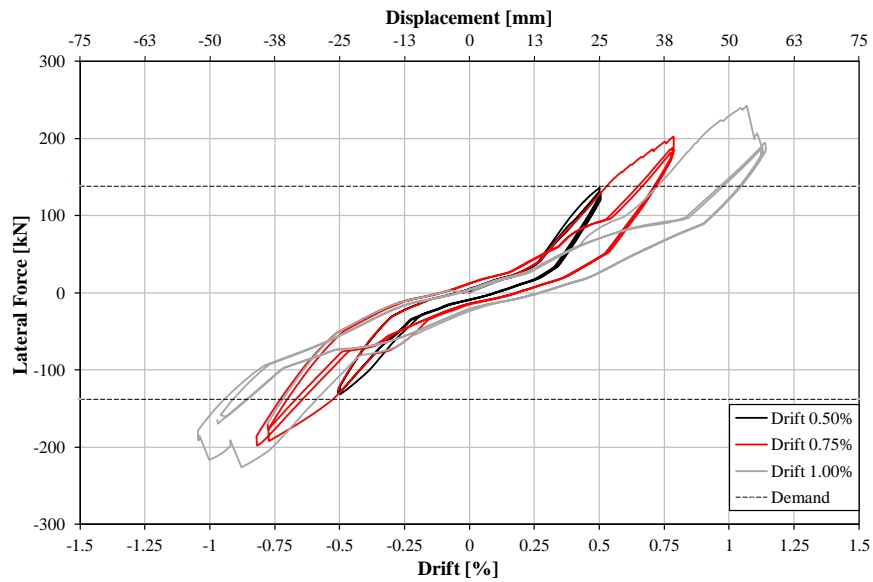


Fig. 7.33 Lateral force vs drift before reaching 1% drift level

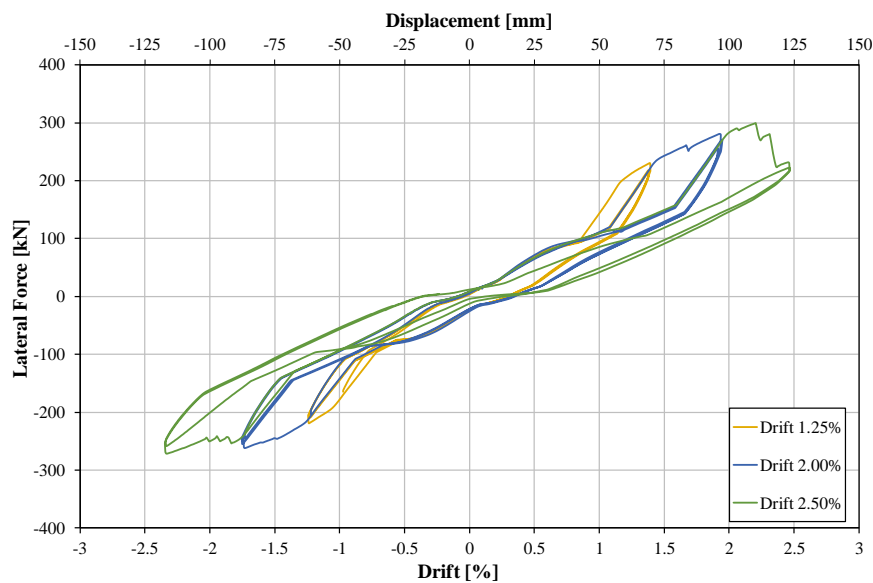


Fig. 7.34 Lateral force vs drift after reaching 1% drift level

7.5.3. Overturning moment vs drift

The overturning moment versus drift response is presented for the single CLT rocking wall test. The overturning moment has been determined by the actuator load values by the actuator height.

As for the lateral loading response, Fig. 7.35 shows the hysteretic response of the test for all imposed drift levels, while in Fig. 7.36 and Fig. 7.37 the results are divide respectively before and after the design drift ratio level.

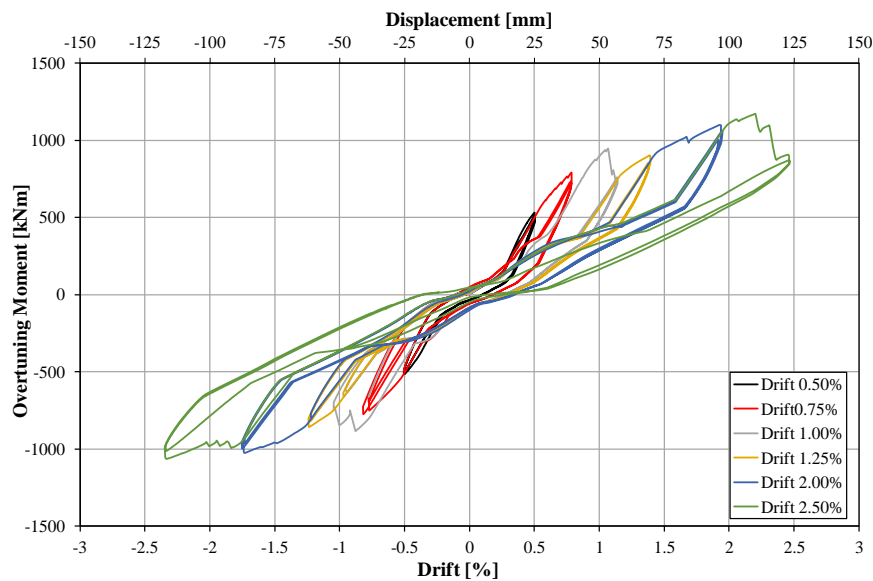


Fig. 7.35 Overturning moment vs drift

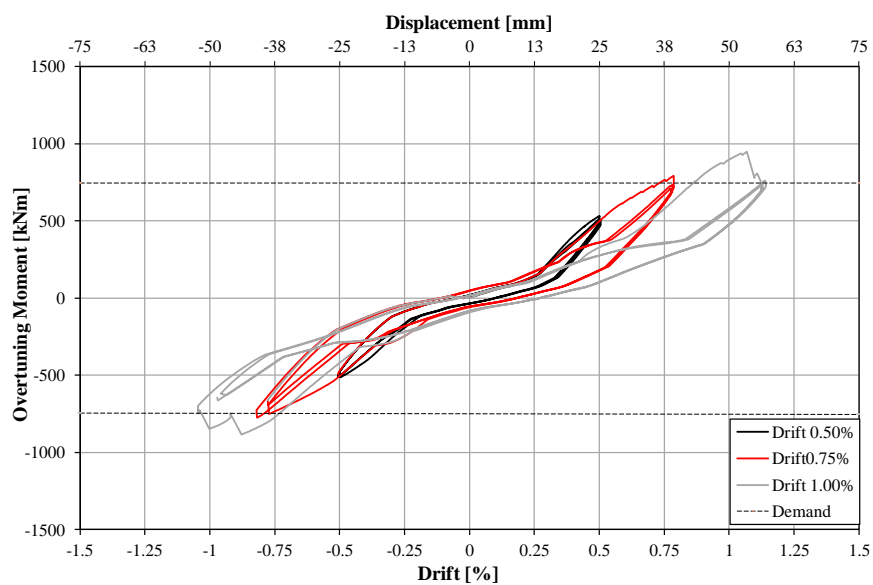


Fig. 7.36 Overturning moment vs drift before reaching 1% drift level

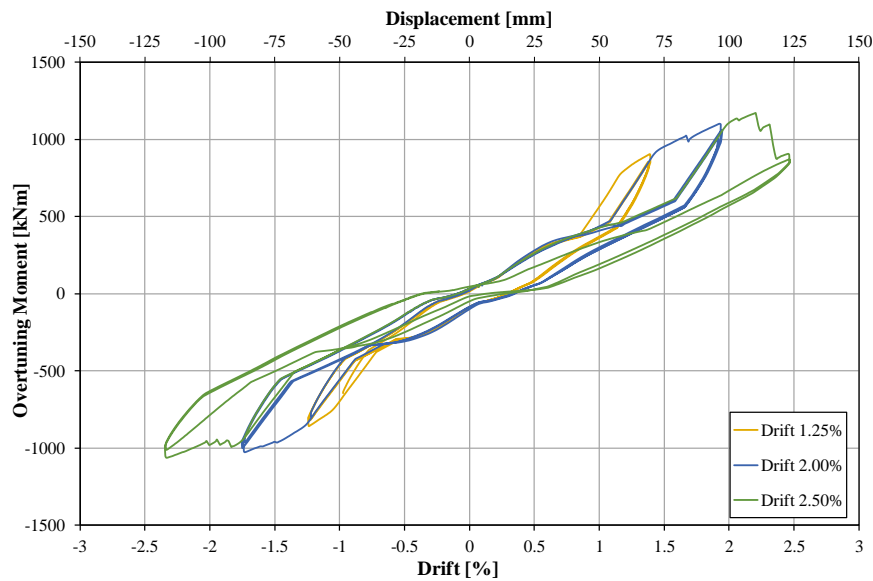


Fig. 7.37 Overturning moment vs drift after reaching 1% drift level

Similar observations to the lateral load history can be done for the overturning moment, since are directly dependent quantities. The moment demand for the 1% drift ratio have also been satisfied.

7.5.4. Post-tensioning force

Fig. 7.38 shows the post tensioning force trend versus drift for the CLT wall test. The initial value of the applied axial load was about 175 kN (40 kip).

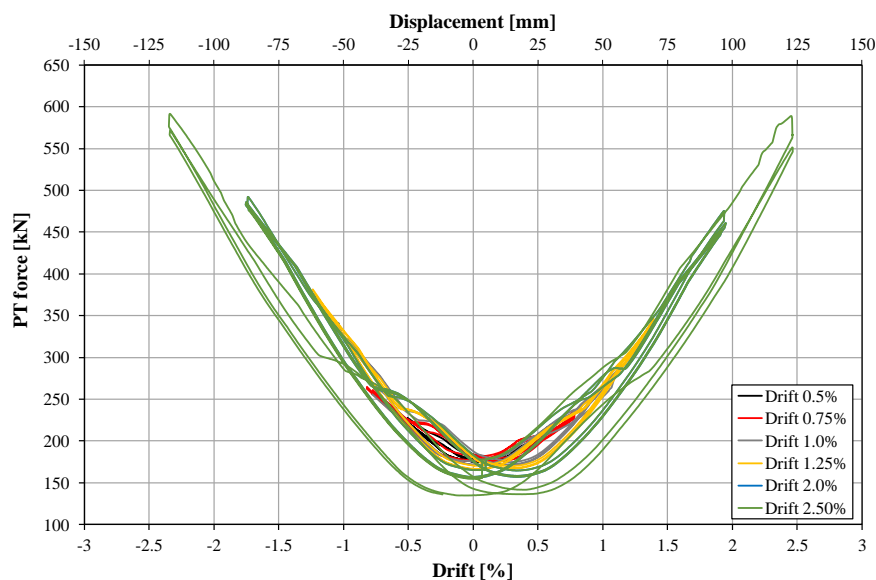


Fig. 7.38 Post-tension force vs drift

Post-tensioning force has been measured by the top load cell, therefore reported results refer to the total PT load that is considered to be equally divided for the two bars since no out-of-plane displacement were observed.

Fig. 7.39 shows that there were not significant losses of the initial post-tension force up to the design drift level. The PT reverse trend is not properly symmetric because of the embracing solution was probably moving up while trying to push the panel. This behaviour more evident for low values of drift.

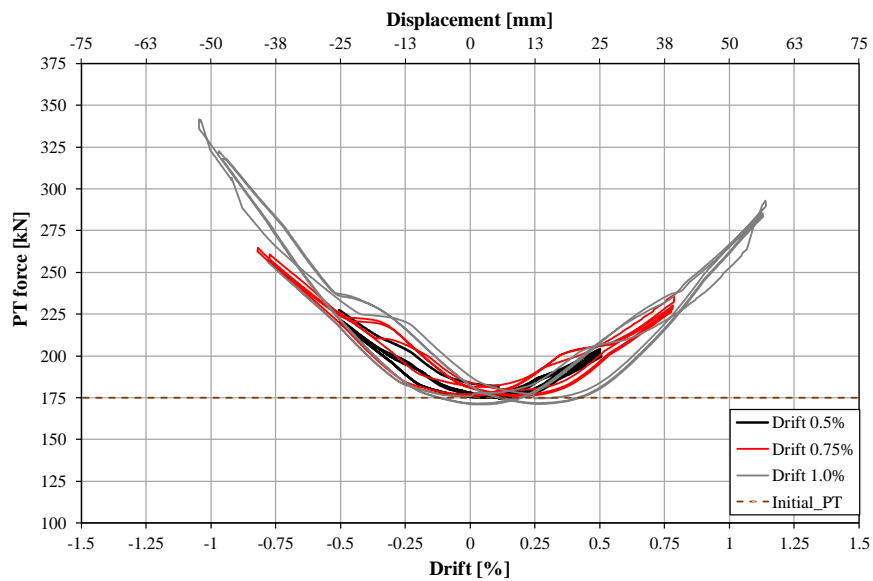


Fig. 7.39 Post-tension force vs drift before reaching 1% drift level

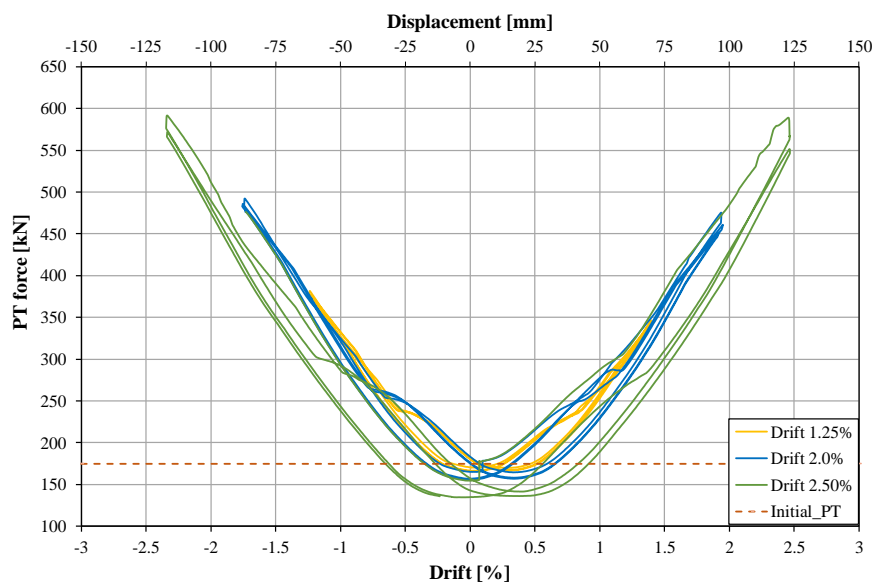


Fig. 7.40 Post-tension force vs drift after reaching 1% drift level

Differently, for increasing values of drift the trend became almost symmetric, while the initial post-tensioning force starts getting lower (Fig. 7.40). The loss in terms of initial post-tensioning is probably because of the small deformations at the base of the wall panel more some localised plasticity in the anchorage.

Fig. 7.41 show the PT strength ratio over drift, results are derived from the registered force divided by the double area of a PT bar. The PT bar could have been used also with a smaller diameter.

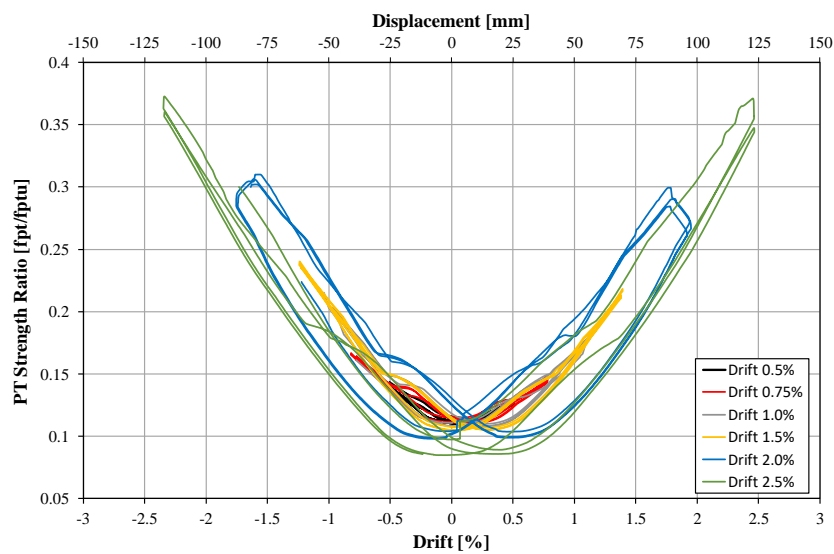


Fig. 7.41 PT strength ratio vs drift

Fig. 7.42 illustrates the value of the PT force correspondent to the overturning moment, for higher level of drift the reached PT force dropped down because of the progressing loose of rigidity in the panel-dissipater connection.

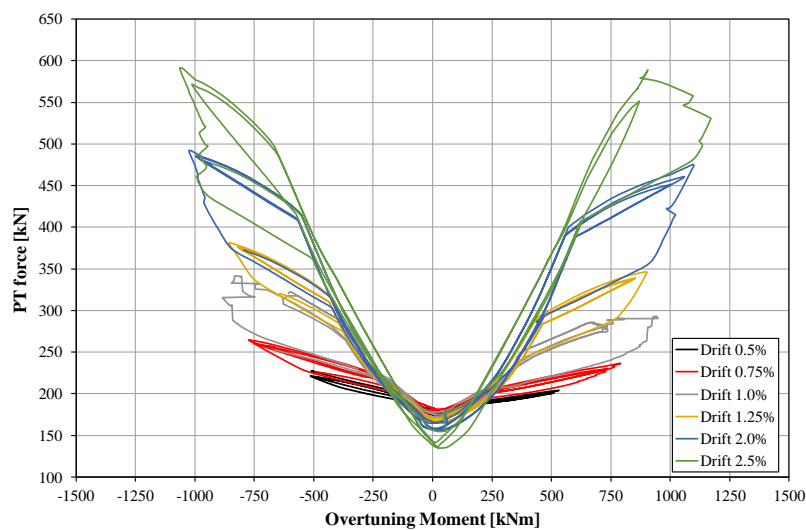


Fig. 7.42 PT force vs overturning moment

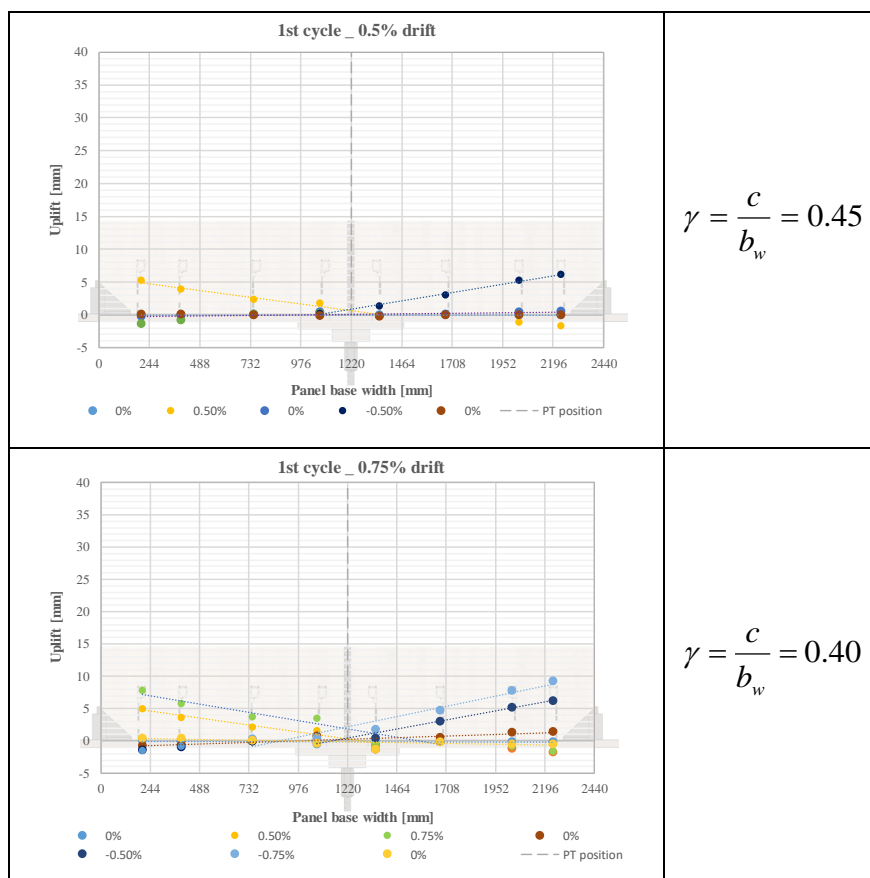
7.5.5. Neutral axis oscillation

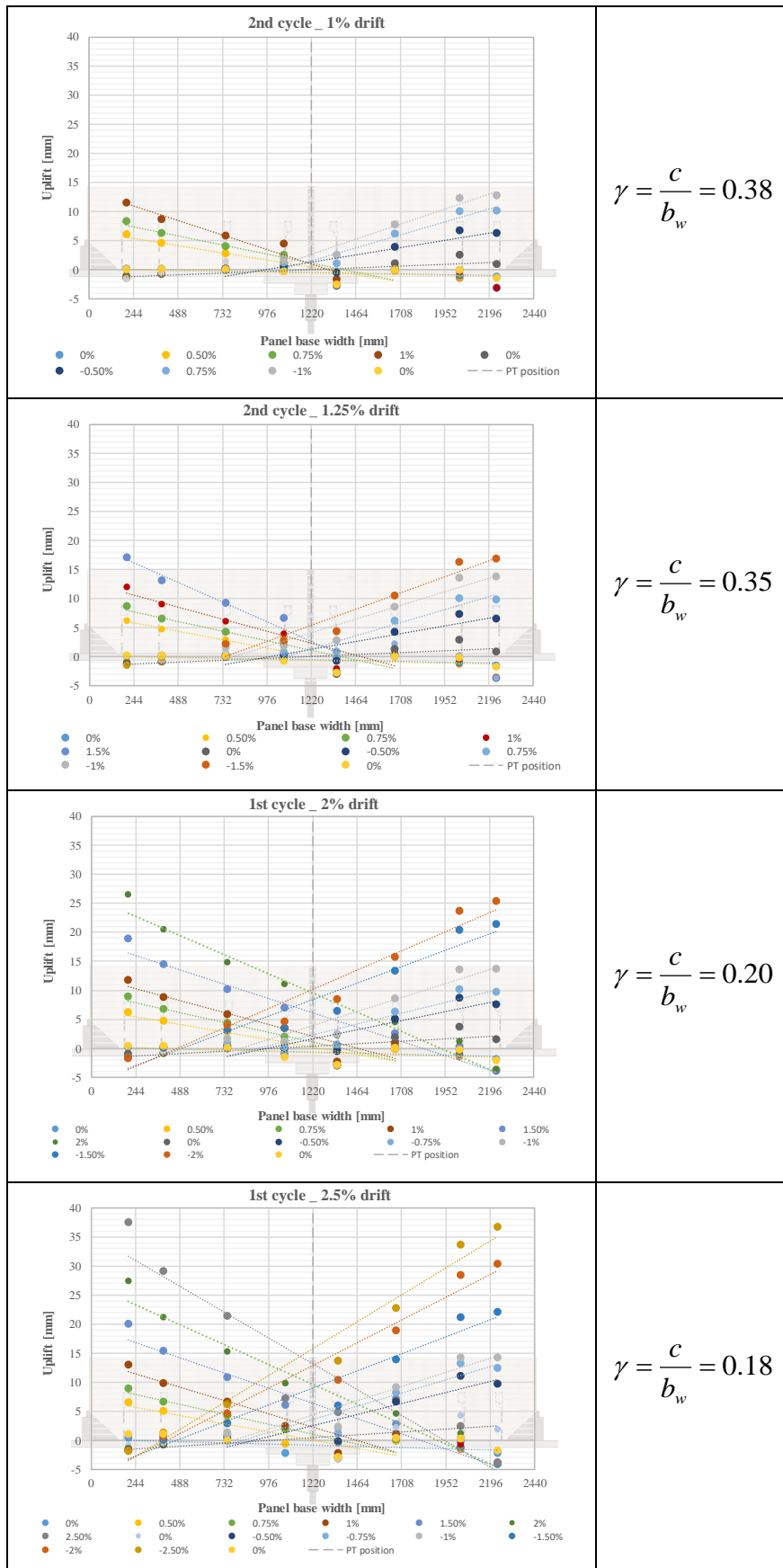
The neutral axis depth (c) is an important characteristics that can be used for calibration of analytical and numerical models of timber rocking wall. Neutral axis position is defined as the location of the rocking wall where the wall start losing contact with its bearing surface.

The base displacement string potentiometers (SP13-14-15-16-17-18-19-20) were spaced along the length of the wall and used to give an estimation of the neutral axis. All the instruments were positioned after the imposed initial PT. The neural axis position has been derived by linearly interpolating the positive (uplift) potentiometers readings. The depth of the contact portion correspond to the location where the linearization cross the horizontal axis (zero displacement).

Table 21 reports the obtained dimensionless neutral axis depth for the first cycle for each imposed drift level.

Table 21 Neutral axis depth ratio for the first cycle of each drift level





The same procedure has been repeated for all the cycles of each drift level, in order to evaluate the possible variation of the neutral axis depth within increasing deformation at base of the CLT, the resume is reported in Fig. 7.43.

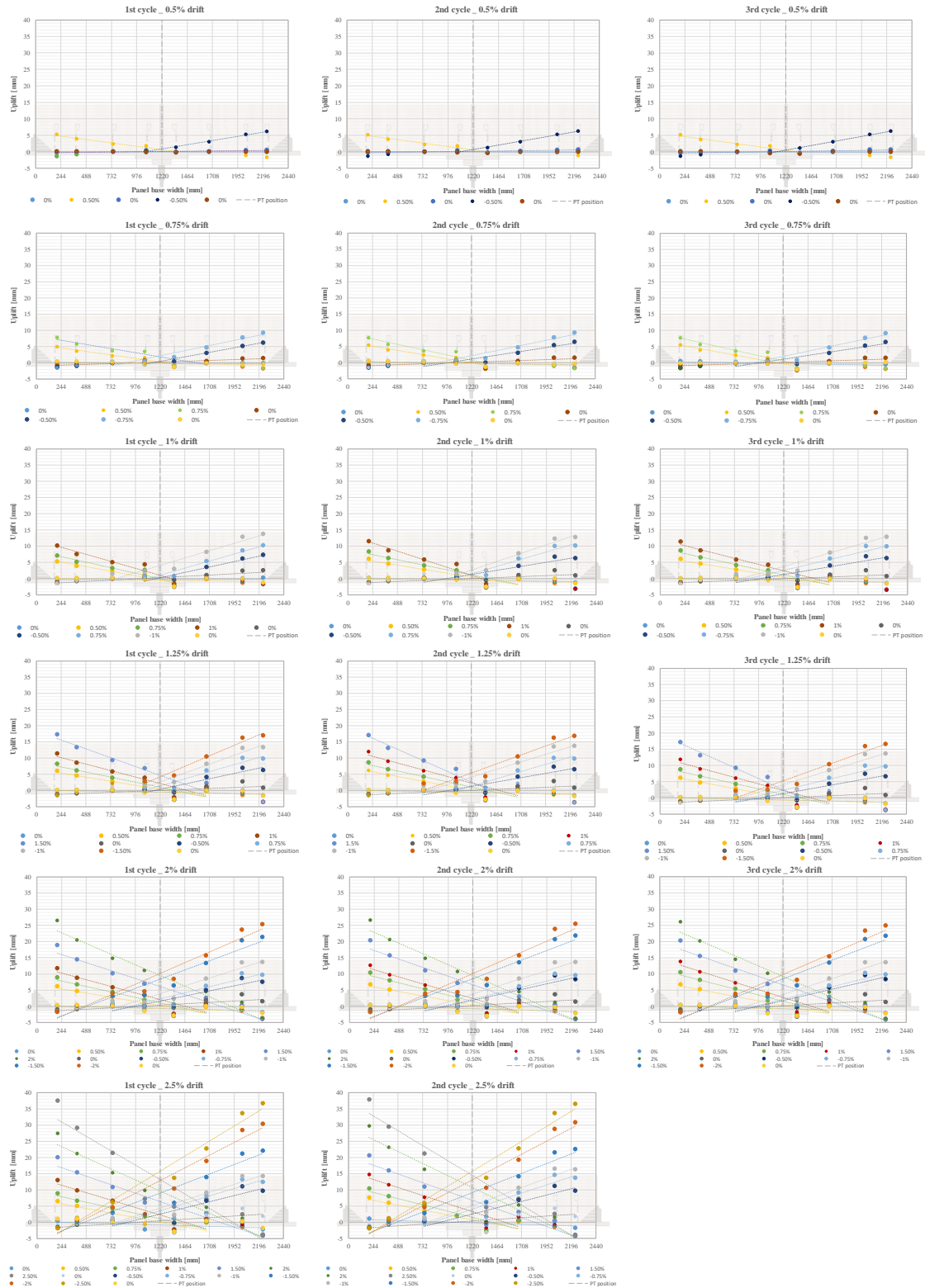


Fig. 7.43 Oscillation of the neutral axis depth for the given drift levels during repeated cycles

The results showed that the deformation at the base panel (especially close to the steel toe) were correlated to the increasing drift level, but were not particularly affected by the repeated cycles in the north-south direction.

Table 22 reports the progressive distances of the base string potentiometer.

Table 22 Progressive distances from the left corner of the base string potentiometers

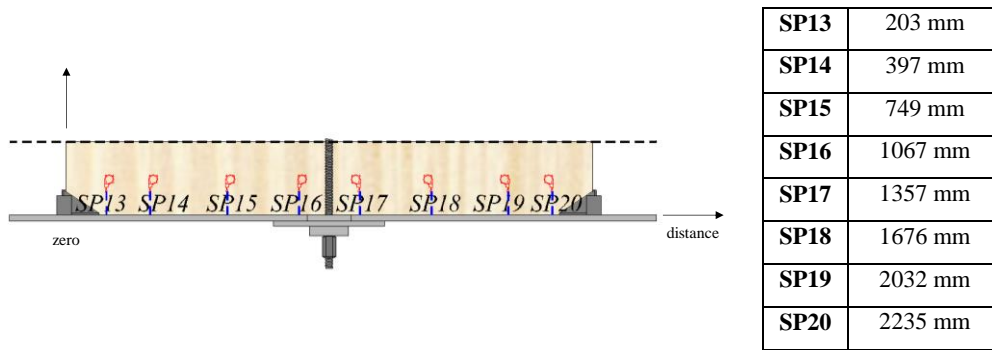
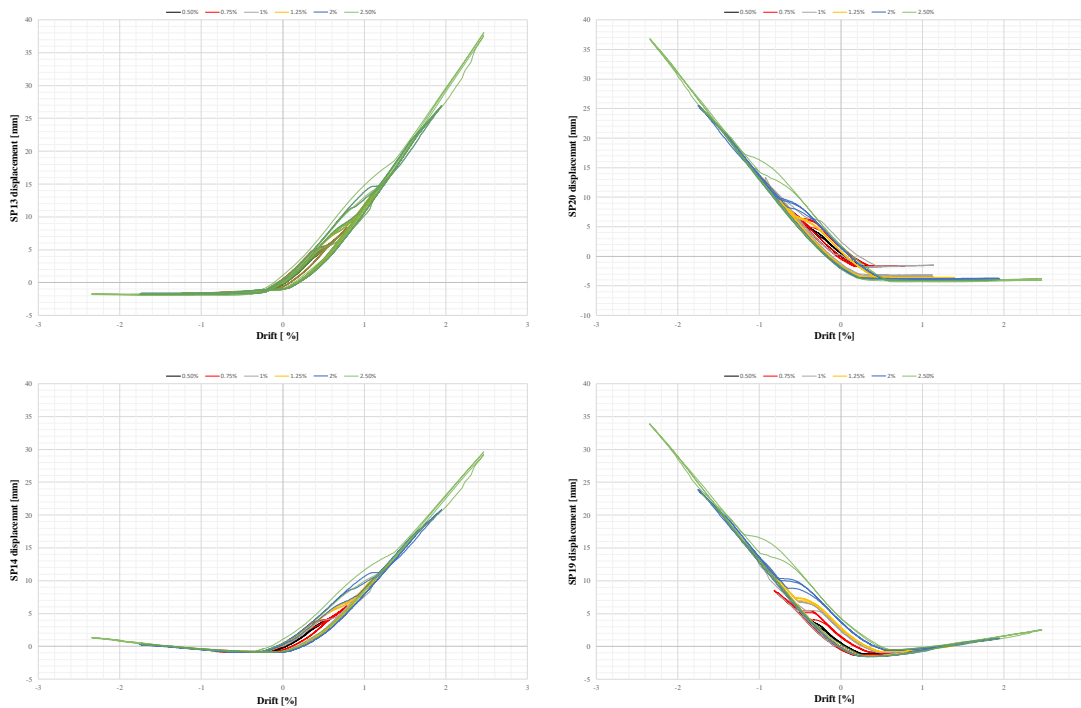


Fig. 7.44 shows the recorded vertical displacement for each symmetrically positioned string pot during the rocking motion of the CLT panel.



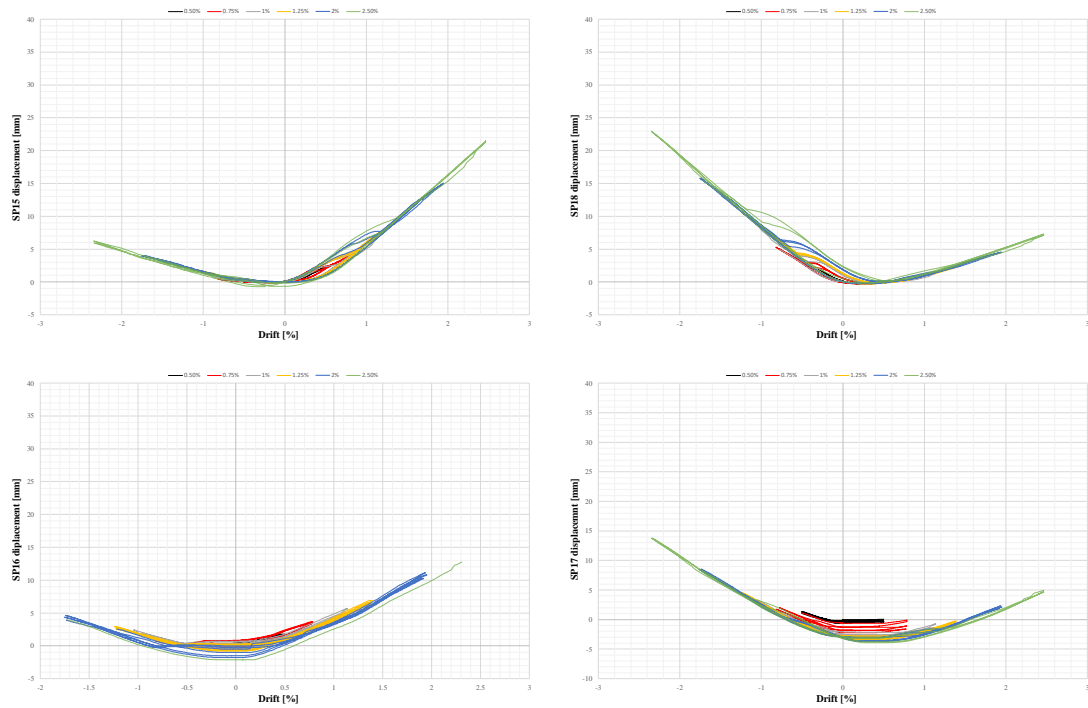


Fig. 7.44 Symmetrical positioned (respect PT bar) string pot uplift measures

Also from Fig. 7.44 it is easy to understand where and when the CLT panel was uplifting for reversed cycles. As previously mentioned, the valuation of the neutral axis depth varies with drift levels and it is fundamental to predict the response of the rocking panel in terms of forces and consequently to design it properly, optimizing each constructive details.

Chapter 8. Numerical model

Summary of Chapter 8

This chapter presents the numerical model development for the tested CLT wall. Nonlinear Time History Analysis have been conducted using Software CSI SAP 2000 v. 19.0. The key features of the numerical model were validated considering physical effects that could affect the system parameters. After validation against the experimental data, the chapter focuses on numerical simulation performed to investigate the behaviour of the panel at higher drift levels, examining in detail the dissipater behaviour and the capacity of the post-tension system.

8.1. Numerical Modelling - Simplified model description

Nonlinear push – pull numerical analyses were performed to reproduce the cyclic behaviour of the CLT panel, investigating how the unbonded post tension bars, combined with energy dissipating elements, affect the structural response.

The developed numerical model allowed to assess what the response of the rocking system would be, going beyond the drift levels reached during the experimental test.

In fact, horizontal displacements were limited by two aspects: unexpected failure in the connection between the CLT panel and the dissipater and the anchorage solution for post-tensioned bars.

The loss of strength in the panel-dissipater connection have been overtaken in the numerical schematization through the use of a rigid link, in order to simulate a rigid connection and understand real capacity of the hybrid rocking system.

The anchorage of post-tension bars has been modelled with a multilinear elastic behaviour, to take into account its axial stiffness reduction.

Analysis have been carried out using FEM Software SAP 2000 v19.0. This software is widely used for design of structures; therefore, it has been chosen to understand how a common software can face complex numerical problems.

The method of nonlinear time-history analysis used by the software is an extension of the Fast-Nonlinear Analysis (FNA), developed by Wilson (Ibrahimbegovic & Wilson 1989). This method is extremely efficient, particularly for structural systems which are primarily linear elastic but have a limited number of predefined nonlinear elements.

Analysis has been conducted applying the displacement history of the test to a lumped plasticity model.

Nonlinearities of the model have been introduced and concentrated using links characterized by non-linear behaviour (see Fig. 8.1). These elements are briefly described:

- **Axial dissipaters** were modelled using a nonlinear law, defined on the basis of tension behaviour of steel. These elements have allowed to simulate the cyclic behaviour of energy dissipaters;
- **Lateral restraints** were modelled introducing multilinear elastic elements, which were characterized by an incremental axial stiffness. This aspect has allowed to model how lateral restraint forces evolves with horizontal base displacements. This behaviour has allowed to consider initial sliding of the panel at the base.

- **The rocking oscillation** at the base of the panel has been simulated using specific friction/gap elements. These elements are characterized by an only compression behaviour and a friction dissipation capacity. This property was fundamental to simulate dissipation induced by sliding contact of the base of the panel during push – pull cycles, and representing correctly the base compressed area.

The CLT wall has been modelled using a simple elastic beam elements, as suggested by Kovacs (Kovacs 2016) and Palermo (Palermo et al. 2012).

The panel exhibits a behaviour that is substantially elastic, therefore a 2D element can be reduced to a beam without losing information on the model response. At the same time, rigid links have been introduced to simulate effective dimensions of the panel, modelling the base contact behaviour of a 2D panel using a 1D element.

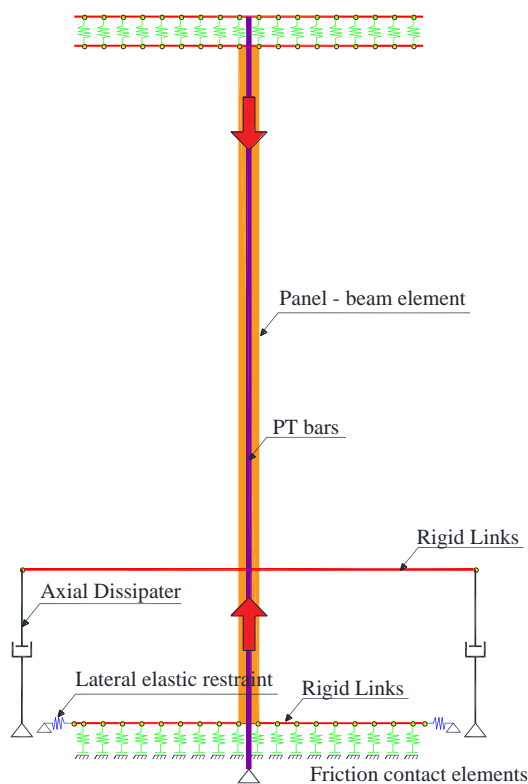


Fig. 8.1 Schematization of lumped plasticity model

8.1.1. Model Development – Definition of Elastic Elements

As previously mentioned, the CLT panel is characterized by a linear-elastic behaviour and it is modelled by a 1D beam element. The timber material in the model has been defined as isotropic, since is subjected mainly to compression loads (refer to Table 23).

The assumed elastic modulus has been defined as a percentage (55%) of elastic modulus parallel to fibres, as suggested by Newcombe (Newcombe et al. 2008b).

Table 23 Material properties specified for CLT wall

Density [kg/m ³]	Elastic Modulus [MPa]
530	6600

Tendon elements have been used to represent the effect of the post-tensioning bars. The base and the top of the panel are linked to each other by two pinned ends beams, which represent Dywidag post-tension bars, the steel material properties are defined in Table 24. Post-tension force is assigned to the panel by tendon elements, which are modelled as loads. The base restraint of each PT bar has been modelled considering its effective axial stiffness with a multilinear elastic link. Observation of experimental results has shown that the base restraints of the PT system do not act as rigid restraints; on the contrary, their deformations increase with post tension axial force levels transferred by rocking mechanism. This phenomenon would be reduced in a real system where the post-tensioned elements are directly anchored to the concrete footing. Fig. 8.2 shows how for low PT loads, induced by rocking mechanism, the behaviour of the restraint is substantially rigid. When PT loads increase the stiffness of restraint decreases if compared to rigid behaviour, which is never totally feasible in real systems.

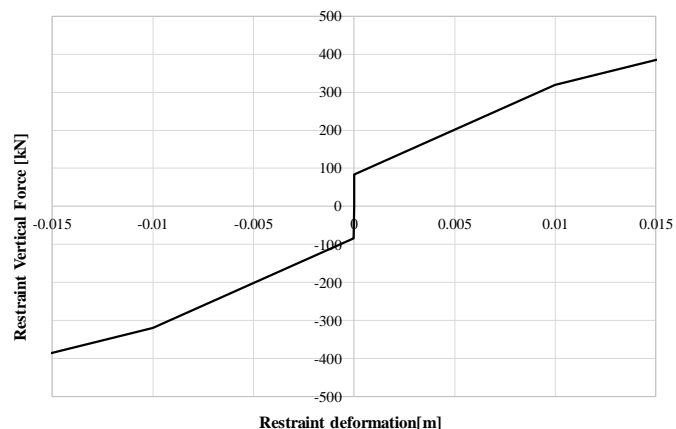


Fig. 8.2 Detail of anchorage of PT bar and the behaviour implemented in the model

Table 24 Material properties specified for Post-Tension Bars

Elastic Modulus [MPa]	Axial Force [kN]
20000	90

8.1.2. Model Development – Non-linear behaviour of Base Rocking Interaction

The interface behaviour at the base of the wall has been simulated introducing zero length non-linear friction elements. These elements resist only to compression and can also reproduce the friction between contacting surfaces, in this case, between wood and steel. The rocking at the base interface can be correctly reproduced considering the real width of the CLT panel, for this reason the ends of the beam have been extended horizontally through rigid links. These links are connected in series, and transfer forces from the beam to a series of vertical Friction/Gap spring element disposed at the base (Fig. 8.3).

Each spring at the base represent a portion of the CLT base length, clearly the number of springs introduced has been calibrated to well represent the evolution of the neutral axis depth during push-pull cycles.

The compression stiffness of contact elements has been defined as a function of the global axial stiffness of the panel, dividing it by the total number of vertical springs introduced in the model. These elements were characterized also by a friction dissipation capacity. In fact, before reaching the shear-keys, which restraint the horizontal displacements, the panel has shown a small sliding at the base (8 mm for each side), due to specimen construction tolerances and to the growing crushing on the sacrificial interposed plywood during test.

The friction between contacting surfaces induces the initial amount of dissipation observed for low levels of force and displacements.

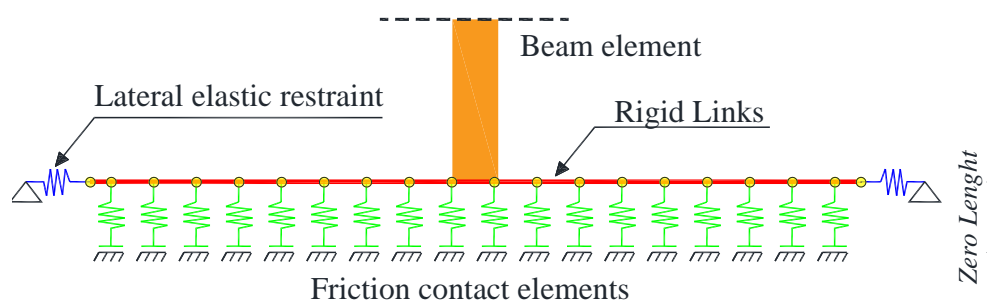


Fig. 8.3 Rocking mechanism – Schematization of friction - contact non-linear links

Table 25 Parameters of friction - contact non-linear links disposed at the base of the panel

Axial Stiffness [kN/m]	Friction coefficient
70000	0.15

Therefore lateral base restraints have been modelled by multilinear elastic links, characterized by an initial low stiffness branch that considers initial horizontal gap of the panel between shear keys and corner skirting. During push-pull cycles, the panel is pushed toward lateral shear keys and the gap progressively decreases.

When the sliding of the panel is stopped by the shear key, the rocking behaviour starts. It is important to notice that the small timber block interposed between the panel and shear keys is subjected to a progressive degradation, that is the reason why it has been considered an initial lower stiffness of lateral restraint (see Fig. 8.4 and Fig. 8.5).

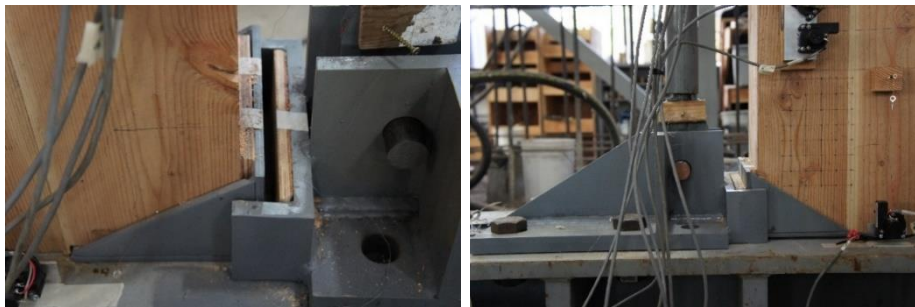


Fig. 8.4 Behaviour of lateral restraints: Initial slip between shear key and corner skirting and contact between corner skirting and shear key

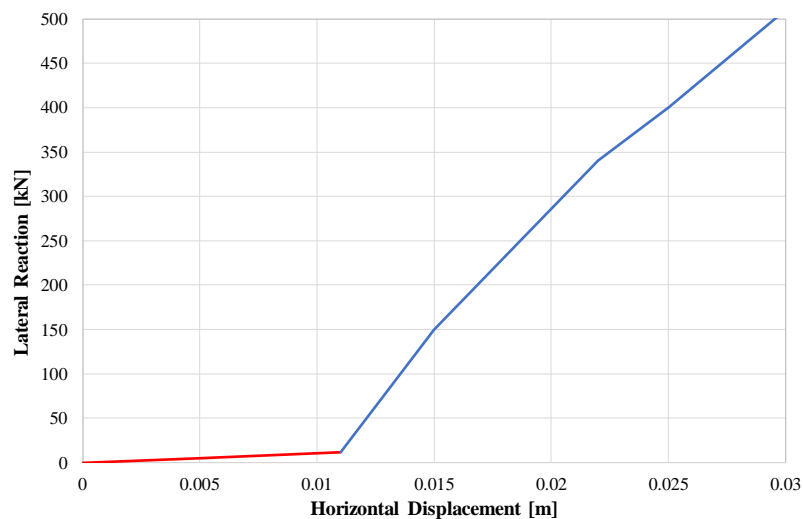


Fig. 8.5 Behaviour of lateral restraints: Initial slip between shear key and corner skirtings (red line).
Contact between corner skirtings and shear key (blue line)

8.1.3. Numerical Model Development – Non-linear behaviour of steel dissipaters

Axial steel dissipaters have been modelled as *Multilinear Plastic Non-Linear Elements*, described with a non-linear force deformation relationship given by a multilinear curve. The trend is defined on the basis of the stress-strain law of S275 (A36) steel (Kramer et al. 2013), as reported in Fig. 8.6 The first branch of implemented behaviour is elastic, while the remaining segments define the evolution of plastic deformation. The parameters that define the structural steel force-displacement curve are reported in Table 26. The strain hardening and softening behaviour after elastic branch has been defined by adopting the expression from Holzer et al. (1975).

$$\sigma = \varepsilon_y \left(1 + r \left(\frac{\sigma_u}{\sigma_y} - 1 \right) e^{(1-r)} \right) \quad (1)$$

Where:

- ε_y is steel yield strain;
- ε_{sh} is steel strain at onset of strain hardening;
- ε_u is strain corresponding to steel maximum stress;
- σ_y is steel yield stress;
- σ_u is steel maximum stress;
- $r = \frac{\varepsilon - \varepsilon_{sh}}{\varepsilon_u - \varepsilon_{sh}}$.

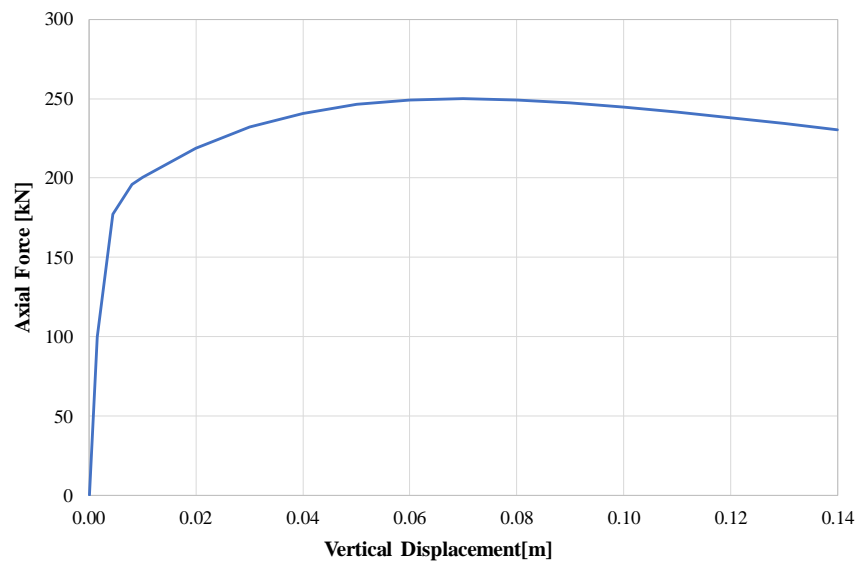


Fig. 8.6 Force Displacement behaviour of *Multilinear Plastic Links*

Table 26 Parameters which define the stress strain curve of dissipater

Yield Stress [MPa]	Max Stress [MPa]	Yielding deformation [%]	Maximum Deformation [%]
275	450	0.14	20

The pivot rule has been chosen among the different hysteretic models of the SAP2000 library, as there is no specific hysteretic model for wooden structures, and this is the only model that can take into account, although approximately, the pinching effect and the stiffness degradation of dissipater. The name of adopted hysteretic model derives from the presence of the pivot points in the force-displacement diagram, which define the slopes of unloading and reloading branches, as illustrated in Fig. 8.7. This model is fully described in Dowell, Seible, and Wilson (1998). The following parameters have been provided and the values implemented into the model are reported in Table 27:

- α_1, α_2 which define the pivot points for the unloading from the positive part of the backbone curve and the negative part, respectively;
- β_1, β_2 , which define the pivot points for the reloading towards a positive force and a negative force, respectively;
- η which determines the amount of degradation of the elastic slopes after plastic deformation.

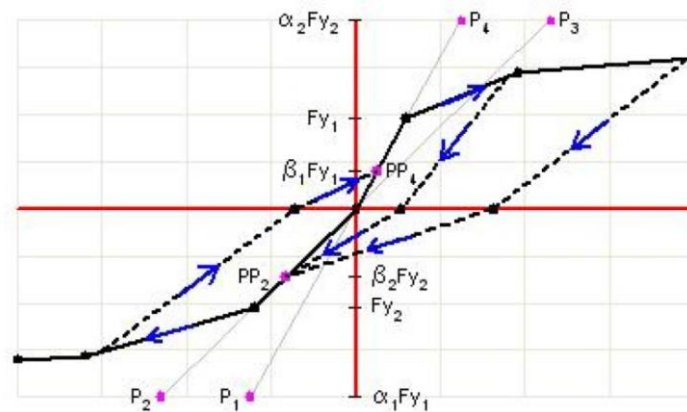


Fig. 8.7 Multilinear Pivot hysteresis relationship used in SAP2000 for dissipater hysteresis modelling

Table 27 Parameters which define the Pivot Hysteresis Model

α_1	α_2	β_1	β_2	η
50	2	0.1	1	0

8.2. Numerical Model Validation

In the present paragraph comparisons between experimental and numerical results are presented. Validation of the model has been conducted comparing nonlinear analysis results with experimental test until 1% of lateral drift. As previously described, an undesired failure started around 1% drift level in the connection between the CLT panel and the external dissipater. One of the principal aim of the model is to overcome the failure of connection, so its validation has been calibrated until experimental results were not affected by undesired failure mechanisms. Obtained results, compared in terms of load - displacement curves, exhibit a good agreement, as report in Fig. 8.8.

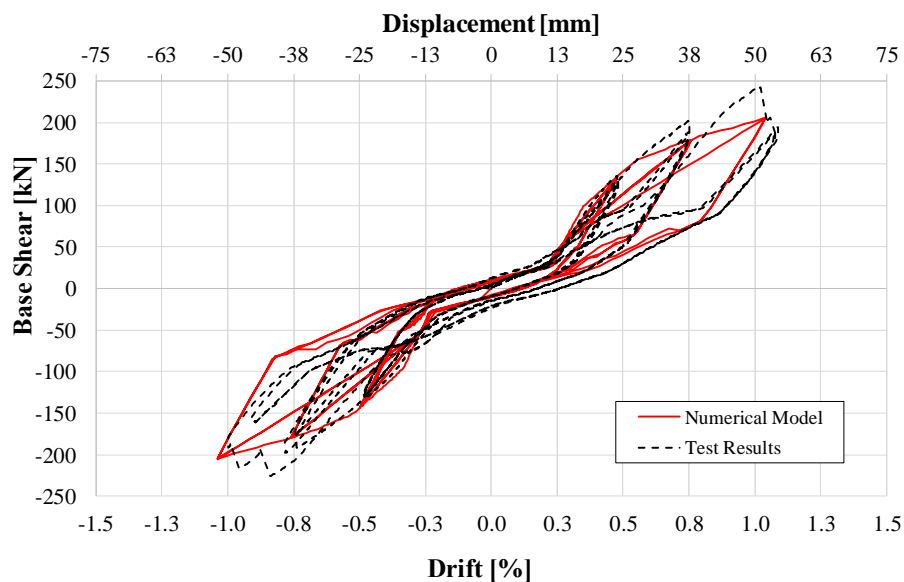


Fig. 8.8 Comparison between experimental and numerical results for drifts 0.5% - 0.75% - 1 %

Fig. 8.9, Fig. 8.10 and Fig. 8.11 show the comparisons of base shear – displacement curves obtained from numerical model and test results for each drift level until 1% lateral drift.

Accordance between curves decreases starting from 1% drift cycles, as reported in Fig. 8.11, because of the progressive degradation of the CLT panel - external dissipater.

In addition, experimental behaviour is in general “smoother” with respect to numerical results, this is due to inevitable approximations in the numerical model.

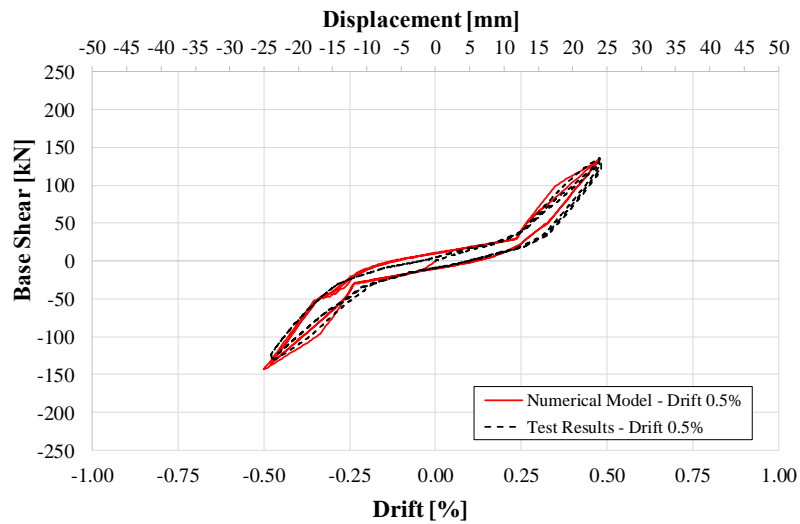


Fig. 8.9 Comparison between experimental and numerical results – drift level 0.5%

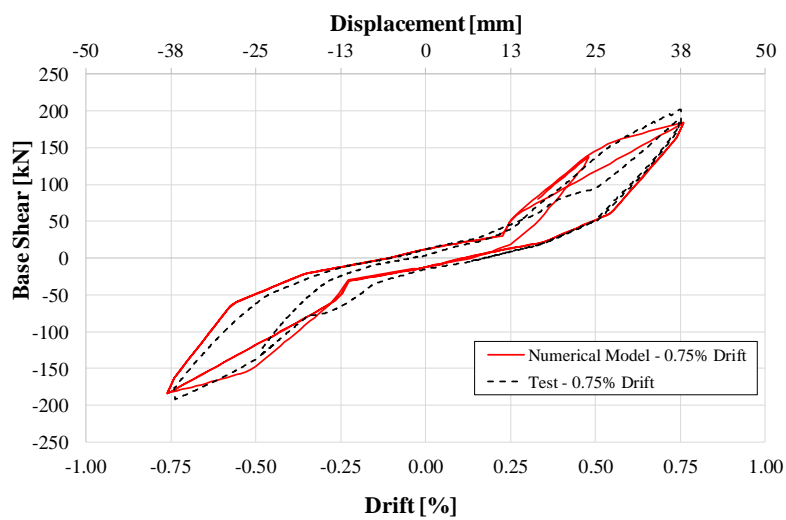


Fig. 8.10 Comparison between experimental and numerical results – drift level 0.75%

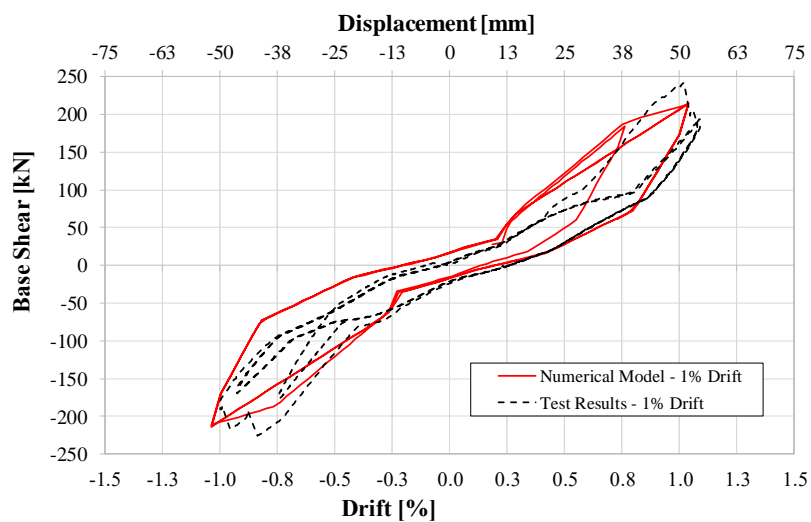


Fig. 8.11 Comparison between experimental and numerical results – drift level 1%

The overturning moment also exhibit a good accordance between numerical and test values, as reported in Fig. 8.12, confirming what has been already discussed for the base shear – displacement comparisons.

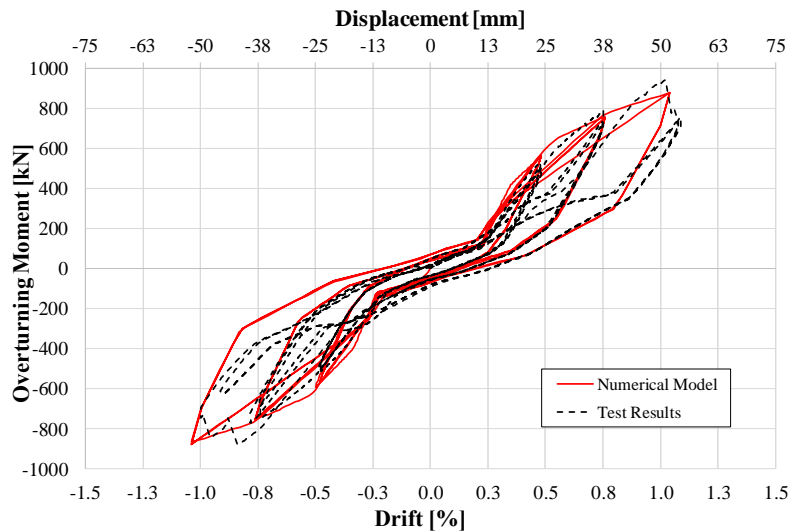


Fig. 8.12 Overturning Moment - Comparison between experimental and numerical results for drifts 0.5% - 0.75% - 1 %

Examination of model and experimental results have been conducted also for axial force in PT bars, exhibiting a positive accordance. Results for drift until 1% are reported in Fig. 8.13. Furthermore, the graph obtained from the numerical model is perfectly symmetric while the experimental one is not. This is a consequence of some adjustments of experimental set up occurred during the test, which are not reproducible by the model.

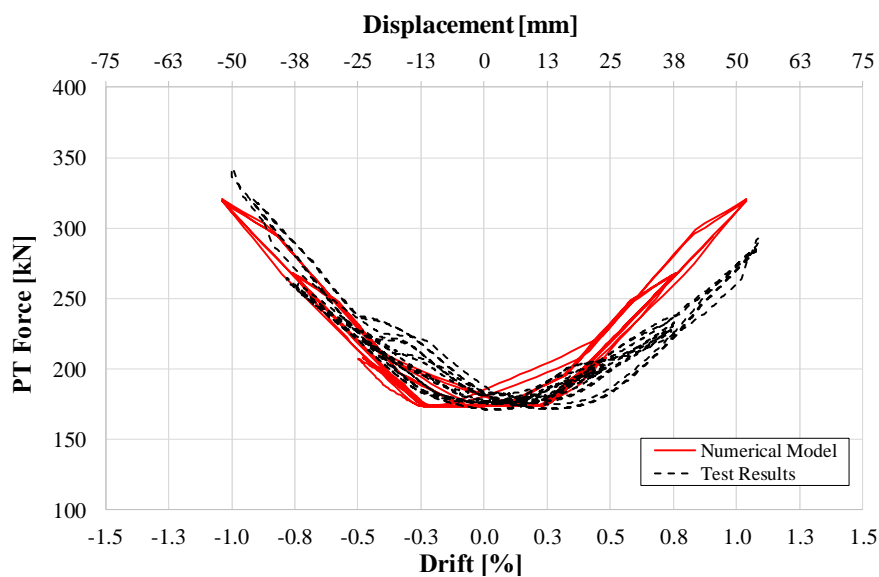


Fig. 8.13 PT force: Comparison of experimental and numerical results for drifts 0.5% - 0.75% - 1 %

In Fig. 8.14, Fig. 8.15 and Fig. 8.16 comparisons of PT - displacement curves obtained from the numerical model and experimental results for each drift level, are illustrated in detail until 1% drift.

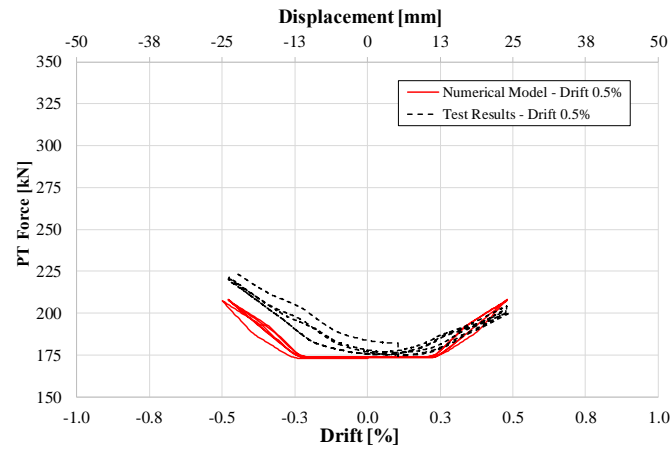


Fig. 8.14 Comparison of test and numerical results: Post-tension force – drift level 0.5%.

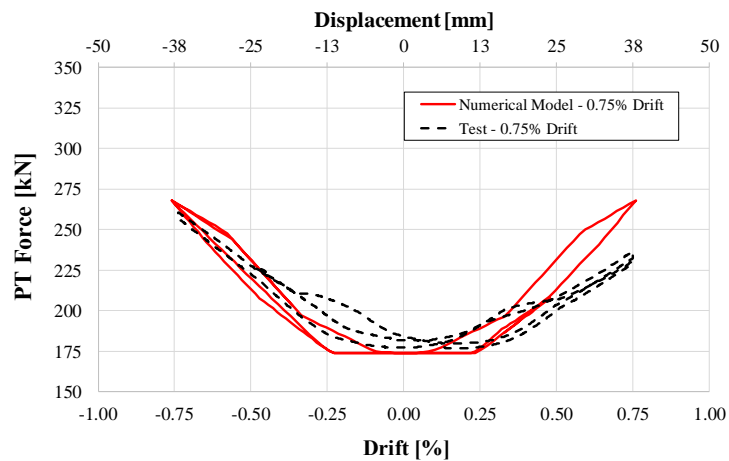


Fig. 8.15 Comparison of test and numerical results: Post-tension force – drift level 0.75%

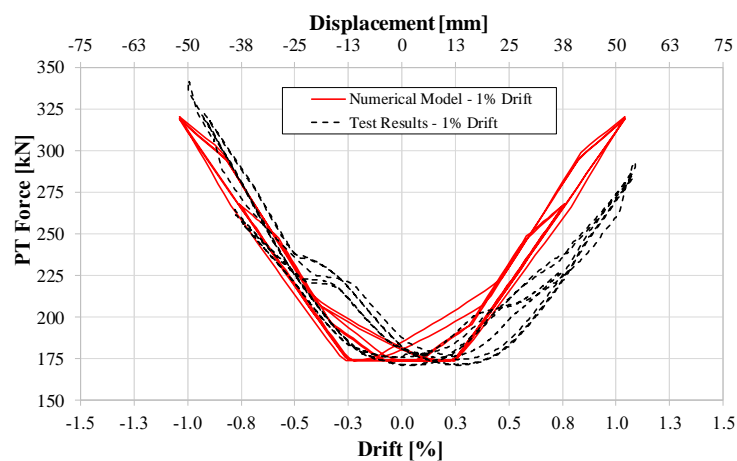


Fig. 8.16 Comparison of test and numerical results: Post-tension force – drift level 1%

Table 28 reports the comparison between experimental and numerical values for the resulting horizontal forces. The comparison in term of displacement was automatically satisfied because of the imposed displacement history equal to the drift levels applied in the experimental test. Comparison of values show a good agreement between numerical and experimental behaviour, above all for 0.5% and 0.75% drift levels. The gap between experimental and numerical model values, as expected, increase around 1% drift.

Table 28 Comparison of horizontal load measured during test with numerical model.

Drift	Test -Base Shear[kN]	Numerical Model – Base Shear[kN]	Difference [%]
0.5%	130	133	+2%
0.75%	200	190	-5%
1%	230	216	-8%

To understand if the parameters introduced in the model were correctly determined, a comparison between experimental and numerical values in terms of amount of dissipated energy has also been carried out.

In Fig. 8.17 dissipated energy values are shown for each cycle of experimental and numerical model, the percentage ratio of variation between obtained values is also reported above the numerical energy results. In this case the maximum difference between numerical and experimental behaviour is 9%, demonstrating a valid correspondence between experimental and numerical results. However, around 9th cycle (1% drift) the loss of strength of dissipater -CLT panel connection starts and the experimental test energy dissipation capacity decreases respect to the model.

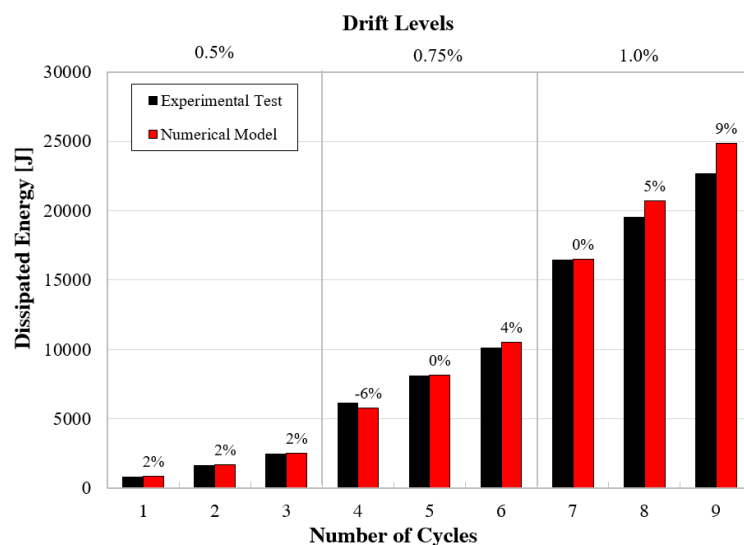


Fig. 8.17 Comparison between dissipated energy obtained by experimental and numerical results

8.3. Simulation of test and calculation of Area -based Equivalent viscous damping

The validated model has been used to reproduce test, overtaking the unexpected failure of panel-dissipater connection. The base shear – displacement response has been evaluated until 2.5% drift, as reported in Fig. 8.18. Numerical results show overall a good accordance with experimental data, also for drift above 1%, however the dissipation capacities of the model are higher if compared to the test.

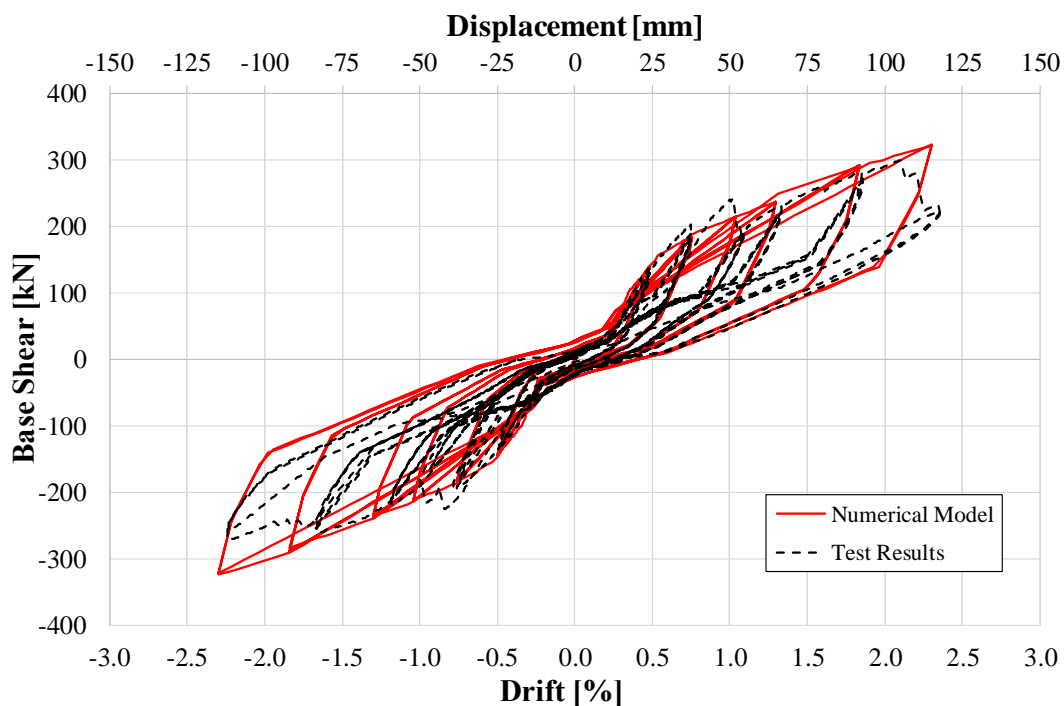


Fig. 8.18 Comparison between dissipated energy obtained by experimental and numerical results for drift until 1%

In the model the dissipaters preserve sufficient energy dissipation capacities until drift 2.5%, while during test their dissipation capacities decrease after 1%.

The evidence of this behaviour is given by the comparison of dissipated energy calculated as the area of every force – displacement cycle, respectively for test and numerical results. The energy dissipation obtained from experimental results is lower if compared to dissipation energy values obtained from numerical model, the percentage ratio of difference between dissipation values starts to increase clearly from 1.25% drift.

At 2.5% of drift the percentage reduction of dissipation capacity, after loss of resistance of dissipater connection registered during test, is approximately -30%, if compared to numerical model results (see Fig. 8.19).

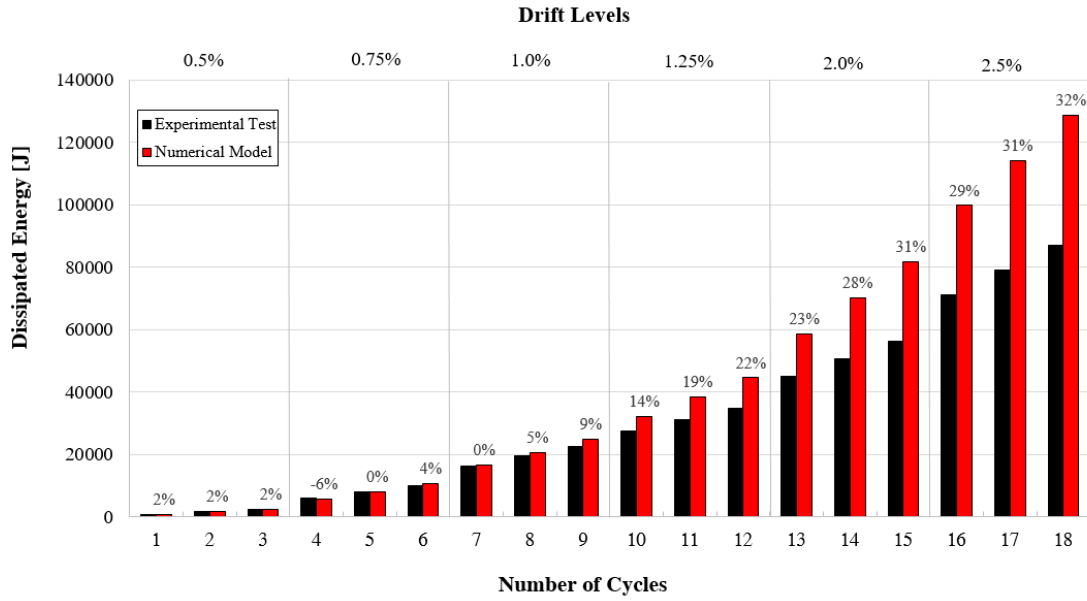


Fig. 8.19 Comparison between dissipated energy obtained by experimental and numerical results for drift until 2.5%.

This effect had some influence on the system behaviour also in terms of hysteretic damping. To highlight the magnitude of the reduction of the energy dissipated through hysteresis, the area-based viscous damping has been evaluated for each cycle of the experimental tests.

The area – based equivalent viscous damping (EVD) ζ_{hist} derives from the following formula:

$$\zeta_{hist} = \frac{1}{2\pi} \frac{A_h}{F_m \Delta_m} \quad (2)$$

Where:

- A_h is the area within one complete cycle of stabilized force-displacement response;
- $F_m \Delta_m$ are maximum force and displacement achieved in the stabilized loops.

The EVD values have been calculated respectively for model and test results. The evolution of EVD has been evaluated comparing results obtained by every 1st cycle of each drift level and results obtained by 2nd and 3rd cycle.

As shown, in Fig. 8.20 and Fig. 8.21, It is comprehensible that maximum dissipation occurs at every 1st cycle for each drift level, while at 2nd and 3rd cycles dissipation capacity decreases.

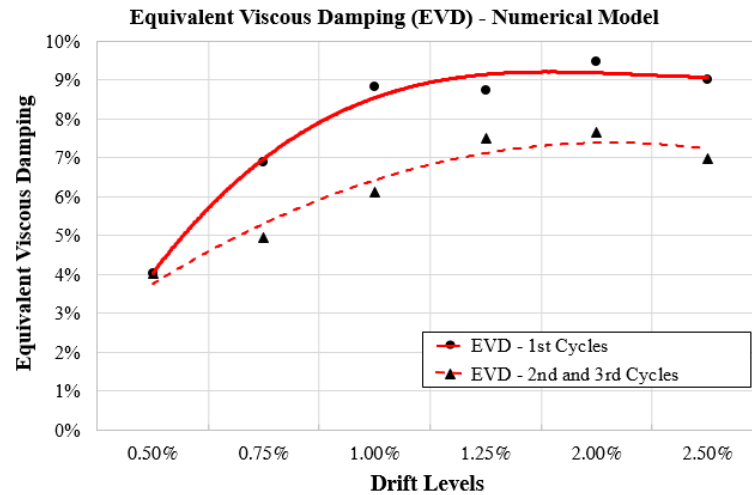


Fig. 8.20 Comparison of EVD values for 1st, 2nd and 3rd Cycles of drifts until 2.5% for numerical model

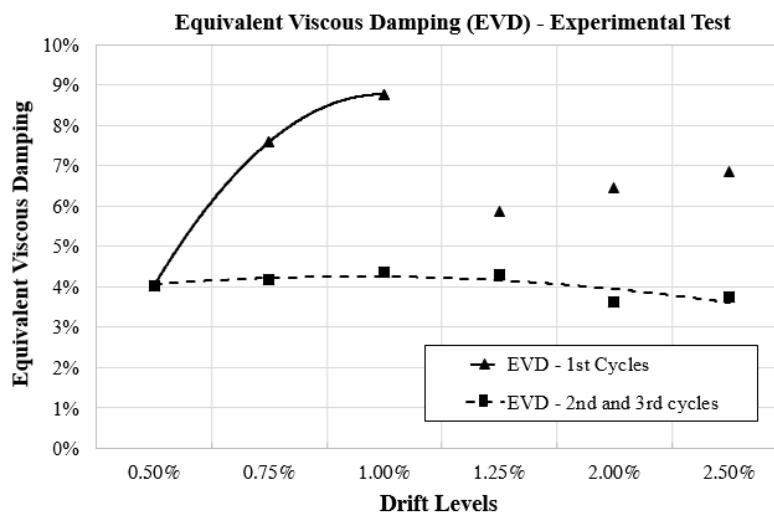


Fig. 8.21 Comparison of EVD values for 1st, 2nd and 3rd Cycles of drifts until 2.5% for experimental results

The EVD values are compared between numerical model and experimental test, as reported in Fig. 8.22 and Fig. 8.23.

Numerical model results calculated for 1st cycle exhibit an increasing trend from 0.5% to 2.5% drifts, while test results show a clear decrease at 1.25% drift, highlighting how the loss of resistance in the connection of dissipater influences dissipation capacities of the system.

EVD values calculated for 2nd and 3rd cycle exhibit an increasing trend from 0.5% to 2.5% drifts for numerical model, while the test values are substantially constant.

In this case, anyway, the loss of dissipation capacities after 1.25% is not so clear as for 1st cycles EVD values.

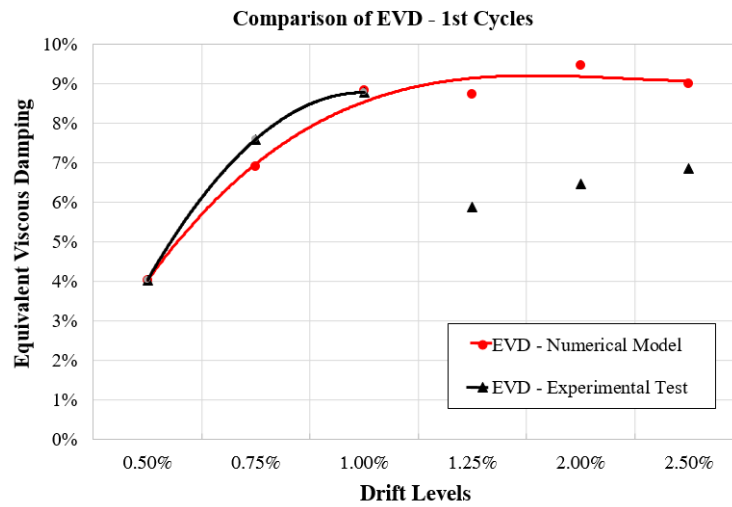


Fig. 8.22 Comparison of EVD values obtained by experimental and numerical results for 1st Cycles of drifts until 2.5%

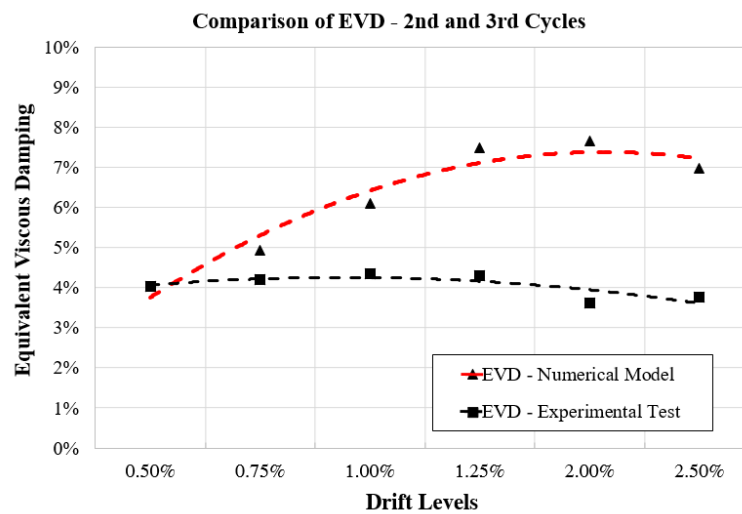


Fig. 8.23 Comparison of EVD values obtained by experimental and numerical results for 2nd and 3rd Cycles of drifts until 2.5%

8.4. Numerical simulation for high drift levels

The validated model has been used to overcome drift levels reached during test, trying to reach effective limit capacity of the system.

On the basis of experimental test results, the simple numerical model developed, although with some approximations, allows to reproduce in a satisfying way the behaviour of hybrid rocking-dissipating system.

The displacement loading history has been extended to a drift level of 5%, which is two times higher than the maximum drift reached during test (2.5%), as reported in Fig. 8.24.

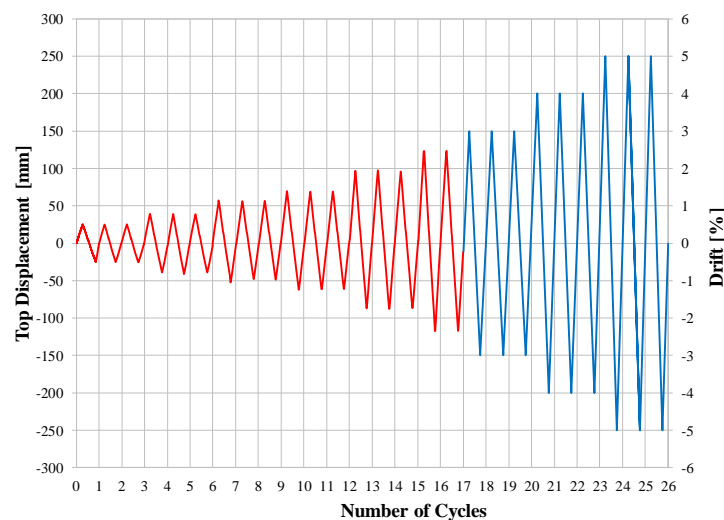


Fig. 8.24 Drift levels reached during experimental test and developed numerical model (red line) and incremental drift levels investigated by numerical model (blue line)

The base shear – displacement curve obtained, as reported in Fig. 8.25, shows that the dissipation capacities of the model are high until 5% drift, and continue to increase in addition to a good re-centring capacity, which is guaranteed by the post-tensioned bars. The energy dissipation capacity obtained from experimental results, except for cycles under 1% drift, is lower if compared to dissipated energy values obtained from numerical model.

In Fig. 8.26 the dissipated energy is computed for every extended target cycle in the numerical representation. In addition, for drift levels under 2.5% results obtained by experimental test are reported, and previously commented.

It is clear how high level drift cycles contribute decisively to increase dissipation capacity of the system.

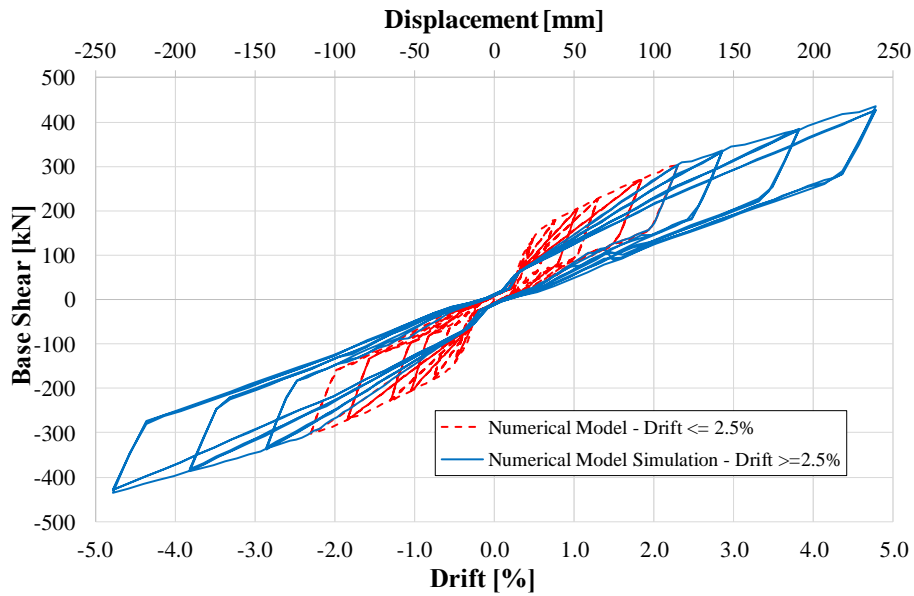


Fig. 8.25 Base shear – top displacement curve: Drift levels reached during experimental test (red line) and incremental drift levels investigated by numerical model (blue line)

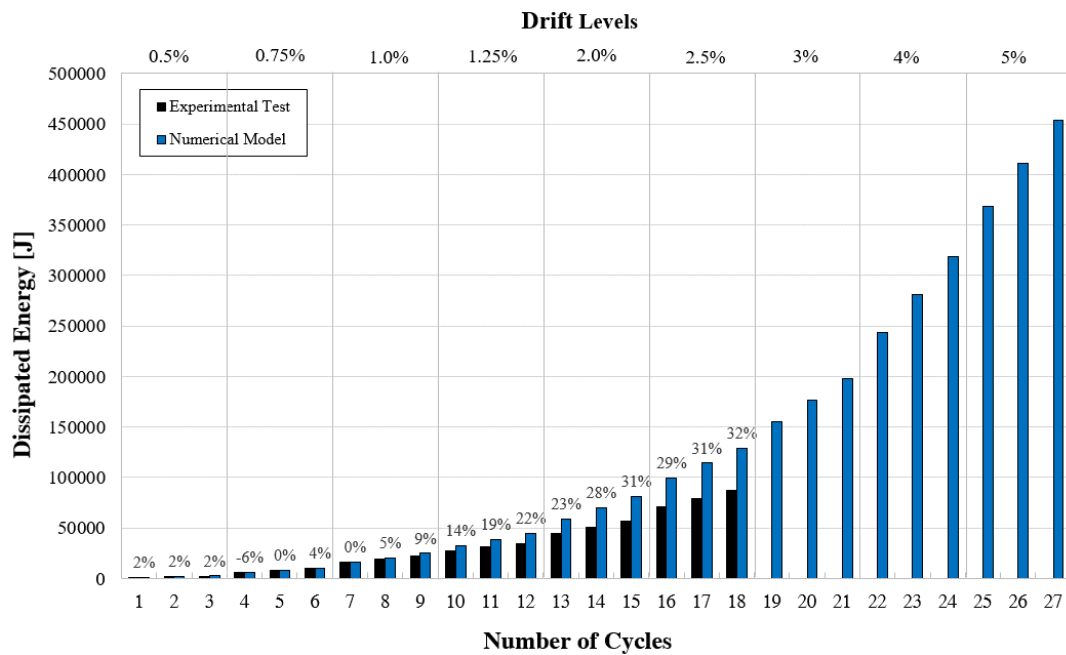


Fig. 8.26 Comparison between dissipated energy obtained by experimental and numerical results for drift until 5%

For every cycle of numerical simulation, the equivalent viscous damping coefficient (EVD) has been calculated. In Fig. 8.27 are reported envelope curves of calculated values of EVD for different drift levels. The blue line is the interpolation of EVD values of 1st cycles, while the red one interpolates EVD values of 2nd and 3rd cycles of each drift level.

How previously discussed the higher contribute to damping is given by 1st cycles with a maximum equivalent viscous damping of about 10%, while the 2nd and 3rd cycles give a EVD of 7.5%.

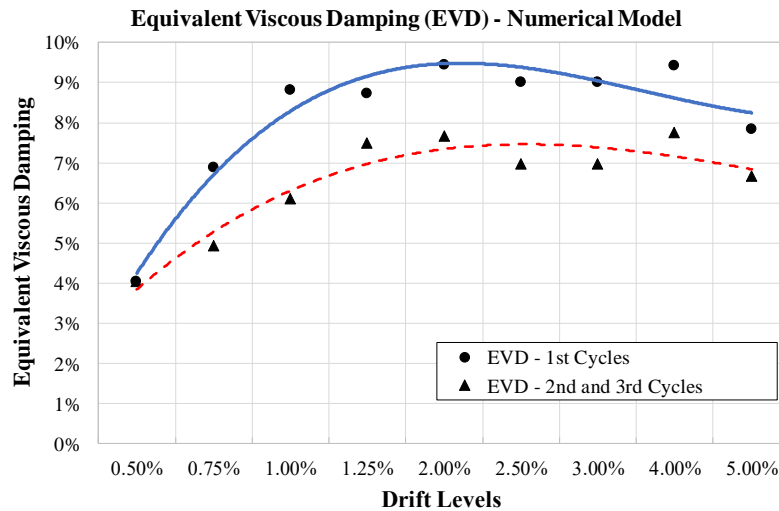


Fig. 8.27 Comparison of EVD values for 1st, 2nd and 3rd Cycles of drifts until 5% for numerical model

In conclusion, the objective of numerical simulation has been investigating the basic parameters that defines the structural response of a CLT panel equipped with a hybrid rocking/dissipative system.

These parameters are substantially the dissipater nonlinear behaviour, the elastic stiffness of the PT bars/anchorage and the friction/rocking gap behaviour at the base of the panel. The knowledge of those parameters allows to reproduce a complex non-linear behaviour with simple models and to predict structural response without repeat experimental tests. The characterized finite elements modelling can be fairly easily implemented in more complex 3D representations of CLT structures, that could be designed to face intense seismic action with lateral resistant hybrid rocking low-damage CLT walls solutions.

Chapter 9. Conclusions

In this thesis the interaction between coupled actions in traditional CLT building connections and the lateral force-displacement response of a hybrid CLT rocking wall were examined using experimental testing, analytical and numerical modelling. The keys objective of this work were: investigating the actual response of the traditional CLT connectors when subjected to seismic solicitation to help defining guidelines and models for a safety design of metal connectors in CLT structures, and to provide an input and more information on the behaviour and design of low-damage solutions for CLT shear walls. To achieve these objectives, different experimental tests have been performed. Conclusions drawn from each of these researches are summarized below, together with possible future improvements and further research programs.

9.1. Experimental campaign on CLT traditional steel connections remarks

The first part presents an experimental study on the effect of lateral deformation on the axial behavior of typical hold-down and angle bracket connections. The results of tests performed on 15 specimens each (10 cyclic plus 5 monotonic tests) subjected to different levels of imposed secondary deformation confirm that stiffness, yielding displacement, and load-carrying capacity are affected by the coupling shear-tension action on both types of connections. Experimental results compared to analytical estimation of the load-carrying capacity demonstrate that adopting mean values for the mechanical parameters (i.e. wood density, fastener yielding moment etc..) in the general model suggested by Johansen (Johansen 1949) provides reliable estimation of the load-carrying capacity of nailed hold-down and angle bracket connections. The resulting analytical capacity of the connection is close to the value obtained experimentally when the metal bracket connectors are subjected to actions towards the main axis (without imposed secondary direction displacements). On the other hand, the load-carrying capacity of the

configuration with imposed secondary displacement cannot be predicted with the standard approach, thus specifically developed models are necessary.

Results from monotonic and cyclic tests on hold-down and angle bracket connections could be used to define guidelines and models for a safety and optimized design of metal connectors in CLT structures. Additionally, they provide a basic information for advanced and reliable investigation on CLT structures, by means of specifically calibrated analytical models suitable to define the actual hold-down axial resistance and angle bracket shear capacity at different level of secondary direction displacements.

The laboratory campaign demonstrates that engineering design practice is not coherent with experimental evidences and may represent an unsafe calculation assumption when conventional CLT connections are subjected to coupled tension-shear action.

Last but not least, undesired connection response has been highlighted especially when the angle bracket was loaded in the secondary. The yielding of the steel part occurred before the shear plastic mechanism of nails in the wood wall was activated. These types of failure modes demonstrate that capacity based design should not only be implemented at the building level (i.e. no brittle failures on the wood element), but also at the connection level (i.e. failure in tension of the hold-down metal plate) and, even more, at the fastener level (i.e. by ensuring a desired ductile failure as two plastic hinges in the fastener). The basic principle of capacity based design at the connection levels is that nail plasticization should be always ensured, whereas the steel parts of the connector should be overdesigned to prevent any plasticization. In this way all energy dissipation is concentrated in the nailed CLT panel-metal bracket connections (in both directions), and even more, the same connector could be possibly reused after undergoing major seismic events.

9.2. Experimental test CLT hybrid rocking wall remarks

The response of different, conventional and innovative, connection systems for lateral load resisting CLT walls have been investigated in this thesis. In addition to the first part, a damage free connection solution that included external dissipative devices was tested.

The feasibility of the application of hybrid rocking principles on a CLT wall and its response was numerically and experimentally studied. The 2-storey 2/3 scaled test on a CLT post-tensioned wall with external axial dissipaters showed that this is a good prospective solution for timber shear resistant wall.

Drift amplitudes up to 2.5% drift were applied and some unexpected damages on the connection were observed after 1% design drift level. The applicability of the selected connection solution between dissipaters and CLT wall has been tested for the first time. The chosen connection solution between the external dissipative device and the timber wall, which was realized using innovative ZD-plate connectors (MyTiCon), was found to be not appropriate for the study case. Although, this new connectors are really efficient for joints subjected to pure shear action, and overcome the problems showed with typical double crossed screws when subjected to reverse cycles (Closen 2012).

The post-tensioning bars worked, as expected, in the role of elastic springs ensuring to the CLT panel a re-centring capability after cycles. No damages were observed in the compression zone at the base of the CLT panel, and neither in the contact portion with the lateral shear keys. Test results are reported in terms of lateral force, overturning moment and oscillation of the neutral axis depth, this information is fundamental to design properly the entire system components.

In addition, a numerical model has been developed for the tested CLT wall using SAP 2000. The key features of the numerical model were validated considering physical effects that could affect the system parameters. After validation against the experimental data, the numerical simulation is used to investigate the behaviour of the rocking system components at higher drift levels, overcoming the experimental test limits.

Experimental and numerical test results can be used to provide more details and starting points on CLT rocking wall systems performances to the scientific and engineering design community to be used in the near future for further researches and several CLT projects. Allowing CLT structural systems to go way beyond the limitation of classic distributed connections and at the same time relying on higher performances with less residual damages.

9.3. Suggestions for future work

During the work of this thesis some key areas have been addressed which require further experimental or analytical studies to verify and/or strengthen the presented results.

Regarding the first part, additional experimental tests are required to describe more in detail the variation of the connection's capacity under coupled actions and to provide further input data for numerical simulation.

An interesting next step could be the contemporary application of cyclic load input in the two directions, to simulate a realistic evolution of the seismic force in the connector's behaviour and defining a resistant domain.

In addition, with reference to the second part, the stimulating outcomes of the hybrid rocking wall test supports an application of this system in CLT structures. Further tests are needed to improve the presented results. Also, additional tests should be carried out at higher drift levels. In this context the vertical load or the pre-stress force in PT bars should be varied to draw conclusions on the different behaviour varying the re-centring ratio parameter. Details require to be better planned to abate the effect of "pinching" in the overall hysteresis loop.

The dissipater disposition need to optimized to reduce as possible the secondary moment due to the distance with the panel, this is an aspect that strongly influences the correct design of the connection. To activate and exploit with maximum benefits the dissipater contribution, the connection need to remain rigid, which for elevate force requests means that should be highly oversized. Especially for timber element this aspect is not easy to achieve, because the connection portion end up to be a quite big steel plaque, losing this way the benefit of reducing the number of needed fasteners and taking advantage of using wood instead of steel as constructive material. Moreover, by relying on wood-metallic connector resistant mechanism the problem of embedment in the wood after repeated cycles can be hardly prevented. Therefore, an alternative solution to repeat the test could be adapting, to the present study case, a system already implemented for wood-concrete slab. The idea is using as attach for the external dissipater a support that is glued together with the side of the panel, giving to the connection a sort of material continuity, as shown in Fig. 9.1.



Fig. 9.1 HSK system (TiComTec)

The HSK system consist of perforated metal plates with a corresponding adhesive. This forms the bond between the wood and the steel. The wood is cut parallel to the grain, the cavity is filled with a special adhesive and finally, the perforated metal plate is inserted. The holes in the steel plate acts as adhesive anchors and can withstand enormous force. The selected plate thickness and rating are intended to ensure that, in the event of failure, the steel plate begins to yield before the wood cracks, protecting the connections from brittle failures and providing additional ductility. The presented option is just a hypothesized alternative solution so far, additional financial support will be needed to repeat more tests.

References

- American National Standard-ANSI/APA PRG 320, 2012. Standard for Performance-Rated Cross-Laminated Timber.
- Blaß, H. J. ; Uibel, T., 2006. Load carrying capacity of joints with dowel type fasteners in solid wood panels. In *Proceedings of the Institution of Civil Engineers - Structures and Buildings, CIB*. Florence.
- Blaß, H. J. ; Uibel, T., 2007. *Tragfähigkeit von stiftförmigen Verbindungsmitteln in Brettsperrholz*. K. Universitätsverlag Karlsruhe, ed., Karlsruhe, Germany: Karlsruher Berichte zum Ingenieurholzbau.
- Buchanan, A. & Fairweather, R.H., 1993. Seismic Design of Glulam Structures. *Bulletin of the New Zealand Society for Earthquake Engineering, NZSEE*, 26(4), pp.415–436.
- Ceccotti, A., 2008. New technologies for construction of medium-rise buildings in seismic regions: the XLAM case. *Structural Engineering International*, 18(2), pp.156–165.
- Ceccotti, A., 2007. Progetto SOFIE - Sistema Costruttivo Fiemme. Relazione scientifica finale.
- Ceccotti, A. et al., 2013. SOFIE project - 3D shaking table test on a seven-storey full-scale cross-laminated timber building. *Earthquake Engineering & Structural Dynamics*, 42(13), pp.2003–2021.
- Ceccotti, A. et al., 2006. SOFIE project - Cyclic tests on cross-laminated wooden panels. In *9th World Conference on Timber Engineering, WCTE*. pp. 805–812.
- Ceccotti, A. & Sandhaas, C., 2010. A proposal for a standard procedure to establish the seismic behaviour factor q of timber buildings. In *10th World Conference on Timber Engineering, WCTE*.
- Christopoulos, C. et al., 2002. Posttensioned energy dissipating connections for moment-resisting steel frames. *Journal of Structural Engineering*, 128(9), pp.1111–1120.

- Closen, M., 2012. *Self-Tapping screw assemblies under monotonic loading*. University of British Columbia.
- Dujič, B., 2004. Testing of Racking Behaviour of Massive Wooden Wall Panels. In *International Council for Research and Innovation in Building and Construction, CIB*.
- Dunbar, A.J.M., Pampanin, S. & Buchanan, A.H., 2014. Seismic performance of core-walls for multi-storey timber buildings. In *Bulletin of the New Zealand Society for Earthquake Engineering, NZSEE*.
- Eatherton, M.R. et al., 2014. Design concepts for controlled rocking of self-centering steel-braced frames. *Journal of Structural Engineering*, 140(11), p.4014082.
- EN-12512, 2011. Timber structures-Test methods: Cyclic testing of joints made with mechanical fasteners.
- EN-1380, 2009. Timber structures. Test methods. Load bearing nails, screws, dowels and bolts.
- EN-14358, 2006. Timber structures - Calculation of characteristic 5-percentile values and acceptance criteria for a sample.
- EN-1995-1-1, 2009. Eurocode 5 - Design of timber structures, Part 1-1, General: Common rules and rules for buildings.
- EN-1998-1, Eurocode 8: Design of structures for earthquake resistance.
- EN-26891, 1991. Timber structures: Joints made with mechanical fasteners. General principles for the determination of strength and deformation characteristics.
- EN-338, 2009. Structural timber - Strength classes.
- ETA-04/0013, 2015. Nails and Screws for Use in Nailing Plates in Timber Structures.
- ETA-09/0323, 2009. Three-dimensional nailing plate (angle bracket for wood to wood connections).
- ETA-11/0086, 2011. Hold-downs for timber-to-timber or timber-to-concrete or steel connections.
- ETA-14/0349, 2014. CLT – Cross Laminated Timber: Solid wood slab elements to be used as structural element in buildings.
- Ganey, R. et al., 2016. Experimental investigation of self-centering cross laminated timber walls. In *World Conference on Timber Engineering, WCTE*.
- Gavric, I. et al., 2012. Experimental-numerical analyses of the seismic behaviour of cross-laminated wall systems. In *15th World Conference of Earthquake Engineering, WCEE*.

- Gavric, I., Fragiaco, M. & Ceccotti, A., 2014. Cyclic behaviour of typical metal connectors for cross-laminated (CLT) structures. *Materials and Structures*, 48(6), pp.1–17.
- Guerrini, G. et al., 2015. Seismic behavior of posttensioned self-centering precast concrete dual-shell steel columns. *Journal of Structural Engineering*, 141(4), pp.1–11.
- Guerrini, G. et al., 2012. Self-centering precast concrete dual-shell steel columns. In *15th World Conference on Earthquake Engineering, WCEE*.
- Gülkan, P. & Langenbach, R., 2004. The earthquake resistance of traditional timber and masonry dwellings in turkey. In *13th World Conference on Earthquake Engineering, WCEE*.
- Gupta, A. & Krawinkler, H., 1999. *Seismic demands for performance evaluation of steel moment resisting frame structures*. Report No.132, Stanford University.
- Hilson, B.O., 1995. Joints with dowel-type fasteners – Theory, Timber Engineering STEP 1: Basis of design, material properties, structural components and joints. , p.C3/1-11.
- Ibrahimbegovic, A. & Wilson, E.L., 1989. Simple numerical algorithms for the mode superposition analysis of linear structural systems with non-proportional damping. *Computers & Structures*, 33(2), pp.523–531.
- Iqbal, A. et al., 2012. Seismic response of post-tensioned LVL walls coupled with plywood sheets. In *World Conference on Timber Engineering, WCTE*. pp. 5–10.
- Iqbal, A., Pampanin, S. & Buchanan, A., 2007. Improved seismic performance of LVL post-tensioned walls coupled with UFP devices. In *8th Pacific Conference on Earthquake Engineering*.
- Izzi, M. et al., 2016. Experimental investigations and design provisions of steel-to-timber joints with annular-ringed shank nails for Cross-Laminated Timber structures. *Construction and Building Materials*, 122, pp.446–457.
- Johansen, K.W., 1949. Theory of timber connections. *International Association of Bridge and Structural Engineering*, 9, pp.249–262.
- Jorissen, A. & Fragiaco, M., 2011. General notes on ductility in timber structures. *Engineering Structures*, 33(11), pp.2987–2997.
- Kovacs, M., 2016. *Seismic design of heavy timber in low-to-moderate seismic hazard regions*. Master Thesis, McMaster University.
- Kramer, A., Barbosa, A.R. & Sinha, A., 2013. Performance of steel energy dissipators

- connected to Cross-Laminated Timber wall panels subjected to tension and cyclic loading. *Journal of Earthquake Engineering*, 142(2007), pp.1–10.
- Langenbach, R., 2010. Earthquake resistant traditional construction. *International Conference on Disaster Management and Cultural Heritage*, pp.1–25.
- Marriott, D.J. et al., 2008. Dynamic Testing of Precast, Post-Tensioned Rocking Wall Systems with Alternative Dissipating Solutions. In *Bulletin of the New Zealand Society for Earthquake Engineering, NZSEE*. pp. 90–103.
- Moroder, D. et al., 2014. Experimental investigation of wall-to-floor connections in post-tensioned timber buildings. In *Bulletin of the New Zealand Society for Earthquake Engineering, NZSEE*.
- Munoz, W. et al., 2008. Determination of yield point and ductility of timber assemblies: in search for a harmonised approach. In *World Conference on Timber Engineering, WCTE*.
- Nakaki, S.D., Stanton, J.F. & Sritharan, S., 1999. An overview of the PRESSS five-story precast test building. *Precast Concrete Institute Journal*, 44(2), pp.26–39.
- Newcombe, M., 2007. *Seismic design of multistorey post-tensioned timber buildings*.
- Newcombe, M.P. et al., 2008a. Section analysis and cyclic behavior of post-tensioned jointed ductile connections for multi-story timber buildings. *Journal of Earthquake Engineering*, 12(sup1), pp.83–110.
- Newcombe, M.P. et al., 2008b. Section analysis and cyclic behavior of post-tensioned jointed ductile connections for multi-story timber buildings. *Journal of Earthquake Engineering*, 12, pp.83–110.
- Palermo, A. et al., 2012. From theory to practice: design, analysis and construction of dissipative timber rocking post-tensioning wall system for Carterton Events Centre, New Zealand. In *15th World Conference on Timber Engineering, WCEE*. Lisboa.
- Palermo, A. et al., 2006. Innovative seismic solutions for multi-storey LVL timber buildings overview of the research program. In *9th World Conference on Timber Engineering, WCTE*.
- Palermo, A. & Pampanin, S., 2006. Experimental investigations on LVL seismic resistant wall and frame subassemblies. In *European Conference on Earthquake Engineering and Seismology, ECEES*.
- Palermo, A., Pampanin, S. & Calvi, G.M., 2004. Use of “controlled rocking” in the seismic design of bridges. In *13th World Conference of Earthquake Engineering, WCEE*.

- Palermo, A., Pampanin, S. & Marriott, D., 2007. Design, modeling, and experimental response of seismic resistant bridge piers with posttensioned dissipating connections. *Journal of Structural Engineering*, 133(11), pp.1648–1661.
- Palermo, a. et al., 2006. Quasi-static cyclic tests on seismic-resistant beam-to-column and column-to-foundation subassemblies using Laminated Veneer Lumber (LVL). In *19th Australasian Conference on Mechanics of Structures and Materials, ACMSM*.
- Palermo, a. et al., 2005. Seismic design of multi-storey buildings using laminated veneer lumber (LVL). In *Bulletin of the New Zealand Society for Earthquake Engineering, NZSEE*.
- Pampanin, S. et al., 2006. Code provisions for seismic design of multi-storey post-tensioned timber buildings. In *International Council for Research and Innovation in Building and Construction, CIB*.
- Pampanin, S., Priestley, M.J.N. & Sritharan, S., 2001. Analytical modelling of the seismic behaviour of precast concrete frames designed with ductile connections. *Journal of Earthquake Engineering*, 5(3), pp.329–367.
- Piazza, M., Polastri, A. & Tomasi, R., 2011a. Ductility of timber joints under static and cyclic loads. *Proceedings of the ICE-Structures and Buildings*, 164(2), pp.79–90.
- Piazza, M., Polastri, A. & Tomasi, R., 2011b. Ductility of timber joints under static and cyclic loads. *Proceedings of the Institution of Civil Engineers - Structures and Buildings*, 164(2), pp.79–90.
- Popovski, M. et al., 2014. Force modification factors for CLT structures for NBCC. In *Materials and Joints in Timber Structures*. Dordrecht: Springer Netherlands, pp. 543–553.
- Popovski, M., Schneider, J. & Schweinsteiger, M., 2010. Lateral load resistance of cross-laminated wood panels. In *World Conference on Timber Engineering, WCTE*. pp. 3394–3403.
- Pozza, L. et al., 2015. Behaviour factor for innovative massive timber shear walls. *Bulletin of Earthquake Engineering*, 13(11), pp.3449–3469.
- Pozza, L. et al., 2016. Experimentally based q -factor estimation of cross-laminated timber walls. *Proceedings of the Institution of Civil Engineers - Structures and Buildings*, 169(7), pp.492–507.
- Pozza, L. & Scotta, R., 2015. Influence of wall assembly on behaviour of cross-laminated timber buildings. *Proceedings of the ICE-Structures and Buildings*, 168(4), pp.275–

- 286.
- Priestley, M.J.N., 1991. Overview of PRESSSS research program. *Precast Concrete Institute Journal*, 36(4), pp.50–57.
- Priestley, M.J.N. et al., 1999. Preliminary results and conclusions from the PRESSSS five-story precast concrete test building. *Precast Concrete Institute Journal*, 44(6), pp.42–67.
- Priestley, M.J.N. et al., 1999. Preliminary test results from the PRESSSS 5-story precast concrete building. *Precast Concrete Institute Journal*, 44(6), pp.42–67.
- Rahman, A. & Restrepo, J., 2000. *Earthquake resistant precast concrete buildings: Seismic Performance of cantilever walls prestressed using unbonded tendon*,
- Restrepo, J.I., Tobolski, M.J. & Matsumoto, E.E., 2011. *NCHRP Report 681: Development of a precast bent cap system for seismic regions*,
- Ricles, J.M. et al., 2001. Posttensioned seismic-resistant connections for steel frames. *Journal of Structural Engineering*, 127(2), pp.113–121.
- Sandhaas, Carmen; Mergny, E., Yield moment of nails. In *INTER proceedings*. pp. 2–4.
- Sandhaas, C. et al., 2009. Analysis of X-lam panel-to-panel connections under monotonic and cyclic loading. In *International Council for Research and Innovation in Building and Construction, CIB*.
- Sarti, F., 2015. *Seismic design of low - damage post - tensioned timber wall systems*. Doctoral thesis, University of Canterbury.
- Sarti, F., Palermo, A. & Pampanin, S., 2014. Quasi static cyclic tests of 2 / 3 scale post-tensioned timber wall and column-wall-column (CWC) systems. In *Bulletin of the New Zealand Society for Earthquake Engineering, NZSEE*. pp. 1–9.
- Sarti, F., Palermo, A. & Pampanin, S., 2012. Simplified design procedures for post-tensioned seismic resistant timber walls. In *15th World Conference of Earthquake Engineering, WCEE*.
- Smith, T. et al., 2007. Seismic response of hybrid-LVL coupled walls under quasi-static and pseudo-dynamic testing. In *Bulletin of the New Zealand Society for Earthquake Engineering, NZSEE*. pp. 1–8.
- Stanton, J.F., 2003. Self-centering structures for use in seismic regions. In *Proceedings of the ASCE Structures Congress*. Seattle,WA, p. 8 on CD-ROM.
- Stanton, J.F. & Nakaki, S.D., 2002. *Design Guidelines for Precast Concrete Structural Systems*, PRESSSS Report No. 01/03-09.
- Stanton, J.F., Stone, W.C. & Cheok, G.S., 1997. A hybrid reinforced precast frame for

- seismic regions. *Precast Concrete Institute Journal*, 42(2), pp.20–32.
- Tampone, G., 1996. *Il restauro delle strutture di legno*, Hoepli.
- Tomasi, R. & Sartori, T., 2013. Mechanical behaviour of connections between wood framed shear walls and foundations under monotonic and cyclic load. *Construction and Building Materials*, 44, pp.682–690.
- Tomasi, R. & Smith, I., 2015. Experimental characterization of monotonic and cyclic loading responses of CLT panel-to-foundation angle bracket connections. *Journal of Materials in Civil Engineering*, 27(6), p.4014189.
- Toranzo, L., 2002. *The use of rocking walls in confined masonry structures: a performance-based approach*. Doctoral thesis, University of Canterbury.
- Toranzo, L.A. et al., 2004. Rocking confined masonry walls with hysteretic energy dissipators and shake-table validation. In *13th World Conference on Earthquake Engineering, WCEE*.
- Toranzo, L. a. et al., 2009. Shake-table tests of confined-masonry rocking walls with supplementary hysteretic damping. *Journal of Earthquake Engineering*, 13(6), pp.882–898.
- Yasumura, M., 2012. Determination of failure mechanism of CLT shear walls subjected to seismic action. In *International Council for Research and Innovation in Building and Construction, CIB*.
- Yenidogan, C. & Erdik, M., 2016. A comparative evaluation of design provisions for seismically isolated buildings. *Soil Dynamics and Earthquake Engineering*, 90, pp.265–286.

Figure Captions

Fig. 1.1 Flow-chart of thesis organization.....	8
Fig. 2.1 (a) <i>Today-ji Daibutsu-den</i> Buddhist temple (b) <i>Horyu-ji</i> temple and its structure.....	13
Fig. 2.2 Japanese tenon and mortise splices joints (<i>mechiire</i>)	14
Fig. 2.3 Traditional half-timber frame constructions in (a) Portugal: <i>gaiola</i> walls,.....	15
Fig. 2.4 Example and schematic representation of <i>quincha</i> (Perù) construction system	16
Fig. 2.5 Modern timber structures : (a) <i>The Globe of Science and Innovation</i> , CERN Museum, (b) <i>Fondation Jérôme Seydoux-Phaté</i> by Renzo Piano, (c) <i>Brock Commons</i> , the tallest mass timber building under construction in Canada.	18
Fig. 2.6 <i>Baloon Frame</i> vs. <i>Platform Frame</i> system.....	19
Fig. 2.7 Examples of <i>Platform Frame</i> structural system (left) and <i>Heavy Timber</i> construction (right).....	20
Fig. 2.8 (a) Glue Laminated Timber, (b) PSL, (c) LVL and (d) sawn lumber wood element	20
Fig. 2.9 Examples of wood joints in timber frame constructions.....	21
Fig. 2.10 Various solutions of wood-steel connections.....	22
Fig. 2.11 Mass timber constructions are a complement to light wood and post-and-beam systems	22
Fig. 2.12 (a) Milled logs (<i>log house</i>), (b) plank orientation glulam (<i>floor or roof</i>), (c) wood-concrete element (<i>floor</i>), (d) CLT panel, (e) NLT panel, (f) DLT panel	23
Fig. 2.13 Houses built with <i>log house</i> system.....	24
Fig. 2.14 Cross-Laminated Timber (CLT) panel	25
Fig. 2.15 Examples of types of connections typically used to establish panel-to-panel and wall-to-floor connections in CLT construction	27
Fig. 2.16 In-plane CLT wall tests and CLT building shaking table tests conducted by CNR-IVALSA under SOFIE project.	28
Fig. 2.17 Examples of CLT building: (a) Family house (Austria); (b) Kindergarten in Poggio Picenze (Aquila); (c) Hotel Nautilus, 7-storey (Pesaro); (d) Social housing-Via Cenni, 9-storey (Milano);	29
Fig. 3.1 Lateral load path in a platform system and detail of CLT wall consequent deformation	39

Fig. 3.2 Schematic representation of a CLT wall and typical joints (i.e. hold-down and angle bracket).....	40
Fig. 3.3 Case of CLT wall test with hold-downs and angle brackets, hysteresis loop response and uplift corner detail (Popovski et al. 2010)	42
Fig. 3.4 Experimental setup on full scale CLT walls: single wall and coupled wall (Gavric et al. 2012)	43
Fig. 3.5 Unidirectional cyclic tests on typical CLT connections conducted by Gavric et al.(Gavric et al. 2014).....	44
Fig. 4.1 Pictures of the test setup without the CLT specimen	51
Fig. 4.2 Test setup representation with the specimen and description of load directions	51
Fig. 4.3 Distribution and detail of the CLT panel layer thickness	52
Fig. 4.4 Hold-down WHT540 dimensions (Rothoblass catalogue)	53
Fig. 4.5 Specimen details and assembly.....	53
Fig. 4.6 Standard monotonic and cyclic loading procedure for timber structures.....	54
Fig. 4.7 Protocol followed for monotonic tests (LD-30 as example).....	55
Fig. 4.8 Protocol followed for cyclic tests (LD-30 as example)	55
Fig. 4.9 Side views of the test setup and position of measurement instruments	56
Fig. 4.10 Deformed shapes of specimens for different values of lateral and axial displacements	57
Fig. 4.11 Deformed nails with double plastic hinge formations	58
Fig. 4.12 Localized embedment of wood caused by loaded fasteners	58
Fig. 4.13 Detail of rigid rotation of the ribbed based portion of hold-down for large value of lateral displacement imposed (i.e., LD-45): (a) out-of-plane deformation of the steel plate with accompanied extraction of nails, (b) localized crushing of wood panel below the ribbed portion of connection.....	59
Fig. 4.14 Lateral displacement along the hold-down plate at the end of lateral displacement phases	60
Fig. 4.15 Axial force vs. axial displacement curves for the 5 test series with different prescribed lateral displacement values (LD-0, 7.5, 15, 30, 45 mm): comparison of results from monotonic and cyclic tests	62
Fig. 4.16 Axial force vs. axial displacement: (a) monotonic and (b) cyclic curves for the 5 test series with different prescribed lateral displacement values (0, 7.5, 15, 30, 45 mm)	63
Fig. 4.17 Force evolution during the cyclic axial phase - Mean values of shear force	63
Fig. 4.18 Force evolution during the cyclic axial phase - Mean values of axial force.....	64
Fig. 4.19 Shear force vs. lateral displacement curves for the tests with different values of prescribed lateral displacement (0, 7.5, 15, 30, 45 mm)	65

Fig. 4.20 EN-12512 definition of yield values for a load-slip curve with (a) with two well defined liner parts, (b) without two well-defined linear parts	66
Fig. 4.21 Schematic representation of (a) ENb and (b) EEH methods for the definition of yielding point and corresponding tri-linear approximation.....	67
Fig. 4.22 Tri-linear approximations superimposed to the monotonic experimental curves for the specimen subjected to different prescribed lateral displacement (0, 7.5, 15, 30, 45 mm)	68
Fig. 4.23 Displacement values of the tri-linear curves for the specimens with different prescribed lateral displacement (LD=0, 7.5, 15, 30, 45 mm).....	70
Fig. 4.24 Force values of the tri-linear curves for the specimens with different prescribed lateral displacement (LD=0, 7.5, 15, 30, 45 mm)	71
Fig. 4.25 Stiffness values of the backbone curves for specimens with different prescribed lateral displacement (LD=0, 7.5, 15, 30, 45 mm)	72
Fig. 4.26 Mean values of the dissipated energy for each axial cycle at prescribed values of lateral displacement (0, 7.5, 15, 30, 45 mm)	79
Fig. 5.1 Drawing of the test setup for angle bracket connection.....	86
Fig. 5.2 Angle bracket connection setup	87
Fig. 5.3 CLT panel layer configuration.....	88
Fig. 5.4 Angle bracket and nail geometry (Rothoblaas catalogue)	88
Fig. 5.5 Explode view and assembly of the test specimen	89
Fig. 5.6 Protocol followed for monotonic tests (AD-20 as example)	90
Fig. 5.7 Protocol followed for cyclic tests (AD-20 as example).....	90
Fig. 5.8 Side view of the specimen and position of the measurement instruments.....	91
Fig. 5.9 Deformed shapes of test specimens for different values of axial displacement.....	93
Fig. 5.10 Failure of the connection with plasticization in the nails.....	93
Fig. 5.11 Failure of the connection with consequent embedment in the panel and deformed steel bracket.....	94
Fig. 5.12 In-plane and out-of-plane rotation of the angle-bracket	94
Fig. 5.13 Corner wood crushing and nails pull out	95
Fig. 5.14 Imposed axial displacement on the connection and nails deformations for cyclic (left) and monotonic (right) tests.....	96
Fig. 5.15 Axial force vs. axial displacement for monotonic tests (AD 0-5-10-15-20).....	98
Fig. 5.16 Axial force (mean value) vs. axial displacement for cyclic tests (AD 0-5-10-15-20) .	98
Fig. 5.17 Shear force vs. lateral displacement curves for the five test series (AD 0-5-10-15-20): comparison of monotonic and cyclic results	99
Fig. 5.18 Shear force vs. lateral displacement for monotonic (right) and cyclic (left) tests	100
Fig. 5.19 Axial force (mean value) evolution during the cyclic loading.....	100
Fig. 5.20 Shear force (mean value) evolution for repeated lateral displacement cycles	101

Fig. 5.21 Equivalent Energy Plastic Curve (EEEP) method	102
Fig. 5.22 <i>Yasumura and Kawai analysis method for the determination of the yield point</i>	103
Fig. 5.23 Tri-linearization of experimental curve	103
Fig. 5.24 Tri-linear approximation curves for cyclic and monotonic results for imposed AD-XY levels	104
Fig. 5.25 Displacement point values of the tri-linearization curves (mean value) for different prescribes axial displacement (AD 0-5-10-15-20)	105
Fig. 5.26 Force point values of the tri-linearization curves (mean value) for different prescribes axial displacement (AD 0-5-10-15-20)	106
Fig. 5.27 Stiffness values of the backbone curves for different prescribes axial displacement (AD 0-5-10-15-20)	107
Fig. 5.28 Influence of the angle bracket geometry on force patterns on the nails fastener group (Tomasi & Sartori 2013)	109
Fig. 5.29 Resulting forces in the angle bracket connector	109
Fig. 5.30 Comparison between experimental and analytical angle-bracket connection capacity	110
Fig. 5.31 Mean values of the dissipated energy for each axial cycle at prescribed values of axial displacement (0, 5, 10, 15, 20 mm)	112
Fig. 6.1 Hysteretic response of various structural systems	122
Fig. 6.2 Gap opening and schematic representation of a self-centering wall (Rahman & Restrepo 2000)	122
Fig. 6.3 Idealized hysteresis loops	123
Fig. 6.4 Hybrid rocking system mechanisms: (a) decompression, (b) tensile yielding of the steel dissipater, (c) PT elements elongation, (d) compressive yielding in the steel dissipater and (e) re-centring (Sarti 2015)	124
Fig. 6.5 Passive energy dissipation devices in earthquake resistant buildings.....	125
Fig. 6.6 Buckling-resistant unbonded brace (BRB)	126
Fig. 6.7 Joined precast hybrid frame (Nakaki et al. 1999)	127
Fig. 6.8 Precast concrete post-tensioned rocking wall with u-shaped lateral dissipator (Stanton 2003)	127
Fig. 6.9 Hybrid precast concrete dual-shell steel columns (Guerrini et al. 2015)	128
Fig. 6.10 Steel Moment Resisting Frame joint (Ricles et al. 2001)	128
Fig. 6.11 Controlled rocking self-centring steel-braced frames (Eatherton et al. 2014)	129
Fig. 6.12 Rocking confined masonry system (Toranzo et al. 2009).....	130
Fig. 6.13 Flexural energy dissipation devices (Toranzo et al. 2004)	130
Fig. 6.14 (a) Nailed and (b) epoxied steel rods connection for gluelam beam-column joint ...	131
Fig. 6.15 LVL beam-column hybrid solutions under Pres-Lam program	132

Fig. 6.16 Post-tensioned LVL rocking wall system with externally mounted plug-and-play dissipaters	132
Fig. 6.17 Internal mild steel bars on the left, LVL-exopoxied steel dissipaters on the centre and <i>plug-and play</i> solution on the right (Sarti et al. 2012)	133
Fig. 6.18 Scheme of Coupled Wall System with UFP devices (left), Test set up of Coupled Wall System (centre), Particular of UFP devices (right) (Iqbal et al. 2007).....	133
Fig. 6.19 NMIT building with steel UFP devices (<i>top</i>) and Carterton Events Centre with internal dissipater bars (<i>bottom</i>), New Zealand.....	134
Fig. 6.20 CLT self-centering timber wall with supplemental UFPs dissipating devices (Ganey et al. 2016).....	135
Fig. 6.21 Tests on pinned axial energy dissipaters for CLT rocking wall: (a) with reduced restrained buckling length, (b) increase in restrained length for the dissipater (Kramer et al. 2013)	136
Fig. 7.1 3D model and different views of the adopted case study.....	141
Fig. 7.2 Hypothesize wall-to-beam pinned connection (Moroder et al. 2014).....	142
Fig. 7.3 Seattle (WA) elastic response spectra and design spectra with a <i>q-factor</i> of 2	143
Fig. 7.4 Summary flow-chart of the section equilibrium procedure	145
Fig. 7.5 Rocking wall section balance.....	147
Fig. 7.6 Base layers subdivision of the CLT panel	149
Fig. 7.7 Setup descriprion	151
Fig. 7.8 Side view of the setup.....	151
Fig. 7.9 Out-of-plane retains detail (left), global view of CLT wall in position (right).....	152
Fig. 7.10 Multiple full views of the test specimen	153
Fig. 7.11 North-East side view instrumentation.....	154
Fig. 7.12 North-West side view instrumentation	154
Fig. 7.13 CLT wall panel dimensions and thickness layers detail	155
Fig. 7.14 Moisture content measure instrument.....	156
Fig. 7.15 Post-tensioning solution for the test.....	157
Fig. 7.16 Axial energy dissipater with non-assembled parts.....	158
Fig. 7.17 Simplified scheme of buckling	159
Fig. 7.18 Execution phases for the external axial dissipater	161
Fig. 7.19 Alternative connection solution for the panel-to-dissipater link.....	163
Fig. 7.20 ZD-plate (MyTiCon).....	164
Fig. 7.21 Force distribution in ZD-plate connection	164
Fig. 7.22 Panel-to-axial dissipater connection assembly	165
Fig. 7.23 Double function of the shear key solution	166

Fig. 7.24 Base corner solution shear key, working also as bottom attachment of the axial dissipater	167
Fig. 7.25 Steel skirting protection for the CLT wall toe	167
Fig. 7.26 Lateral loading protocol (displacement control)	168
Fig. 7.27 Failure started at 1% drift in the connection	169
Fig. 7.28 Previous test on a moment connection using ZD-plates (Closen 2012)	170
Fig. 7.29 Breaking in the panel-to-dissipater connection.....	170
Fig. 7.30 Uplift in the base corner and subsequent repositioning contact for the reverse cycle	171
Fig. 7.31 PT bars bottom anchoring	171
Fig. 7.32 Lateral force vs drift.....	172
Fig. 7.33 Lateral force vs drift before reaching 1% drift level.....	173
Fig. 7.34 Lateral force vs drift after reaching 1% drift level.....	173
Fig. 7.35 Overturning moment vs drift	174
Fig. 7.36 Overturning moment vs drift before reaching 1% drift level.....	174
Fig. 7.37 Overturning moment vs drift after reaching 1% drift level.....	175
Fig. 7.38 Post-tension force vs drift	175
Fig. 7.39 Post-tension force vs drift before reaching 1% drift level	176
Fig. 7.40 Post-tension force vs drift after reaching 1% drift level	176
Fig. 7.41 PT strength ratio vs drift	177
Fig. 7.42 PT force vs overturning moment	177
Fig. 7.43 Oscillation of the neutral axis depth for the given drift levels during repeated cycles	180
Fig. 7.44 Symmetrical positioned (respect PT bar) string pot uplift measures	182
Fig. 8.1 Schematization of lumped plasticity model	188
Fig. 8.2 Detail of anchorage of PT bar and the behaviour implemented in the model.....	189
Fig. 8.3 Rocking mechanism – Schematization of friction - contact non-linear links	190
Fig. 8.4 Behaviour of lateral restraints: Initial slip between shear key and corner skirting and contact between corner skirting and shear key.....	191
Fig. 8.5 Behaviour of lateral restraints: Initial slip between shear key and corner skirtings (red line). Contact between corner skirtings and shear key (blue line)	191
Fig. 8.6 Force Displacement behaviour of <i>Multilinear Plastic Links</i>	192
Fig. 8.7 Multilinear Pivot hysteresis relationship used in SAP2000 for dissipater hysteresis modelling.....	193
Fig. 8.8 Comparison between experimental and numerical results for drifts 0.5% - 0.75% – 1 %	194
Fig. 8.9 Comparison between experimental and numerical results – drift level 0.5%	195
Fig. 8.10 Comparison between experimental and numerical results – drift level 0.75%	195

Fig. 8.11 Comparison between experimental and numerical results – drift level 1%	195
Fig. 8.12 Overturning Moment - Comparison between experimental and numerical results for drifts 0.5% - 0.75% – 1 %	196
Fig. 8.13 PT force: Comparison of experimental and numerical results for drifts 0.5% - 0.75% – 1%	196
Fig. 8.14 Comparison of test and numerical results: Post-tension force – drift level 0.5%.	197
Fig. 8.15 Comparison of test and numerical results: Post-tension force – drift level 0.75%	197
Fig. 8.16 Comparison of test and numerical results: Post-tension force – drift level 1%	197
Fig. 8.17 Comparison between dissipated energy obtained by experimental and numerical results	198
Fig. 8.18 Comparison between dissipated energy obtained by experimental and numerical results for drift until 1%	199
Fig. 8.19 Comparison between dissipated energy obtained by experimental and numerical results for drift until 2.5%.	200
Fig. 8.20 Comparison of EVD values for 1 st , 2 nd and 3 rd Cycles of drifts until 2.5% for numerical model.....	201
Fig. 8.21 Comparison of EVD values for 1 st , 2 nd and 3 rd Cycles of drifts until 2.5% for experimental results	201
Fig. 8.22 Comparison of EVD values obtained by experimental and numerical results for 1 st Cycles of drifts until 2.5%.....	202
Fig. 8.23 Comparison of EVD values obtained by experimental and numerical results for 2 nd and 3 rd Cycles of drifts until 2.5%	202
Fig. 8.24 Drift levels reached during experimental test and developed numerical model (red line) and incremental drift levels investigated by numerical model (blue line)	203
Fig. 8.25 Base shear – top displacement curve: Drift levels reached during experimental test (red line) and incremental drift levels investigated by numerical model (blue line).....	204
Fig. 8.26 Comparison between dissipated energy obtained by experimental and numerical results for drift until 5%	204
Fig. 8.27 Comparison of EVD values for 1 st , 2 nd and 3 rd Cycles of drifts until 5% for numerical model.....	205
Fig. 9.1 HSK system (TiComTec)	212

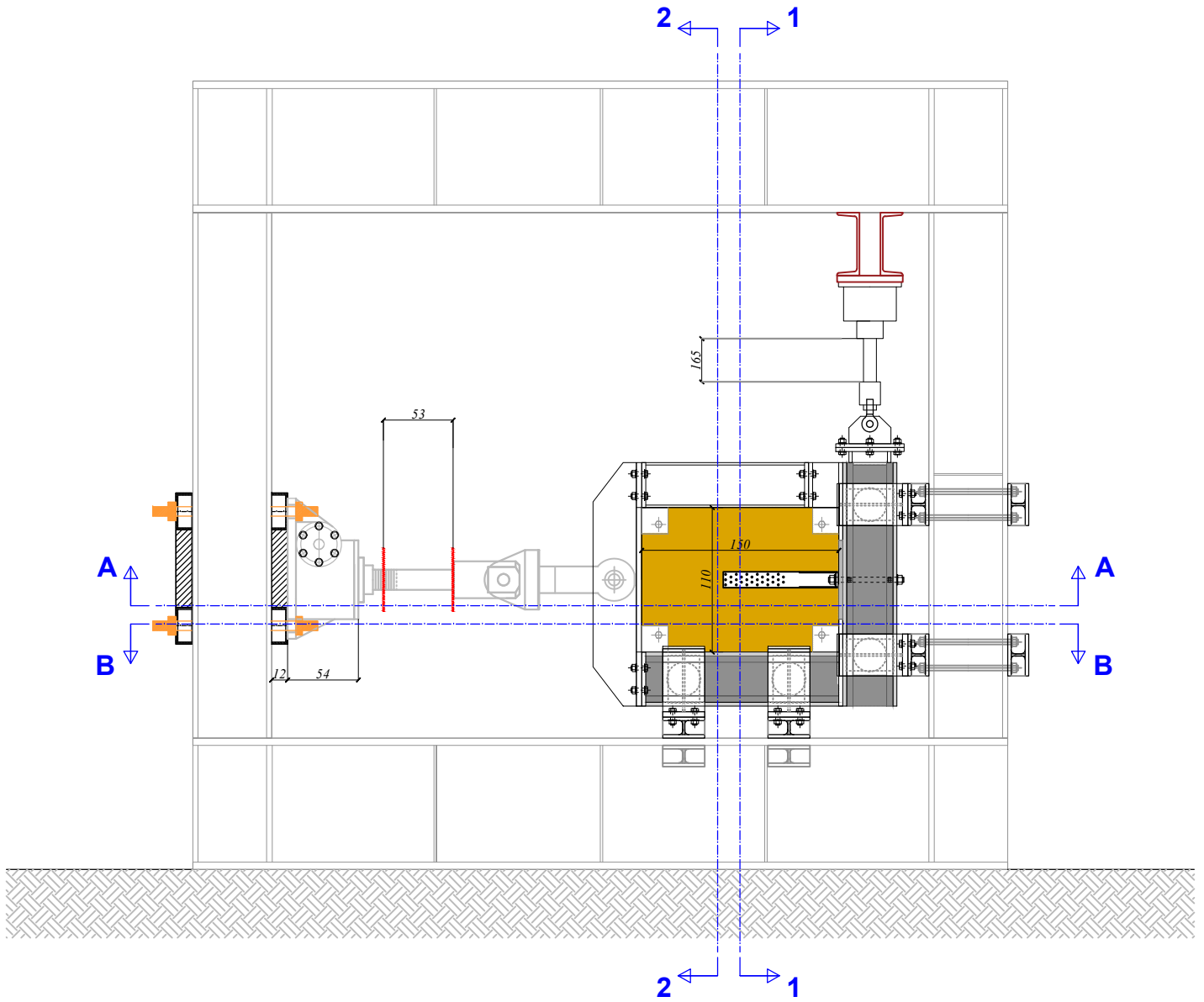
Table Captions

Table 1 Mean values of hold-down axial elongation at different levels of the axial cyclic displacement.....	60
Table 2 Resulting values from the different tri-linearization methods	69
Table 3 Mean values of ductility in traction (μ) for different levels of lateral displacement (LD=0, 7.5, 15, 30, 45 mm)	72
Table 4 Adopted parameters for computing connection's load-carrying capacity.....	75
Table 5 Comparison between the estimation of elastic stiffness of hold-down connection for the configuration LD-0.....	76
Table 6 Mean values of strength degradation (ΔF) registered during the cyclic tests at different levels of the axial displacement (4,5 - 24 mm)	77
Table 7 Mean values of equivalent viscous damping (v_{eq}) from cyclic tests conducted at different levels of axial displacements	78
Table 8 Different levels of imposed axial displacement	89
Table 9 Comparison between the imposed axial displacement and nails deformation for lateral cyclic loading	97
Table 10 Comparison between the imposed axial displacement and nails deformation for lateral monotonic loading.....	97
Table 11 Mean values of ductility (μ) for different levels of axial displacements (AD 0-5-10-15-20)	108
Table 12 Analytical and experimental angle bracket connection capacity results	110
Table 13 Mean values of strength degradation (ΔF) registered during the cyclic tests at different levels of the axial displacement (4,5 - 24 mm)	111
Table 14 Mean values of equivalent viscous damping (v_{eq}) from cyclic tests conducted at different levels of axial displacements	112
Table 15 Scale factors according to Cauchy similitude	144
Table 16 Post-tension bars steel properties	Table 17 Axial dissipater steel (S275)..... 146
Table 18 Douglas fir (Oregon pine) physical and mechanical characteristics	149
Table 19 Moisture content records.....	156
Table 20 Loading profile of CLT rocking wall test	168
	233

Table 21 Neutral axis depth ratio for the first cycle of each drift level.....	178
Table 22 Progressive distances from the left corner of the base string potentiometers	181
Table 23 Material properties specified for CLT wall.....	189
Table 24 Material properties specified for Post-Tension Bars.....	189
Table 25 Parameters of friction - contact non-linear links disposed at the base of the panel ...	190
Table 26 Parameters which define the stress strain curve of dissipater	193
Table 27 Parameters which define the Pivot Hysteresis Model	193
Table 28 Comparison of horizontal load measured during test with numerical model.....	198

**ANNEX A: Setup drawings for coupled actions
tests on CLT traditional connections**





CLT TRADITIONAL CONNECTIONS TESTS

Test Setup - Front view

TAV.01

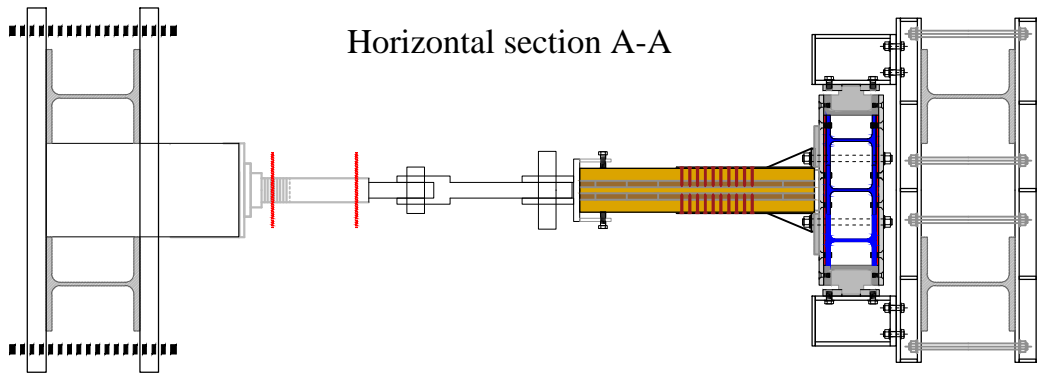
Author: Ph. D Milena Massari

Date: 2/24/2016

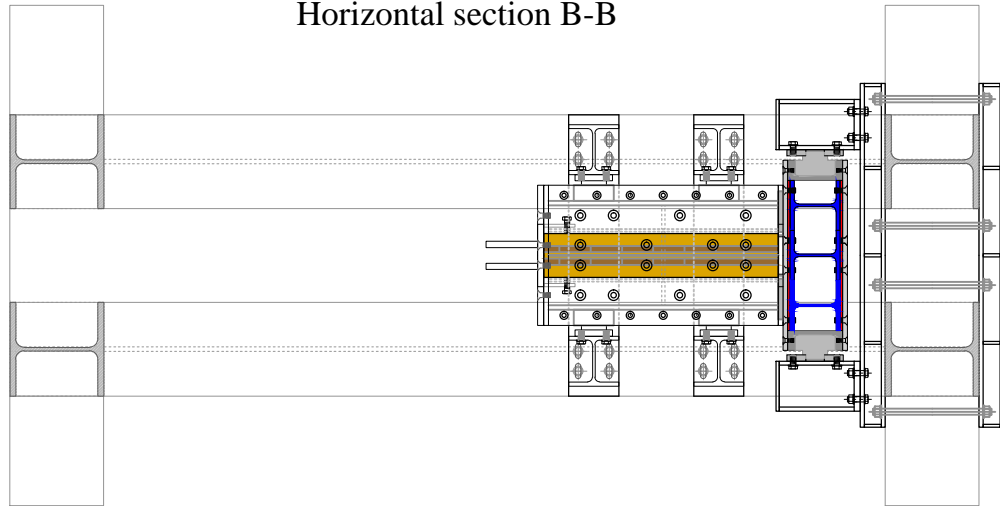
Rev. 1

DRAFT PACKAGE FOR INFORMATION ONLY

PROPRIETARY AND CONFIDENTIAL
ALMA MATER STUDIORUM
UNIVERSITY OF BOLOGNA

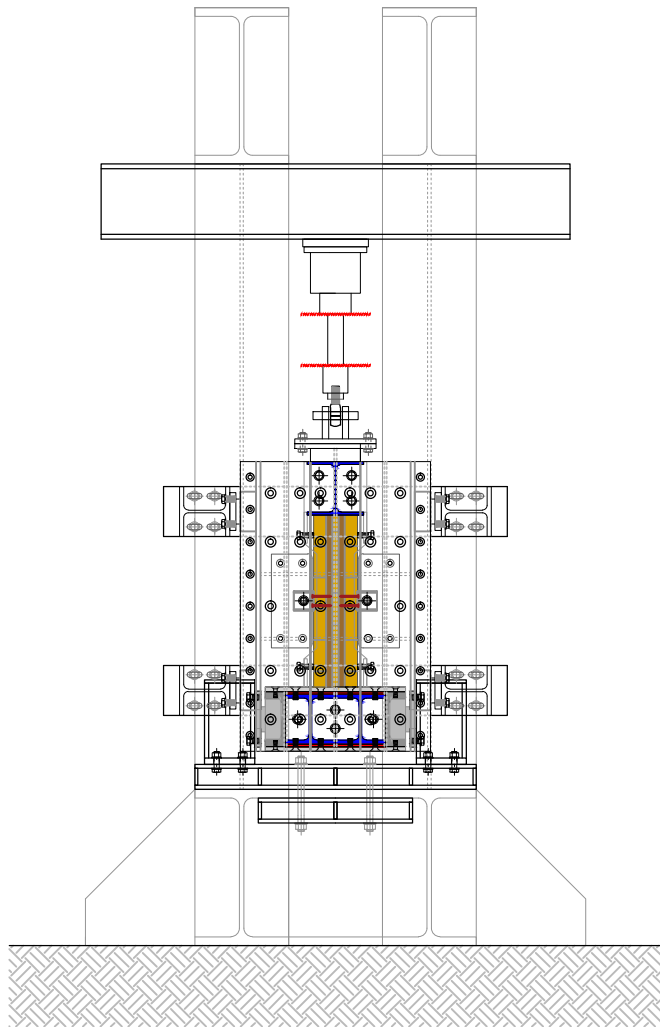


Horizontal section A-A

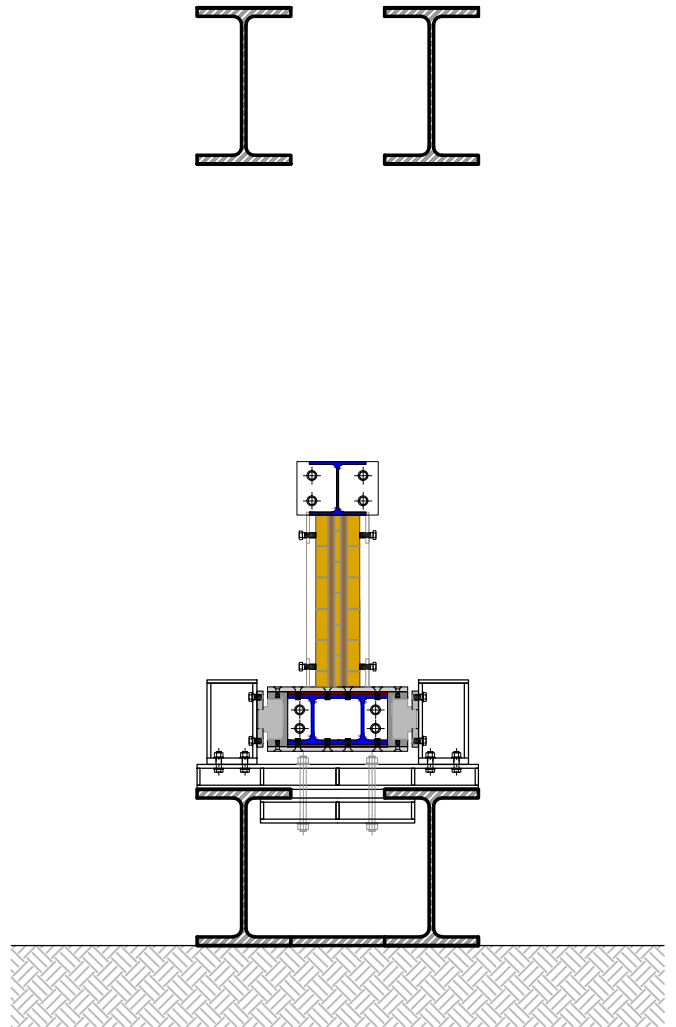


Horizontal section B-B

Vertical Section 1-1



Vertical Section 2-2



CLT TRADITIONAL CONNECTIONS TESTS

TAV.02

Test Setup - Horizontal Sections

Author: Ph. D Milena Massari

Date: 2/24/2016

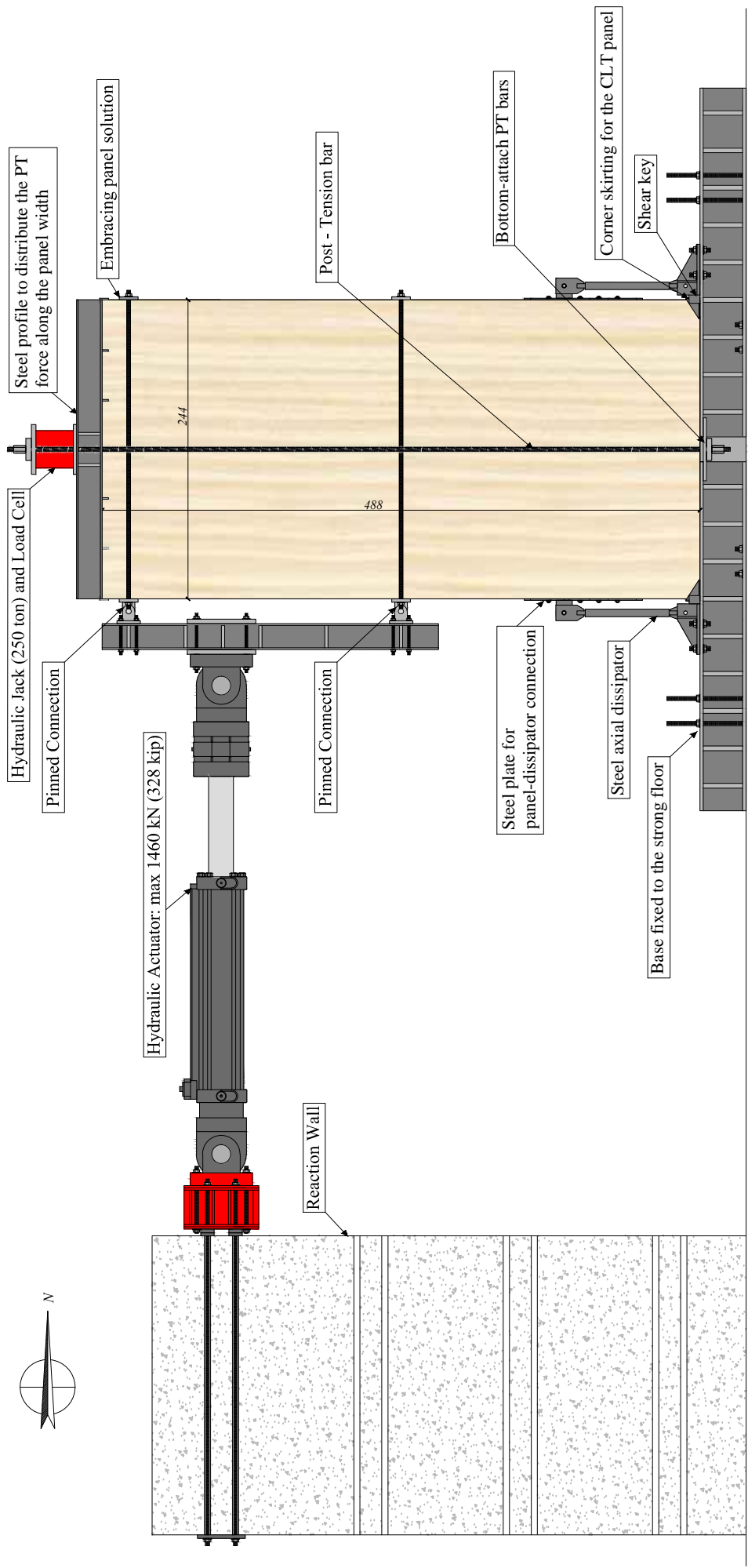
Rev. 1

DRAFT PACKAGE FOR INFORMATION ONLY

PROPRIETARY AND CONFIDENTIAL
ALMA MATER STUDIORUM
UNIVERSITY OF BOLOGNA

**ANNEX B: Setup drawings for hybrid rocking
CLT wall test**





TAV.03

CROSS-LAMINATED TIMBER ROCKING WALL TESTS

Test Setup - Frontal Overview

Author: Ph. D Milena Massari

Date: 2/24/2016

Rev. 1

DRAFT PACKAGE FOR INFORMATION ONLY
 PROPRIETARY AND CONFIDENTIAL
 © OREGON STATE UNIVERSITY
 101 KEARNEY HALL
 CORVALLIS, OR 97331

